ESL-TR-88-08

SPECTROSCOPIC STUDIES OF METAL-LIGAND-SURFACE INTERACTIONS

C.T. JOHNSTON, W.B. PERSON, M.T. VALA,
T.L. TIPTON, D.A. STONE

UNIVERSITY OF FLORIDA
DEPARTMENTS OF CHEMISTRY AND SOIL SCIENCE
GAINESVILLE FL 32611

OCTOBER 1988

FINAL REPORT

JANUARY 1986 - SEPTEMBER 1987

ENGINEERING & SERVICES LABORATORY
AIR FORCE ENGINEERING & SERVICES CENTER
TYNDALL AIR FORCE BASE, FLORIDA 32403

NOTICE

PLEASE DO NOT REQUEST COPIES OF THIS REPORT FROM HQ AFESC/RD (ENGINEERING AND SERVICES LABORATORY). ADDITIONAL COPIES MAY BE PURCHASED FROM:

NATIONAL TECHNICAL INFORMATION SERVICE
5285 PORT ROYAL ROAD
SPRINGFIELD, VIRGINIA 22161

FEDERAL GOVERNMENT AGENCIES AND THEIR CONTRACTORS REGISTERED WITH DEFENSE TECHNICAL INFORMATION CENTER SHOULD DIRECT REQUESTS FOR COPIES OF THIS REPORT TO:

DEFENSE TECHNICAL INFORMATION CENTER
CAMERON STATION
ALEXANDRIA, VIRGINIA 22314

UNCLASSIFIED

SECURITY CLASSIFICATION OF THIS PAGE

REPORT DOCUMENTATION PAGE

Form Approved OMB No. 0704-0188

1a. REPORT SECURITY CLASSIFICATION	1b. RESTRICTIVE MARKINGS
2a. SECURITY CLASSIFICATION AUTHORITY	3. DISTRIBUTION/AVAILABILITY OF REPORT Approved for Public Release Distribution Unlimited
2b. DECLASSIFICATION/DOWNGRADING SCHEDULE	
4. PERFORMING ORGANIZATION REPORT NUMBER(S)	5. MONITORING ORGANIZATION REPORT NUMBER(S) ESL-TR-88-08
6a. NAME OF PERFORMING ORGANIZATION University of Florida 6b. OFFICE SYMBOL (If applicable)	7a. NAME OF MONITORING ORGANIZATION Air Force Engineering and Services Center
6c. ADDRESS (City, State, and ZIP Code) Departments of Chemistry and Soil Science Gainesville FL 32611	7b. ADDRESS (City, State, and ZIP Code) HQ AFESC/RDVS Tyndall AFB FL 32403
8a. NAME OF FUNDING/SPONSORING ORGANIZATION HQ AFESC 8b. OFFICE SYMBOL (If applicable) RDV	9. PROCUREMENT INSTRUMENT IDENTIFICATION NUMBER F08635-83-C0-136, Task 86-4
8c. ADDRESS (City, State, and ZIP Code) HQ AFESC/RDVS Tyndall AFB FL 32403-6001	10. SOURCE OF FUNDING NUMBERS PROGRAM ELEMENT NO. 1900 / PROJECT NO. 20 / TASK NO 90 / WORK UNIT ACCESSION NO. NA

11. TITLE (Include Security Classification)

Spectroscopic Studies of Metal-Ligand-Surface Interactions

12. PERSONAL AUTHOR(S)

C. T. Johnston, W. B. Person, M. T. Vala, T. L. Tipton, and D. A. Stone

13a. TYPE OF REPORT	13b. TIME COVERED	14. DATE OF REPORT (Year, Month, Day)	15. PAGE COUNT
Final	FROM Jan 86 TO Sep 87	October 1988	223

16. SUPPLEMENTARY NOTATION

Availability of this report is specified on reverse of front cover

17. COSATI CODES		
FIELD	GROUP	SUB-GROUP
07	02	
07	04	

18. SUBJECT TERMS (Continue on reverse if necessary and identify by block number)

Spectroscopy; Raman and Infrared Studies; Metal-Ligand-Surface Interactions.

19. ABSTRACT (Continue on reverse if necessary and identify by block number)

A four part program of research on the vibrational spectroscopy of hydrazine, aromatic hydrocarbons, metals and clays and their interactions has been carried out. Vibrational spectra of hydrazine and its deuterated analogs have been obtained in cold rare gas matrices. A theoretical study of the vibrational frequencies and intensities of these systems has been carried out and used to interpret the observed spectra. Hydrazine has been reacted with various metal atoms and ions and their Raman or infrared spectra recorded and interpreted. Finally, the vibrational spectra of specific clay minerals and the effect of adsorbed metal cations and aromatic hydrocarbons were obtained and used to study the interactions between these species.

20. DISTRIBUTION/AVAILABILITY OF ABSTRACT	21. ABSTRACT SECURITY CLASSIFICATION
☒ UNCLASSIFIED/UNLIMITED ☐ SAME AS RPT. ☐ DTIC USERS	UNCLASSIFIED
22a. NAME OF RESPONSIBLE INDIVIDUAL Dr Daniel A. Stone	22b. TELEPHONE (Include Area Code) 904-283-4298 / 22c. OFFICE SYMBOL HQ AFESC/RDVS

DD Form 1473, JUN 86 Previous editions are obsolete. SECURITY CLASSIFICATION OF THIS PAGE

(The reverse of this page is blank.)

UNCLASSIFIED

EXECUTIVE SUMMARY

This research program was designed to conduct fundamental vibrational spectroscopic studies on the interaction of certain small organic molecules with transition metal ions and with clay minerals. The principal objective was to determine the chemical mechanisms of interaction of these organic molecules with targeted metal cations and clay minerals. Specifically, the major goals were:

* Develop noninvasive, in situ vibrational spectroscopic techniques.
* Better understand the electronic and vibrational spectra of certain targeted clay minerals, organic molecules, and metal cations and atoms.
* Determine the primary mechanisms of metal-molecules interactions
* Observe how metal cations influence the adsorption and transformation of organic-surface complexes.

To accomplish these goals, a four-pronged program of research was carried out. First, the vibrational spectra of hydrazine and its deuterated derivatives were obtained in frozen rare gas matrices at low temperatures (12K). Second, to aid in the interpretation of the spectra of these minimally-perturbed species, a theoretical study of the vibrational frequencies and intensities of hydrazine and its deuterated isomers was performed. Third, the interaction of certain neutral metal atoms and ions with hydrazine was investigated by Raman and Fourier transform infrared spectroscopy. Finally, the vibrational spectra of specific clay minerals and the effect of adsorbed metal cations and aromatic hydrocarbons were obtained and used to understand the interactions between these species.

(The reverse of this page is blank)

PREFACE

This report was prepared by members of the Departments of Chemistry and Soil Science of the University of Florida, Gainesville FL 32611. The work was sponsored by the Air Force Engineering and Services Center, Engineering and Services Laboratory (AFESC/RDVS), Tyndall Air Force Base FL 32403-6001.

This report describes experimental and theoretical work on the electronic and vibrational spectra of certain targeted metals, ligands and surfaces. The goal of this program was to understand the mechanisms of metal-ligand interactions and how they are perturbed near environmentally significant surfaces.

The work was carried out between January 1986 and September 1987, under the direction of professors Martin T. Vala and Willis B. Person of the Department of Chemistry and Clifford T. Johnston of the Department of Soil Science.

Dr Daniel A. Stone was the AFESC/RDVS project officer for this contract.

This report has been reviewed by the Public Affairs Office and is releasable to the National Technical Information Service (NTIS). At NTIS, it will be available to the general public, including foreign nationals.

This technical report has been reviewed and is approved for publication.

DANIEL A. STONE, PhD
Project Officer

THOMAS J. WALKER, Lt Col, USAF, BSC
Chief, Environics Division

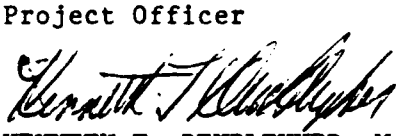

KENNETH T. DENBLEYKER, Maj, USAF
Chief, Environmental Sciences Branch

LAWRENCE D. HOKANSON, Colonel, USAF
Director, Engineering and Services Laboratory

(The reverse of this page is blank)

TABLE OF CONTENTS

TABLE OF CONTENTS
(Concluded)

LIST OF FIGURES

LIST OF FIGURES

(Continued)

LIST OF FIGURES

(Continued)

LIST OF FIGURES

(Continued)

LIST OF FIGURES

(Continued)

LIST OF FIGURES

(Continued)

LIST OF FIGURES

(Continued)

LIST OF FIGURES

(Concluded)

LIST OF TABLES

LIST OF TABLES

(Continued)

LIST OF TABLES

(Continued)

LIST OF TABLES

(Concluded)

SECTION I

INTRODUCTION

A. OBJECTIVE

The objective of this research was to conduct fundamental studies of the mechanisms by which small molecules, coordinated with metal ions, interact with environmentally significant surfaces. The major goal of the program was to better understand the vibrational spectra of certain targeted metals, ligands and surfaces and the changes observed during interaction of these species.

B. BACKGROUND

This research program was carried out jointly at the Air Force Engineering and Services Center, Engineering and Services Laboratory (ESL), Tyndall Air Force Base, and in the Departments of Chemistry and Soil Science at the University of Florida.

The research at the ESL consisted of: (1) assembling and testing an FT-IR matrix-isolation apparatus; and (2) using this apparatus to study individual toxic chemicals in a minimally perturbing environment. The primary substances studied were hydrazine and its deuterated derivatives. Spectra were also obtained for monomethylhydrazine (MMH), unsymmetrical dimethylhydrazine (UDMH), and benzene. Each of these compounds was investigated via mid-infrared spectroscopy to obtain information on fundamental molecular vibrations.

The analysis of the hydrazine spectra was aided by quantum mechanical calculations carried out concurrently at the University of Florida under this contract. Comprehensive vibrational assignments were obtained for normal hydrazine (N_2H_4) and all nine deuterated hydrazines. Only one of the latter had previously been studied at all. These new results for hydrazines are expected to be of use in interpreting the spectra of N_2H_4 in more highly perturbed environments similar to those of natural soils.

The research at the University of Florida Department of Chemistry consisted of: (1) a theoretical study of the vibrational frequencies and intensities of hydrazine and its derivatives, (2) an experimental study of the matrix-isolation vibrational (infrared) spectroscopy of certain metal atom complexes of hydrazine and ammonia, and (3) an experimental investigation of the vibrational (Raman) spectroscopy of polycrystalline complexes of metals ions with hydrazine.

The research at the University of Florida Department of Soil Science consisted of : (1) evaluation of three methods to study clay-organic complexes; and (2) using the best method (controlled environment transmission) to study the vibrational spectra of certain clay-organic complexes using Fourier transform infrared spectroscopy. The following paragraphs outline background for the research performed in these different areas.

To understand the observed vibrational spectra of interacting molecules and ions and thus to be able to use these observations to learn about the nature and mechanism of these interactions, it is first necessary to understand completely the spectra of the isolated molecules. As a first step in the interpretation of the spectra of hydrazine and its complexes, ab initio molecular orbital calculations were carried out for the vibrational spectra of hydrazine. These calculations were made at the SCF level, with a 6-31G** basis-set, and were made to predict both the frequencies and the intensities of the fundamental absorption bands of N_2H_4. Based on previous experience, it was expected that these predicted spectra would agree with experimental spectra for the isolated molecule. This proved to be the case. Furthermore, calculations with a 3-21G basis-set examined the basis-set dependence and found it to be small. In addition, independent calculations by Magers and Bartlett, including the effects of electron correlation, showed that those effects are also small for this molecule.

The force constants and dipole moment derivatives derived from our calculations for hydrazine appear to form a reliable first approximation to the true values of these parameters. This conclusion was tested by predicting spectra for all possible deuterated isotopic derivatives of N_2H_4. These predicted spectra were in good agreement with the experimental spectra,

proving that the calculated vibrational parameters (force constants and dipole moment derivatives) are indeed a good first approximation to the true experimental parameters.

The agreement between the spectra calculated for the gauche conformer of hydrazine and the experimental spectra establish that the gauche conformer is predominant (>95%) in the matrices. The changes observed in the spectrum from the gas phase show that even the very weak interaction between hydrazine and the matrix has an observable effect on the vibrational spectra. One of the unfinished goals of the theoretical studies would be to calculate the effect of intermolecular interaction (for example, dimer formation) on the vibrational parameters and to follow these effects as the interaction increases to the strength found for those that occur with metal ions.

An important phase of this project involved the development of the Fourier transform-infrared (FT-IR) and Raman spectroscopic techniques used to study the metal-ligand-surface complexes. This task included the development of a matrix-isolation FT-IR apparatus, upgrading an existing laser Raman spectrometer, and the development of controlled environment diffuse reflectance, attenuated total reflectance and transmission FT-IR sample presentation capabilities used to characterize the vibrational spectra of the soil constituents. In addition, computer codes were developed on various computers to collect Raman data and drive the monochromator, process matrix-isolation FT-IR data, and to display, manipulate, and output the FT-IR and Raman data.

To better understand the possible interaction of hydrazine with the transition metals found in clays, two different spectroscopic studies of possible complexation between transition metals and hydrazine were undertaken. In the first study, a complexation investigation of neutral copper and iron atoms with hydrazine in the nonperturbing medium of a rare gas matrix was performed. The method developed for this study involved the codeposition of a metal effused from a high-temperature Knudsen cell with a room temperature mixture of hydrazine and argon onto a spectroscopic sample window held at 12K by a closed-cycle cryogenic refrigerator. Fourier transform infrared spectroscopic measurements were taken and vibrational band shifts from uncomplexed hydrazine noted. Parallel studies were also performed, with ammonia as the ligand.

The shifted bands were interpreted as resulting from the 1:1 complexes $Cu \cdot NH_3$, $Fe \cdot NH_3$ or $Cu \cdot N_2H_4$. The $Cu \cdot NH_3$ and $Fe \cdot NH_3$ complexes displayed relatively large frequency shifts, with the $Fe \cdot NH_3$ complex showing a larger shift than $Cu \cdot NH_3$. The $Cu \cdot N_2H_4$ and $Fe \cdot N_2H_4$ complexes showed identical, but considerably smaller shifts than the ammonia complexes. These observations were found to be completely consistent with recent calculations by Bauschlicher. In this theoretical study the complexes' bonding was attributed to an electrostatic interaction between the ligand's dipole moment and the effective polarized metal atom dipole moment. Normal mode calculations fit to the observed shifted complex bands are consistent with the deduced relative bonding strength in the different complexes.

In the second study of the complexation of hydrazine, the Raman spectra of the known $Zn(N_2H_4)_2X_2$ (X = Cl, Br) complexes were studied for polycrystalline solids and assigned for the first time. In the region between 300 cm^{-1} and 3500 cm^{-1} Raman bands due to perturbed vibrations of the hydrazine ligands were observed and assigned. Where previously observed, the present bands correspond well although, because of the higher resolution used in the present study, several additional bands have been observed in this region. In the low-energy region between 100 and 300 cm^{-1}, vibrations due to the ZnN_4X_2 core were observed for the first time. A reasonable assignment scheme for this region has been found with the aid of a normal coordinate calculation of the complexes' core.

Three diverse sample presentation FT-IR techniques were evaluated in order to determine the optimum method for studying clay-organic complexes: powder spectra were obtained using a controlled environment diffuse reflectance (CE-DR) cell, aqueous solutions in a cylindrical internal reflectance cell, and a controlled environment transimission (CE-TR) cell was used to study self-supporting clay films and deposits. Of the three methods compared, controlled environment transmission was shown to provide the highest signal-to-noise ratio and greatest spectral resolution.

The selection rules for Raman- and infrared-active vibrational transitions are different; consequently, a more complete vibrational analysis can be

obtained by the combined application of Raman and FT-IR methods. Raman and FT-IR spectra of KGa-1 kaolinite were compared, and in the high frequency hydroxyl stretching region, good agreement between the Raman and FT-IR spectra was obtained. However, much longer data collection times were required for the Raman spectra than were required for FT-IR spectra to obtain a comparable signal-to-noise ratio. In contrast to the high frequency results, there was generally poor agreement between the Raman and FT-IR spectra of kaolinite in the lower frequency region; many of the lower frequency vibrational bands were unique to the Raman or the FT-IR spectrum, i.e., few bands were both IR- and Raman-active. In addition, the low-frequency vibrational spectra of clay minerals below 400 cm^{-1} was more accessible using Raman spectroscopy than by using far-FT-IR methods.

FT-IR spectra of clay-organic complexes were shown to be influenced significantly by the nature of the exchangeable metal cation on the surface of the clay mineral. As expected, Na-exchanged montmorillonites did not perturb the vibrational spectrum of adsorbed p-xylene significantly. The CE-TR spectrum of adsorbed p-xylene on the Na-exchanged clay was similar to the vapor phase spectrum of p-xylene. In comparison, however, there was clear evidence that a chemical transformation of adsorbed p-xylene did occur on the same montmorillonite clay but exchanged with Cu^{+2} rather than with Na^{+} cations. As the water content decreased, the metal-ligand-surface complex developed a dark orange color, and a suite of new vibrational bands which could not be assigned to p-xylene fundametals were observed in the FT-IR spectrum of the p-xylene: Cu-exchanged montmorillonite complex. Thus, unambiguous vibrational data obtained indicated that p-xylene was transformed on the surface of Cu-exchanged montmorillonite under anhydrous conditions.

FT-IR spectra of clay-arene complexes have not been reported previously in the literature. These vibrational results agree with published electron spin resonance (ESR), dispersive-IR, and ultraviolet (uv)-visible results and indicate that, under anhydrous conditions, a single electron transfer reaction takes place between the organic adsorbate, p-xylene, and the exchangeable metal cation, Cu^{+2}. Consequently, the Cu^{+2} cation on the surface of the clay is reduced to Cu^{+1}, or to Cu metal, and the aromatic adsorbate is oxidized to form a radical organic cation. Polymerization of the radical cation is

minimized in the case of p-xylene because the para position on the ring are occupied by methyl groups. Thus, radical organic cations of p-xylene are stabilized on the surface of the Cu-exchanged montmorillonite under anhydrous conditions.

C. SCOPE

This report is arranged in the following order. In Section II the experimental studies of the infrared spectra of matrix-isolated hydrazine and its deuterated isomers is presented. The theoretical studies of these species, are given in Section III. The next two sections, IV and V, report the experimental investigations of the complexes formed between hydrazine and the metal atoms copper and iron, between ammonia and the same metal atoms and between hydrazine and zinc chloride and bromide. Finally, the studies on the vibrational spectra of the organic adsorbates with clay minerals are presented in Section VI.

SECTION II

EXPERIMENTAL VIBRATIONAL SPECTROSCOPIC STUDIES OF MATRIX-ISOLATED HYDRAZINE AND ITS DEUTERATED ISOMERS

A. INTRODUCTION

Matrix-isolation FTIR experiments were conducted at Tyndall AFB to assist in the understanding of clay spectra described in Section VI of this report. The intention was to characterize the vibrational spectra of toxic molecules in an inert environment, and proceed to more complicated systems. Infrared matrix-isolation spectra were obtained for hydrazine, deuterated hydrazine, methylhydrazine (MMH), unsymmetrical dimethylhydrazine (UDMH), and benzene. A complete data analysis was performed on the first two of these substances. The remaining spectra were recorded for future reference.

Hydrazine is of interest to the Air Force because of its use as a fuel for rockets, thrusters, and small electrical power-generating units. The current matrix-isolation study of N_2H_4 expands the single previous matrix study (Reference II-1) and revises some of the earlier vibrational assignments.

Ab initio calculations, described in Section III, were instrumental in assigning all of the hydrazine spectra. These calculations enabled most of the observed fundamental vibrations to be assigned unambiguously. In some cases, vapor-phase data were also beneficial (References II-2-5).

Most of the currently accepted vapor-phase assignments for N_2H_4 are based on the work of Giguere and Liu (Reference II-2). Additional data have since been reported for ν_7 (Reference II-3) and ν_{12} (Reference II-4); and a renumbering of the fundamental frequencies has been adopted (Reference II-5). A summary of the renumbered vapor frequencies has been given by Durig et al., along with gas- and liquid-phase data (Reference II-5).

The experiments on deuterated hydrazine comprise the first exhaustive study of the nine constituent species of this substance (two isomers of N_2H_3D, four of $N_2H_2D_2$, two of N_2HD_3, and one of N_2D_4). Previous work on deuterated hydrazines has been limited to N_2D_4. Durig et al. (Reference II-5) investigated the gas-, liquid-, and solid-phase infrared spectra of N_2D_4, as

well as the Raman spectrum of liquid N_2D_4. Tanaka et al. (Reference II-6) performed ab initio calculations on N_2D_4 and revised some of the earlier gas-phase assignments and band centers. No matrix-isolation spectra have been reported for deuterated hydrazines. The present data for N_2D_4 confirm the assignments of Reference II-6, except for the ordering of the ν_1 and ν_8 NH-stretching frequencies.

B. EXPERIMENTAL

The matrix-isolation apparatus consisted of four major components: (1) a closed-cycle refrigerator (Air Products Displex model CSA-202) with an infrared window attached to the cold head; (2) a vacuum shroud to house the refrigerator; (3) a gas-handling manifold; and (4) an FT-IR spectrometer (Nicolet 6000C upgraded to model 160SX hardware and software). The infrared beam was transmitted through the vacuum shroud via KBr windows. Usually, the matrix was produced by mixing the vaporized sample with nitrogen or argon solvent, and spraying the resulting solution onto the cryogenically cooled deposit window. In some cases, the solute and solvent were sprayed through separate nozzles, as shown in Figure 1.

In the single-nozzle configuration, hydrazine vapor was premixed with the matrix gas in a 1.0-liter Pyrex® bulb and directed to the deposit window through 1.5 meters of 1/4-inch Pyrex® and stainless steel tubing. Pyrex® was desirable for low-concentration runs because it adsorbed less hydrazine than the stainless steel. The deposit line had to be exposed to hydrazine for several minutes to establish an equilibrium between vapor-phase and adsorbed hydrazine.

The solvent deposit rate was in the range of 4 to 8 mmol/hour for both argon and nitrogen. The rate was controlled by a metering valve (Granville-Phillips series 203) which was periodically adjusted to maintain a steady flow while the pressure in the gas-mixing bulb dropped. The deposits were limited to about 20 mmol because scattering increased rapidly beyond this point. For some runs, deposits were made on both sides of the window to increase the intensities of weak absorptions.

MATRIX ISOLATION

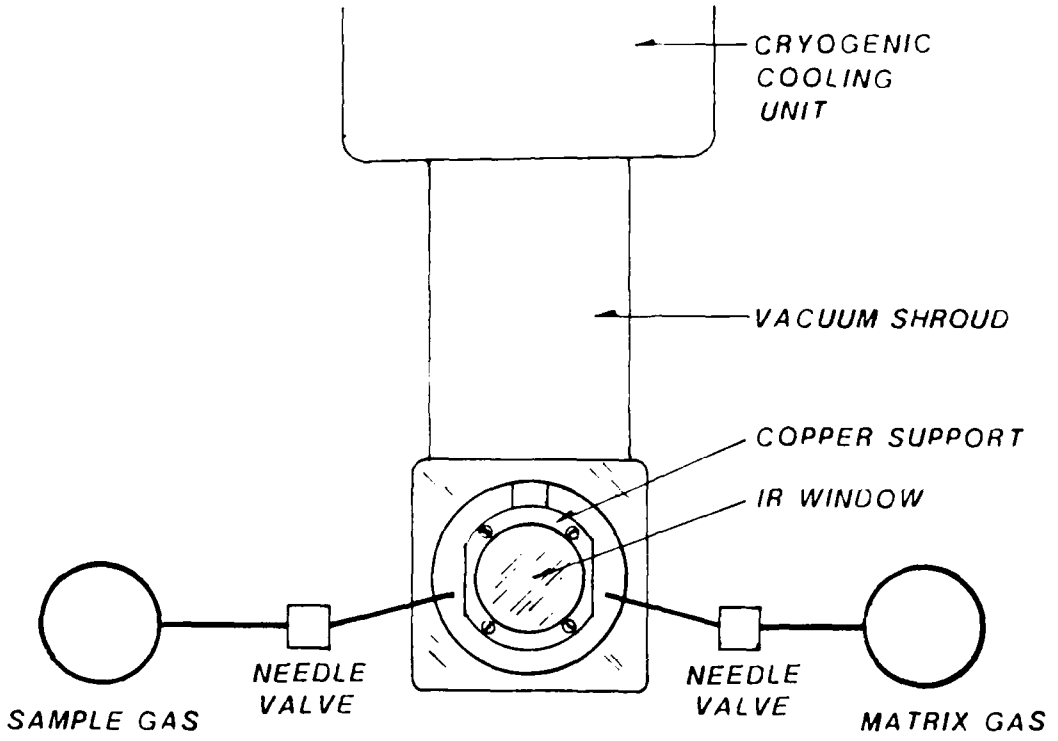

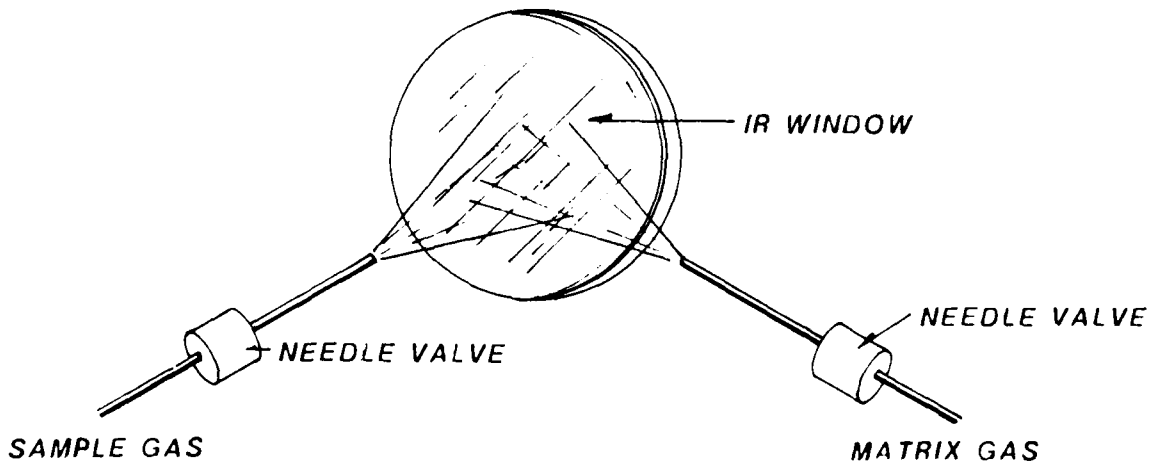

Figure 1. Matrix-Isolation Apparatus

The primary nozzle consisted of a 12-mm length of 0.25-mm inner diameter stainless steel tube. The small nozzle diameter permitted faster argon deposits although it is not clear why. Supersonic-expansion cooling may have been a factor. The nitrogen matrices were not sensitive to deposit tube diameter. The distance between the end of the nozzle and the deposit window was approximately 10 mm.

The secondary nozzle consisted of a 1/32-inch inner diameter stainless steel tube, preceded by a variable length (3 to 10 cm) of 0.1-mm inner diameter glass capillary to control the minute flow rate of the solute. This configuration reduced the exposure of the solute to impurities because there was no need for a mixing bulb or a long flow tube. It also permitted a cooling jacket to be placed around the solvent flow tube to condense water and other impurities that would otherwise reach the matrix window. This jacket consisted of a 60-cm length of 1/2-inch plastic tubing through which the vapor from a liquid-nitrogen dewar was passed. Such a jacket could not be used when the solute and solvent were premixed since the solute would have condensed onto the flow tube.

The deposit window was a 25- x 2-mm disk of CsI or Irtran-II.® The former has a lower frequency cutoff (420 versus 700 cm^{-1}), while the latter is much easier to clean. The amount of scattering of the nitrogen matrices was very sensitive to the amount of contact between the window and window holder. Indium washers (25-mm outer diameter, 15-mm inner diameter) and cryogenic grease were used to improve the contact between the window and the holder. The window surface was oriented about 20 degrees from the perpendicular to the infrared beam to reduce the intensities of interference fringes.

Matrix temperature measurements were made using an iron-doped gold versus chromel thermocouple sandwiched between the window surface and an indium washer. Cryogenic grease was applied to the region around the thermocouple junction, and a copper plate was used to press the indium washer against the window. All deposits were made at the minimum attainable temperature of 13 K. It should be noted that the matrix temperatures were probably slightly higher than the observed thermocouple readings since the thermocouple was not in direct contact with the matrix. Warming and annealing experiments were

done, using the temperature controller (Model APD-E) supplied with the closed-cycle refrigerator.

The N_2H_4 sample (Aldrich, 98 percent purity) was transferred under argon to a distillation apparatus, refluxed over reagent grade NaOH for 4 hours, and distilled. The fraction collected at 113.5 °C comprised the purified sample. The N_2D_4 sample (MSD Isotopes, 98.6 atom percent D, 2.7 percent D_2O) was used without further purification. The room-temperature vapor pressures of the liquid hydrazine samples were sufficient to produce the desired vapor-phase depositing mixtures. The nitrogen and argon samples were research grade (Air Products). Before use, they were passed through a 1.2-meter coil of 1/8-inch stainless-steel tubing immersed in a 178 K acetone bath.

Water was a significant impurity in all of the spectra reported here, even when the two-nozzle setup was used. Therefore, some of the minor features in the spectra may be due to a hydrazine-water complex. Typically, the ν_2 impurity band of H_2O/N_2 at 1597 cm^{-1} was similar in intensity to the ν_4 band of N_2H_4/N_2. Two other likely contaminants, aniline and ammonia, were not observed in significant quantities in the matrix spectra.

Both the N_2H_4/Ar and N_2H_4/N_2 spectra were run at five different hydrazine concentrations: 1:200, 1:500, 1:1000, 1:2000, and 1:5000. Concentrations less than 1:5000 were not used because of poor signal/noise and because of the tendency of hydrazine to be adsorbed on the walls of the deposit tube. The concentration dependence of the observed hydrazine bands, in combination with annealing studies, enabled monomer peaks to be distinguished from aggregate peaks.

In the N_2D_4 experiments, the extent of hydrogen-deuterium isotopic exchange was a more useful variable than the solute concentration itself. Isotopic exchange of the N_2D_4 with H_2O took place in the normal course of depositing the sample since residual H_2O was always present in the gas-handling manifold. The relative amounts of the $N_2H_nD_{4-n}$ (n = 0, 1, ...4) species could be readily manipulated by changing the length or diameter of the flow tube, or by changing the overall solute concentration. The highest N_2D_4 percentage was obtained using the two-nozzle configuration and a 1:1000

solute/solvent ratio. A high percentage of N_2H_3D was produced by replacing the usual deposit line with 3/8-inch stainless steel tubing. The amount of exchange was also increased by reducing the solute/solvent ratio to 1:5000 from the usual 1:1000.

All runs reported here were made at 0.5 cm^{-1} resolution since higher resolutions did not reveal any additional structure in the observed bands. The number of averaged interferometer scans was 100 and 500 for the sample and background spectra, respectively. Very little reduction in signal/noise was obtained by scanning more than 100 times. The detector was liquid-nitrogen-cooled HgCdTe-B (5000 - 400 cm^{-1}).

C. RESULTS

1. Matrix-Isolation Spectra of N_2H_4

a. Overview

Hydrazine has seven bending modes and five stretching modes in accordance with its C_2 point group symmetry (Reference II-5). All of these except the torsion mode, ν_7, are expected to lie in the 4000 - 420 cm^{-1} region investigated in the present FT-IR study. An overview of the N_2H_4/Ar and N_2H_4/N_2 spectra is given in Figure 2, and a listing of all monomer bands in these spectra is given in Table 1.

Table 2 shows the frequencies and infrared intensities of the fundamental modes of N_2H_4 obtained from vapor-phase (References II-2-5), ab initio, and matrix-isolation studies. Vibrational assignments for the matrix-isolation spectra were obtained from comparisons of data in this table.

Both argon and nitrogen matrices were studied to determine whether hydrazine rotates in a matrix environment. Nitrogen has been found to be less conducive to rotation of trapped species than argon (Reference II-7). Water, for example, has rotational structure in argon but not in nitrogen (Reference II-8). No evidence of rotational structure was found in the present hydrazine spectra. However, the presence of rotation cannot be ruled out for hydrazine

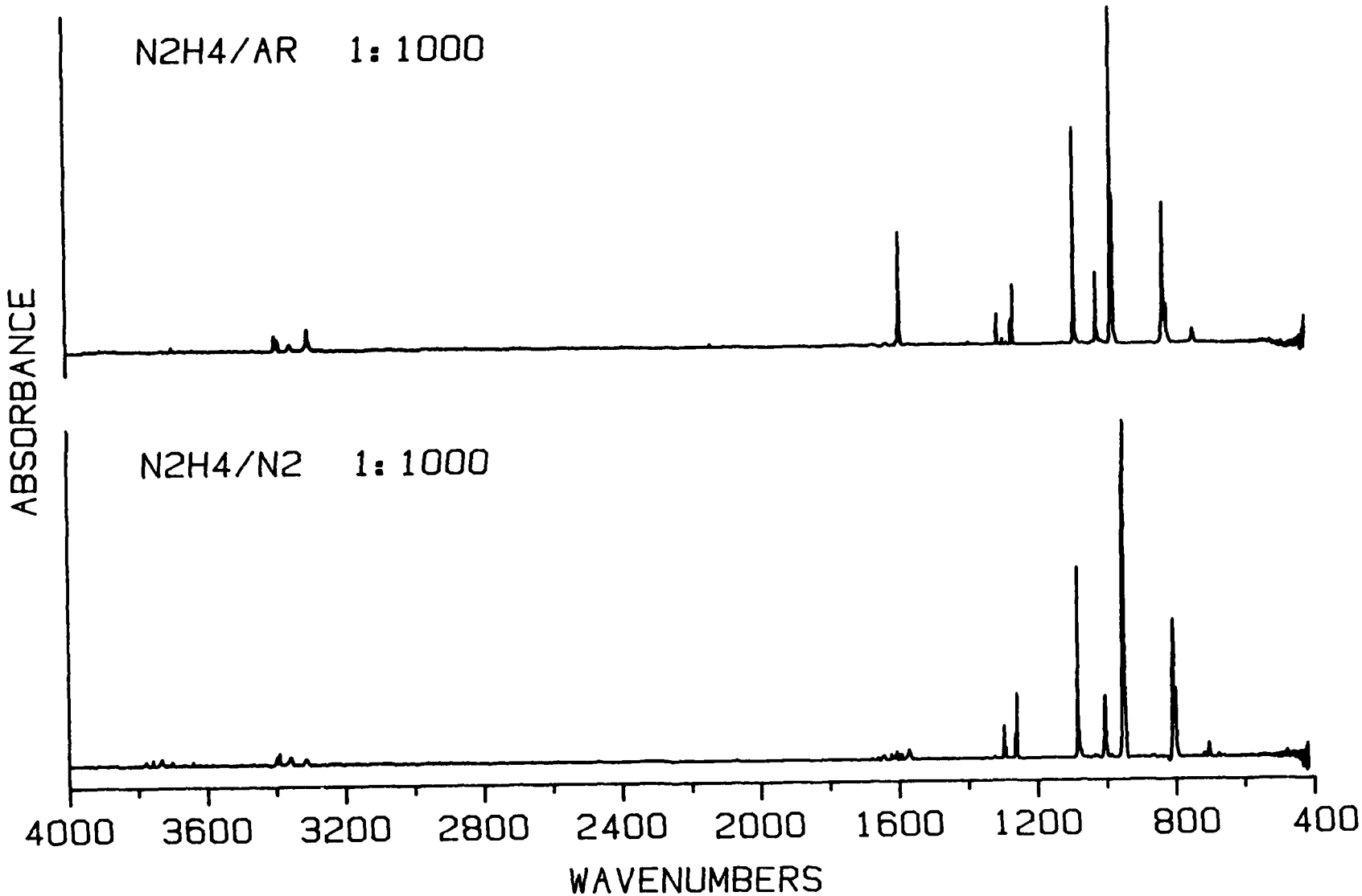

Figure 2. N_2H_4 Matrix-Isolation Spectra. Matrix-Isolated Water has been Subtracted from the N_2H_4/N_2 Spectrum but not the N_2H_4/Ar Spectrum.

TABLE 1. WAVENUMBERS AND RELATIVE INTENSITIES OF MONOMER ABSORPTION BANDS OF N_2H_4 OBSERVED IN ARGON AND NITROGEN MATRICES

Vibrational Mode	N_2H_4/Ar		N_2H_4/H_2	
	cm^{-1}	I[a]	cm^{-1}	I[a]
7 (v = 2)	679	2	749	12
	706	5		
6	803	86	825	71
	810		834	
	812			
	815			
12	953	206	977	203
	956		983	
	958			
5	1086	39	1091	38
11	1262	8	1267	5
	1264			
	1266			
4	1293	5	1314	5
	1299			
3,10			1595	17
?	1662	0.8		
?	1679	0.6		
?	2071	0.4	2101	0.5
9	3312	4	3301	6
1	3390	2	3387	3
8	3398	3	3396	5

[a] The values given for the relative intensities were obtained using the method described in Table 2. Intensities are not given for individual components of bands because those values changed with deposit conditions.

TABLE 2. WAVENUMBERS, PREDICTED INTENSITIES (KM/MOL), AND EXPERIMENTAL RELATIVE INTENSITIES OF N_2H_4 FUNDAMENTALS

	Approximate Vibrational Mode[a]	Predicted		Ar Matrix		N_2 Matrix		Vapor[d]
		cm^{-1}	A[b]	cm^{-1}	I[c]	cm^{-1}	I[c]	cm^{-1}
7	torsion	427	50.7	----		----		377[e]
6	s-wag	841	98.5	810	86	834	71	780
12	a-wag	954	190.5	953	206	983	203	937[f]
5	NN str.	1087	5.5	1086	39	1091	38	1098
11	a-HNH twist	1258	7.8	1262	8	1267	5	1275
4	s-HNH twist	1290	5.8	1299	5	1314	5	----
10	a-scissor	1624	14.3	----		1595	17	1608
3	s-scissor	1639	13.7	----		1595		1493
9	a-s-HNH str.	3309	15.0	3313	4	3301	6	3297
2	s-s-HNH str.	3317	0.50	----		----		----
1	s-a-HNH str.	3410	0.01	3390	2	3387	3	3325
8	a-a-HNH str.	3415	1.8	3398	3	3396	5	3350

[a] The initial s/a label on the stretching modes indicates the direction of one $NH_i(NH_o)$ stretch with respect to the other NH_i (NH_o) stretch. The second s/a label describes the relative motions of the two NH stretches within a given amino group.

[b] These are absolute integrated absorption coefficients in km/mol.

[c] These are relative intensities scaled so that their sum is the same as the corresponding sum of predicted A values.

[d] The vapor data are taken from Reference II-2 except where noted otherwise. The assignments of Reference II-2 have been renumbered as suggested in Reference II-5.

[e] Reference II-3.

[f] Reference II-4.

because the instrumental resolution may have been too low to permit rotational fine structure to be observed.

b. Bending and NN-Stretching Modes of N_2H_4

All of the observed modes, except those consisting of NH stretching, lie in the 1900 - 700 cm^{-1} region shown in Figure 3. The vapor-phase spectrum shown in this figure was reexamined to check the assertion of Catalano et al.(Reference II-1) that the previously observed bands (Reference II-2) in the 6.3 micrometer region are artifacts. The present vapor spectrum is essentially the same as that given in Reference II-2 and does not show any features resulting from hydrazine reacting with the KBr cell windows. Thus, the band assigned to ν_{10} (1608 cm^{-1}) in the vapor phase spectrum appears to be correct. The assignment of ν_3 (1493 cm^{-1}) for the vapor phase is more questionable (vide infra).

Most of the monomer bands in Figure 3 can be assigned readily by comparing the matrix data with predicted data and with vapor-phase data (Table 2). The assignment of the $2\nu_7$ torsional mode (Table 1) in argon is tentative due to the 27 cm^{-1} splitting between the absorptions assigned to this mode. This splitting could be the result of tunnelling through the barrier to torsion. Alternatively, the higher-frequency component may be a combination band involving a librational mode of N_2H_4 in the lattice. Such bands have been observed for other molecules such as water (Reference II-8) and ammonia (Reference II-9). A complete analysis of the above observations would require an examination of the far infrared region of the spectrum, and therefore will be deferred to the future.

The present assignments of ν_3 and ν_{10} to a single band at 1595 cm^{-1} in N_2H_4/N_2 are based primarily on the theoretical prediction (Table 2) that these bands should be closely spaced and nearly equal in intensity. Additional support for these assignments was obtained from the observation of two scissor-bending frequencies in N_2D_4/N_2 which have roughly equal intensities and are separated by only 2 cm^{-1} (vide infra). The 1595 cm^{-1} band was not reported in the previous matrix study of N_2H_4/N_2. Evidently, this band was obscured by the strong H_2O/N_2 impurity band at 1597 cm^{-1}, and was

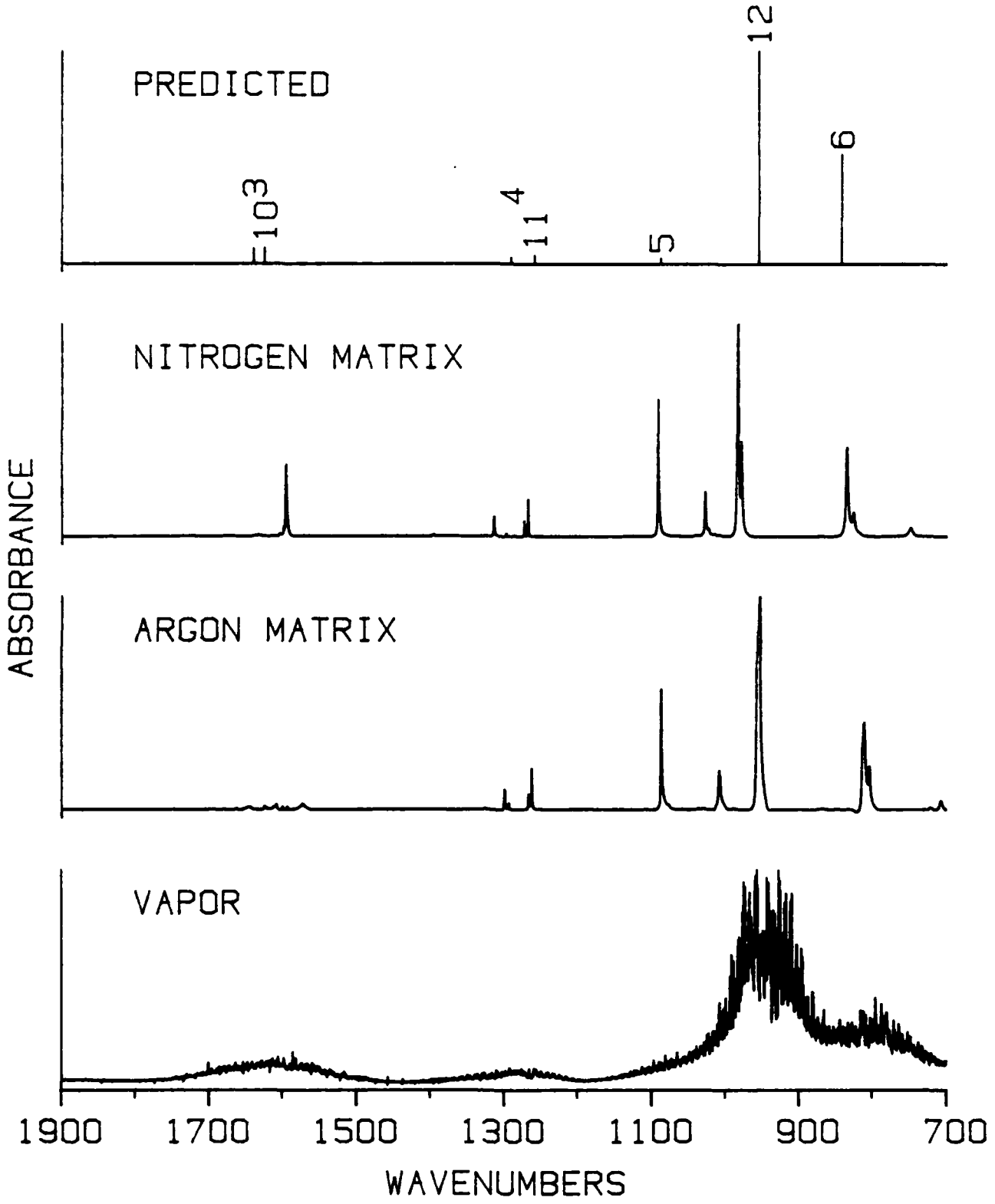

Figure 3. N_2H_4 Matrix-Isolation Spectra in the Bending and NN-Stretching Region.

subtracted from the spectrum along with the water band. The surprising absence of both ν_3 and ν_{10} from the present and previous (Reference II-1) argon matrix spectra remains unexplained. The weak bands that appear near 1600 cm^{-1} in the N_2H_4/Ar spectrum in Figures 2 and 3 are due to water.

The wagging modes of hydrazine can produce inversion splittings but none were seen in either argon or nitrogen. According to Hamada et al. (Reference II-4), the inversion of the asymmetric wagging mode should produce a closely spaced doublet with two smaller bands equally spaced on either side. The absence of inversion splittings in N_2H_4/N_2 (vapor-phase barrier = 2620 cm^{-1}) (Reference II-4) is consistent with the reported absence of such splittings (Reference II-10) in NH_3/N_2 (vapor-phase barrier = 2022 cm^{-1}) (Reference II-11).

c. NH-Stretching Modes of N_2H_4

Spectra of the NH-stretching region are shown in Figure 4, and the corresponding mode assignments are given in Table 2. Although there are four NH-stretching modes in hydrazine, only three monomer matrix bands were observed. A fourth band, which occurs near 3350 cm^{-1} in both argon and nitrogen matrices, is due to hydrazine dimer.

The assignments of the monomer bands in Figure 4 were deduced primarily by comparison of matrix wavenumbers with predicted wavenumbers (Table 2). The close resemblance of these two sets of data is sufficient to establish the assignment of ν_9 for both matrix spectra in Figure 4. The broad shoulder that accompanies the ν_9 band of N_2H_4/Ar is caused by an aggregate. The assignments of ν_1 and ν_8 to the two matrix bands near 3400 cm^{-1} are also straightforward but the the ordering is uncertain. Confusion arises because the intensity of the ν_1 band is much greater in relation to ν_8 than expected.

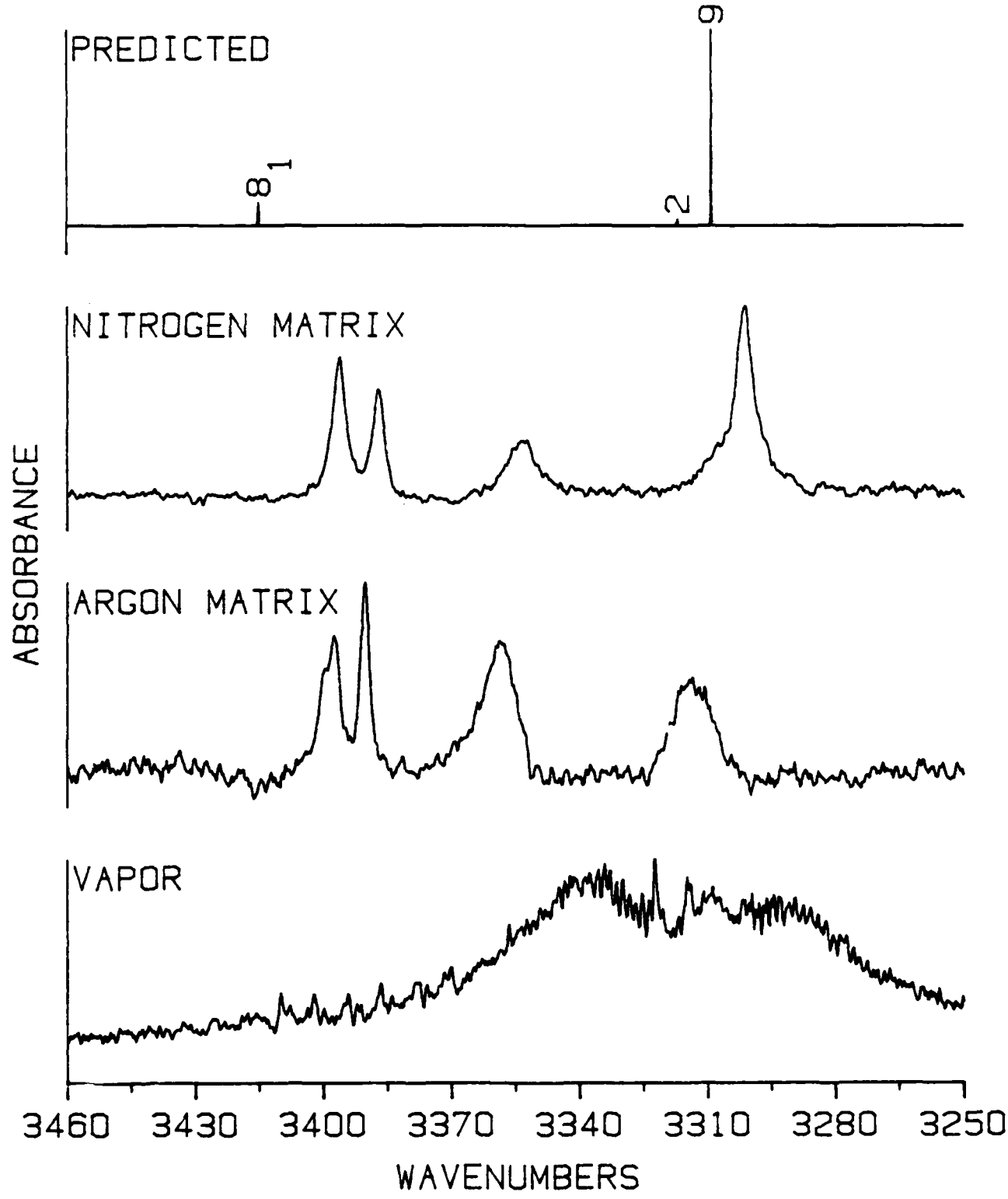

Figure 4. N_2H_4 Matrix-Isolation Spectra in the NH-Stretching Region.

A comparison of the present NH-stretching data to the previously reported data (Reference II-1) for matrix-isolated hydrazine indicates that the latter were obtained at an excessively high hydrazine concentration. The N_2H_4/N_2 bands which are found at 3396 cm^{-1} and 3387 cm^{-1} in Figure 4 were previously blended. Also, the dimer band at 3353 cm^{-1} was previously reported to be ν_8.

d. Concentration-Dependence Studies of N_2H_4

Differentiation between monomer and aggregate hydrazine bands was accomplished by using plots such as those shown in Figures 5-9. The band intensities in these plots have been scaled so that the absorbance of each monomer peak is approximately the same at all three concentrations that are shown. Aggregate bands can be easily recognized on the basis of their variations in absorbance as a function of concentration.

In principle, the above procedure could permit aggregates of varying sizes to be distinguished from each other. However, the relatively high dilutions used in the present experiments restricted the usefulness of this method to the point where only a few dimer lines could be assigned. A summary of the observed aggregate peaks in the N_2H_4 matrix spectra is given in Table 3.

A justification of the dimer assignments can be made by plotting a growth curve such as those given by Barnes and Hallam (Reference II-12) for methanol. Such a curve is plotted in Figure 10 for the 1008 cm^{-1} absorption of N_2H_4/Ar. This curve resembles the dimer curve of Reference II-12 and not any of the higher multimer curves. Indeed, one would not expect aggregates larger than a dimer to be observed at concentrations as dilute as 1:5000.

Two peaks (977 and 825 cm^{-1}) appearing in Figures 8 and 9, respectively, exhibited irregular, but mutually proportional, variations in intensity as a function of N_2H_4 concentration. Both were determined to be monomer absorptions by integrating them in combination with their assumed

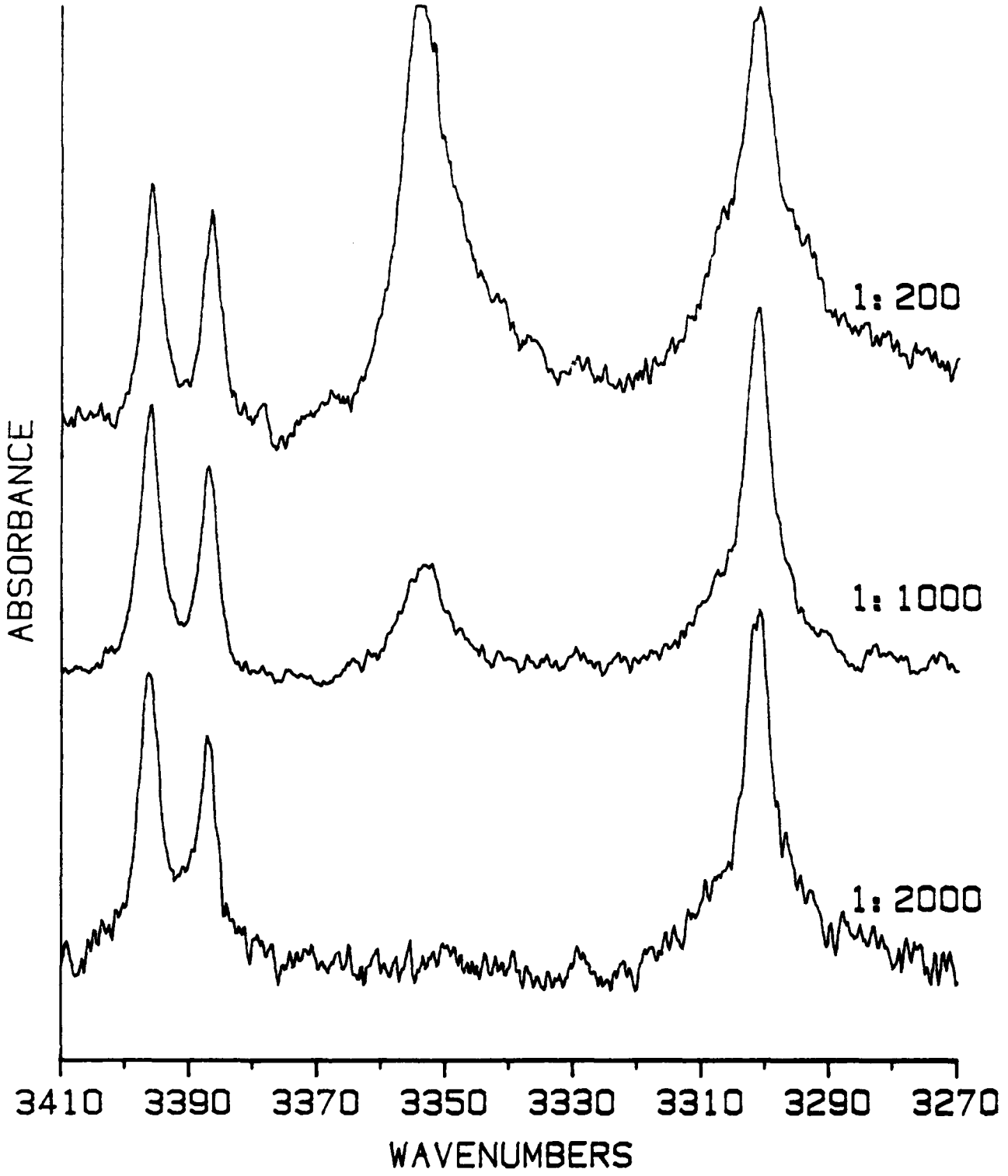

Figure 5. Concentration-Dependence for N_2H_4/N_2; 3410 - 3270 cm^{-1}.

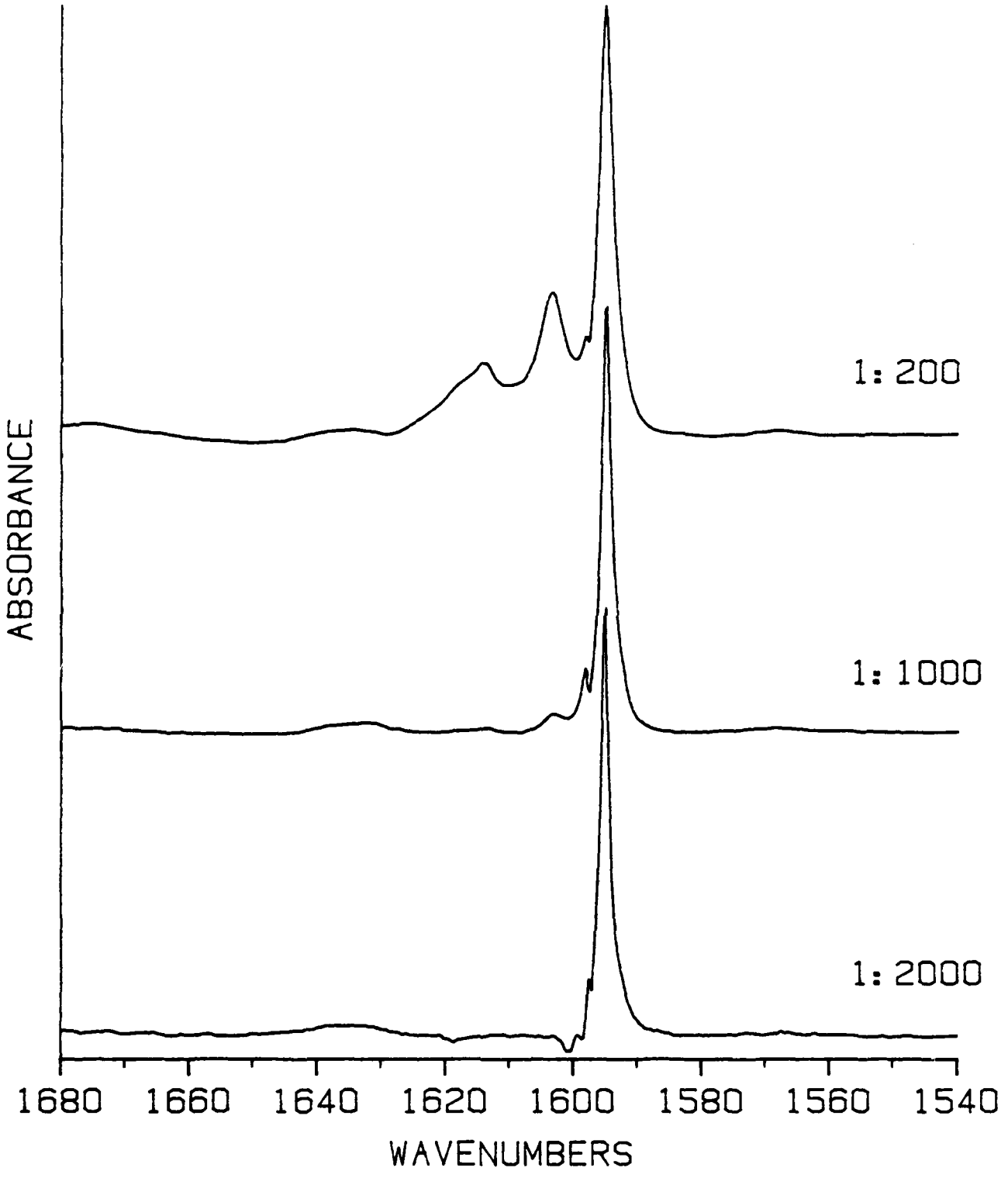

Figure 6. Concentration-Dependence for N_2H_4/N_2; 1680 - 1540 cm^{-1}.

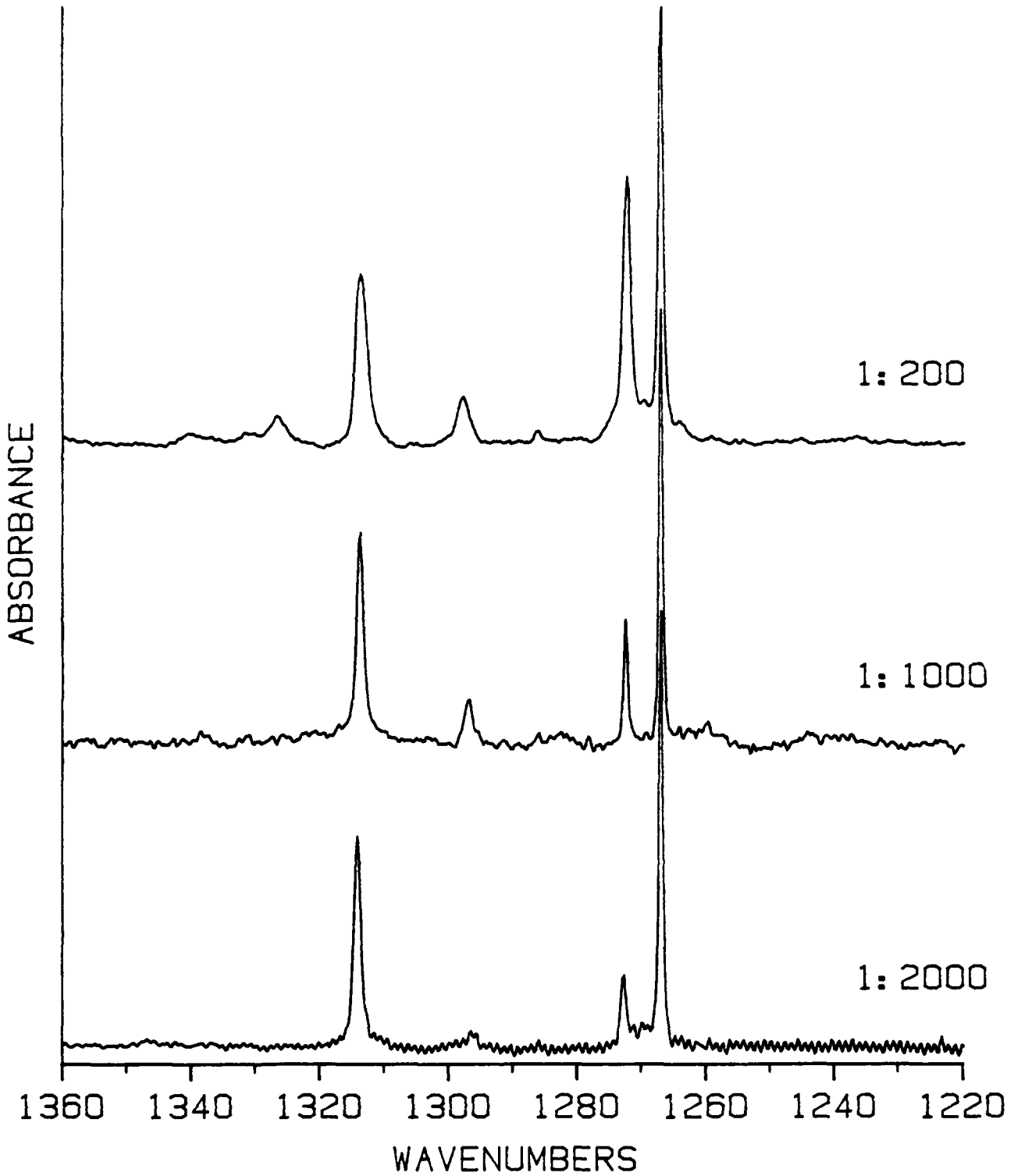

Figure 7. Concentration-Dependence for N_2H_4/N_2; 1360- 1220 cm^{-1}.

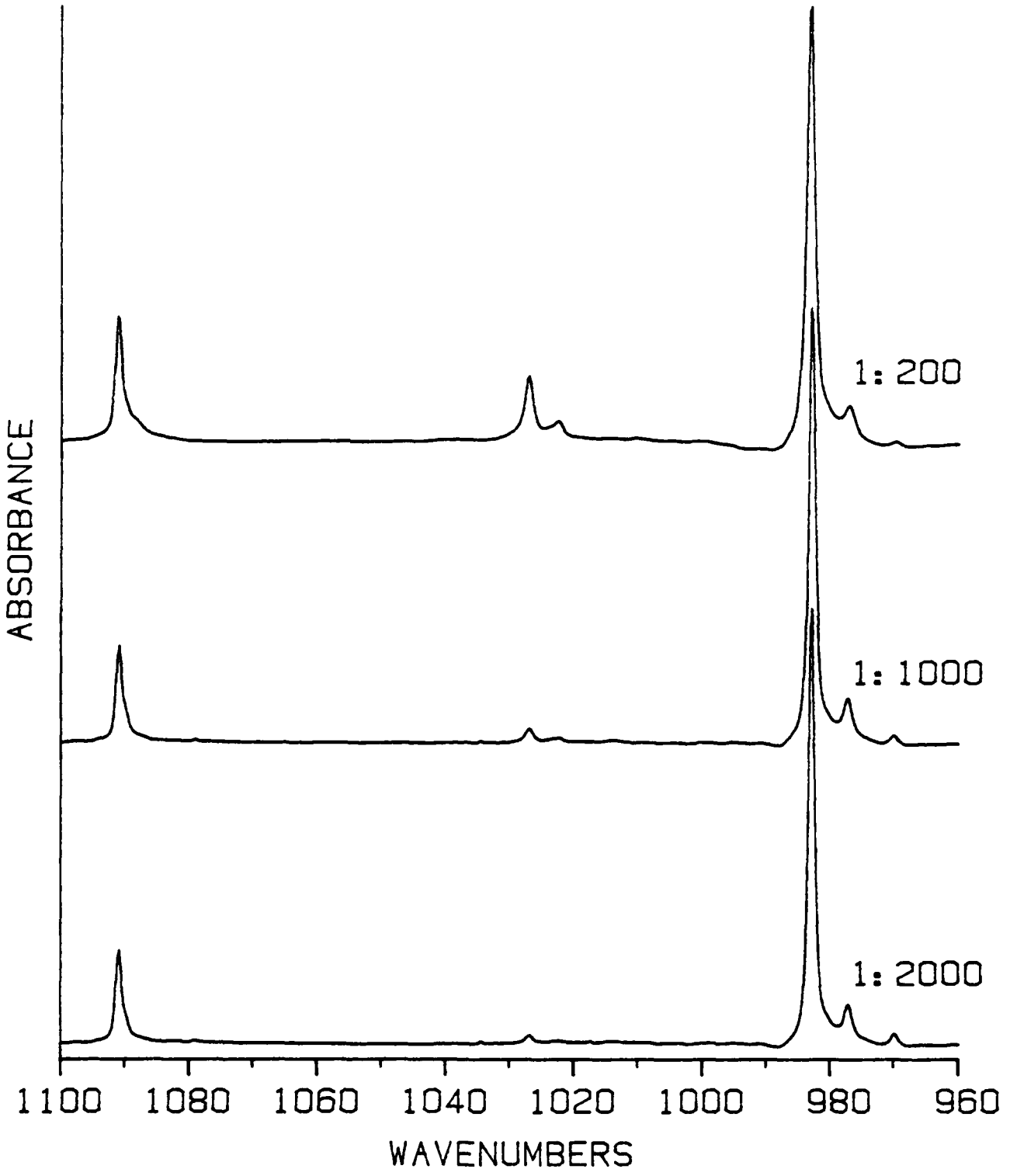

Figure 8. Concentration-Dependence for N_2H_4/N_2; 1100- 960 cm^{-1}.

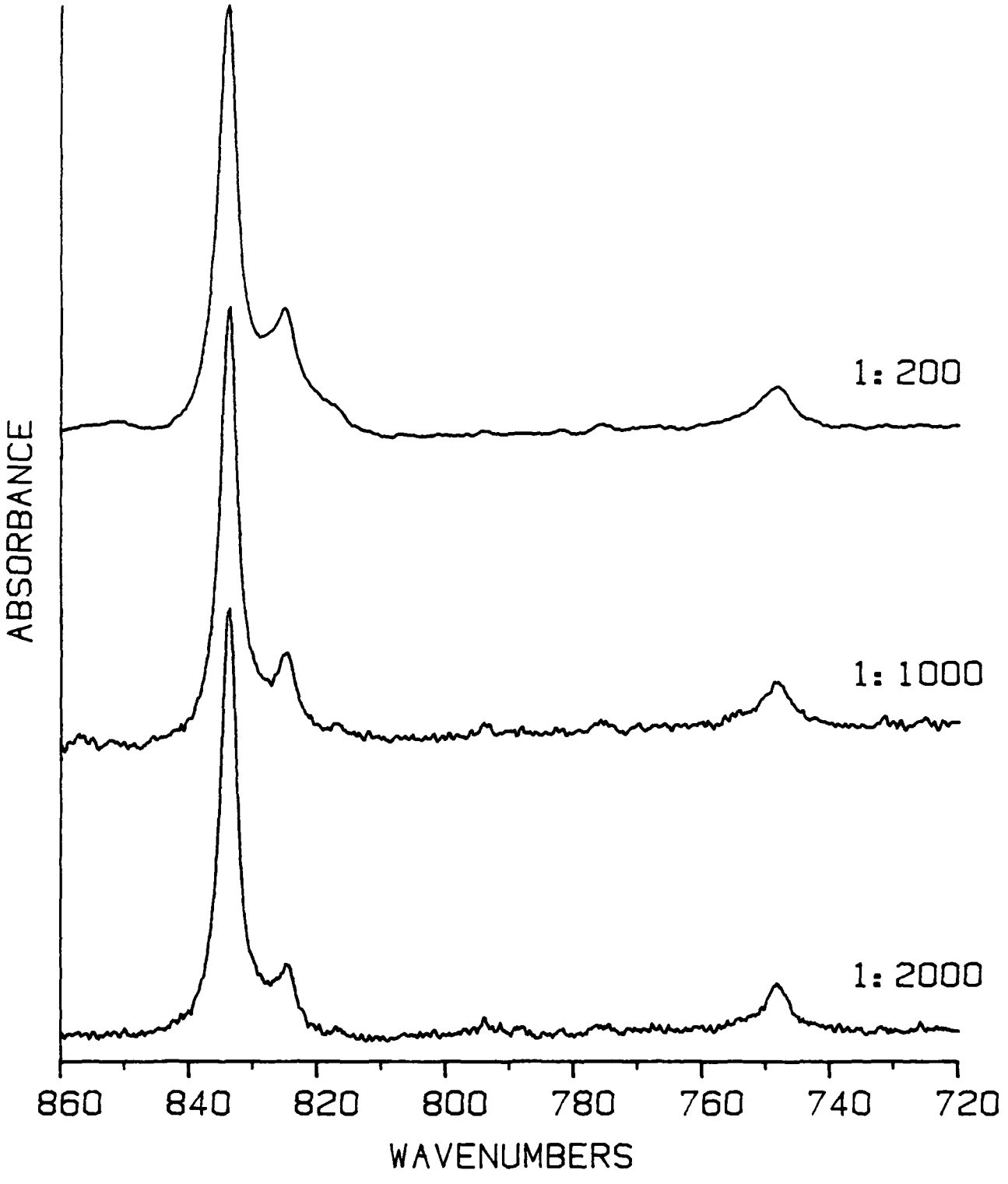

Figure 9. Concentration-Dependence for N_2H_4/N_2; 860- 720 cm^{-1}.

TABLE 3. ABSORPTIONS DUE TO HYDRAZINE AGGREGATES

Argon Matrix			Nitrogen Matrix		
cm^{-1}	Relative Intensity[a]	Assignment[b]	cm^{-1}	Relative Intensity[a]	Assignment[b]
480	8	dimer	492	14	dimer
824	1	unassigned	1023	30	unassigned
835	2	"	1027	100	dimer
849	7	"	1272	5	unassigned
867	6	"	1297	2	"
1008	110	dimer	1326	2	dimer
1029	19	unassigned	1331	0.8	"
1038	0.5	"	1603	8	unassigned
1044	3	"	1614	5	"
1320	0.5	dimer	3353	60	dimer
1325	3	"	3379	2	unassigned
3358	31	"			
3381	1	unassigned			

[a] Relative intensities are given for a dilution ratio of 200:1. They are based on the intensity calibration described in Table 2.

[b] Some aggregate bands were not assigned because: (1) they were observed only at the highest matrix concentration that was used; or (2) they changed with matrix concentration differently from the dimer bands but could not be assigned to a specific aggregate.

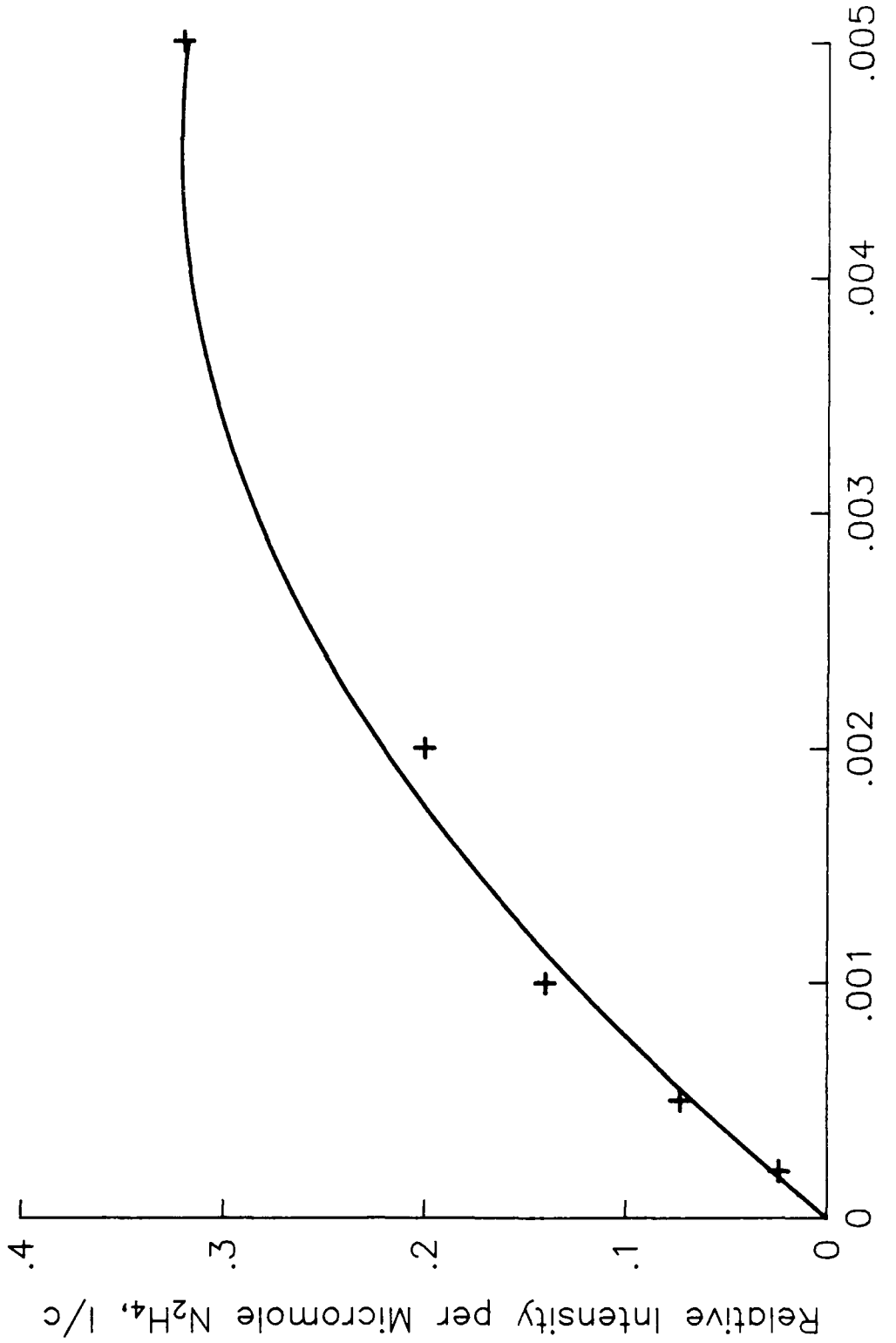

Figure 10. Concentration-Dependence of the 1008 cm^{-1} Dimer Band of N_2H_4/Ar.

partners at 983 and 834 cm^{-1}, respectively. Upon annealing, these peaks decreased irreversibly in intensity. The combination of the above evidence suggests that the 977 and 825 cm^{-1} absorptions are due to a secondary lattice site.

e. Temperature-Dependence Studies of N_2H_4

The intensities and the frequencies of all of the hydrazine monomer band components exhibited temperature dependences which were completely reversible at temperatures below 30 K for both nitrogen and argon matrices. This behavior has been previously reported for other molecules (References II-9, II-13). Temperature-dependence data for N_2H_4/N_2 monomer bands are given in Table 4. This table indicates that the components of site-split modes begin to merge as the temperature increases.

Annealing did not produce any significant sharpening of the bands although some changes in the relative intensities of the sites did occur. These changes were much less, however, than those produced by changing the deposit rate, the deposit window temperature, and the dimensions of the deposit nozzle.

The identification of aggregate bands could be confirmed by subtracting an annealed spectrum from its unannealed counterpart. Aggregate bands then become entirely negative, and have absolute intensities which are larger relative to the monomer intensities than they are in the original spectrum. A typical difference spectrum is shown in Figure 11. For some of the modes in this figure, annealing revealed the presence of additional sites which could not otherwise be resolved by the spectrometer.

2. Matrix-Isolation Spectra of Deuterated Hydrazine

a. Identification of Isomers and $N_2H_nD_{4-n}$ Species

The number of isomers of each $N_2H_nD_{4-n}$ specie can be deduced by referring to Figure 12. Hydrazine has a pair of inner and a pair of outer hydrogen-atom sites. Normally, substitution by another chemical species would

TABLE 4. TEMPERATURE-DEPENDENT WAVENUMBER SHIFTS AND INTENSITY CHANGES OF N_2H_4/N_2 MONOMER BANDS

Vibrational Mode	cm^{-1}(14K)	cm^{-1}(26K)-cm^{-1}(14K)	I(26K)/I(14K)
7 (v = 2)	748.7	-0.7	0.3
6 (1)[a]	824.4	0.6	4
(2)	834.0	-0.4	0.7
12 (1)	976.8	0.6	6
(2)	983.0	-0.7	0.6
5	1091.2	-0.4	0.8
11	1266.8	0.1	0.7
4	1314.1	-0.8	0.7
10	1594.9	-0.1	0.7
9	3301.0	0.3	0.8
1	3386.7	0.1	1
8	3396.3	-0.4	0.7

[a] The digits in parentheses are used to label multiple components of the same mode.

take place predominantly at the outer sites on the basis of steric factors. However, for deuterium, substitution at the inner sites is comparable to that at the outer sites, and all possible isomeric configurations can be readily produced. A listing of these deuterated isomers is given in Table 5. The notation shown in this table is used in the remainder of this report.

Both argon and nitrogen matrices were studied to distinguish absorption bands for hydrazine which were overlapped in one matrix material but not the other. A portion of a typical spectrum containing a mixture of $N_2H_nD_{4-n}$ species is given in Figure 13. The usefulness of the matrix-isolation technique is apparent from this figure. Clearly, the vapor-phase analog of this spectrum would be difficult to analyze.

The $N_2H_nD_{4-n}$ species assignments for the matrix-isolated absorptions were deduced by examining several spectra containing different relative amounts of $N_2H_nD_{4-n}$ species. These spectra were plotted so that the absorbance of a chosen reference band had the same value for each spectrum.

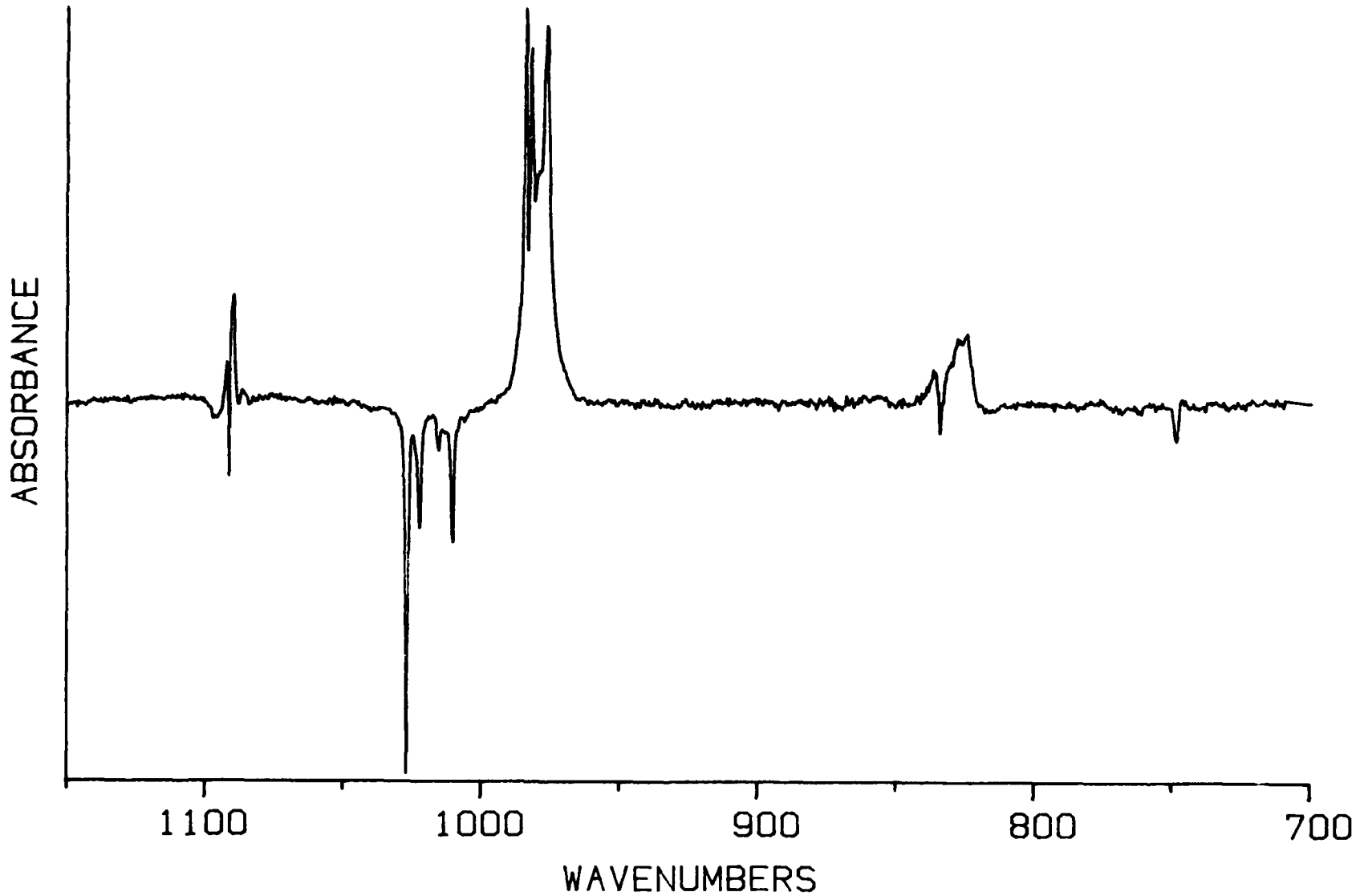

Figure 11. N_2H_4/N_2 Difference Spectrum: (Unannealed)-(Annealed).

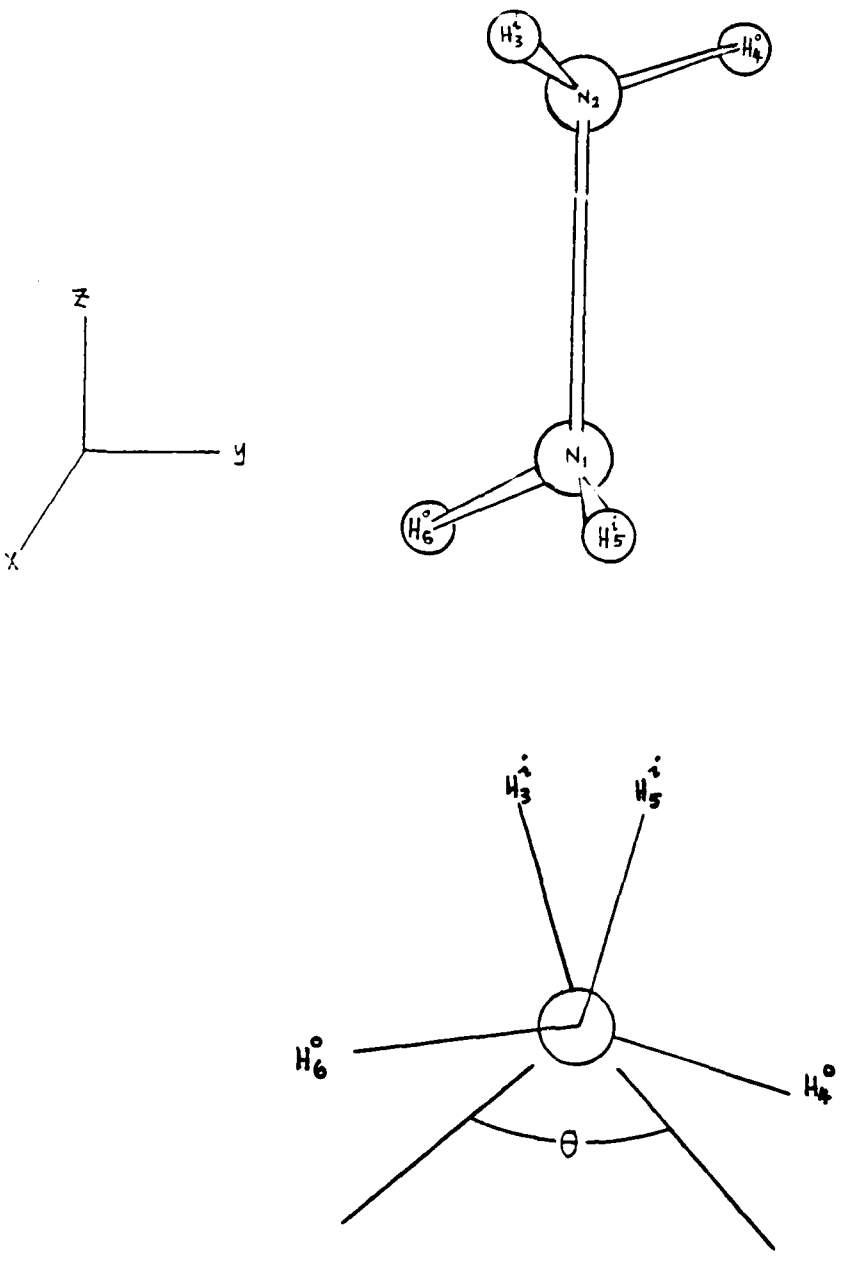

Figure 12. Hydrazine Molecule Viewed Along the Perpendicular Direction (Above) and Along the NN Bond (Below).

TABLE 5. DEUTERATED ISOMERS OF HYDRAZINE

N_2H_3D[a]	$N_2H_2D_2$[b]	N_2HD_3	N_2D_4
i	ii	ioo	iioo
o	oo	iio	
	i1o1		
	i1o2		

[a] i = inner substitutional position for the deuterium atoms
o = outer " " " " " "

[b] Labels 1 and 2 distinguish one amino group from the other. The notation "i1o2" is used here and throughout the text as an abbreviation for i(1)o(2).

Each of the bands belonging to the same $N_2H_nD_{4-n}$ species as this reference band would then also have approximately the same absorbance in all of the plots. The remaining $N_2H_nD_{4-n}$ species assignments could be obtained in a similar manner. Absorptions due to H_2O, HDO, and D_2O were identified, using References II-8, II-14, and II-15.

The isomer ratios for a given $N_2H_nD_{4-n}$ species did not change under the experimental conditions used. Therefore, the isomers could not be distinguished from each other on the basis of experimental data alone.

Ab initio calculations were used to establish normal mode assignments and to confirm the $N_2H_nD_{4-n}$ species assignments. These calculations were done on an assumed gauche configuration, using a 6-31G** basis set. The predicted wavenumbers were multiplied by a scale factor of 0.89 to obtain the best possible match with the argon matrix absorptions. The nitrogen matrix absorptions tended to have larger matrix shifts in the high-frequency direction.

An analysis of the isomer ratios was made by using a statistical model in which the only variable was the probability ratio RD/RH, where RD and RH are the relative probabilities of outer-site substitution versus inner-site substitution for D atoms and H atoms, respectively. The best fit of this model to the experimental data is shown in Table 6. This fit was obtained by

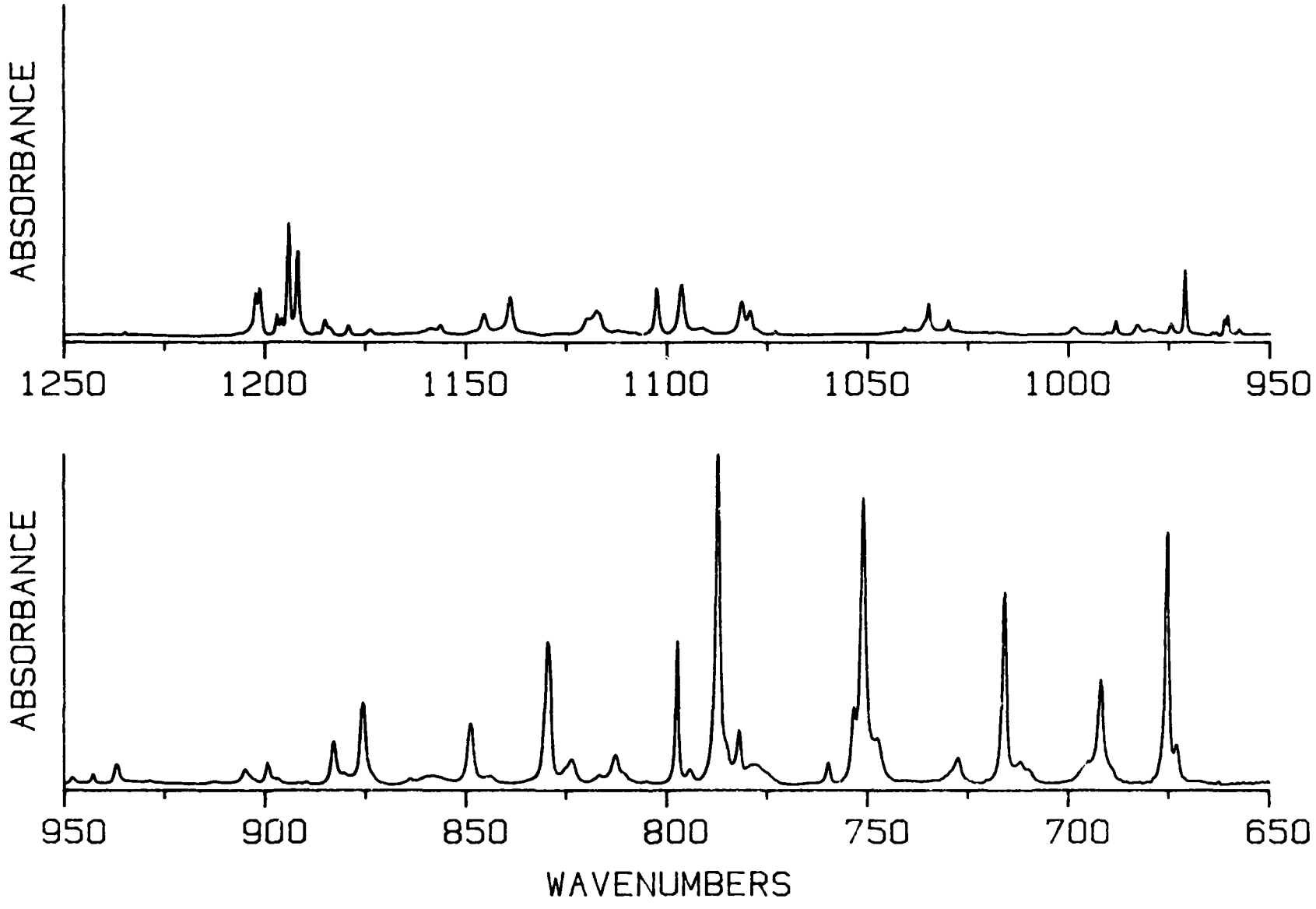

Figure 13. Isotopic Mixture of Deuterated Hydrazine in a Nitrogen Matrix. This Spectrum Corresponds to Run 2 (Nitrogen) in Table 7.

TABLE 6. ISOMER FRACTIONS FOR DEUTERATED HYDRAZINE SPECIES

Specie	Isomer	Experimental[a]	Statistical Model[b]
N_2H_3D	i	0.34	0.35
	o	0.66	0.65
$N_2H_2D_2$	ii	0.11	0.08
	oo	0.28	0.29
	i1o1	0.36	0.31
	i1o2	0.26	0.31
N_2HD_3	iio	0.35	0.35
	ioo	0.65	0.65

[a] See discussion in text. The isomer fractions were calculated separately for each $N_2H_nD_{4-n}$ specie.

[b] Calculated using R_D/R_H = 1.9, where R_D and R_H are the relative probabilities of outer versus inner substitution for D and H atoms, respectively.

assuming that RD/RH = 1.9. All of the predicted spectra of deuterated hydrazine that appear in this report were generated using this ratio.

The substantial difference between the experimental i1o1 and i1o2 isomer fractions indicated in Table 3 may result from: (1) errors in the predicted relative band intensities; (2) absorption bands of multimers, impurities, or complexes which escaped identification; or (3) a real population difference not explained by the above statistical model. A possible flaw in this model is that it assumes that only one H/D exchange occurs during a single molecular collision. If two such exchanges were to occur in some collisions, the relative i1o1 and i1o2 isomer fractions would not necessarily be identical since the outcome would then depend on the details of the molecular geometry.

Once the isomer ratios were determined, it was possible to calculate $N_2H_nD_{4-n}$ percentages for each experimental run. These percentages are shown in Table 7, along with the estimated quantities of solute deposited. The relative $N_2H_nD_{4-n}$ specie percentages could not be changed in a

TABLE 7. $N_2H_nD_{4-n}$ SPECIE PERCENTAGES[a]

Matrix	Run	N_2H_4	N_2H_3D	$N_2H_2D_2$	N_2HD_3	N_2D_4	Micromoles of Solute Deposited
N_2	1	1	2	9	31	57	13
	2	0	4	16	36	43	14
	3	54	33	10	2	0	0.9
	4	12	26	31	26	5	2
	5	0	2	8	31	59	20
Ar	1	0	3	11	37	49	4
	2	31	36	21	8	3	2
	3	0	2	9	39	49	20
	4	24	36	24	13	3	3
	5	0	0	5	27	68	0.8
	6	23	36	26	13	2	2

[a] This table lists data from all experimental runs.

very systematic manner but enough variation was obtained to permit $N_2H_nD_{4-n}$ assignments to be made for all but the weakest absorptions.

b. Spectra of N_2D_4

The N_2D_4 matrix spectra were the simplest to assign because of the existence of only one isomer, and the availability of literature data for the vapor phase (Reference II-5). N_2D_4/Ar and N_2D_4/N_2 spectra are displayed in Figure 14 along with the corresponding predicted spectrum and vapor spectrum. All lines not due to monomeric N_2D_4 were blanked from the matrix spectra to facilitate the comparison of these spectra with the others.

The vibrational assignments and intensities of the N_2D_4 matrix spectra are presented in Table 8. The assignment for N_2D_4 is similar to that for N_2H_4 except that in N_2D_4 the NN-stretching symmetry coordinate mixes strongly with the symmetric-amino-twisting coordinate in the mixed ν_4 and ν_5 modes, in contrast with N_2H_4 where they are nearly pure. According to the prediction ν_4 is 52 percent NN-stretch / 34 percent DND twist; and ν_5 is 34 percent NN-stretch / 59 percent DND twist. The assignments of all but one of

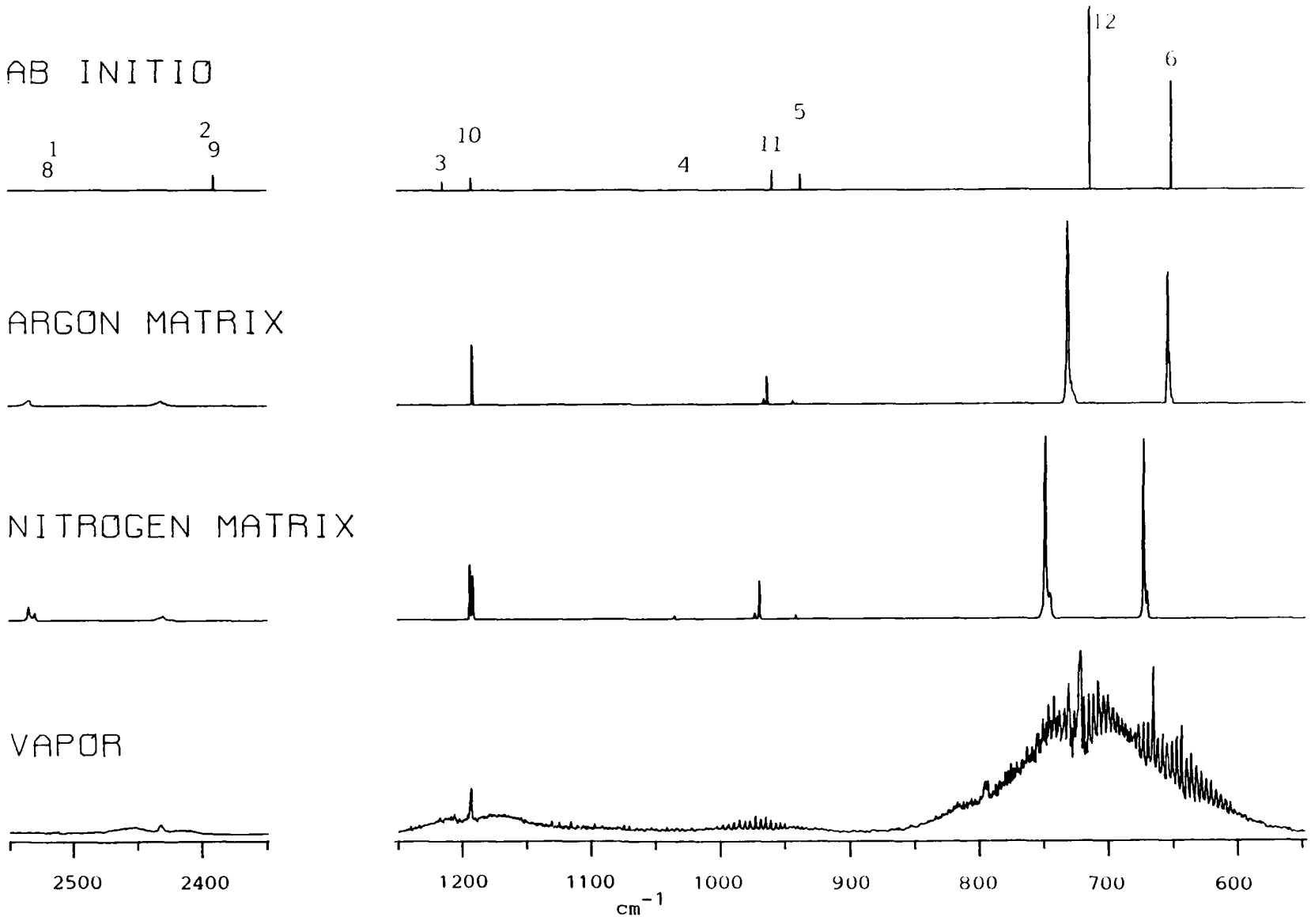

Figure 14. N_2D_4 Spectra. All Matrix Absorptions Other than Those of N_2D_4 Have Been Blanked.

TABLE 8. WAVENUMBERS, PREDICTED INTENSITIES (KM/MOL), AND EXPERIMENTAL RELATIVE INTENSITIES OF N_2D_4 FUNDAMENTAL VIBRATIONS

Mode #	PED[a]	Predicted		Ar Matrix		N_2 Matrix		Vapor[e]
		(cm^{-1})[b]	A[c]	cm^{-1}	I[d]	cm^{-1}	I[d]	cm^{-1}
8	a-a-DND str(95)	2519	1.0	2534	5	2535	7	2532
1	s-a-DND str(98)	2517	0.01	2533	7	2530	4	2542
2	s-s-DND str(98)	2399	0.03					
9	a-s-DND str(96)	2391	8.2	2431	5	2430	1	2436
3	s-sci(85) + NN str(14)	1215	4.8	1192	17	1194	10	1140[f]
10	a-sci(99)	1193	7.2	1192		1192	9	1194
4	NN str(52) + s-DND twi(34)	1027	0.002	1034?		1036	1	1009[f]
11	a-DND twi(85) + a-wag(13)	961	10.8	964	11	971	9	972
5	s-DND twi(59) + NN str(34)	939	8.7	945	2	943	1	933[f]
12	a-wag(87) + a-DND twi(13)	716	98.0	733	96	751	99	723
6	s-wag(94)	654	57.8	656	63	675	56	645
7	torsion(100)	307	26.6					291

[a] See Table 2 for an explanation of the s/a labels. The numbers in parentheses are component percentages. Abbreviations: sci=scissor, twi=twist, str=stretch.

[b] The original predicted frequencies were multiplied by 0.89 to obtain the values listed here.

[c] These are absolute integrated absorption coefficients in km/mol.

[d] These are relative integrated intensities which have been scaled so that their sum is the same as the corresponding sum of predicted A values.

[e] Reference II-6 except where noted otherwise.

[f] Reference II-5.

the matrix absorptions of N_2D_4 were straightforward due to the good agreement between the predicted and matrix frequencies. The ν_4 mode could not be identified in N_2D_4/Ar because it was weak and probably buried under a stronger N_2HD_3 absorption.

In principle, the ratio of wavenumbers $\nu(N_2H_4)/\nu(N_2D_4)$ should be nearly identical in the matrix and vapor phases (Reference II-16). An examination of this relationship is given in Table 9. The nitrogen and argon data are consistent but some of the vapor ratios differ substantially from the matrix ratios. These discrepancies may be due to interaction of hydrazine with the matrix, or possibly to inaccuracies in the vapor data. The former is more likely since at least some of the frequency ratios from the vapor are based on N_2H_4 and N_2D_4 bands which have both been analyzed in considerable detail (References II-2, II-4, II-5, and II-6).

c. Spectra of N_2HD_3

The matrix spectra of N_2HD_3 are presented in Figure 15, along with the corresponding predicted spectrum. Again, the vibrational assignments (Table 10) are straightforward due to the good agreement between the predicted and matrix absorption frequencies. The only uncertain assignments are those for the weak absorption bands that lie above 1400 cm^{-1}.

Two different sets of intensities are given in Table 10 for the matrix spectra. One of these is scaled to the predicted km/mol values as described for N_2D_4 in Table 8. For this set, a separate computation was made for each isomer since the ab initio calculations yielded no information regarding relative isomer abundances. The other set accounts for these abundances and thus describes the overall relative band intensities as they appear in the matrix spectra of Figure 15.

d. Spectra of $N_2H_2D_2$

The matrix spectra for $N_2H_2D_2$ are plotted in Figure 16, where they are compared with the predicted spectrum. To avoid confusion, the vibrational modes of all four isomers have been numbered in order of frequency. Normally,

TABLE 9. N_2D_4 MATRIX AND VAPOR SHIFTS[a].

Mode[b] #	Approximate Mode Description	Freq(N_2H_4) / Freq(N_2D_4)		
		Argon Matrix	Nitrogen Matrix	Vapor[c]
6	s-wag	1.235	1.236	1.209
12	a-wag	1.300	1.309	1.296[d]
5	s-DND twist	1.149	1.157	1.177[e]
11	a-DND twist	1.308	1.300	1.312
4	NN str.	1.256	1.268	
10	a-scissor		1.338	1.347
3	s-scissor		1.336	
9	a-s-DND str.	1.363	1.358	1.353
1	s-a-DND str.	1.338	1.342	1.308
8	a-a-DND str.	1.340	1.340	1.323

[a] The uncertainties in the matrix frequency ratios are approximately 1 unit in the last digit.
[b] Matrix wavenumbers are given in Table 2 for N_2H_4, and Table 8 for N_2D_4.
[c] References II-6 (N_2D_4) and II-2 (N_2H_4) except where indicated otherwise.
[d] Reference II-4 (N_2H_4).
[e] Reference II-5 (N_2D_4).

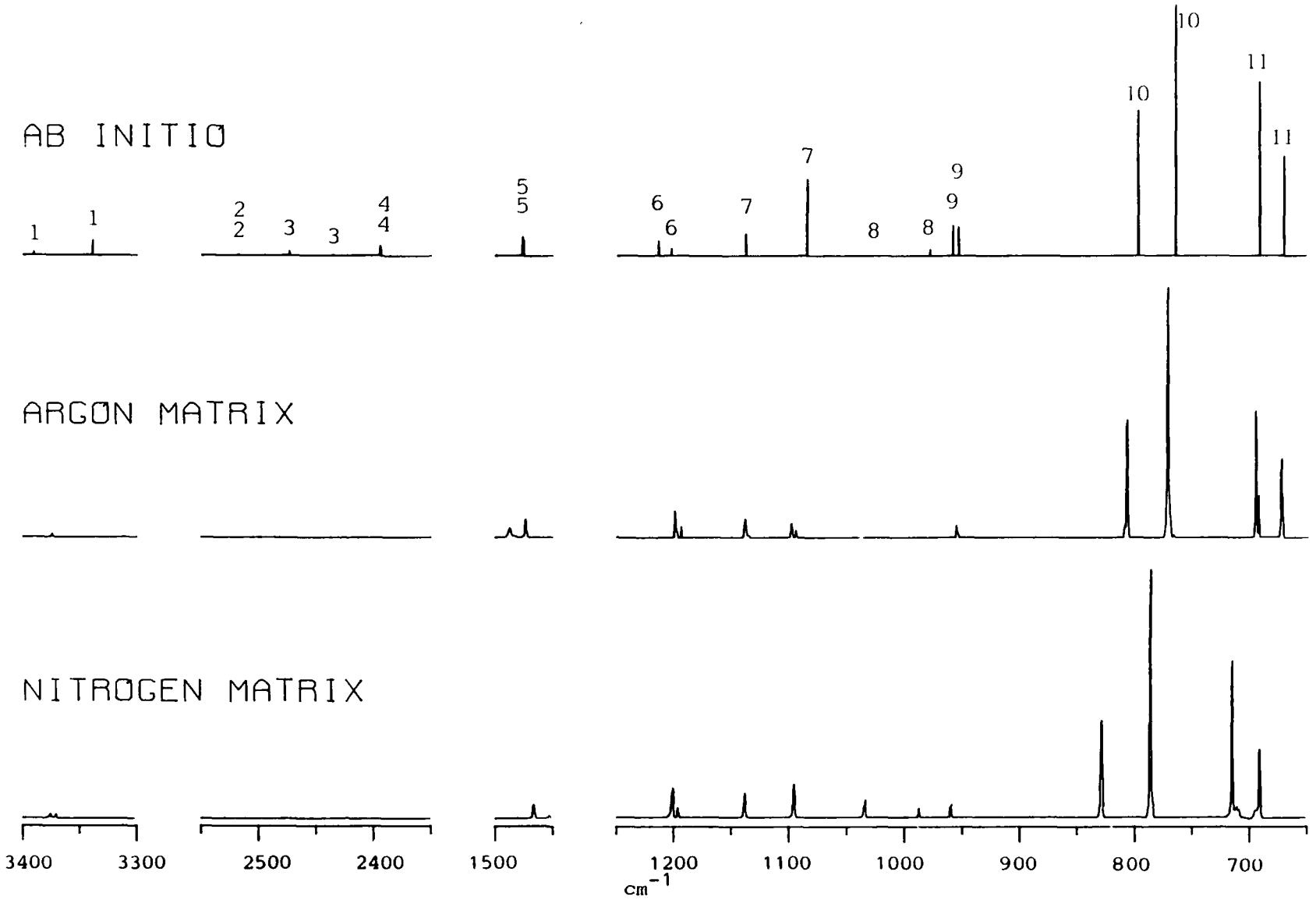

Figure 15. N_2HD_3 Spectra. All Matrix Absorptions Other than Those of N_2HD_3 Have Been Blanked.

TABLE 10. WAVENUMBERS, PREDICTED INTENSITIES (KM/MOL), AND EXPERIMENTAL RELATIVE INTENSITIES OF N_2HD_3 FUNDAMENTAL VIBRATIONS[a]

Isomer and Mode #	PED	Predicted		Ar Matrix		N_2 Matrix	
		cm^{-1}	A[b]	cm^{-1}	I[c]	cm^{-1}	I[c]
iio 1	NH str(100)	3391	2.9				
ioo 1	" " (100)	3339	5.8	3374	(*,1.7)	3371	(*,1.2)
ioo 2	a-DND str(96)	2518	0.6				
iio 2	" " " (97)	2518	0.5				
ioo 3	ND str(98)	2474	1.9				
iio 3	" " (97)	2436	1.7				
ioo 4	s-DND str(97)	2395	4.0			2423	(*,1.1)
iio 4	" " " (95)	2394	5.0			2423	
ioo 5	HND sci(86) + HND twi(14)	1477	7.6	1487	(*,5.1)	1467	(*,6.8)
iio 5	" " (87) + " " (13)	1476	11.1	1474	(*,6.0)	1453	(*,1.9)
ioo 6	DND " (80) + NN str(12)	1214	6.3	1199	(9,6.0)	1201	(24,16)
iio 6	" " (91)	1203	6.0	1194	(7,2.6)	1196	(6,1.9)
iio 7	HND twi(47) + NN str(29) + HND wag(10)	1138	16.8	1140	(23,8.1)	1139	(27,9.5)
ioo 7	" " (56) + DND sci(15) + " " (13)	1085	30.1	1098	(16,10)	1096	(21,14)
ioo 8	NN str(56) + DND twi(16) + HND twi(14)	1028	0.01			1035	(7,4.3)
iio 8	DND twi(46) + HND twi(25) + NN str(16)	979	5.5			988	(6,2.1)
ioo 9	" " (67) + NN str(24)	959	12.3	956	(4,2.8)	961	(3,1.7)
iio 9	NN str(48) + DND twi(33)	954	21.3	956	(3,1.1)	960	(7,2.3)
iio 10	HND wag(60) + DND wag(21) + DND twi(16)	798	103.5	807	(114,41)	829	(124,43)
ioo 10	" " (72) + DND twi(15)	765	98.0	772	(131,83)	787	(99,64)
ioo 11	DND " (92)	692	67.9	695	(67,43)	716	(68,45)
iio 11	" " (76) + HND wag(17)	671	71.0	673	(87,31)	692	(60,21)
iio 12	torsion(99)	332	28.6				
ioo 12	" (99)	329	33.9				

[a] See Table 8 for additional explanation not supplied here.
[b] These are absolute integrated absorption coefficients in km/mol.
[c] The numbers in parentheses are relative intensities per mole of isomer and N_2HD_3 specie, respectively. Asterisks denote bands whose assignments are uncertain.

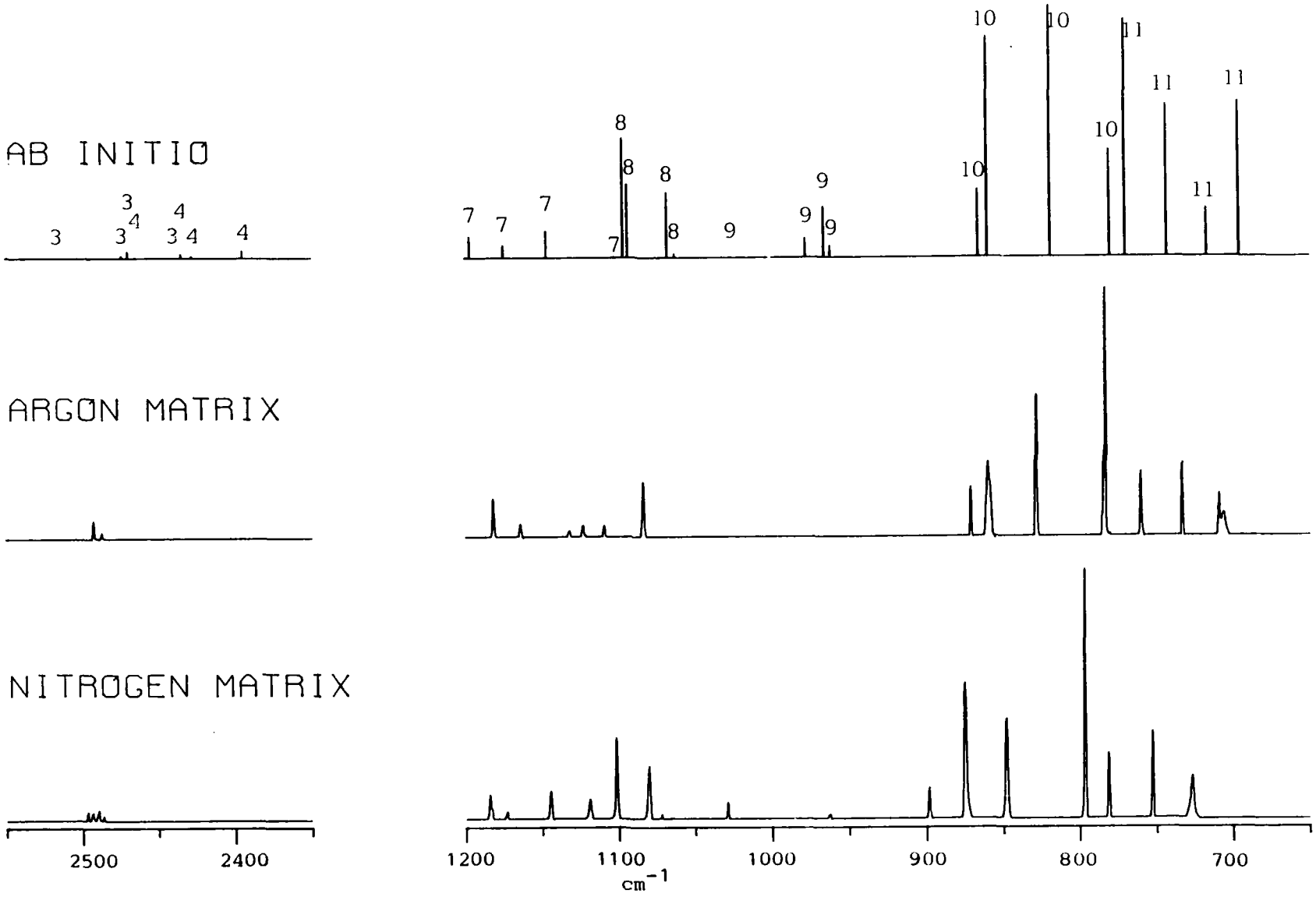

Figure 16. $N_2H_2D_2$ Spectra. All Matrix Absorptions Other than Those of $N_2H_2D_2$ Have Been Blanked.

the C_2 symmetry of the ii and oo isomers would dictate a numbering system analagous to that used for N_2H_4.

$N_2H_2D_2$ was more difficult to analyze than the other $N_2H_nD_{4-n}$ vibrational species for two reasons. First, there is a higher density of absorption bands for the matrix spectra of the former compared with the latter. Second, $N_2H_2D_2$ was always accompanied by significant amounts of virtually all other $N_2H_nD_{4-n}$ species.

The $N_2H_2D_2/N_2$ spectrum appears puzzling in the 950 to 650 cm^{-1} region because there are only seven lines out of the expected eight. However, the $N_2H_2D_2/Ar$ spectrum reveals that modes ν_{10} and ν_{11} of the oo isomer are nearly coincident and are probably blended in the $N_2H_2D_2/N_2$ spectrum.

The 1250 to 1050 cm^{-1} region is puzzling because some of the lines are shifted substantially from their predicted frequencies. One clue for assigning this region is that the predicted frequencies for the scissor-bending modes of hydrazine have a greater tendency to be lower than the observed frequencies than any of the other modes. Hence, the observed line at 1182 cm^{-1} in $N_2H_2D_2/Ar$ (1185 cm^{-1} in N_2) probably corresponds to the ν_7 scissor-bending mode of the i1o1 isomer (ν(calc.) = 1197 cm^{-1}). An alternative is to assume that this absorption is missing from the matrix spectra. The key to assigning the remaining lines in the 1250 to 1050 cm^{-1} region is to deduce the identity of the ν_7 s-HND-twisting absorption of the ii isomer. The proposal that leads to the most satisfying result for the remaining lines is to attribute the 1184 cm^{-1} absorption of $N_2H_2D_2/N_2$ to this mode. This absorption is probably not a site-split component of the scissor-bending mode (1185 cm^{-1}) discussed above because none of the other modes of $N_2H_2D_2/N_2$ has such a component. The corresponding absorption in $N_2H_2D_2/Ar$ must be assumed to be completely blended with the 1182 cm^{-1} scissor-bending mode. If this interpretation is correct, a straightforward one-to-one correspondence is obtained for the remaining predicted versus experimental absorptions in the 1250 to 1050 cm^{-1} region. The only remaining uncertainty would be in the relative ordering of the ν_7(oo), ν_8(oo), and ν_8(i1o2) modes. The assignments shown in Table 11 are based on this interpretation. Alternatively, if it is assumed that the 1184 and 1185 cm^{-1} absorptions of

TABLE 11. WAVENUMBERS, PREDICTED INTENSITIES (KM/MOL), AND EXPERIMENTAL RELATIVE INTENSITIES OF $N_2H_2D_2$ FUNDAMENTAL VIBRATIONS[a]

Isomer and Mode #		PED	Predicted		Ar Matrix		N_2 Matrix	
			cm^{-1}	A	cm^{-1}	I	cm^{-1}	I
i1o1	1	a-HNH str(92)	3412	0.9				
ii	1	a-NH str(100)	3398	5.6				
i1o2	1	NHo str (100)	3391	2.9				
ii	2	s-NH str(100)	3384	0.06				
oo	1	" " " (100)	3347	0.2				
i1o2	2	NHi str (100)	3339	5.8				
oo	2	a-NH str(100)	3330	11.4				
i1o1	2	s-HNH str(92)	3314	7.9				
i1o1	3	a-DND str(97)	2518	0.5			2497	(*,1.4)
oo	3	a-ND str (99)	2478	3.7	2492	(15,4.5)	2494	(*,3.1)
i1o2	3	NDo str (99)	2474	1.8	2487	(6,1.5)	2490	(*,3.5)
oo	4	s-ND str (99)	2470	0.01			2487	(*,0.9)
ii	3	" " " (99)	2443	0.2				
i1o2	4	NDi str (99)	2435	2.6				
ii	4	a-ND str(100)	2428	5.1				
i1o1	4	s-DND str(97)	2395	4.0				
i1o1	5	HNH sci (100)	1628	15.0				
ii	5	s-HND sci(82) + s-HND twi(19)	1515	9.3				
oo	5	a-HND sci(81) + a-HND twi(18)	1501	10.3				
i1o2	5	HiNDo sci(55) + HoNDi sci(33)	1478	7.6				
i1o2	6	HoNDi sci(54) + HiNDo sci(32)	1475	11.1				
oo	6	s-HND sci(91)	1453	3.7				
ii	6	a-HND sci(93)	1437	10.2				
i1o1	6	HNH twi (87) + DND sci(12)	1286	0.3				

TABLE 11. WAVENUMBERS, PREDICTED INTENSITIES (KM/MOL), AND EXPERIMENTAL RELATIVE INTENSITIES OF $N_2H_2D_2$ FUNDAMENTAL VIBRATIONS

(Concluded)

Isomer and Mode #	PED	Predicted		Ar Matrix		N2 Matrix	
		cm^{-1}	A	cm^{-1}	I	cm^{-1}	I
i1o1 7	DND sci(71) + NN str(16)	1197	10.5	1182	(*,7.6)	1185	(*,6.9)
ii 7	s-HND twi(38) + NN str(36) + s-wag(18)	1175	24.9	1164	(*,4.2)	1174	(*,2.2)
i1o2 7	HoNDi twi(42) + NN str(38)	1147	13.2	1132	(*,0.8)	1145	(*,8.6)
oo 7	s-HND twi(60) + NN str(34)	1103	1.0				
oo 8	a-HND twi(58) + a-wag(26) + a-HND sci(16)	1097	61.9	1123	(*,3.0)	1120	(*,6.9)
i1o2 8	HiNDo (twi(66) + sci(10)) + HoNDi wag(10)	1094	35.3	1110	(*,1.9)	1102	(*,18)
i1o1 8	NN str(41)+DND(sci(14)+twi(14))+HNH wag(31)	1068	31.6	1084	(35,11)	1081	(40,16)
ii 8	a-HND twi(92)	1063	9.4			1073	(9,1.0)
oo 9	NN str(57) + s-HND twi(31)	1028	0.01			1030	(13,3.3)
i1o2 9	NN str(59) + HoNDi twi(33)	978	9.5				
i1o1 9	DND twi(47) + NN str(38) + HNH wag(11)	966	24.7			964	(*,0.4)
ii 9	NN str(66) + s-HND twi(28)	962	22.2			963	(*,0.4)
ii 10	a-wag(100)	866	121.6	871	(85,8.3)	899	(62,7.3)
i1o1 10	HNH wag(53) + DND twi(37)	860	105.4	860	(145,48)	876	(115,44)
i1o2 10	HiNDo (wag(39) + twi(16)) + HoNDi wag(41)	819	120.3	829	(140,38)	849	(139,35)
oo 10	s-wag(90)	780	55.7	784	(47,14)	797	(165,41)
oo 11	a-wag(74) + a-HND twi(23)	770	122.8	783	(120,37)	797	
i1o2 11	HiNDo wag(45) + HoNDi wag(44)	743	72.7	760	(49,13)	782	(54,14)
ii 11	s-wag(82) + s-HND twi(14)	717	87.1	733	(124,12)	753	(148,18)
i1o1 11	DND wag(94)	696	74.3	709	(31,10)	727	(56,22)
i1o1 12	torsion(100)	372	43.4				
ii 12	" (97)	356	27.2				
i1o2 12	" (98)	353	34.7				
oo 12	" (98)	350	41.0				

[a] See Tables 8 and 10.

$N_2H_2D_2/N_2$ are site-split components of the same mode, then one of the remaining modes in the 1250 to 1050 cm^{-1} region must be either missing or blended with another mode. The most likely candidate for a missing mode is the ν_7 absorption of the oo isomer since it is predicted to be the weakest of the set. This interpretation would necessitate the following reassignments in Table 11: ν_7(ii) = 1164 cm^{-1} (Ar), 1174 cm^{-1} (N2); ν_7(i1o2) = 1132 cm^{-1} (Ar), 1145 cm^{-1} (N2); and ν_7(oo) absent. None of the uncertain assignments were used in determining isomer and isotope percentages.

e. Spectra of N_2H_3D

Matrix spectra of N_2H_3D are presented in Figure 17, along with the predicted spectrum. The quantity of this species was never large in any of the matrix experiments because it was difficult to optimize the production of this specie using N_2D_4 starting material. Nevertheless, all expected modes between 1300 and 700 cm^{-1} were observed and assigned without difficulty. These assignments are presented in Table 12, along with intensity data.

3. Matrix-Isolation Spectra of MMH, UDMH, AND Benzene

Matrix spectra of MMH are presented in Figures 18 and 19, where they are compared with the vapor spectrum and the predicted spectrum. Tentative assignments for the matrix spectra, based primarily on previous vapor-phase findings (Reference II-17), are presented in Table 13. Additional analysis of the ab initio calculation is needed to confirm these assignments. Difficulties arise in correlating the predicted and matrix data because the predicted frequencies are less accurate for MMH than for hydrazine. These difficulties are due to a computer-imposed limitation on the size of the basis set that can be used.

The vapor-phase spectrum and argon-matrix spectrum of UDMH are compared in Figures 20 and 21. No assignments have been attempted for the matrix spectrum because no ab initio calculation has been made yet. The assignments that have been proposed for the vapor phase (Reference II-18) are indicated in the figure.

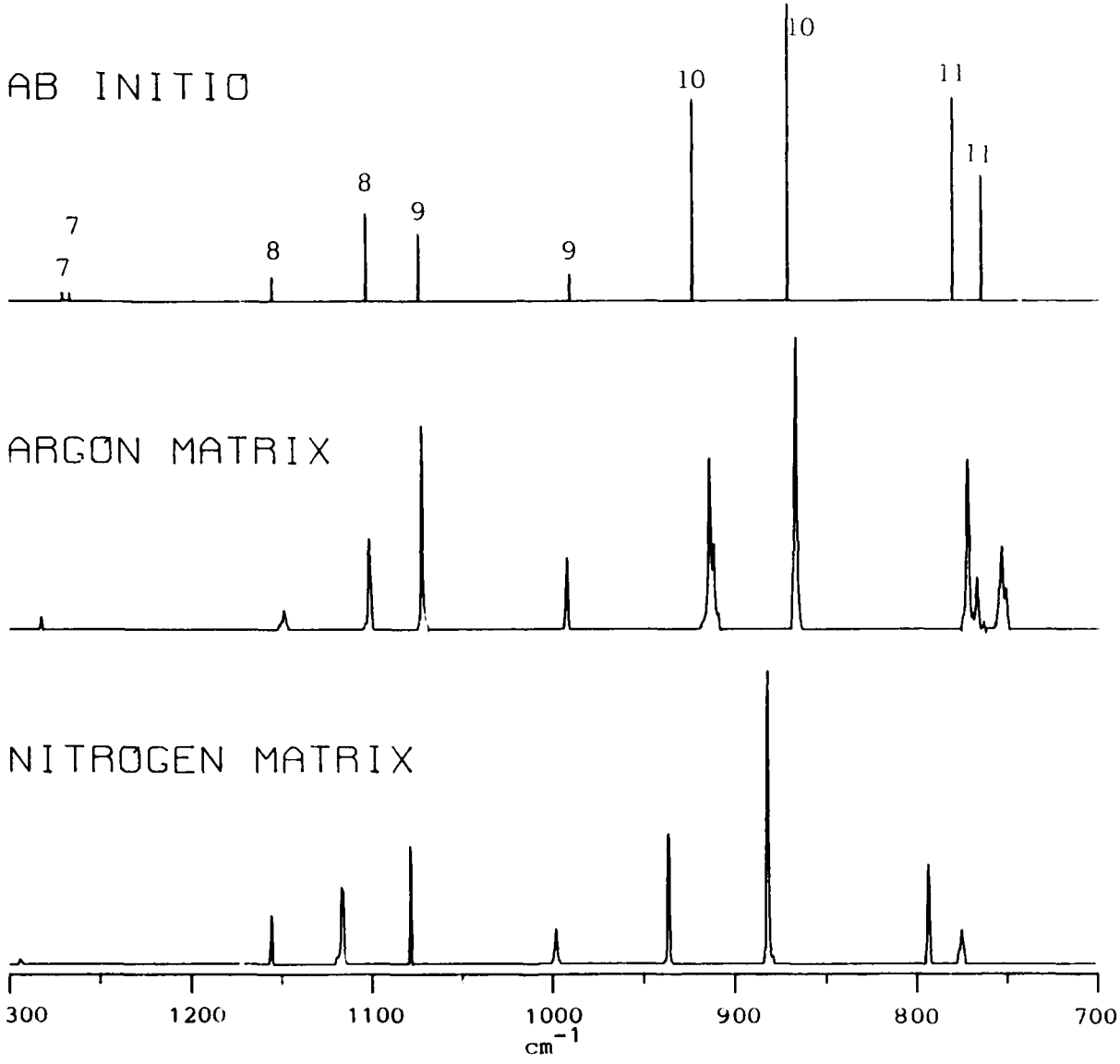

Figure 17. N_2H_3D Spectra. All Matrix Absorptions Other Than Those of N_2H_3D Have Been Blanked.

TABLE 12. WAVENUMBERS, PREDICTED INTENSITIES (KM/MOL), AND EXPERIMENTAL RELATIVE INTENSITIES OF N_2H_3D FUNDAMENTAL VIBRATIONS[a]

Isomer and Mode #		PED	Predicted		Ar Matrix		N_2 Matrix	
			cm^{-1}	A	cm^{-1}	I	cm^{-1}	I
i	1	a-HNH str(87)	3414	1.4				
o	1	" " " (92)	3412	0.8				
i	2	NH str(94)	3390	2.7				
o	2	" " (93)	3340	2.9				
i	3	s-HNH str(92)	3313	7.4				
o	3	" " " (86)	3311	10.8				
o	4	ND str(99)	2474	1.8				
i	4	" " (99)	2435	2.6				
i	5	HNH sci(98)	1632	14.5				
o	5	" " (100)	1630	15.2				
o	6	HND " (84) + HND twi(12)	1480	6.1				
i	6	" " (82) + " " (12)	1479	8.7				
o	7	HNH twi(93)	1271	4.1	1283	(*,1.5)	1294	(*,1.9)
i	7	" " (89)	1267	6.7				
i	8	HND " (38) + NN str(36) + HNH wag(15)	1156	18.7	1149	(15,5.4)	1156	(33,10)
o	8	" " (61) + " " (13) + HND " (12)	1104	36.0	1102	(37,23)	1117	(43,29)
o	9	NN str(67) + HNH wag(27)	1075	27.8	1073	(59,37)	1079	(38,26)
i	9	" " (50) + HND twi(41)	991	20.4	992	(31,11)	999	(56,18)
i	10	HNH wag(68) + HND wag(21)	924	150.5	914	(133,49)	937	(134,43)
o	10	" " (64) + HND twi(17) + NN str(14)	872	121.4	867	(102,64)	883	(140,95)
o	11	HND " (83)	781	83.2	772	(70,44)	794	(48,32)
i	11	" " (71) + HNH wag(16)	765	92.7	754	(104,38)	776	(59,19)
i	12	torsion(99)	393	38.9				
o	12	" (99)	390	49.6				

[a] See Tables 8 and 10.

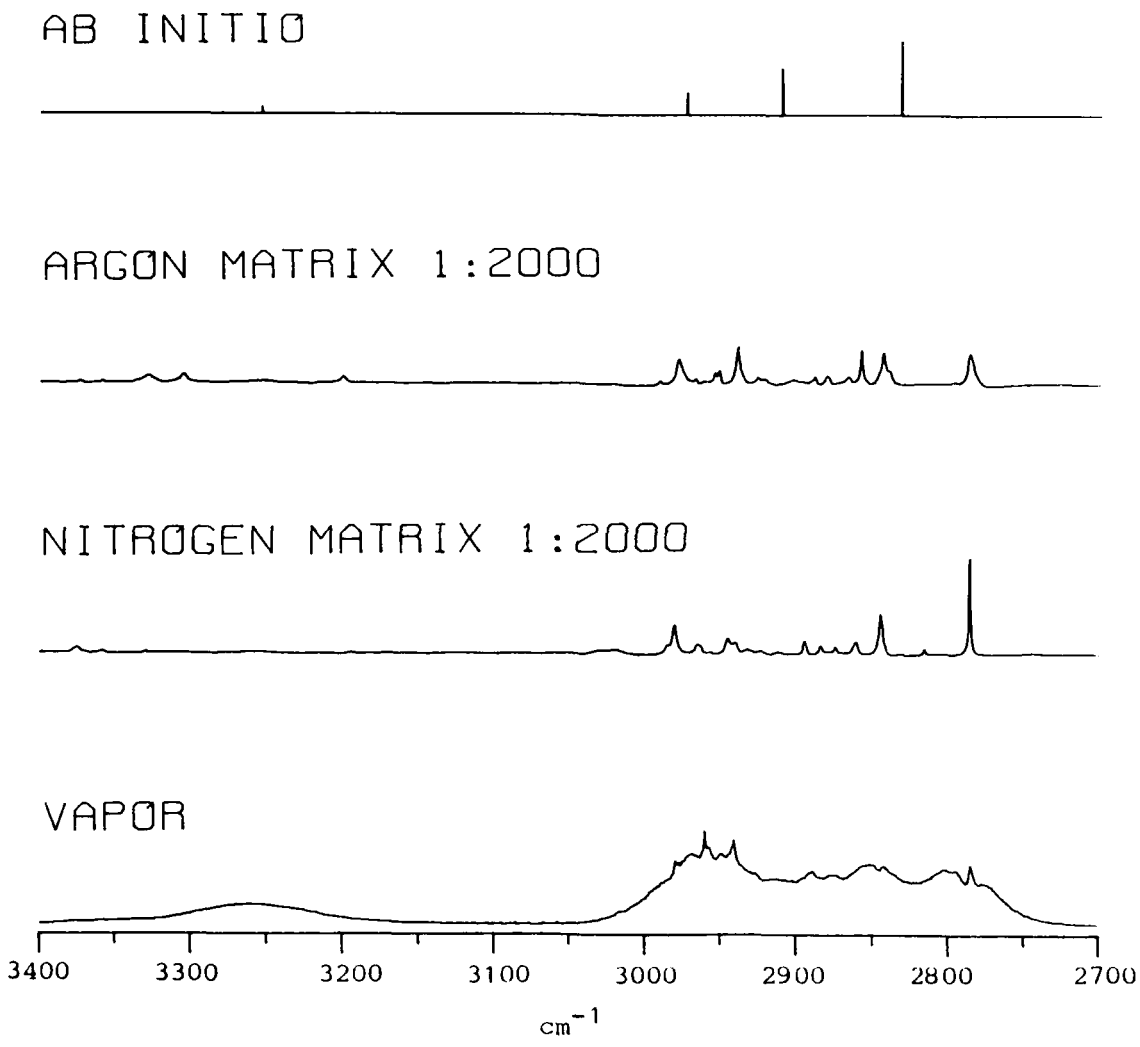

Figure 18. Monomethylhydrazine Survey Spectra: 3400-2700 cm^{-1}.

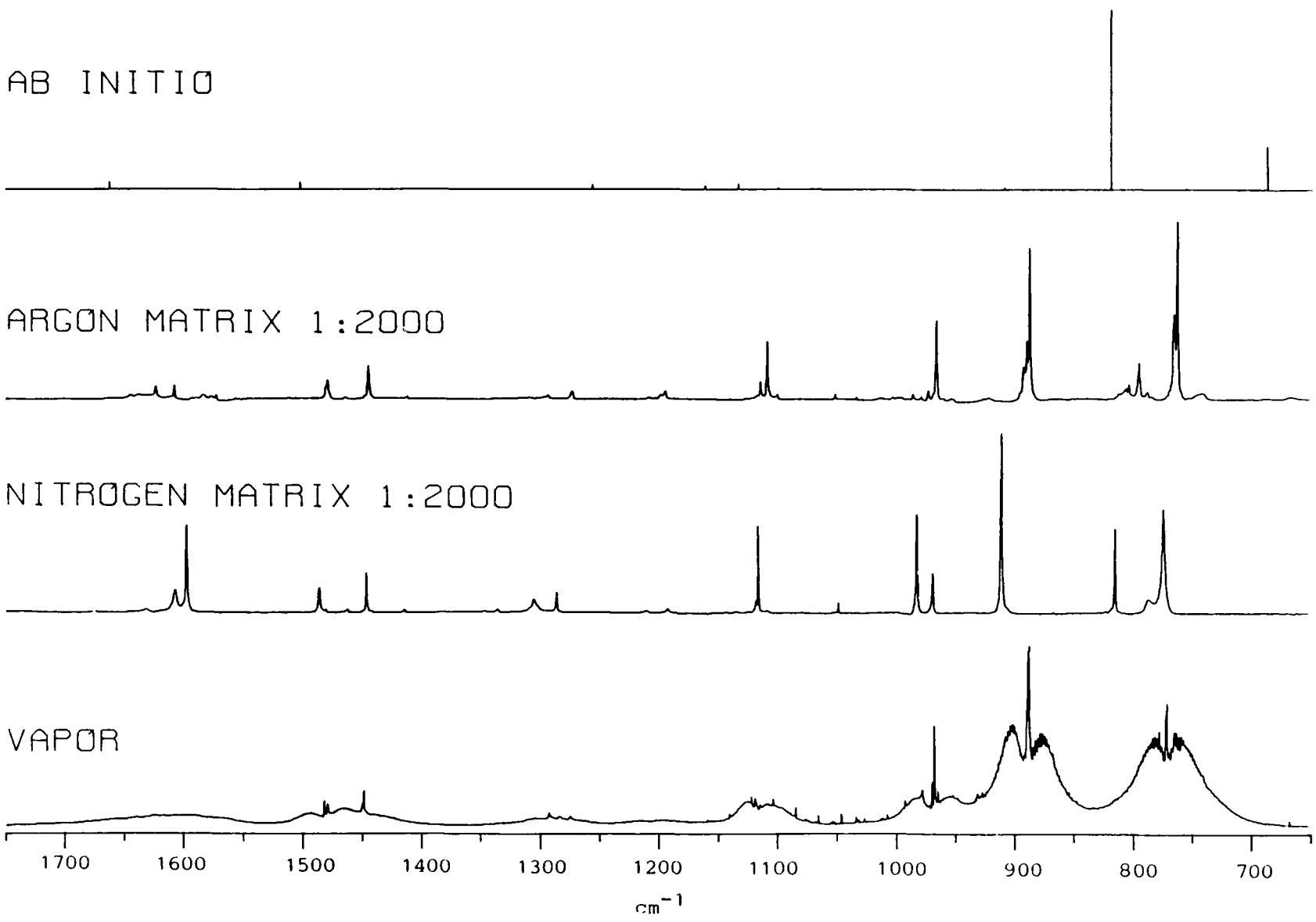

Figure 19. Monomethylhydrazine Survey Spectra: 1750-650 cm^{-1}.

TABLE 13. WAVENUMBERS, PREDICTED INTENSITIES (KM/MOL), AND EXPERIMENTAL RELATIVE INTENSITIES OF NH_2NHCH_3 FUNDAMENTAL VIBRATIONS[a]

Mode #	Predicted		Ar Matrix		N_2 Matrix		Vapor[b]
	cm^{-1}	A	cm^{-1}	I	cm^{-1}	I	cm^{-1}
1	3381	1.14	3374	1	3376	9	
2	3281	3.29	3359	1	3359	1	
3	3255	8.20	3306	7			
4	2974	23.74	2979	25	2981	31	2967
5	2911	48.53	2939	28	2945	21	2951
6	2833	74.56	2786	36	2786	43	2784
7	1663	10.02	1584	10	1607	22	1597
8	1527	2.29	1479	15	1487	13	1479
9	1503	9.59	1445	20	1447	15	1465
10	1476	1.00	1413	1	1415	1	1449
11	1441	0.18	1274	6	1287	9	1282
12	1257	6.50	1195	7	1193	1	1210
13	1162	5.78	1115	6	1118	3	1118
14	1134	7.64	1109	21	1117	21	1124
15	1100	2.78	1101	1			1108
16	910	3.73	967	39	984	47	968
17	820	231.47	888	121	912	99	888
18	688	55.74	764	150	775	148	777
19	411	21.11					425
20	296	62.78					316
21	225	2.54					257

[a] See Table 8 for an explanation of the intensity data.
[b] Reference II-17.

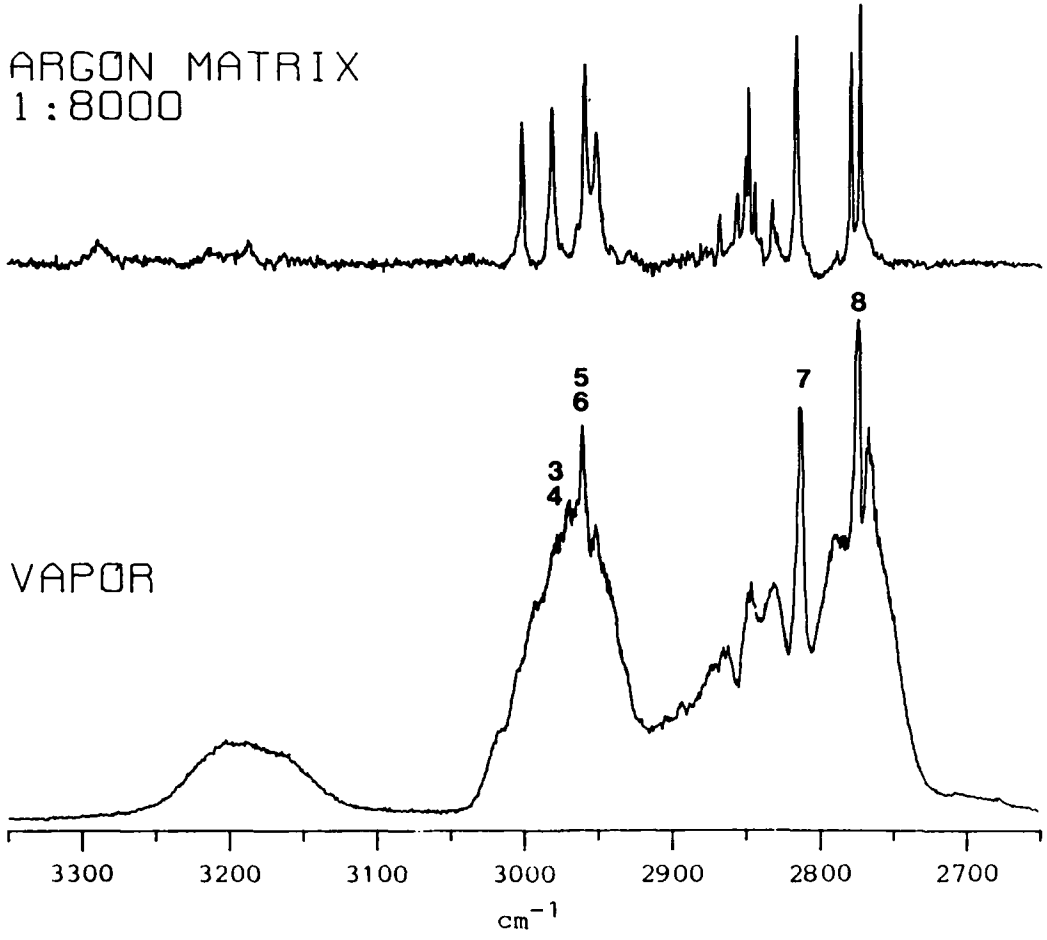

Figure 20. UDMH Survey Spectra: 3350-2650 cm^{-1}.

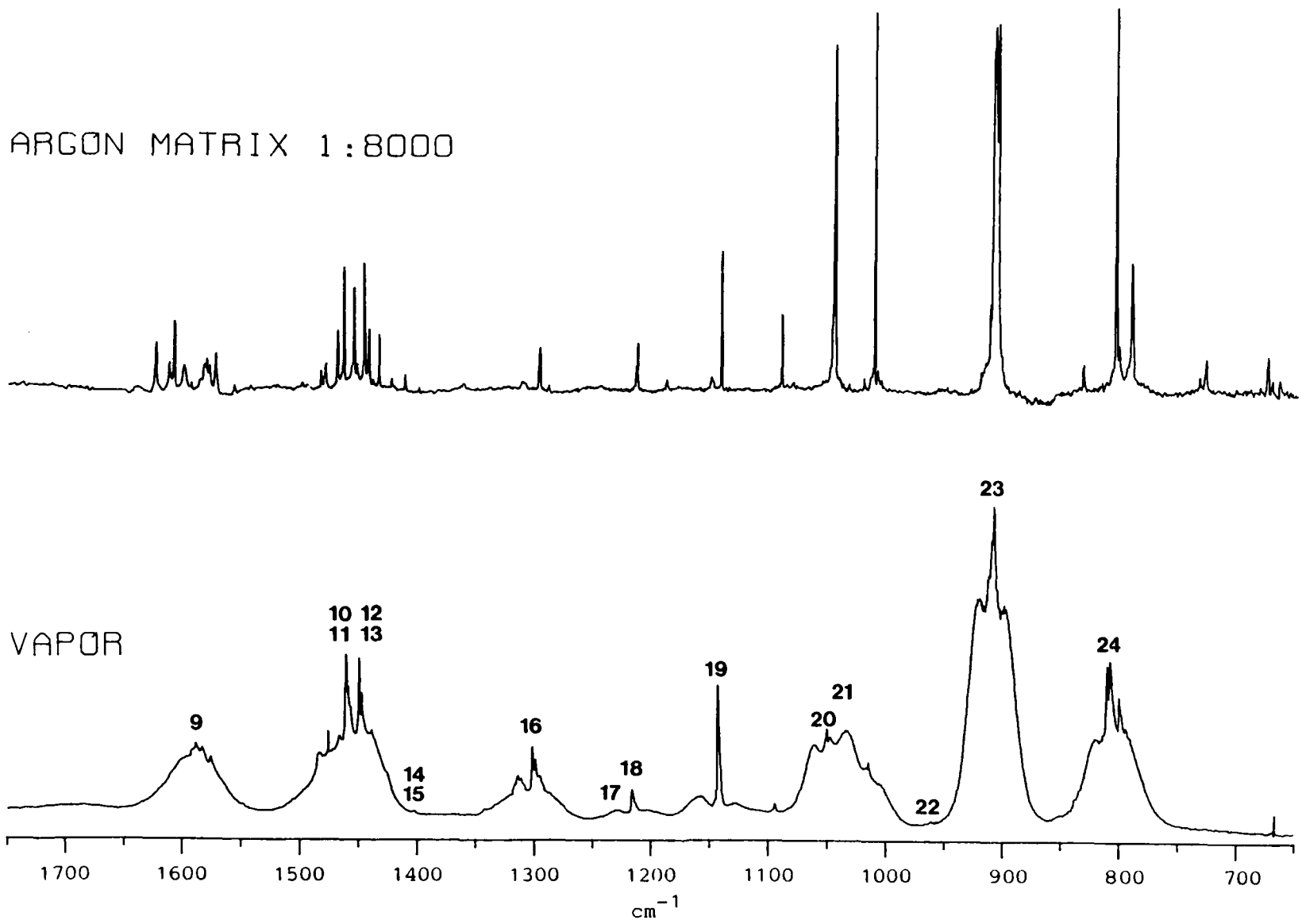

Figure 21. UDMH Survey Spectra: 1750-650 cm^{-1}.

The vapor-phase spectrum and argon-matrix spectrum of benzene are compared in Figures 22 and 23. These spectra have been included in this report only as a convenient reference. Benzene has already been studied extensively in both the vapor-phase (Reference II-19) and in various matrices (Reference II-20).

C. CONCLUSIONS

The FT-IR matrix-isolation studies of $N_2H_nD_{4-n}$ species have demonstrated the usefulness of the matrix-isolation technique for studying small molecules. The extension of such studies to larger molecules is limited only by the availability of accurate predicted spectra. The consistently close agreement between the predicted and experimental fundamental frequencies of the present hydrazine spectra has enabled most of the experimental vibrations to be assigned confidently. It is hoped that these results will be a step toward understanding the behavior of hydrazine in clays.

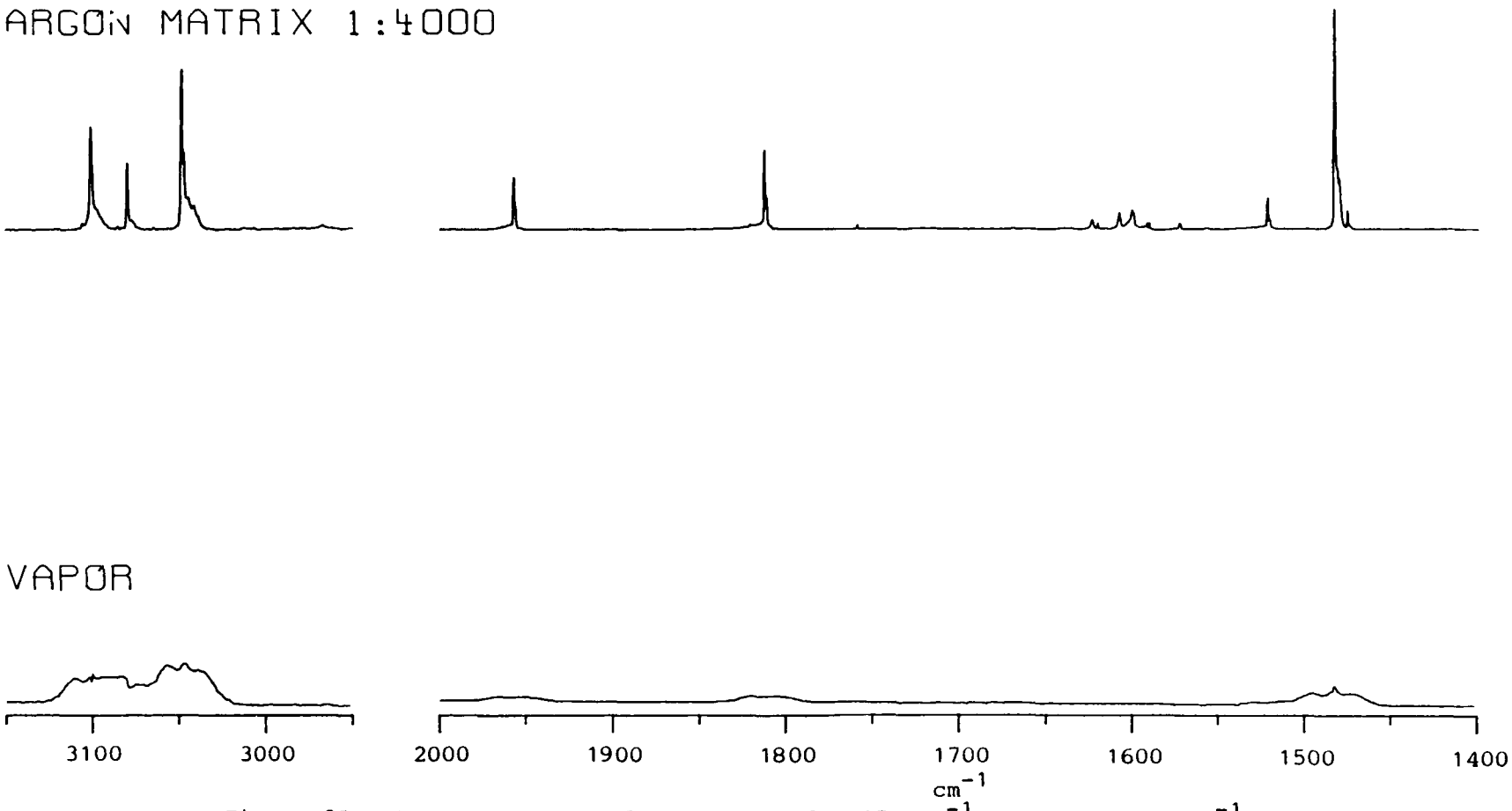

Figure 22. Survey Spectra of Benzene: 3150-2950 cm^{-1} and 2000-1400 cm^{-1}.

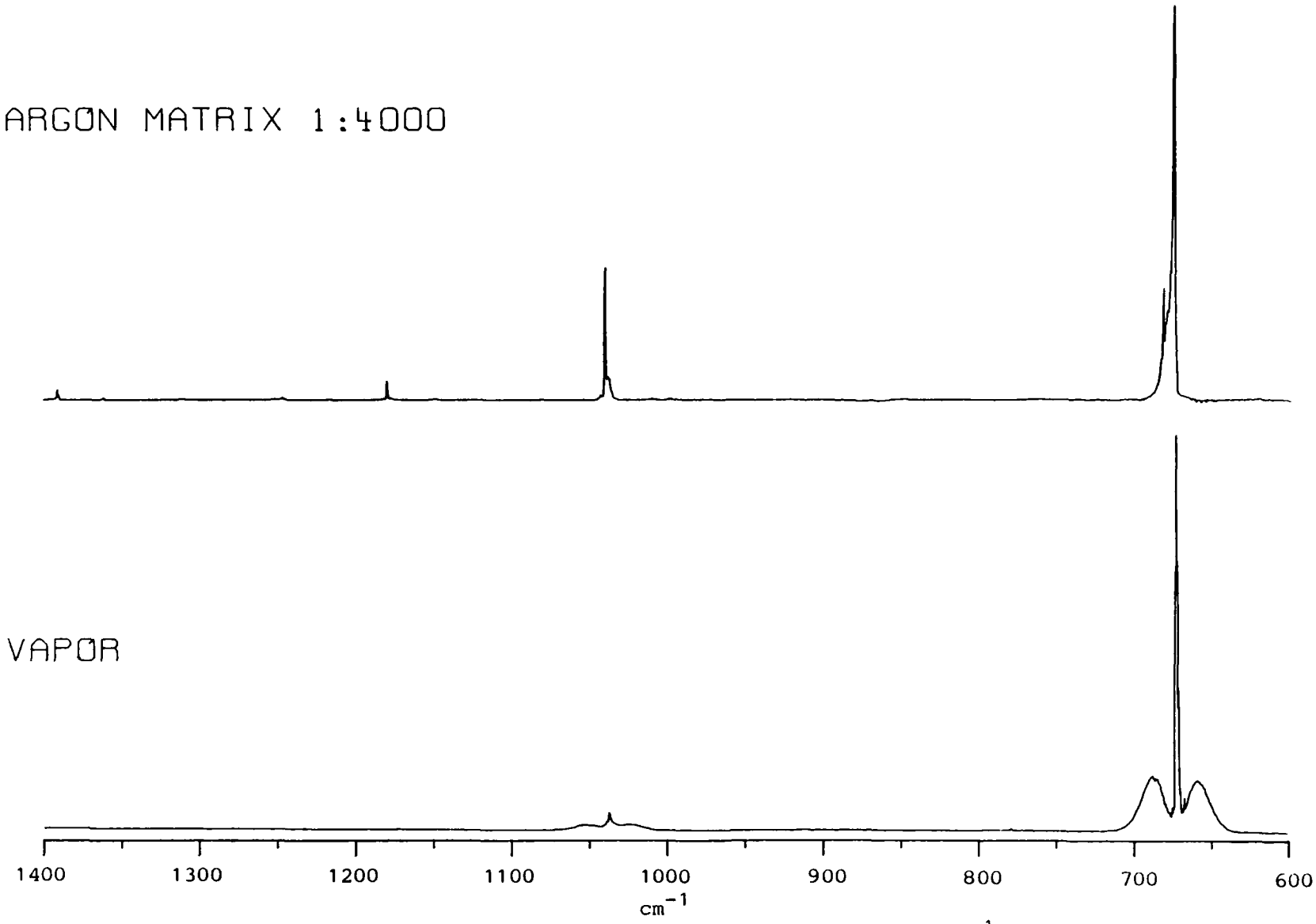

Figure 23. Survey Spectra of Benzene: 1400-600 cm^{-1}.

SECTION III

CALCULATIONS OF THE VIBRATIONAL SPECTRA OF N_2H_4, ALL OF ITS DEUTERATED DERIVATIVES AND $CH_3N_2H_3$

A. INTRODUCTION

A detailed and complete understanding of the spectrum of the isolated molecule is essential to interpreting changes in vibrational spectra of a ligand as it interacts with a surface such as clay. The experimental infrared spectrum for the isolated hydrazine molecule has been reported in Section II. It is first necessary to assign each of the absorption bands observed in the spectrum of the matrix isolated molecules to one of the 12 fundamental modes of vibration of the predominant conformer, to combination band or overtones, to different conformers, to impurities, or to dimers or complexes of N_2H_4 with H_2O or other impurities. This problem is exceedingly difficult and it has not been done carefully before. The assignment of the matrix spectrum is discussed in Section II, where it generally agrees with previous assignments of the infrared spectrum of isolated N_2H_4 to the fundamental modes of vibration. Remaining absorption bands have been assigned to the hydrazine dimer, but not yet to specific fundamental modes.

Calculations play a very important role in the process of understanding the spectrum of N_2H_4. In particular, ab initio quantum mechanical calculations of the spectra provide an objective prediction that allows an extremely valuable test of previous assignments based largely on an intuitive knowledge of characteristic group frequencies. As the name implies, an ab initio quantum mechanical calculation, in contrast with empirical or semiempirical quantum mechanical calculations, does not make any assumptions about the molecule, but calculates the vibrational spectrum (for example) by a direct solution of the Schrödinger equation with no simplifying assumptions. An ab initio calculation evaluates the properties of interest for a system described by approximate wavefunctions, to make it possible to carry out the calculation. These approximate wavefunctions are obtained by following standard procedures that express them in different basis sets. In order of increasing complexity and sophistication, typical basis sets for ab initio calculations may be STO-3G, 3-21G, 4-31G or 6-31G** (see Reference III-1). Previous experience has shown that calculated vibrational spectra using an STO-3G basis

set do not agree with experiment and so are essentially useless, with the reliability of the calculated spectrum increasing up through calculations made with the 6-31G** basis set. It is known that the latter calculations give frequencies and intensities for each predicted band that are in the correct order, when compared with experiment, and the remaining errors in the calculation are reasonably well-known so that allowances may be made for them in the interpretation of spectra.

The ultimate goal of the calculations reported here was not simply to predict frequencies and intensities for the fundamental modes in the infrared spectrum of hydrazine. Such "bare bones" predictions have been made before (References III-1-3) but not enough details have been reported to make possible the extensive interpretation required for complete understanding of changes in hydrazine spectra that occur as a result of intermolecular interactions. Our calculations have provided these details whenever work is resumed on this interpretation in the future.

The objectivity and accuracy of an ab initio quantum mechanical prediction of the vibrational parameters (force constants and dipole moment derivatives (known as Atomic Polar Tensors or APTs) are sufficient to provide values that are more accurate representations of the true values that can be obtained from experimental data alone using traditional methods of vibrational analysis. References were given in Section II to earlier assignments and calculations of force constants and qualitative intensities. This work is not reviewed again here because we are not interested in this study in confirming or contradicting these previous empirical estimates of force constants. Rather, our calculations are intended to give the best present estimate of force constants and APTs for hydrazine. From previous experience, the probable errors in these parameters are known or can be estimated.

From these parameters it was possible to predict the spectra of all possible deuterated derivatives of N_2H_4. It is expected that many of these parameters may be transferred judiciously to predict the spectra of the methylated hydrazines. It is also expected that changes in these parameters due to intermolecular interactions (or interactions with the clay surface, for example) will provide considerable detailed information about the structure of

hydrazine in complexes or on surfaces.

In this section we present first a description of the method of calculation. Some of the results from these calculations were used in Section II, where the calculated spectra formed the basis for the assignments. However, the complete calculated spectra (frequencies, intensities, definitions of coordinates, and complete calculations of the Potential Energy Distributions (PEDs)) for all hydrazine molecules in this study are summarized here. The calculated results are summarized briefly; their significance is apparent by reference to Section II or to the manuscript (Reference III-4) prepared from the work from Sections II and III.

B. CALCULATIONS

Ab initio molecular orbital calculations were carried out using the GAUSSIAN 82 program (Reference III-5) first with a 3-21G basis set (Reference III-6), and later with a 6-31G** basis set (Reference III-7). The geometry optimization finds that the minimum energy configuration is the gauche form shown in Figure 24, in agreement with previous calculations (References III-1-3) and with the experimental gas electron-diffraction study by Kohata, et al. (Reference III-8). The predicted structure and relative energies of conformers from our study, shown in Figure 24, agree very well with the result from the previous studies (References III-2, III-3, III-8). The Cartesian force constants were calculated using the program option to calculate the gradients of the force analytically and these were then mass weighted and diagonalized in the program option to obtain frequencies. The calculated values, shown in Table 24, agree very well with the values reported by Riggs and Radom (Reference III-3). The normal coordinate transformation matrix, ℓ (defined by $q = \ell Q$ - see Reference III-9) is obtained as the transformation

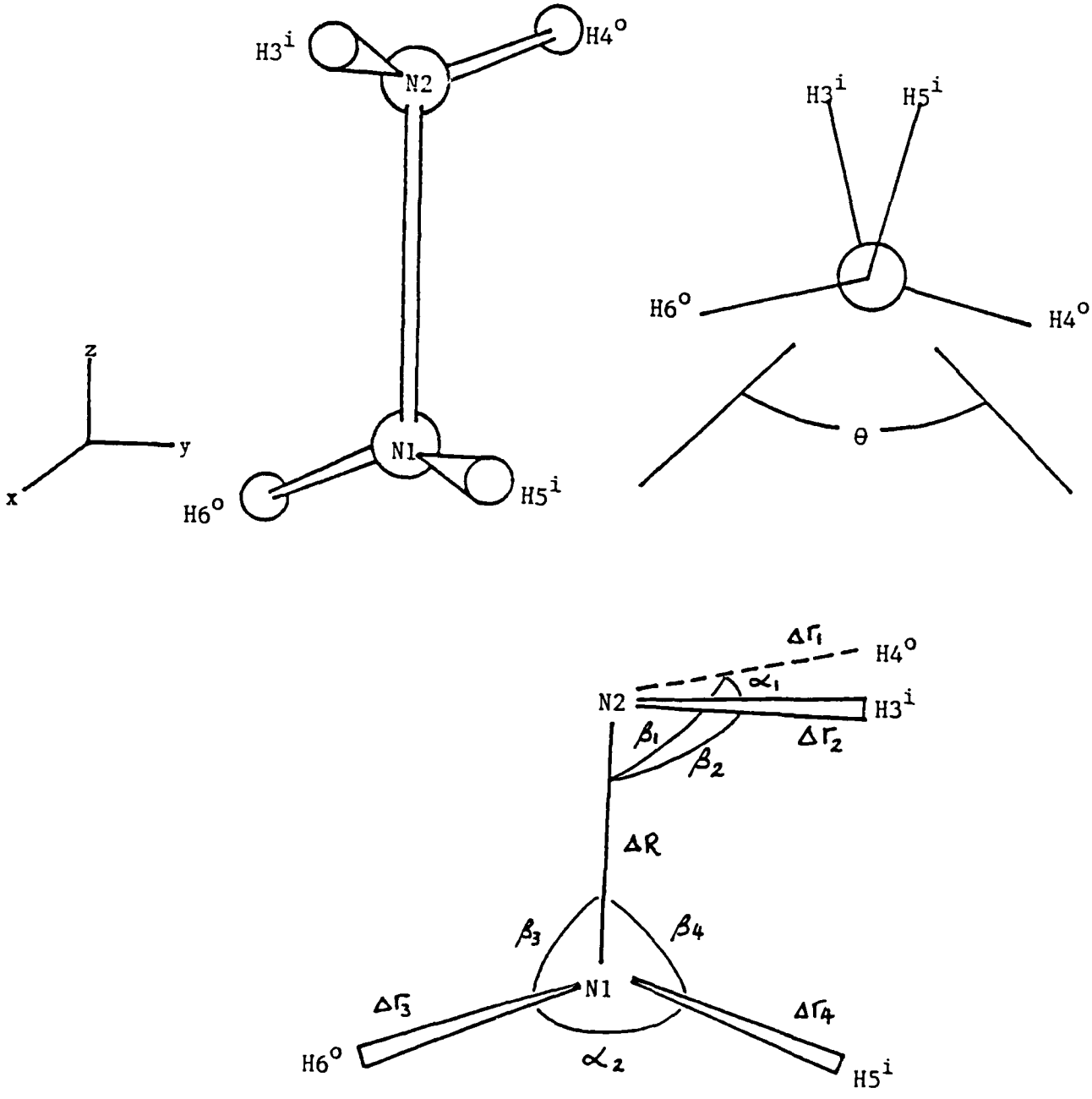

Figure 24. The Most Stable (Gauche) Conformation for the Isolated Hydrazine Molecule. The Lower Sketch Includes the definition of the Internal Coordinates.

matrix that diagonalizes F_q, the force constant matrix in mass-weighted Cartesian coordinates.

In order to use these predicted wavenumbers to interpret experimentally observed spectra it is desirable to carry out additional calculations. The most important of these is to calculate the dipole moment derivatives (APTs) (References III-10-12) and transform these to obtain the predicted intensities of each fundamental vibration band. The APTs are calculated using the method described by Komornicki and McIver (Reference III-13) as applied specifically (Reference III-14) for GAUSSIAN 82. When the APTs are transformed to obtain the P_Q polar tensor (Reference III-11, III-12), the integrated molar absorption coefficients, A/km $mole^{-1}$, are calculated to give the values shown in Table 14.

Another useful modification of the frequency calculations before comparing them with experimental observations is to "scale" the predicted spectrum. The wavenumbers predicted by calculations at this level of theory are generally 10 percent too high, and various procedures have been recommended (Reference III-15-17; and Reference III-1) for adjusting them to the experimental values. Initially, the predicted wavenumbers here were multiplied by a factor of 0.9 to get a predicted spectrum. Later, this factor was adjusted to 0.89 to obtain frequencies (Table 14) that agree better with the experimental values (Reference III-4) from the N_2H_4/Ar matrix spectrum. Such scaling of all frequencies by a single factor corresponds to scaling every calculated force constant by that factor squared. It may be expected that each force constant might better be scaled by a different factor to force an exact fit to the experimental spectrum, but the general agreement between predicted and experimental spectra (as seen in Section II) supports the hypothesis that the scaling factors are all nearly the same.

It is also useful to calculate the PEDs (Reference III-18, III-19) when one is trying to understand experimental spectra. The PEDs give the contribution of each symmetry coordinate to each one of the normal modes. They provide a basis for chemical interpretation of each of the normal modes in the spectra in terms of combinations of pure symmetry coordinate displacements. (For example, the absorption calculated at the scaled wavenumber of

TABLE 14. VIBRATIONAL SPECTRUM OF HYDRAZINE (GAUCHE) CALCULATED AT 6-31G**//6-31G** LEVEL.[a]

Frequency (cm^{-1})		Intensity	
Unscaled	Scaled[b]	A (km mol^{-1})	PED[c]
a Class			
3832	3410	0	s-a-HNH str (96)
3727	3317	0.5	s-s-HNH str (96)
1842	1639	13.7	s-scissor (100)
1449	1290	5.8	s-HNH twist (91)
1221	1087	5.5	NN str (78) + s-wag (17)
945	841	98.5	s-wag (79) + NN str (20)
480	427	50.7	torsion (100)
b Class			
3837	3415	1.8	a-a-HNH str (88) + a-s-HNH str (11)
3718	3309	15.0	a-s-HNH str (89) + a-a-HNH str (11)
1825	1624	14.3	a-scissor (99)
1414	1258	7.7	a-HNH twist (94)
1072	954	190.5	a-wag (95)

[a] The notation comes from Reference III-1; the first "6-31G**" refers to the basis set used for this calculation, and the second gives the basis set used to obtain the optimized reference geometry.

[b] Frequencies are scaled by a constant factor of 0.89.

[c] PED calculated using symmetry coordinate definition in Table 15. The initial s/a label on the stretching modes indicates the direction of one NH_i (NH_o) stretch with respect to the other NH_i (NH_o) stretch. The second s/a label describes the relative motions of the two NH stretches within a given amino group. Here the i and o refer to "inner" and "outer" H atoms, respectively. See Figure 24.

3317 cm^{-1} is assigned as an almost pure (96 percent) symmetric combination of the two symmetric N-H stretches of the individual NH_2 groups (the "s-s-HNH stretch" in Table 14). The numerical values given for the PEDs depend very strongly on the definition of symmetry coordinates. Those given in Table 14 are based on symmetry coordinates defined in Table 15.

Table 14 shows that most of the modes of vibration are nearly pure symmetry coordinate displacements; for another example, the first mode at a scaled predicted wavenumber of 3410 cm^{-1} is (96 percent) the symmetric (or in-phase) combination of the two asymmetric NH_2 stretching modes (s-a-HNH_2 str in Table 14, defined as S_2 in Table 15). However, the two symmetric (a class) modes predicted at scaled wavenumbers of 1087 and 841 cm^{-1} are seen in Table 14 to be quite strong mixtures of N-N stretch with the s-wag (defined in Table 15). Such predictions of mixing (or nonmixing) of symmetry coordinates depend quite strongly on the values of the force constants used in the normal coordinate calculations. Since there is some error in the predicted force constants, the PEDs could be expected to be somewhat approximate descriptions of the true normal modes in the molecule.

To complete the summary of results from predictions for N_2H_4, the values calculated here for the energies of the gauche and anticonformers (the two most stable conformers - see Reference III-3) are shown in Table 16. The calculation predicts the gauche conformer to be more stable than the anti form by about 7 kJ/mole (in agreement with Riggs and Radom (Reference III-3)). This rather large predicted energy difference is in agreement with the experimental observation in Section II that the observed spectrum of N_2H_4 in the matrices have no extra absorption bands that could be attributed to the presence of some concentration of anti form in the matrix.

The infrared spectrum calculated hydrazine in its anti configuration is given in Table 17. When this predicted spectrum is compared with the spectrum predicted for the gauche conformer in Table 14. The spectrum for the anti conformer is predicted to be much simpler, with only two bands (at 1587 and 1010 cm^{-1}) predicted strong enough to be observable in the near infrared region studied experimentally. For some time it was thought that the band observed in the spectrum of N_2H_4/Ar at 1010 cm^{-1} might be due to the anti

TABLE 15. SYMMETRY COORDINATE DEFINITION FOR ALL CONFORMERS OF N_2H_4 AND N_2D_4.

Symmetry Coordinate[a]	Name[b]
a Species	
$S_1 = (\Delta r_1 + \Delta r_2 + \Delta r_3 + \Delta r_4) / 2$	s-s-HNH str
$S_2 = (\Delta r_1 - \Delta r_2 + \Delta r_3 - \Delta r_4) / 2$	s-a-HNH str
$S_3 = \Delta R$	NN str
$S_4 = (2\Delta\alpha_1 - \Delta\beta_1 - \Delta\beta_2 + 2\Delta\alpha_2 - \Delta\beta_3 - \Delta\beta_4) /(12)^{1/2}$	s-scissor
$S_5 = (\Delta\alpha_1 + \Delta\beta_1 + \Delta\beta_2 + \Delta\alpha_2 + \Delta\beta_3 + \Delta\beta_4) /(6)^{1/2}$	s-wag
$S_6 = (\Delta\beta_1 - \Delta\beta_2 + \Delta\beta_3 - \Delta\beta_4) / 2$	s-HNH twist
$S_7 = \Delta\theta$	torsion
b Species	
$S_8 = (\Delta r_1 + \Delta r_2 - \Delta r_3 - \Delta r_4) / 2$	a-s-HNH str
$S_9 = (\Delta r_1 - \Delta r_2 - \Delta r_3 + \Delta r_4) / 2$	a-a-HNH str
$S_{10} = (2\Delta\alpha_1 - \Delta\beta_1 - \Delta\beta_2 - 2\Delta\alpha_2 + \Delta\beta_3 + \Delta\beta_4) /(12)^{1/2}$	a-scissor
$S_{11} = (\Delta\alpha_1 + \Delta\beta_1 + \Delta\beta_2 - \Delta\alpha_2 - \Delta\beta_3 - \Delta\beta_4) /(6)^{1/2}$	a-wag
$S_{12} = (\Delta\beta_1 - \Delta\beta_2 - \Delta\beta_3 + \Delta\beta_4) / 2$	a-HNH twist

[a] Internal coordinates are defined in Figure 24.

[b] See text for explanation of s/a labels (symmetric/antisymmetric).

TABLE 16. ENERGIES FOR GAUCHE AND ANTI CONFORMATIONS OF HYDRAZINE.

	Energies in hartrees		
	Conformer:		
	GAUCHE	ANTI	ΔE^a (kJ/mole)
	E_G	E_A	
E(6-31G**)[b]	-111.183523343	-111.178635844	12.83
E(MP2)[c]	-111.542397283	-111.539346494	8.01
Z.p. corr[d]	0.051422830	0.050914981	-1.33
		$\Delta E^{o}_{G,A}$[e] =	6.68

a $\Delta E = E_A - E_G$ = the energy of the anti conformer calculated with respect to the energy of the most stable, gauche, conformer, converted from hartrees to kJ/mole.

b E(HF/6-31G**//HF/6-31G**).

c E(MP2/6-31G**//HF/6-31G**). The values in this line thus include the first estimate of the effect of electron correlation on the calculation of energies.

d Zero-point vibrational energy correction (from real frequencies as calculated with the 6-31G** basis set and scaled by 0.89).

e Best estimate of the difference in energy ($E_A - E_G$) between anti and gauche conformers $\Delta E^{o}_{G,A} = [E_A(MP) - E_G(MP)] + Z.p.\ corr.$

TABLE 17. CALCULATION OF INFRARED SPECTRUM OF HYDRAZINE IN ITS "ANTI" CONFORMATION (6-31G** BASIS).

Normal Coord#[a]	Frequencies (cm^{-1}) Unscaled	Scaled[a]	Intensities km/mole	PED[b]
1	3800	3382	0.3	NH S-A-STR(100).
2	3777	3362	0	NH A-A-STR(100).
3	3718	3310	2.5	NH A-S-STR(100).
4	3703	3296	0	NH S-S-STR(100).
5	1846	1643	0	HNH S-A-BEND(102).
6	1783	1587	59.4	HNH A-A-BEND(99).
7	1623	1444	0	NNH A-A-BEND(100).
8	1331	1185	0	S-UMB BEND(100).
9	1198	1066	0.6	NNH S-A-BEND(100).
10	1135	1010	248	A-UMB BEND(98).
11	1109	987	0	N-N STR(101).
12	86	76	144	NN TORS(100).

[a] Frequencies scaled by constant factor of 0.89.

[b] See Table 15 for definition of symmetry coordinates.

conformer, until concentration dependence studies established definitely that this band was due to the dimer $(N_2H_4)_2$ (see Section II and Reference III-4).

Table 18 reports the infrared spectrum predicted for the trans conformer of N_2H_4. The predicted spectrum is also much simpler for the trans conformer than for the gauche form (again, because of the change of symmetry from C_2 (for gauche) to C_{2h} for trans or anti forms). As for the anti form, only two bands (here at 1605 and 1022 cm^{-1}) are predicted strong enough to be observable in the near infrared spectrum of the trans conformer of N_2H_4. It is concluded that the only conformer of hydrazine present in the matrix sample is the gauche conformer.

C. DEUTERATED HYDRAZINE CALCULATIONS

Force constants from the ab initio calculation for the gauche conformer of N_2H_4 were scaled uniformly by $(0.90)^2$ and used with the APTs to predict the frequencies, infrared intensities, and PEDs for all the fundamental vibrational modes of all possible deuterated isotopic derivatives of hydrazine. These predicted spectra were used to make the assignment of the bands in the experimental spectrum to vibrations of each isomer of the isotopic derivatives (Section II and Reference III-4). Furthermore the calculations of PEDs (References III-18, III-19) form the basis for the assignment of each band to a particular symmetry coordinate vibration, as seen in the following summary Tables 17-32.

The results for N_2D_4 presented in Table 19 are worth some discussion. If these are compared with the results for N_2H_4 in Table 14, a similar pattern is predicted for the spectrum of N_2D_4, with its characteristic shift to lower wavenumber for the modes involving H-atom motion in hydrazine. This shift in the natural frequency causes a change in the normal mode mixing in N_2D_4 from that found for N_2H_4. The comparatively unshifted N-N stretch now mixes with the DND twist instead of with the s-wag, as it did in N_2H_4. Otherwise the shift to lower wavenumbers and the decrease in intensity predicted on deuteration are those expected for this kind of molecule.

TABLE 18. CALCULATION OF INFRARED SPECTRUM OF HYDRAZINE IN ITS "TRANS" CONFORMATION (6-31G** BASIS).

Normal Coord#[a]	Frequencies (cm^{-1}) Unscaled	Scaled[a]	Intensities km/mole	PED[b]
1	3800	3420	0.3	NH S-A-STR(100).
2	3777	3400	0	NH A-A-STR(100).
3	3719	3347	2.5	NH A-S-STR(100).
4	3703	3333	0	NH S-S-STR(100).
5	1846	1662	0	HNH S-A-BEND(102).
6	1783	1605	59.4	HNH A-A-BEND(99).
7	1623	1460	0	NNH A-A-BEND(100).
8	1331	1198	0	S-UMB BEND(100).
9	1198	1078	0.6	NNH S-A-BEND(100).
10	1135	1022	248	A-UMB BEND(98).
11	1109	998	0	N-N STR(101).
12	86	77	144	NN TORS(100).

[a] Frequencies scaled by constant factor of 0.89.

[b] See Table 15 for definition of symmetry coordinate.

TABLE 19. CALCULATION OF INFRARED SPECTRUM OF N_2D_4 (DDNNDD) (6-31G** BASIS) GAUCHE CONFORMATION.

Frequency (cm^{-1})		Intensity	
Unscaled	Scaled[b]	A (km mol^{-1})	PED[c]
a Class			
2828	2517	0	s-a-DND str(98)
2696	2399	0	s-s-DND str(98)
1365	1215	5	NN str(14) + s-scissor (85)
1154	1027	0	NN str(52) + s-DND twist (34)
1055	939	9	NN str(34) + s-DND twist (59)
735	654	58	s-wag (94)
345	307	27	torsion (100)
b Class			
2830	2519	1	a-a-DND str (95)
2686	2391	8	a-s-DND str (96)
1341	1193	7	a-scissor (99)
1080	961	11	a-wag (13) + a-DND twist (85)
805	716	98	a-wag (87) + a-DND twist (13)

[a] See Table 15 for definition of symmetry coordination.

[b] Frequencies scaled by constant factor of 0.89.

Most of the remaining partially deuterated molecules have little or no symmetry, so the calculated spectrum is not separated into symmetric (A Class) or antisymmetric (B Class) vibrations, but presented in order of decreasing frequency. The possible deuterated isomers of hydrazine were listed in Table 5. Tables 20 through 32 present the calculated spectra for all possible deuterium-containing hydrazine molecules. In each case the spectrum was calculated for the gauche conformer of the molecule, using the vibrational parameters calculated for the gauche conformer of N_2H_4, thus, taking into account the change in spectrum as H atoms are replaced by the heavier D atoms.

These tables are arranged in a manner similar to those discussed previously in this section. Table 20 defines the symmetry coordinates used to describe the vibrations of one of the monohydrogen isomers ($DDNND^iH^o \equiv$ iio of Table 5). The calculated wavenumbers (both unscaled and scaled), intensities, and PEDs (defined in terms of the symmetry coordinates of Table 7) are presented for this molecule in Table 21. The results for the other N_2D_3H isomer are presented in Table 22.

The wavenumbers and intensity predicted for the two isomers of N_2D_3H are quite different, showing how different are the dynamical effects when the heavy atom is substituted for an inner hydrogen atom from those for substitution of an outer H atom.

Table 23 defines the symmetry coordinates for one of the isomers of $N_2H_2D_2$; here it is HHNNDD (i1o1 in the notation of Table 5). The vibrational spectrum predicted for this molecule is presented in Table 24.

Table 25 defines symmetry coordinates for both $H^iD^oNND^oH^i$ (oo) and $H^oD^iNND^iH^o$ (ii.) The calculated spectrum for the former molecule (oo) is presented in Table 26, and for (ii) in Table 27.

Table 28 defines the symmetry coordinates for the final isomer of $N_2H_2D_2$, namely for $D^oH^iNND^iH^o$ (i1o2). The calculated vibrational spectrum for this molecule is presented in Table 29.

TABLE 20. SYMMETRY COORDINATE DEFINITION FOR TRIDEUTEROHYDRAZINE $DDNND^{i}H^{o}$.[a]

$S_1 = \Delta r_1$	N_2H^o str.
$S_2 = \Delta r_2$	N_2D^i str.
$S_3 = (1/\sqrt{6})(2\Delta\alpha_1 - \Delta\beta_1 - \Delta\beta_2)$	$H^oN_2D^i$ a-bend
$S_4 = (1/\sqrt{3})(\Delta\alpha_1 + \Delta\beta_1 + \Delta\beta_2)$	$H^oN_2D^i$ umb bend.
$S_5 = (1/\sqrt{2})(\Delta\beta_1 - \Delta\beta_2)$	$N_1N_2H^o/D^i$ a-bend
$S_6 = \Delta R$	NN str
$S_7 = (1/\sqrt{2})(\Delta r_3 + \Delta r_4)$	N_1D s-str
$S_8 = (1/\sqrt{2})(\Delta r_3 - \Delta r_4)$	N_1D a-str
$S_9 = (1/\sqrt{6})(2\Delta\alpha_2 - \Delta\beta_3 - \Delta\beta_4)$	N_1D a-bend
$S_{10} = (1/\sqrt{3})(\Delta\alpha_2 + \Delta\beta_3 + \Delta\beta_4)$	N_1D umb bend
$S_{11} = (1/\sqrt{2})(\Delta\beta_3 - \Delta\beta_4)$	N_2N_1D a-bend
$S_{12} = \Delta\theta$	NN torsion

[a] iio in the notation of Table 5. These are the symmetry coordinates also for the $DDNNH^{i}D^{o}$ (ioo) molecule when D^i is replaced by H^i and H^o by D^o.

Table 30 defines the symmetry coordinates for the two isomers of N_2H_3D. The predicted spectrum for $HHNND^{i}H^{o}$ (i) is presented in Table 31 and that for the other isomer ($HHNND^{o}H^{i}$ (o)) in Table 32.

These tables reveal the rather remarkable dynamic effect from substitution of one deuterium atom in the different positions in N_2H_4 and show how these effects result in quite different vibrational spectra for each possible deuterated isomer of N_2H_4. These predicted spectra have been used to reach the assignments of the experimental spectra already presented in Section II. Further discussion of the significance of the dynamic effects may be possible if these studies are extended.

TABLE 21. CALCULATION OF INFRARED SPECTRUM OF DDNND^{i}H^{o} (iio) (6-31** BASIS).

Frequencies (cm^{-1}) Unscaled	Scaled[a]	Intensities km/mole	PED[b]
3810	3429	3	H_2H^o STR(100).
2829	2546	0.5	N_1D A-STR(97)
2737	2463	2	N_2D^i STR(97)
2690	2421	5	N_1D S-STR(95)
1658	1493	11	$H_oN_2D^i$ A-BEND(87) + $N_1N_2H^o/D^i$ A-BEND(13)
1352	1217	6	N_1D A-BEND(91)
1279	1151	17	$H^oN_2D^i$ UMB BEND(10) + $N_1N_2H^o/D^i$ A-BEND(47) + NN STR(29)
1100	990	5	$N_1N_2H^o/D^i$ A-BEND(25) + NN STR(16) + N_2N_1D A-BEND(46)
1072	965	21	NN STR(48) + N_2N_1D A-BEND(33)
896	807	103	$H^oN_2D^i$ UMB BEND(60) + N_1D UMB BEND(21) + N_2N_1D A-BEND(16)
754	679	71	$H^oN_2D^i$ UMB BEND(17) + N_1D UMB BEND(76)
373	336	29	NN TORS(99)

[a] Frequencies scaled by constant factor of 0.89.

[b] See Tables 14 and 15 for definition of normal modes.

TABLE 22. CALCULATION OF INFRARED SPECTRUM OF $DDNNH^{i}D^{o}$ (ioo) (6-31G** BASIS).

Frequencies (cm^{-1}) Unscaled	Scaled[a]	Intensities km/mole	PED[b]
3751	3376	6	N_2H^i STR(100)
2829	2546	0.6	N_1D A-STR(96)
2779	2501	2	N_2D^o STR(98)
2691	2422	4	N_1D S-STR(97)
1659	1493	8	$D^oN_2H^i$ A-BEND(86) + $N_1N_2D^o/H^i$ A-BEND(14)
1364	1228	6	NN STR(12) + N_1D A-BEND(80)
1219	1097	30	$D^oN_2H^i$ UMB BEND(13) + $N_1N_2D^o/H^i$ A-BEND(56) + N_1D A-BEND(15)
1155	1039	0	$N_1N_2D^o/H^i$ A-BEND(14) + NN (STR(56) + N_2N_1D A-BEND(16)
1077	969	12	NN STR(24) + N_2N_1D A-BEND(67)
859	773	98	$D^oN_2H^i$ UMB BEND(72) + N_2N_1D A-BEND(15)
778	700	68	N_1D UMB BEND(92)
370	333	34	NN TORS(99)

[a] Frequencies scaled by constant factor of 0.89.

[b] See Table 15 for definition of symmetry coordinates.

TABLE 23. SYMMETRY COORDINATE DEFINITION OF DIDEUTEROHYDRAZINE HHNNDD (i1c1).

$S_1 = (1/\sqrt{2})(\Delta r_1 + \Delta r_2)$	ND s-str
$S_2 = (1/\sqrt{2})(\Delta r_1 - \Delta r_2)$	ND a-str
$S_3 = (1/\sqrt{6})(2\Delta\alpha_1 - \Delta\beta_1 - \Delta\beta_2)$	DND a-bend
$S_4 = (1/\sqrt{3})(\Delta\alpha_1 + \Delta\beta_1 + \Delta\beta_2)$	ND umb bend
$S_5 = (1/\sqrt{2})(\Delta\beta_1 - \Delta\beta_2)$	NND a-bend
$S_6 = \Delta R$	NN str
$S_7 = (1/\sqrt{2})(\Delta r_3 + \Delta r_4)$	NH s-str
$S_8 = (1/\sqrt{2})(\Delta r_3 - \Delta r_4)$	NH a-str
$S_9 = (1/\sqrt{6})(2\Delta\alpha_2 - \Delta\beta_3 - \Delta\beta_4)$	HNH a-bend
$S_{10} = (1/\sqrt{3})(\Delta\alpha_2 + \Delta\beta_3 + \Delta\beta_4)$	NH umb bend
$S_{11} = (1/\sqrt{2})(\Delta\beta_3 - \Delta\beta_4)$	NNH a-bend
$S_{12} = \Delta\theta$	NN torsion

TABLE 24. CALCULATION OF INFRARED SPECTRUM OF HHNNDD (i1o1) (6-31G** BASIS).

Frequencies (cm^{-1}) Unscaled	Scaled[a]	Intensities km/mole	PED[b]
3834	3451	1	NH A-STR(92)
3723	3351	8	NH S-STR(92)
2829	2546	0.5	ND A-STR(97)
2691	2422	4	ND S-STR(97)
1829	1646	15	HNH A-BEND(101)
1444	1300	0.3	DND A-BEND(12) + NNH A-BEND(87)
1345	1211	10	DND A-BEND(71) + NN STR(16)
1200	1080	31	DND A-BEND(14) + NND A-BEND(14) + NN STR(41) + NH UMB BEND(31)
1086	977	25	NND A-BEND(47) + NN STR(38) + NH UMB BEND(11)
966	869	105	NND A-BEND(37) + NH UMB BEND(53)
782	704	74	ND UMB BEND(94)
418	376	43	NN TORS(100)

[a] Frequencies scaled by constant factor of 0.89.

[b] See Table 23 for definition of symmetry coordinates.

TABLE 25. SYMMETRY COORDINATE DEFINITION OF DIDEUTEROHYDRAZINE $H^oD^iNND^iH^o$ (ii).[a]

$S_1 = (1/\sqrt{2})(\Delta r_1 + \Delta r_3)$	NH^o s-str
$S_2 = (1/\sqrt{2})(\Delta r_1 - \Delta r_3)$	NH^o a-str
$S_3 = (1/\sqrt{2})(\Delta r_2 + \Delta r_4)$	ND^i s-str
$S_4 = (1/\sqrt{2})(\Delta r_2 - \Delta r_4)$	ND^i a-str
$S_5 = (1/\sqrt{12})[(2\Delta\alpha_1 - \Delta\beta_1 - \Delta\beta_2) + (2\Delta\alpha_2 - \Delta\beta_3 - \Delta\beta_4)]$	HND s-a-bend
$S_6 = (1/\sqrt{12})[(2\Delta\alpha_1 - \Delta\beta_1 - \Delta\beta_2) - (2\Delta\alpha_2 - \Delta\beta_3 - \Delta\beta_4)]$	HND a-a-bend
$S_7 = (1/\sqrt{6})[(\Delta\alpha_1 + \Delta\beta_1 + \Delta\beta_2) + (\Delta\alpha_2 + \Delta\beta_3 + \Delta\beta_4)]$	s-umb bend
$S_8 = (1/\sqrt{6})[(\Delta\alpha_1 + \Delta\beta_1 + \Delta\beta_2) - (\Delta\alpha_2 + \Delta\beta_3 + \Delta\beta_4)]$	a-umb bend
$S_9 = (1/2)[(\Delta\beta_1 - \Delta\beta_2) + (\Delta\beta_3 - \Delta\beta_4)]$	NND/H s-a-bend
$S_{10} = (1/2)[(\Delta\beta_1 - \Delta\beta_2) - (\Delta\beta_3 - \Delta\beta_4)]$	NND/H a-a-bend
$S_{11} = \Delta R$	NN str
$S_{12} = \Delta\theta$	NN torsion

[a] The symmetry coordinate for $D^oH^iNNH^iD^o$ (oo) will be the same as given here, if the symbol H^o is replaced by D^o and D^i by H^i.

TABLE 26. CALCULATION OF INFRARED SPECTRUM OF $D^{o}H^{i}NNH^{i}D^{o}$ (oo) (6-31G** BASIS).

Frequencies (cm^{-1}) Unscaled	Scaled[a]	Intensities km/mole	PED[b]
3761	3385	0.2	NH^{i} S-STR(100)
3742	3367	11	NH^{i} A-STR(100)
2785	2506	4	ND^{o} A-STR(99)
2775	2498	0	ND^{o} S-STR(99)
1686	1518	10	HND A-A-BEND(81) + NND/H A-A-BEND(18)
1633	1470	4	HND S-A-BEND(91)
1239	1115	1	NND/H S-A-BEND(60) + NN STR(34)
1232	1109	62	HND A-A-BEND(16) + A-UMB BEND(26) + NND/H A-A-BEND(58)
1155	1040	0	NND/H S-A-BEND(31) + NN STR(57)
876	788	56	S-UMB BEND(90)
865	778	123	A-UMB BEND(74) + NND/H A-A-BEND(23)
393	353	41	NN TORS(98)

[a] Frequencies scaled by constant factor of 0.89.

[b] See Table 23 for definition of symmetry coordinates.

TABLE 27. CALCULATION OF INFRARED SPECTRUM OF $H^{o}D^{i}NND^{i}H^{o}$ (ii) (6-31G** BASIS).

Frequencies (cm^{-1}) Unscaled	Scaled[a]	Intensities km/mole	PED[b]
3818	3426	6	NH^{o} A-STR(100)
3802	3422	0.1	NH^{o} S-STR(100)
2744	2470	0.2	ND^{i} S-STR(99)
2728	2455	5	ND^{i} A-STR(100)
1702	1532	9	HND S-A-BEND(82) + NND/H S-A-BEND(19)
1615	1453	10	HND A-A-BEND(93)
1321	1189	25	S-UMB BEND(18) + NND/H S-A-BEND(38) + NN STR(36)
1194	1074	9	NND/H A-A-BEND(92)
1081	973	22	NND/H S-A-BEND(28) NN STR(66)
973	875	122	A-UMB BEND(100)
806	725	87	S-UMB BEND(82) + NND/H S-A-BEND(14)
400	360	27	NN TORS(97)

[a] Frequencies scaled by constant factor of 0.89.

[b] See Table 25 for definition of symmetry coordinate.

TABLE 28. SYMMETRY COORDINATE DEFINITION OF DIDEUTEROHYDRAZINE $D^{o}H^{i}NND^{i}H^{o}$ (i1o2).

$S_1 = \Delta r_1$	N_2H^o str
$S_2 = \Delta r_2$	N_2D^i str
$S_3 = (1/\sqrt{6})(2\Delta\alpha_1 - \Delta\beta_1 - \Delta\beta_2)$	$H^oN_2D^i$ a-bend
$S_4 = (1/\sqrt{3})(\Delta\alpha_1 + \Delta\beta_1 + \Delta\beta_2)$	$H^oN_2D^i$ umb bend
$S_5 = (1/\sqrt{2})(\Delta\beta_1 - \Delta\beta_2)$	$N_1N_2H^o/D^i$ a-bend
$S_6 = \Delta R$	NN str
$S_7 = \Delta r_3$	N_1D^o str
$S_8 = \Delta r_4$	N_1H^i str
$S_9 = (1/\sqrt{6})(2\Delta\alpha_2 - \Delta\beta_3 - \Delta\beta_4)$	$D^oN_1H^i$ a-bend
$S_{10} = (1/\sqrt{3})(\Delta\alpha_2 + \Delta\beta_3 + \Delta\beta_4)$	$D^oN_1H^i$ umb bend
$S_{11} = (1/\sqrt{2})(\Delta\beta_3 - \Delta\beta_4)$	$N_2N_1D^o/H^2$ a-bend
$S_{12} = \Delta\theta$	NN tors

TABLE 29. CALCULATION OF INFRARED SPECTRUM OF $D^{o}H^{i}NND^{i}H^{o}$ (i1o2) (6-31G** BASIS).

Frequencies (cm^{-1}) Unscaled	Scaled[a]	Intensities km/mole	PED[b]
3810	3429	3	N_2H^{o} STR(100)
3751	3376	6	N_1H^{i} STR(100)
2780	2502	2	N_1D^{o} STR(99)
2736	2463	3	N_2D^{i} STR(99)
1661	1495	8	$H^{o}N_2D^{i}$ A-BEND(33) + $D^{o}N_1H^{i}$ A-BEND(55)
1657	1492	11	$H^{o}N_2D^{i}$ A-BEND(54) + $D^{o}N_1H^{i}$ A-BEND(32)
1288	1159	13	$N_1N_2H^{o}/D^{i}$ A-BEND(42) + NN STR(38)
1229	1106	35	$H^{o}N_2D^{i}$ UMB BEND(10) $D^{o}N_1H^{i}$ A-BEND(10) $N_2N_1D^{o}/H^{i}$ A-BEND(66)
1098	989	9	$N_1N_2H^{o}/D^{i}$ A-BEND(33) + NN STR(59)
920	828	120	$H^{o}N_2D^{i}$ UMB BEND(41) + $D^{o}N_1H^{i}$ UMB BEND(39) + $N_2N_1D^{o}/H^{i}$ A-BEND(16)
835	752	73	$H^{o}N_2D^{i}$ UMB BEND(44) + $D^{o}N_1H^{i}$ UMB BEND(45)
396	357	35	NN TORS(98)

[a] Frequencies scaled by constant factor of 0.89.

[b] See Table 28 for definition of symmetry coordinates.

TABLE 30. SYMMETRY COORDINATE DEFINITION OF MONODEUTEROHYDRAZINE $HHNNH^{o}D^{i}$ (i).[a]

$S_1 = \Delta r_1$	N_2H^o str
$S_2 = \Delta r_2$	N_2D^i str
$S_3 = (1/\sqrt{6})(2\Delta\alpha_1 - \Delta\beta_1 - \Delta\beta_2)$	HN_2D a-bend
$S_4 = (1/\sqrt{3})(\Delta\alpha_1 + \Delta\beta_1 + \Delta\beta_2)$	N_2HD umb bend
$S_5 = (1/\sqrt{2})(\Delta\beta_1 - \Delta\beta_2)$	N_1N_2H/D a-bend
$S_6 = \Delta R$	NN str
$S_7 = (1/\sqrt{2})(\Delta r_3 + \Delta r_4)$	N_1H s-str
$S_8 = (1/\sqrt{2})(\Delta r_3 - \Delta r_4)$	N_1H a-str
$S_9 = (1/\sqrt{6})(2\Delta\alpha_2 - \Delta\beta_3 - \Delta\beta_4)$	HN_1H a-bend
$S_{10} = (1/\sqrt{3})(\Delta\alpha_2 + \Delta\beta_3 + \Delta\beta_4)$	N_1H umb bend
$S_{11} = (1/\sqrt{2})(\Delta\beta_3 - \Delta\beta_4)$	N_2N_1H a-bend
$S_{12} = \Delta\theta$	NN torsion

[a] The symmetry coordinates for $HHNNH^{i}D^{o}$ (o) are the same, if H^o is replaced by D^o and D^i by H^i.

TABLE 31. CALCULATION OF INFRARED SPECTRUM OF HHNND^{i}H^{o} (i) (6-31G** BASIS).

Frequencies (cm^{-1}) Unscaled	Scaled[a]	Intensities km/mole	PED[b]
3835	3452	1	N_1H A-STR(87)
3809	3428	3	N_2H^{o} STR(94)
3723	3350	7	N_1H S-STR(92)
2736	2463	3	N_2D^{i} STR(99)
1834	1650	14	HN_1H A-BEND(98)
1662	1496	9	HN_2D A-BEND(82) + N_1N_2H/D A-BEND(12)
1423	1281	7	N_2N_1H A-BEND(89)
1299	1169	19	N_1N_2H/D A-BEND(38) + NN STR(36) + N_1H UMB BEND(15)
1114	1003	20	N_1N_2H/D A-BEND(41) + NN STR(50)
1037	934	150	HN_2D UMB BEND(21) + N_1H UMB BEND(68)
860	774	93	HN_2D UMB BEND(71) + N_1H UMB BEND(16)
442	397	39	NN TORS(99)

[a] Frequencies scaled by constant factor of 0.89.

[b] See Table 30 for definition of symmetry coordinate.

TABLE 32. CALCULATION OF INFRARED SPECTRUM OF $HHNNH^{i}D^{o}$ (o) (6-31G** BASIS).

Frequencies (cm^{-1})		Intensities	
Unscaled	Scaled[a]	km/mole	PED[b]
3834	3451	0.8	N_1H A-STR(92)
3753	3378	3	N_2H^{i} STR(93)
3721	3349	10	N_1H S-STR(86)
2780	2502	2	N_2D^{o} STR(99)
1831	1647	15	HN_1H A-BEND(100)
1663	1497	6	HN_2D A-BEND(84) + N_1N_2H/D A-BEND(12)
1428	1285	4	N_2N_1H A-BEND(93)
1240	1116	36	HN_2D UMB BEND(12) N_1N_2H/D A-BEND(61) + NN STR(13)
1208	1087	28	NN STR(67) + N_1H UMB BEND(27)
980	882	121	N_1N_2H/D A-BEND(17) + NN STR(14) + N_1H UMB BEND(64)
878	790	83	HN_2D UMB BEND(83)
438	394	50	NN TORS(99)

[a] Frequencies scaled by constant factor of 0.89.

[b] See Table 30 for definition of symmetry coordinate.

D. CALCULATIONS FOR MONOMETHYLHYDRAZINE

Finally, calculations of the infrared spectrum for monomethylhydrazine (Figure 15) (CH_3NHNH_2) were made using a 3-21G basis set. These results are attached (Tables 33 and 34) and summarized in Figure 25, which compares the calculated spectrum with a simulation of the experimental spectrum of CH_3NHNH_2 isolated in an Ar matrix (Reference III-19). The quality of the calculation is not as good as reported above for hydrazine and its deuterated derivatives because the basis set for CH_3NHNH_2 is smaller (3-21G here compared with 6-31G** for hydrazine). However, we believe that the calculated spectrum provides a basis for interpretation of the experimental spectrum. The principal uncertainty comes in the prediction of the spectrum in the bending region (1000-650 cm^{-1}) where it would appear that our force constants are somewhat is error, so that the mixing of the N-N stretching mode with the C-N stretch and NH_2 wag is not in agreement with experiment. We believe the errors in predicting these force constants are due to use of the small 3-21G basis set, so that much better agreement could be expected if the calculation were repeated with a 6-31G** basis set. Even so, the present calculation seems good enough to provide a basis for the assignment.

TABLE 33. MONOMETHYL HYDRAZINE SYMMETRY COORDINATE DEFINITION.

$S_1 = \Delta r_{12}$	NN str
$S_2 = \Delta r_{24}$	NC str
$S_3 = (1/\sqrt{2})(\Delta r_{15} + \Delta r_{16})$	NH_2 s-str
$S_4 = (1/\sqrt{6})(2\Delta\alpha_{56} - \Delta\beta_{25} - \Delta\beta_{26})$	NH_2 sciss
$S_5 = (1/\sqrt{2})(\Delta r_{15} - \Delta r_{16})$	NH_2 a-str
$S_6 = (1/\sqrt{2})(\Delta\beta_{25} - \Delta\beta_{26})$	NH_2 twist
$S_7 = (1/\sqrt{3})(\Delta\alpha_{56} + \Delta\beta_{25} + \Delta\beta_{26})$	NH_2 wag
$S_8 = \Delta r_{23}$	N_2H_3 str
$S_9 = (1/\sqrt{2})(\Delta\alpha_{13} - \Delta\alpha_{43})$	NH perpendicular bend
$S_{10} = (1/\sqrt{3})(\Delta\alpha_{13} + \Delta\alpha_{43} + \Delta\beta_{14})$	NH parallel bend
$S_{11} = (1/\sqrt{6})(2\Delta\beta_{14} - \Delta\alpha_{13} - \Delta\alpha_{43})$	NNC bend
$S_{12} = (1/\sqrt{3})(\Delta r_{47} + \Delta r_{48} + \Delta r_{49})$	CH_3 s-str
$S_{13} = 0.38827\Delta\alpha_{89} + 0.41240(\Delta\alpha_{78} + \Delta\alpha_{79})$ $-0.40186\Delta\beta_{27} - 0.40315(\Delta\beta_{28} + \Delta\beta_{29})$	CH_3 s-def
$S_{14} = (1/\sqrt{6})(2\Delta r_{47} - \Delta r_{48} - \Delta r_{49})$	CH_3 in-plane a-str
$S_{15} = 0.83241\Delta\alpha_{89} - 0.39185(\Delta\alpha_{78} + \Delta\alpha_{79})$	CH_3 in-plane a-def
$S_{16} = 0.80990\Delta\beta_{27} - 0.41477(\Delta\beta_{28} + \Delta\beta_{29})$	CH_3 in-plane rock
$S_{17} = (1/\sqrt{2})(\Delta r_{48} - \Delta r_{49})$	CH_3 out-of-plane a-str
$S_{18} = (1/\sqrt{2})(\Delta\alpha_{78} - \Delta\alpha_{79})$	CH_3 out-of-plane a-def
$S_{19} = (1/\sqrt{2})(\Delta\beta_{28} - \Delta\beta_{29})$	CH_3 out-of-plane rock
$S_{20} = \tau_{NN}$	NN torsion
$S_{21} = \tau_{CN}$	CN torsion

Note: Constants used in S_{13}, S_{15} and S_{16} are calculated using method suggested by Matsuura and Tasumi. (H. Matsuura and M. Tasumi, "Force Fields for Large Molecules," Chapter 2, in Vibrational Spectra and Structure, Vol. 12, (J. R. Durig, ed.), Elsevier, Amsterdam, 1983).

TABLE 34. CALCULATION OF INFRARED SPECTRUM OF MONOMETHYL-HYDRAZINE (6-31G** BASIS).

Frequencies (cm^{-1}) Unscaled	Scaled[a]	Intensities km/mole	PED[b]
3757	3343	1	NH_2 s-str(10) NH_2 a-str(90)
3645	3244	3	NH_2 s-str(14) + N_2H_3 str(85)
3616	3218	8	NH_2 s-str(77) + N_2H_3 str(14)
3304	2940	24	CH_3 s-str(10) CH_3 in-pl a-str(10) CH_3 o-o-Pl a-str(80)
3235	2879	49	CH_3s-str(30) + CH_3 in-pl a-str(50) + CH_3 o-o-Pl a-str(20)
3148	2802	75	CH_3 s-str(60) + CH_3 in-pl a-str(40)
1848	1644	10	NH_2 sciss(99)
1697	1510	2	CH_3O-O-Pl a-def(76)
1670	1486	10	CH_3 in-pl a-def(75)
1640	1460	1	NH perpend bend(86)
1602	1425	0	CH_3s-def(90) + CH_3 in-pl a-def(10)
1396	1243	6	NH_2 twist(87)
1291	1149	6	NNC bend(16) + CH_3 O-O-Pl rock(64)
1260	1121	8	NN str(12) + NC str(10) + CH_3 in-pl rock(66)
1222	1087	3	NN str(39) + NC str(25) + CH_3 in-pl rock(17)
1011	900	4	NN str(22) + NC str(35) + NH parallel bend(15) + CH_3O-O-Pl rock(17)

TABLE 34. CALCULATION OF INFRARED SPECTRUM OF MONOMETHYL-HYDRAZINE (6-31G** BASIS).

(Concluded)

Frequencies (cm^{-1}) Unscaled	Scaled[a]	Intensities km/mole	PED[b]
911	811	231	NC str(17) + NH_2 wag(58) + NH parallel bend(11) NNC bend(10)
764	680	56	NN str(25) + NH_2 wag(29) + NH parallel bend(26)
457	406	21	NH parallel bend(21) + NNC bend(58) + NN tors(11)
329	293	63	NH parallel bend (14) + NN tors(82)
250	222	3	CN torrs(94)

[a] Scale factor is 0.89.
[b] See Table 33 for definition of symmetry coordinates.

Monomethyl-hydrazine.

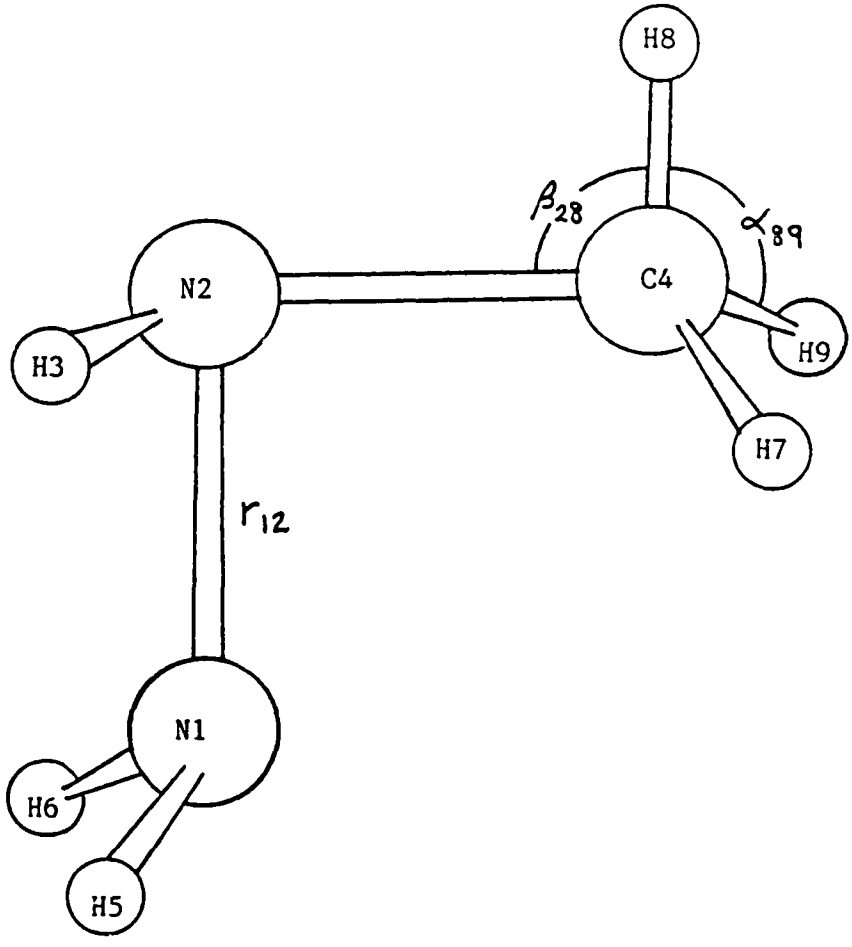

Figure 25. The Expected Most Stable Conformational Form of Monomethylhydrazine, Showing the CH_3 Group Substituted for one of the Outer H Atoms.

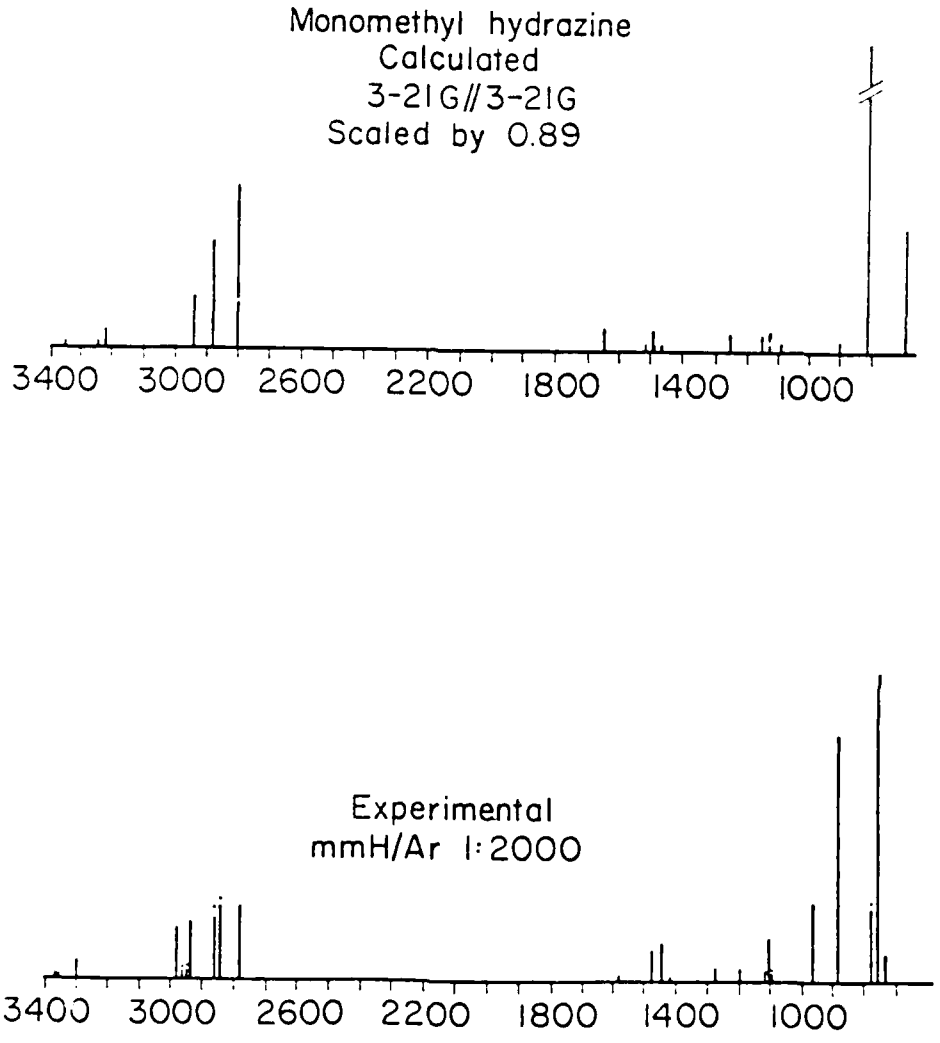

Figure 26. Comparison Between a Simulation of the Calculated Spectrum, Showing Lines Whose Height is Proportional to the Predicted Intensity Plotted Against the Scaled (0.89) Predicted Wavenumber, Compared with the Corresponding Simulation of the Observed Experimental Spectrum of CH_3NHNH_2 in an Ar Matrix (T. Tipton, Reference III-4). The Lines in the Experimental Spectrum Marked by • were not Attributed (Reference III-19) to Absorption by Fundamental Modes of Monomethylhydrazine in its Expected Dominant Tautomeric Form.

SECTION IV

INFRARED SPECTROSCOPY OF MATRIX-ISOLATED COMPLEXES OF HYDRAZINE AND AMMONIA WITH THE NEUTRAL TRANSITION METALS Cu AND Fe

A. INTRODUCTION

Hydrazine is used in auxiliary power units, small thrusters, and as a rocket propellant and is, therefore, of great interest to the Air Force Because of the potential for hydrazine spills the Air Force is interested in developing a data base on the interaction of hydrazine with clay minerals. Since clay minerals often contain transition metals which may attract hydrazine, studies were undertaken on the possible complexation of hydrazine with copper, and iron.

Hydrazine complexes strongly with the ions of the transition metals. Many studies on the infrared spectra of complexes of hydrazine with various transition metal ions have been reported (Reference IV-1). The interaction of neutral transition metal atoms with hydrazine is, however, virtually unknown. This report presents the results of an investigation of the Fourier transform infrared spectra (FTIR) of complexes of hydrazine with neutral copper and iron atoms isolated in argon matrices at 12 K. Parallel studies on the complexes of ammonia with copper or iron are also reported.

The major findings of this study are: (1) the $Cu \cdot NH_3$ and $Fe \cdot NH_3$ complexes exhibit relatively large frequency shifts (particularly in the ν_2 umbrella mode region) with the $Fe \cdot NH_3$ shift being larger than the $Cu \cdot NH_3$; (2) the $Cu \cdot N_2H_4$ and $Fe \cdot N_2H_4$ complexes show practically identical shifts. These shifts are considerably smaller than the analogous ammonia complex shifts. The present observations are consistent with the recent constrained-space-orbital-variation computations reported by Bauschlicher (Reference IV-2) on the $Cu \cdot NH_3$ complex (amongst others). In this theoretical study, the bonding was ascribed to a favorable electrostatic interaction between the NH_3 dipole moment and an effective polarized metal atom dipole moment.

B. EXPERIMENTAL

The matrix deposition apparatus is shown schematically in Figure 35.

Copper or iron metal (Spex Industries) was vaporized from a tantalum Knudsen cell resistively heated in the range 1200-1450 °C for Cu and in the range 1500-1700 °C for iron. The cell temperature was monitored by an optical pyrometer (Leeds and Northrup). The hydrazine/argon and ammonia/argon gas mixtures were prepared in a vacuum line and stored in 5.0-L Pyrex® bulbs. A variety of concentration ratios of complexing gas to argon were tried: the best results were obtained with a ratio of 200:1 of Ar:NH_3 or Ar:N_2H_4. The ammonia (Matheson, 99.9 percent) and argon (Matheson, 99.999 percent) were used as received whereas the hydrazine (Aldrich) was subjected to vacuum distillation before mixing. NH_3 and Ar were run through several freeze (to 77 K)-pump-thaw degassing cycles before preparation of the gas mixtures. Deposition rates of 1 mmol/h were used for 4- to 10-hour periods. Just before deposition the gases (NH_3, Ar) were passed through a coil of stainless steel tubing cooled in a dry-ice/acetone slush bath.

Copper atoms encounter the N_2H_4 or NH_3 ligands in the active region between the nozzle and the deposition window (cf. Figure 35). The deposition window (CsI) is mounted in a copper holder which is secured to the cold finger of a closed-cycle helium refrigerator (Displex 202, Air Products). The sample window was maintained at 10-12 K, as measured by a Fe-Au-chromel thermocouple attached to the Cu window support. After deposition the cryostat was rotated 90° so that the deposition window was aligned in the optical path of the FTIR spectrometer.

Infrared absorption spectra were obtained on a Nicolet 7199 FTIR spectrometer using 2 cm^{-1} resolution (cooled HgCdTe detector). The absolute band positions are, therefore, expected to have an accuracy of better than 1 cm^{-1}.

C. RESULTS

1. Metal•Ammonia Complexes

Ammonia is a symmetric top molecule (C_{3v} group). Four vibrational infrared bands have been observed for NH_3 (Reference IV-3). The ν_2 umbrella mode exhibits a strong integrated intensity (2919 km $mole^{-1}$) in the gas phase. The other modes are significantly weaker (ν_1: 80 km $mole^{-1}$; ν_3: 50

km mole^{-1} and ν_4: 256.9 km mole^{-1}). In matrix studies, impurities can sometimes obscure some of these bands. In the present studies, water impurity interfered with the ν_4 mode in the 1500-1700 cm^{-1} region. As a result, only the vibrational activity due to the ν_1, ν_2 and ν_3 modes (Tables 35, 36 and 37) is reported here.

Isolated in rare gas matrices, ammonia undergoes nearly-free rotation about its threefold axis (Reference IV-4). The generally accepted (Reference IV-4) assignments for the rotational and inversional structure of the ν_2 umbrella mode of matrix-isolated NH_3 are given in Figure 36. In addition, bands due to the NH_3 dimer (Reference IV-5), the $H_2O \cdot NH_3$ complex (Reference IV-6) and the $CO_2 \cdot NH_3$ complex (Reference IV-7) are so indicated in the figure (also Table 37).

Upon deposition of NH_3 with Cu or Fe several new bands have been observed to grow in to higher energies of this intricately structured set of bands. The most prominent of these at 1117 cm^{-1} (Cu/NH_3) and 1130 cm^{-1} (Fe/NH_3) are assigned to perturbed ν_2 bending modes in the 1:1 Metal$\cdot NH_3$ complex. They are shifted 143 cm^{-1} ($Cu \cdot NH_3$) and 156 cm^{-1} ($Fe \cdot NH_3$) to the blue of the free ammonia (in Ar) band at 974 cm^{-1}. The analysis of the other bands in this region is currently being carried out. The shift probably results from a nearly free rotation of the NH_3 portion of the metal$\cdot NH_3$ complex about its threefold axis. Cu and, most probably, Fe occupy substitutional sites (Reference IV-8) in the rare gas lattices and the rotation of the NH_3 in the metal complex may not be greatly different from that in Ar, Kr, or Xe.

The assignment of the 1117 cm^{-1} (1130 cm^{-1}) band to the perturbed ν_2 band in the $Cu \cdot NH_3$ ($Fe \cdot NH_3$) complex is completely consistent with previous assignments by Sūzer and Andrews (Reference IV-7) on the complexes of the alkali metals with NH_3 (cf. Table 36). The shifts in the ν_2 region make it clear that the $Fe \cdot NH_3$ and $Li \cdot NH_3$ complexes have similar strengths. The $Cu \cdot NH_3$ is somewhat weaker.

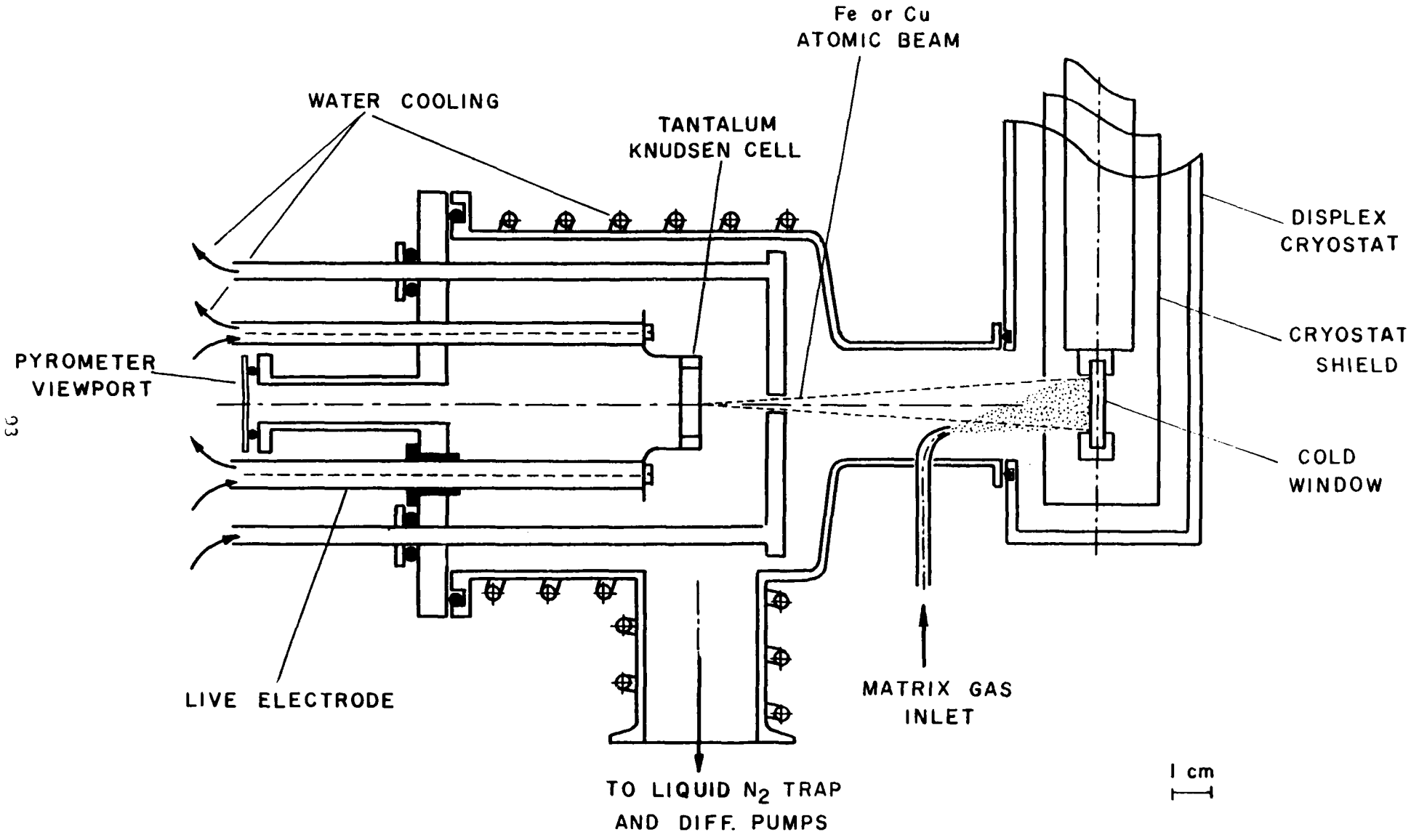

Figure 27. Schematic of the Vacuum Chamber/Furnace and Deposition Cryostat.

TABLE 35. INFRARED ABSORPTION BANDS AND ASSIGNMENTS OF ARGON MATRIX-ISOLATED AMMONIA AND ITS COMPLEXES WITH COPPER AND IRON ATOMS IN THE ν_2 NH BENDING REGION

NH_3[a] (cm^{-1})	$Cu \cdot NH_3$ (cm^{-1})	$Fe \cdot NH_3$ (cm^{-1})	Assignment, Remarks
	1186	1184	
	1176	1171	
	1164	1165	
	1153	1153	
	1142		
		1137	$\nu_2(Fe \cdot NH_3)$
		1130	
	1129		
	1124		$\nu_2(Cu \cdot NH_3)$
	1117		
		1108	
		1100	
	1054	1054sh	(1060, pure solid[b])
		1050?	(1047, aggregate[b])
	1042sh	1042	
1035	1035	1035	$\nu_2(NH_3 \cdot H_2O$[c])
	1027	1027	aggreggate[b]
	1017	1017	trimer[b]
1013	1012sh	1013	$R(1_0^+)$, $R(1_1^-)$[a]
	1000	1000	dimer[a-c]
	991	992	$R(1_1^+)$[a]
		990	
980sh	980sh	980sh	$Q(1_1^-)$[a]
974.2	974	974.7	$R(0_0^-)$[a]
961.6	962	962	$P(1_0^+)$[a]
955	955sh	955	$Q(1_1^+)$[a]

[a] Reference IV-4.
[b] Reference IV-5.
[c] Reference IV-6.

TABLE 36. COMPARISON OF INFRARED ADSORPTION PEAK POSITIONS AND SHIFTS OF AMMONIA AND ITS COMPLEXES WITH THE ALKALI METALS AND COPPER AND IRON

Species	NH Stretch[a]		NH Bend[a]		NH Stretch[a]	
	ν_1	$\Delta\nu_1$	ν_2	$\Delta\nu_2$	ν_3	$\Delta\nu_3$
NH_3	3346	--	974	--	3447	--
$Cu \cdot NH_3$	3212	134	1117	143	3392?	55
$Fe \cdot NH_3$	--	--	1130	156	3381	66
$Li \cdot NH_3$[b]	3277	69	1133	159	3379	68
$Na \cdot NH_3$[b]	3294	52	1079	105	--	--
$K \cdot NH_3$[b]	3292	54	1064	90	--	--
$Cs \cdot NH_3$[b]	3287	59	1049	75	--	--

[a] All entries are in cm^{-1}.
[b] From Reference IV-7.

TABLE 37. INFRARED ABSORPTION BANDS AND ASSIGNMENTS OF ARGON MATRIX-ISOLATED AMMONIA AND ITS COMPLEXES WITH COPPER AND IRON ATOMS

NH_3 (cm^{-1})	$Cu \cdot NH_3$ (cm^{-1})	$Fe \cdot NH_3$ (cm^{-1})	Assignment, Remarks
3450,[a] 3447[b]	3446	3447	$\nu_3(NH_3)$
	3435	3435.6	$\nu_{H_2O}(H_2O \cdot NH_3)$
	3400	3400	Dimer[b]
	3392		$\nu_3(NH_3 \cdot Cu)$
		3381	$\nu_3(NH_3 \cdot Fe)$
3348,[a] 3346[b]			$\nu_1(NH_3)$
	3329	3328	$\nu_{NH_3}(NH_3 \cdot CO_2)$[b]
	3310	3310	Dimer[b]
	3242	3242	Dimer[b]
	3212		$\nu_1(NH_3 \cdot Cu)$
		3209?	$\nu_1(NH_3 \cdot Fe)$
		3204?	

[a] Reference IV-6.
[b] Reference IV-7.

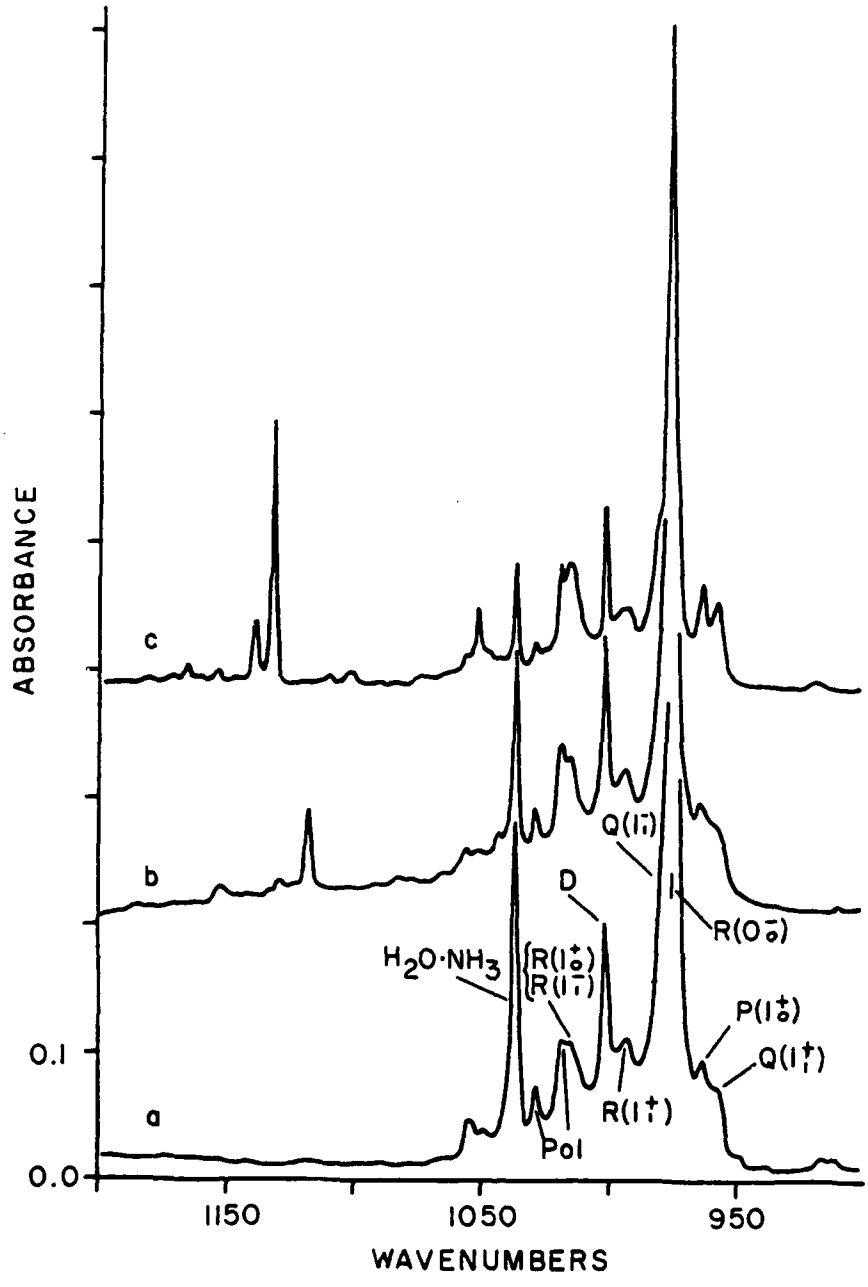

Figure 28. Infrared Spectra of Argon Matrix-Isolated (a) NH_3, (b) Codeposition Mixture of NH_3 and Cu and (c) Codeposition Mixture of NH_3 and Fe.

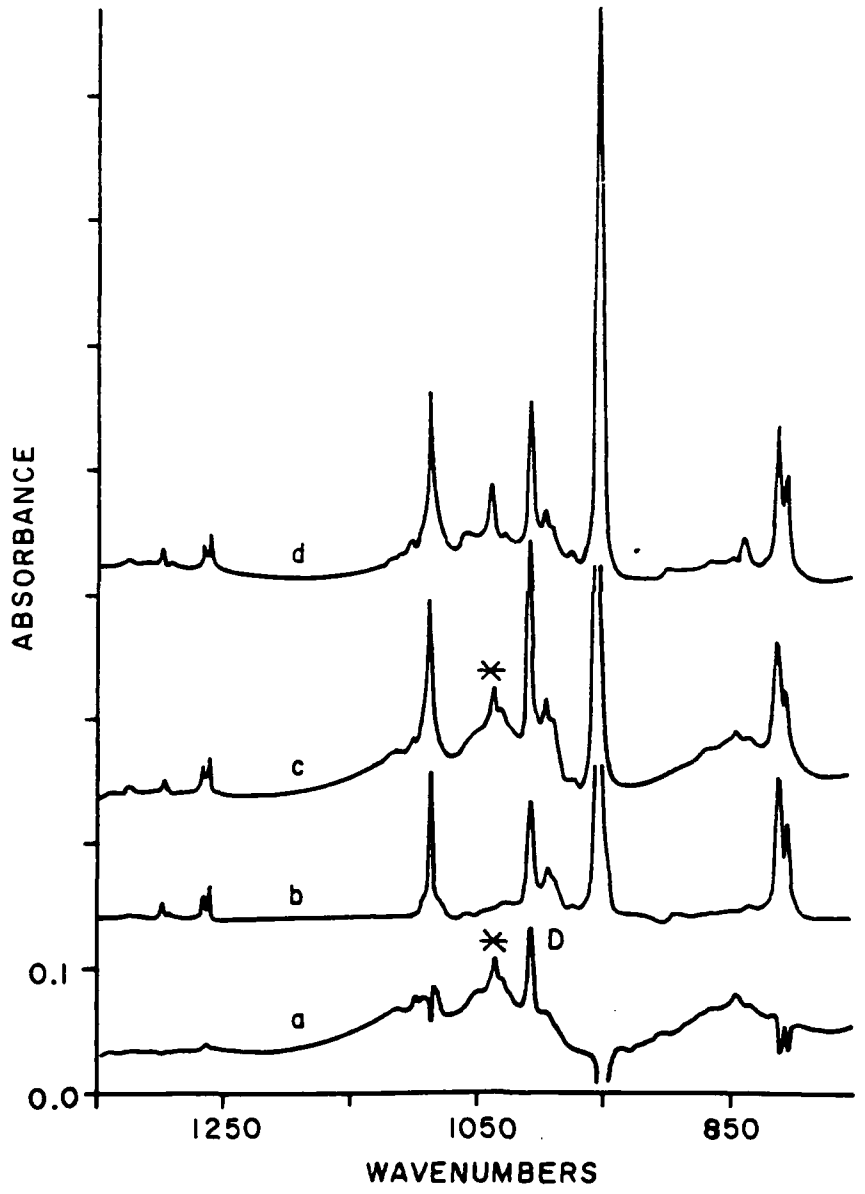

Figure 29. Infrared Spectra of Argon Matrix-Isolated (b) N_2H_4, (c) Codeposition Mixture of N_2H_4 and Cu, (d) N_2H_4 and Fe and (a) Subtraction of (b) from (c).

Shifts are also observed in the NH stretching region (cf. Table 36). The ν_2 mode at ~3450 cm^{-1} shifts to 3392 cm^{-1} and 3381 cm^{-1} in the Cu and Fe complexes, respectively. Similarly, the ν_1 mode at ~3347 cm^{-1} shifts to 3212 cm^{-1} and (probably) 3209 cm^{-1} in the Cu and Fe complexes, respectively. As in the ν_2 region the shifts for the $Fe \cdot NH_3$ complex are greater for the ν_1 and ν_3 bands than they are for $Cu \cdot NH_3$. Interestingly, these shifts (for both the Cu and Fe complexes) are in opposite directions. Upon complexation the ν_1 and ν_3 bands shift to lower energies, while the ν_2 bands shift to higher energies. Similar behavior has been observed previously in complexes involving hydrogen bonding (Reference IV-9).

2. Metal•Hydrazine Complexes

Table 38 and Figure 29 show the results of the metal atom•hydrazine complex formation experiments. Water impurity and low band intensity effectively precluded the precise measurement of any shifted bands in the 1500-1700 cm^{-1} and 3200-3400 cm^{-1} regions. The region from 700-1400 cm^{-1} (the ν_2 region) was therefore the central focus of this phase of these studies.

Figure 29b shows the spectrum of N_2H_4 in an Ar matrix in this region. The assignments of the various N_2H_4 bands are due to Tipton, Stone, Person and Kubulat (Reference IV-10). Also shown in Figure 29 are the spectra obtained upon codeposition of N_2H_4 with Fe atoms (Figure 29d) or Cu atoms (Figure 29c). Several new bands can be discerned at 838 cm^{-1} and 1038 cm^{-1} in Figure 29d (Fe) and at 843 cm^{-1} and 1035 cm^{-1} in Figure 29c (Cu). These bands are assigned as perturbed NNH bending vibrations. Most likely they originate from the ν_6 and ν_{12} free hydrazine motions (Table 38). To accentuate the difference between the $Cu \cdot N_2H_4$ complex and the free N_2H_4 spectra, spectral subtraction of Figure 29b from 29c has been done. The result is shown in Figure 29a. The new $Cu \cdot N_2H_4$ complex bands (marked with *) stand out clearly. The N_2H_4 dimer band at 1007 cm^{-1} is more intense in Figure 29c. Its growth is compared to Figure 29b, and appears as a positive peak in Figure 29a, presumably due to the increased diffusion of hydrazine in the matrix under the deposition conditions used for vaporizing the metals (i.e., radiative heating of the matrix from the hot Knudsen cells).

TABLE 38. INFRARED ABSORPTION BANDS AND ASSIGNMENTS OF ARGON MATRIX-ISOLATED HYDRAZINE AND ITS COMPLEXES WITH COPPER AND IRON ATOMS IN THE 800-1300 cm^{-1} REGION.

N_2H_4 (cm^{-1})	$Cu \cdot N_2H_4$ (cm^{-1})	$Fe \cdot N_2H_4$ (cm^{-1})	Assignments, Remarks
804	804	804	ν_6: δNH_2, δNNH[a]
811	811	811	
	834		
		838	$\nu(N_2H_4 \cdot Fe)$
	843		$\nu(N_2H_4 \cdot Cu)$
954	954	954	ν_{12}: δNNH, δNH_2[a]
974	974	974	ammonia
988	988	988	$\nu_{N_2H_4}(N_2H_4 \cdot H_2O)$
994	994	994	
1007	1007	1007	$\nu_{N_2H_4}$(dimer)[a]
1029	1029	1029	aggregate
	1035		$\nu(N_2H_4 \cdot Cu)$
		1038	$\nu(N_2H_4 \cdot Fe)$
1086	1086	1086	ν_5: νNN[a]
1261	1261	1261	ν_{11}: δNNH
1266	1266	1266	
1193	1293	1293	ν_4: δNNH
1299	1299	1299	

[a] Reference IV-10.

The differences between the $Cu \cdot N_2H_4$ and $Fe \cdot N_2H_4$ complexes' band positions are relatively small. Their shifts are nearly identical. This is particularly evident when the analogous shifts in the metal•ammonia complexes are compared (Tables 35, 36). In these complexes, the shifts are much larger and the differences between the Cu and Fe complexes are greater. These observations are critical to the conclusions drawn in the next section about the bonding mechanisms in the ammonia versus the hydrazine complexes.

3. Normal Coordinate Calculations on Metal•Ammonia Complexes

To study more closely the effect of metal complexation on the various modes of ammonia, normal coordinate calculations were performed on $Cu \cdot NH_3$ and $Fe \cdot NH_3$ complexes. The geometry chosen and internal coordinates used are diagrammed in Figure 30. The atomic cartesian coordinates and the complex symmetry coordinates and overall point group (C_{3v}) symmetries are listed in Tables 31 and 32. The N-metal bond length was arbitrarily chosen as 2.1 Å with the metal atom lying on the C_3 axis where it would best interact with the ammonia lone pair orbital. The internal coordinate force constants (F_{NH} and F_{HNH}) of the NH_3 moiety were determined from Gaussian 82 calculations and were transferred directly to the $metal \cdot NH_3$ complex. The force constant, $F_{HNMetal}$, was varied between 0.05 and 0.6 mdyn/Å while holding the force constant F_{NMetal} fixed at a value in the range 0.05 to 5.0 mdyn/Å. Then the inverse operation was performed. From the result of 60 calculations, it was found for the $Fe \cdot NH_3$ complex that

- $\nu_{as}(NH)$ varies insignificantly (3457 to 3458 cm^{-1}),
- $\nu_s(NH)$ also varies insignficantly (3333 to 3336 cm^{-1}),
- $\delta_{as}(HNH)$ varies slightly (1632 to 1655 cm^{-1}),
- $\delta_s(umb)$ varies significantly (1068 to 1460 cm^{-1}),
- $\delta_{as}(HNFe)$ varies greatly (261 to 893 cm^{-1}), and
- $\nu(NFe)$ varies tremendously (73 to 708 cm^{-1}).

Similar results were found for the $Cu \cdot NH_3$ calculation. Those modes directly involving the metal atom were predicted to vary greatly with the force constants chosen. Of special significance are the large shifts predicted for the δ_s umbrella mode upon metal complexation. (As expected, this mode shifts most for a change in the F_{HNFe} force constant.)

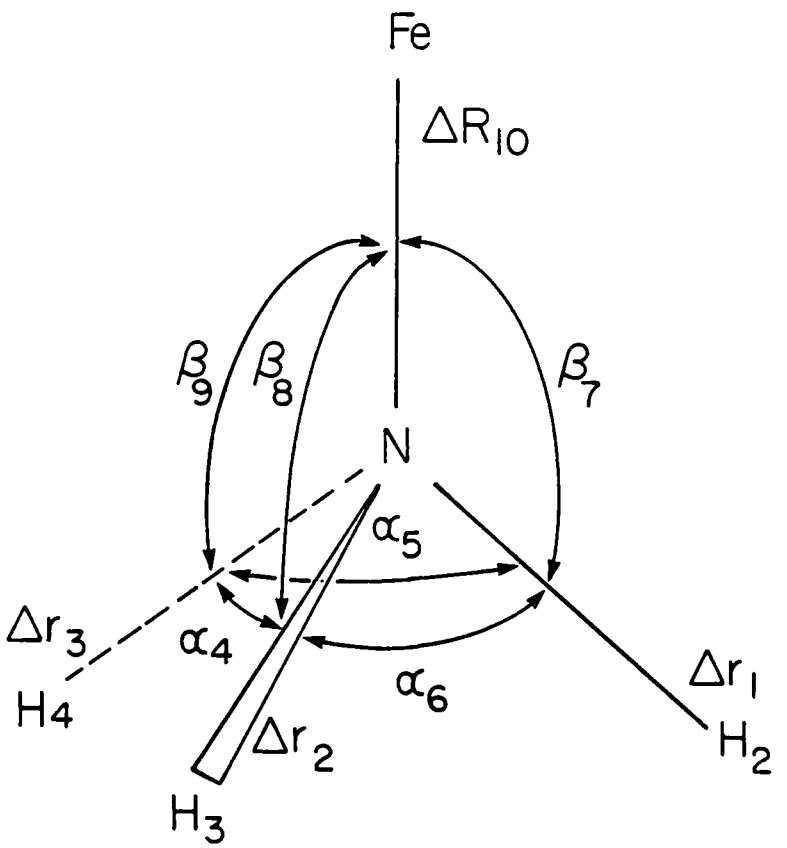

Figure 30. Assumed Geometry and Internal Coordinates of the $Fe \cdot NH_3$ and $Cu \cdot NH_3$ Complexes.

TABLE 39. CARTESIAN COORDINATES FOR THE 1:1 NEUTRAL METAL ATOM-AMMONIA COMPLEX

	x^a	y^a	z^a
N_1	0.000000	0.000000	0.000000
H_2	0.932565	0.000	-0.363764
H_3	-0.466282	-0.807625	-0.363764
H_4	-0.466282	0.807625	-0.363764
$metal_5$	0.00000	0.00000	2.10000

[a] All entries in Å.

TABLE 40. SYMMETRY COORDINATE DEFINITIONS FOR THE 1:1 NEUTRAL METAL ATOM•AMMONIA COMPLEX

$S_1 = \Delta R_{10}$	a_1	ν_s(NFe)
$S_2 = (\Delta r_1+\Delta r_2+\Delta r_3)/\sqrt{3}$	a_1	ν_s(NH)
$S_3 = (\Delta\alpha_4+\Delta\alpha_5+\Delta\alpha_6-\Delta\beta_7-\Delta\beta_8-\Delta\beta_9/\sqrt{6}$	a_1	δ_s(umb)
$S_4 = (2\Delta r_1-\Delta r_2-\Delta r_3)/\sqrt{6}$	e	ν_{as}(NH)
$S_7 = (\Delta r_1-\Delta r_3)/\sqrt{2}$		
$S_5 = (2\Delta\alpha_4-\Delta\alpha_5-\Delta\alpha_6)/\sqrt{6}$	e	δ_{as}(HNH)
$S_8 = (\Delta\alpha_4-\Delta\alpha_6)/\sqrt{2}$		
$S_6 = (2\Delta\beta_7-\Delta\beta_8-\Delta\beta_9)/\sqrt{6}$	e	δ_{as}(NHFe)
$S_9 = (\Delta\beta_7-\Delta\beta_9)/\sqrt{2}$		

This result is confirmation of the assignment given above of the 1117 cm^{-1} ($Cu \cdot NH_3$) and 1130 cm^{-1} ($Fe \cdot NH_3$) bands to perturbed ν_2 modes. The results of the best-fit calculation are shown in Table 41. There it can be seen that both the perturbed umbrella modes and the perturbed ν_{as} NH stretching modes can be fit well. Other bands in the accessible IR range could not be identified with certainty due to interferences from water impurities and weak band strengths. Interestingly, the F_{NMetal} force constant for $Fe \cdot NH_3$ is twice as large as for $Cu \cdot NH_3$ (3.0 mdyn/Å vs. 1.5 mdyn/Å) with $F_{HNMetal}$ = 0.1 mdyn/Å in both complexes. This result is compatible with the qualitative conclusion drawn above that the $Fe \cdot NH_3$ complex is stronger than $Cu \cdot NH_3$.

D. DISCUSSION

Previous matrix isolation studies (References IV-6, IV-11) of NH_3 complexes with strong acids such as HF and weak ones like H_2O have demonstrated substantial shifts of the ν_2 bending vibration (61 cm^{-1} for $NH_3 \cdot H_2O$ and 120 cm^{-1} for $NH_3 \cdot HF$). Comparing these values and $NH_3 \cdot$alkali metal complex results with the present results (Table 36) it is clear that $Cu \cdot NH_3$ and $Fe \cdot NH_3$ are stronger complexes than all these except $Li \cdot NH_3$. The complexes with hydrazine are considerably weaker.

These results are consistent with the recent calculations of Bauschlicher (Reference IV-2) on $Cu \cdot NH_3$ and other complexes (including $Ni \cdot NH_3$). Since the Cu ground state electronic configuration is $3d^{10}4s^1$ and the NH_3 ligand contains a lone pair of electrons on N, one expects in simple terms that interaction between these moieties should lead to repulsion and no complex formation. Bauschlicher shows however that the interaction is much more complicated. The anticipated repulsion is reduced because the metal polarizes the 4s orbital (promotes electron density into the 4p orbital) so that it now has an effective dipole moment. There is then a favorable electrostatic interaction between the metal dipole and the NH_3 dipole moments; this interaction is larger than expected since the charge clouds of the two overlap. Because of this interpenetration of the NH_3 dipoles' negative end (the dipole moment of the free NH_3 is 0.81(N^-H^+)) into the metals' charge cloud, the attraction of the metal nucleus for the negative end of the dipole is enhanced. There is also a small σ donation from the NH_3 to the metal.

TABLE 41. COMPARISON OF BEST-FIT NORMAL COORDINATE CALCULATION WITH EXPERIMENTALLY OBSERVED IR BANDS FOR THE Fe • NH_3 AND Cu • NH_3 COMPLEXES

Mode	Fe • NH_3		Cu • NH_3	
	Calc.[a]	Expt.	Calc.[b]	Expt.
$\nu_{as}(e)NH$	3457	3447	3457	3447
$\nu_s(a_1)NH$	3334	?	3334	?
$\delta_{as}(e)HNH$	1633	--	1633	--
$\delta_s(a_1)umb$	1133	1130	1117	1117
$\nu_{N-M}(a_1)$	548	--	388	--
$\delta_{as}(e)HNM$	369	--	369	--

[a] R_{N-M} = 2.1 Å, F_{HNFe} = 0.1, F_{N-Fe} = 3.0 mdyn/Å, scaled by const. factor of 0.90.

[b] R_{N-M} = 2.1 Å, F_{HNCu} = 0.1 F_{N-Cu} = 1.5 mdyn/Å; scaled by const. factor of 0.90.

These effects are of the same magnitude for all metal•NH_3 systems.

For systems containing 3d holes, an additional factor arises. Fe has a ground state configuration of $3d^64s^2$ with an excited state (0.88 eV above) of $3d^74s^1$ configuration. Bauschlicher remarks (Reference IV-2) that the latter state may be stabilized by strong interactions with one or more neighbors. For such a system, the 4s and $3d_\sigma$ orbitals can mix. Because there are fewer electrons along the internuclear axis in these hybrid orbitals the shielding of the metal nucleus from the NH_3 lone pair is reduced and the bonding in the Fe•NH_3 complex is expected to be stronger. Thus, a larger shift in the ν_3 NH bending frequency is expected compared to Cu•NH_3. This is what is observed (Table 35).

The shifts observed for the hydrazine•metal complexes can also be understood in the above terms. We assume, as seems reasonable, that the N_2H_4 ligand complexes to Cu or Fe in a monodentate fashion via the lone pair on one end of N_2H_4. By analogy to the bonding with NH_3 it is expected that the dipole moment for the ligand $H_2N(NH_2)$ (so written to emphasize its similarity to NH_3) will be considerably less. This will result in a diminished polarization of the metal 4s orbital and a less favorable electrostatic

interaction between the metal effect dipole and the N_2H_4 dipole. Thus, a smaller shift is expected for the N_2H_4•metal complexes. This is as observed. The fact that both $Cu•N_2H_4$ and $Fe•N_2H_4$ complexes exhibit practically the same shift is evidence that the interpenetration and shielding effects which play a role in the stronger ammonia complexes are virtually absent in the present ones.

SECTION V

RAMAN SPECTRA OF THE CHAIN COMPLEXES OF BIS(HYDRAZINE) ZINC CHLORIDE AND ZINC BROMIDE

A. INTRODUCTION

Hydrazine may act as a ligand and complex with transition metals. In principle, hydrazine as a ligand may be unidentate, bidentate or bridging. Complexes of the transition metals with hydrazine in the unidentate or bridging form are now well known (Reference V-1). To date, bidentate hydrazine complexes have not yet been seen. Numerous infrared studies on bridged and unidentate hydrazine complexes of the transition metals have been reported (Reference V-1). However, Raman studies of these species have been limited to one article (Reference V-2) in which bands over only the 950-3300 cm^{-1} region were reported.

In the present study Raman spectra of the $Zn(N_2H_4)_2X_2$ (X = Cl or Br) complexes are presented for the region 100 cm^{-1}-3500 cm^{-1}. Where there is overlap with previous studies (IR and/or Raman) the agreement is good. For the lower wavenumber range (100-400 cm^{-1}) a normal coordinate analysis of the complexes' core was performed and used to aid in the assignment of the spectra.

B. EXPERIMENTAL

The compounds $Zn(N_2H_4)_2X_2$ (X = Cl or Br) were prepared by addition of hydrazine hydrate (Aldrich) to an ethanolic solution of the appropriate metal halide (reagent grade) (Reference V-3). The white solids were rinsed with ethanol and dried in a dessicator. Elemental analysis (Reference V-4) gave for $Zn(N_2H_4)_2Cl_2$: percent N calc. 28.0, percent N found 26.9; percent H calc. 4.03, percent H found 3.66, and for $Zn(N_2H_4)Br_2$: percent N calc. 19.4, percent N found 18.54; percent H calc. 2.79, percent H found 2.25. Infrared spectra of both compounds obtained in KBr discs agreed well with previously published spectra (References V-5, V-6).

Raman spectra of the powdered samples were measured using a Spex double monochromator (Model 1701; slits:400μm, resolution:1cm^{-1}) with a cooled photomultiplier (RCA 3130) in the photon counting mode. Excitation was via the 488nm line (250 mW) of an Ar^+ laser (Spectra Physics 2000 Series). Interfering plasma lines were practically eliminated by a homemade prism prefilter. The sample, contained in a vertically-oriented capillary tube, was rapidly rotated during irradiation; the scattered radiation was collected in a 180° back scatter orientation (Reference V-7). A microcomputer (HP 3000) controlled the wavenumber advance, the signal averaging and the spectral display, storage, and recording.

C. CRYSTAL STRUCTURE

The crystal structure of $Zn(N_2H_4)_2Cl_2$ has been determined by Ferrari, Braibanti and Bighardi (Reference V-8). The space group is monoclinic C^3_{2n} - C2/m. The structure is composed of parallel (to the c axis) chains of bridged complexes with two hydrazines forming bridges between adjacent Zn^{+2} centers (see Figure 31). The coordination about the metal center is pseudo-octahedral with the two remaining apical positions occupied by the chlorides. The symmetry about the zinc is D_{4h}. The metal-N bond length of 2.15Å is described as a weak covalent bond; the Zn-Cl distance of 2.58Å is nearly equal to the sum of the ionic radii. In the crystal the conformation of the hydrazine molecules is staggered, i.e. the angle between the projections of the lone pair orbitals on each N atom of one hydrazine onto a plane perpendicular to the NN axis is 74°. The local symmetry of the hydrazine ligands is thus C_2.

D. NORMAL COORDINATE CALCULATION

To characterize the low energy (< 400 cm^{-1}) Raman spectra of $Zn(N_2H_4)_2X_2$ (X = Cl or Br) a normal coordinate analysis was performed on the ZnN_4X_2 core. For this D_{4h} symmetry center, 15 normal modes are expected, 8 of which are IR active (2 a_{2u}, 3e_u), 6 are Raman active (2a_{1g}, b_{1g}, b_{2g} and e_g) and 1 is inactive (b_{2u}). The internal coordinates are shown in Figure 32, the molecular parameters are listed in Table 35 and the symmetry coordinates are defined in Table 36. Diagonal force constants (F_{dia}) were initially estimated by comparison with those determined by Nakagawa snd Shimanouchi (Reference V-

9) for $Co(NH_3)_6^{2+/3+}$ and trans$[Co(NH_3)_4X_2]^+$ (X = Cl or Br). These are listed in Table 44, along with their corresponding calculated frequencies. All off-diagonal force constants were set equal to zero. Calculations were performed on a VAX/VMS computer and then output to an IBM PC.

E. RESULTS AND DISCUSSION

1. Hydrazine Vibrations

As previously noted many infrared studies of hydrazine and its metal complexes have been reported. Comparison of the observed IR bands with the Raman bands reported here is possible because the local hydrazine symmetry is C_2 and the rule of mutual exclusivity does not hold for these vibrations.

The room temperature Raman spectra of solid $Zn(N_2H_4)_2X_2$ (X = Cl or Br) in the region 300-3800 cm^{-1} are shown in Figures 33-38 and the bands tabulated in Table 45. The spectra for both compounds are similar, with the bromide complex bands shifted ~5-20 cm^{-1} to lower energies. In the 1100-1200 cm^{-1} region an opposite shift is observed (vide infra).

In the NH_2 stretching region, four bands are expected for hydrazine in a staggered conformation; all four should be Raman and IR active. Previous IR investigations (Reference V-5) have reported only three bands in this region; the absence of the fourth band was noted but without explanation. In Figures 33 and 34 where the spectra of the chloride and bromide bis(hydrazine)zinc complexes are shown, the appearance of two strong, well-resolved bands at 3279 cm^{-1}(Cl)/3256 cm^{-1}(Br) and 3232 cm^{-1}(Cl)/3213 cm^{-1}(Br) and two weaker shoulders to lower energy are readily seen (Table 45). These bands are assigned to the expected four NH_2 stretches. These bands appear about 50-150 cm^{-1} lower than the corresponding bands in gaseous hydrazine (References V-10, V-11). This change reflects a weakening of the NH bonds and has been attributed to the shift of electron density away from the nitrogen atom upon coordination to the metal (Reference V-5) and to the dipole-induced dipole attraction of the metal and hydrazine (Reference V-12).

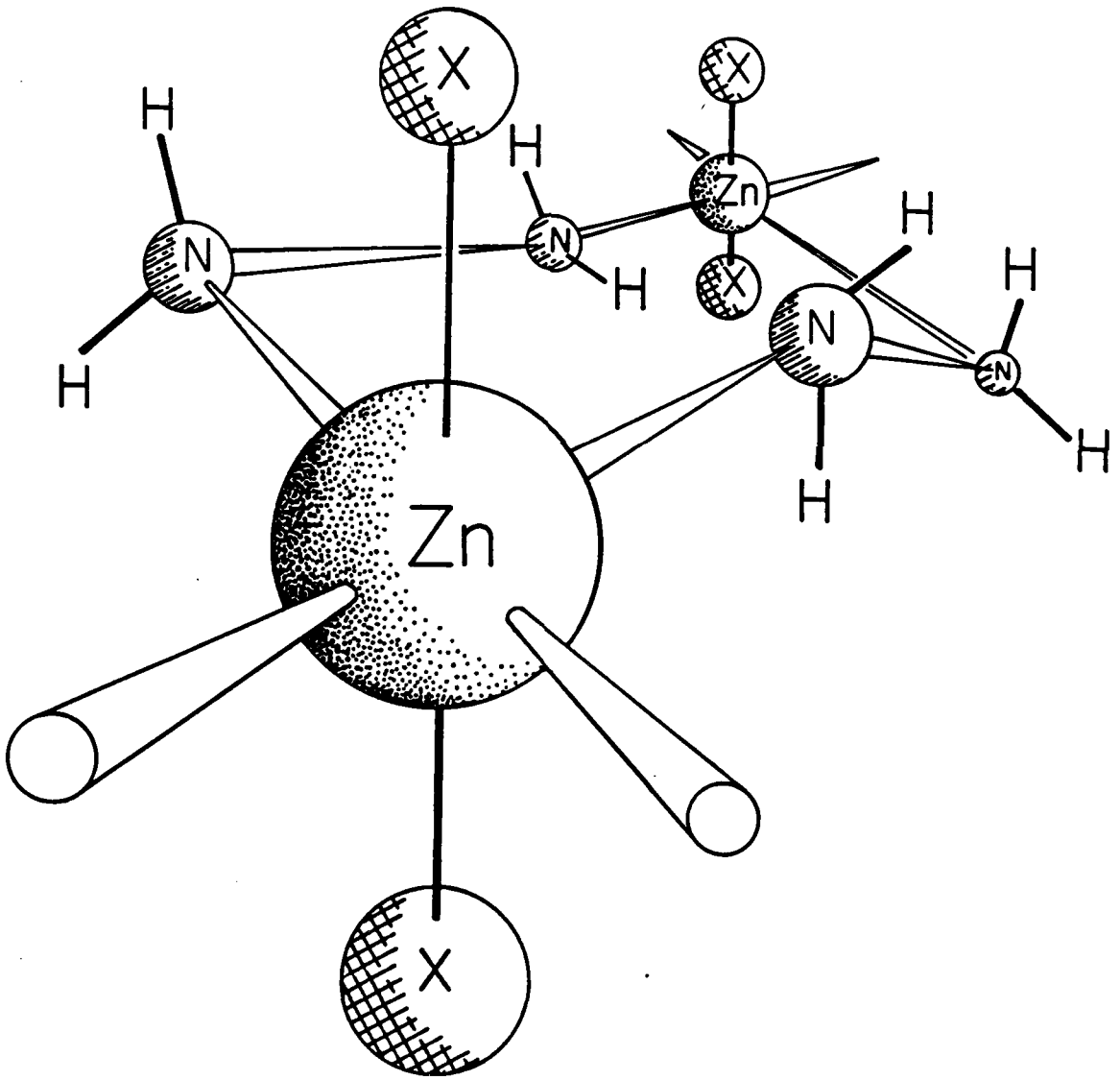

Figure 31. Schematic of Local Structure of the bis(Hydrazine) Zinc Chloride Chain Complex.

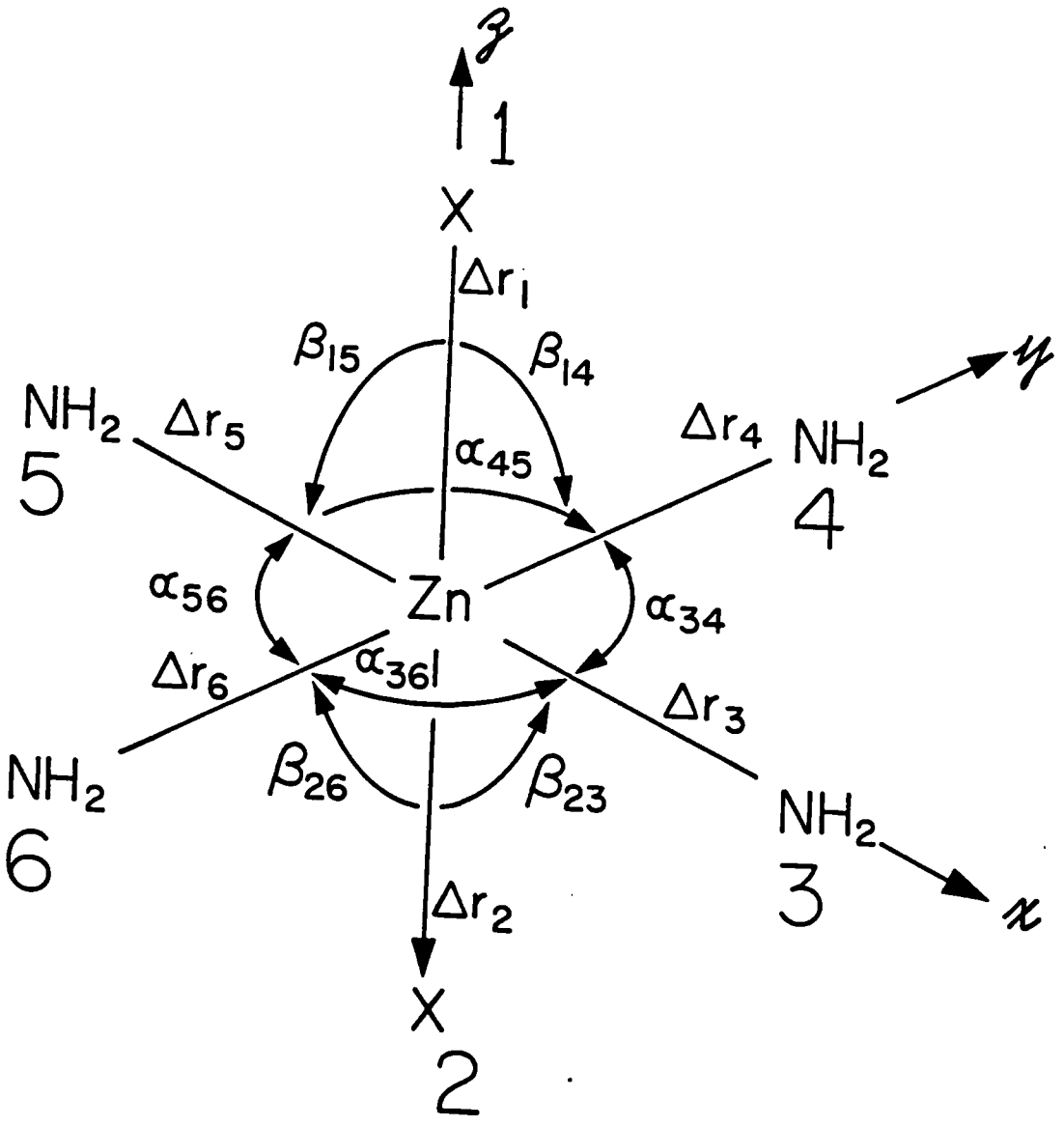

Figure 32. Internal Coordinates and Assumed Geometry for the ZnN_4X_2 Complex Core.

TABLE 42. MOLECULAR PARAMETERS.

Masses		Bond Distances
Zn	65.38 amu	$R(Zn^{II} - N) = 2.15$ Å[b]
NH_2	16.0226[a]	$R(Zn^{II} - Cl) = 2.58$ Å[c]
Cl	35.453	$R(Zn^{II} - Br) = 2.79$ Å[d]
Br	79.904	

[a] One half of each bridging N_2H_4 assigned to Zn^{II}, with NH_2 treated as an atom of mass 16.0226.
[b] Reference V-8. Same for bromide analog.
[c] Reference V-8.
[d] Sum of ionic radii.

NH_2 bending, wagging and twisting vibrations are expected in the 900-1600 cm^{-1} region. Six Raman bands are observed in this range for the chloride (bromide) complex at 1613 (1599), 1580 (1572), 1348 (1342), 1311 (1309), 1186 (1190) and 1127 (1130) cm^{-1}. The first two have previously been assigned (Reference V-5) to the two expected NH_2 bending modes, and the next two attributed to the NH_2 wagging motions. Although the last band (1127 cm^{-1} (Cl)) has been assigned (Reference V-5) to one of the expected NH_2 twisting modes, the other one expected was not identified. A weak IR shoulder at 1190 cm^{-1} was attributed to an impurity (Reference V-5).

We argue here that both the 1127 (1130) and 1186 (1190) cm^{-1} bands in the chloride(bromide) complex should be assigned to the NH_2 twisting vibrations. First, as noted above, the spectral shift in going from the chloride to the bromide complex is ~5-20 cm^{-1} to <u>lower</u> energies, <u>except</u> in the 1100-1200 cm^{-1} region where an <u>opposite</u> shift is observed. Both the 1186 and 1127 cm^{-1} bands increase in frequency when bromine replaces chlorine, indicating a similar vibrational origin. Second, an increase in frequency (going from Cl to Br) indicates a less hindered rotation of the two NH_2 moieties with respect to each other during the twisting motion. This is

TABLE 43. SYMMETRY COORDINATE DEFINITIONS[a]

Symmetry	Symmetry Coordinates	Description
A_{1g}	$S_1 = 1/\sqrt{2}(\Delta r_1 + \Delta r_2)$	MX s-str
A_{2u}	$S_2 = 1/\sqrt{2}(\Delta r_1 - \Delta r_2)$	MX a-str
A_{1g}	$S_3 = 1/2[(\Delta r_3 + \Delta r_5) + (\Delta r_4 + \Delta r_6)]$	MN s-s-str
B_{1g}	$S_4 = 1/2[(\Delta r_3 + \Delta r_5) - (\Delta r_4 + \Delta r_6)]$	MN a-s-str
E_u	$S_5 = 1/2[(\Delta r_3 - \Delta r_5) + (\Delta r_4 - \Delta r_6)]$	MN s-a-str
	$S_6 = 1/2[(\Delta r_3 - \Delta r_5) - (\Delta r_4 - \Delta r_6)]$	MN a-a-str
E_u	$S_7 = 1/\sqrt{8}[(\Delta\beta_{13} + \Delta\beta_{15} - \Delta\beta_{23} - \Delta\beta_{25}) + (\Delta\beta_{14} + \Delta\beta_{16} - \Delta\beta_{24} - \Delta\beta_{26})]$	S-NMN OOPL bend (umb bend)
	$S_8 = 1/\sqrt{8}[(\Delta\beta_{13} + \Delta\beta_{15} - \Delta\beta_{23} - \Delta\beta_{25}) - (\Delta\beta_{14} + \Delta\beta_{16} - \Delta\beta_{24} - \Delta\beta_{26})]$	a-NMN OOPL bend
A_{2u}	$S_9 = 1/2(\alpha_{34} + \alpha_{45} - \alpha_{56} - \alpha_{63})$	s-NMN INPL bend(1)
B_{2u}	$S_{10} = 1/2(\alpha_{34} - \alpha_{45} - \alpha_{56} + \alpha_{63})$	s-NMN INPL bend(2)
B_{2g}	$S_{11} = 1/2(\alpha_{34} - \alpha_{45} + \alpha_{56} - \alpha_{63})$	a-NMN INPL bend
E_u	$S_{12} = 1/\sqrt{8}[(\Delta\beta_{14} + \Delta\beta_{24} - \Delta\beta_{16} - \Delta\beta_{26}) + (\Delta\beta_{13} + \Delta\beta_{23} - \Delta\beta_{15} - \Delta\beta_{25})]$	s-s-MX bend
	$S_{13} = 1/\sqrt{8}[(\Delta\beta_{14} + \Delta\beta_{24} - \Delta\beta_{16} - \Delta\beta_{26}) - (\Delta\beta_{13} + \Delta\beta_{23} - \Delta\beta_{15} - \Delta\beta_{25})]$	a-s-MX bend
	$S_{14} = 1/\sqrt{8}[(\Delta\beta_{14} - \Delta\beta_{24} - \Delta\beta_{16} + \Delta\beta_{26}) + (\Delta\beta_{13} - \Delta\beta_{23} - \Delta\beta_{15} + \Delta\beta_{25})]$	s-a-MX bend
E_g	$S_{15} = 1/\sqrt{8}[(\Delta\beta_{14} - \Delta\beta_{24} - \Delta\beta_{16} + \Delta\beta_{26}) - (\Delta\beta_{13} - \Delta\beta_{23} - \Delta\beta_{15} + \Delta\beta_{25})]$	a-a-MX bend

[a] r_n represents the bond between the Zn^{II} and atom N, $\alpha_{NN'}$ represents the NZnN' angle between nitrogen atoms N and N', and $\beta_{NN'}$ represents the NZnX angle between halogen atom X and nitrogen atom N'. Thus, Δr_N represents stretching modes, $\Delta\alpha_{NN'}$ represents out-of-(xy) plane bends, and $\Delta\beta_{NN'}$ represents in-(xy)-plane bends.

TABLE 44. FORCE CONSTANTS AND CALCULATED FREQUENCIES OF RAMAN ACTIVE MODES.

Type	Symmetry	F(md/Å)	Calculated Frequency (cm^{-1})
$F_{dia}(ZnN)$	A_{1g}, B_{1g}	.535	238.12
		.735[a]	279.10
		.935	314.79
$F_{dia}(ZnCl)$	A_{1g}	.5747	165.91
		.7747[b]	192.63
		.9747	216.07
$F_{dia}(ZnBr)$	A_{1g}	.5621	109.29
		.7621[c]	127.26
		.9621	142.99
$F_{dia}(NZnN)$	B_{2g}	.980	299.79
		1.18[d]	328.96
		1.38	355.75
$F_{dia}(NZnCl)$	E_g	0.6055[e]	190.99
		1.237	272.99
$F_{dia}(NZnBr)$	E_g	0.3408[f]	132.72
		0.886	213.99

[a] All F_{dia} values were estimated by comparing values from Table 44, Ref. V-1. $F_{dia}(ZnN)$ is the average of $F_{dia}(MN)$ values given for $Co(NH_3)_6^{2+}$ [.735 = 1/2(0.65 + 0.89)]. This estimate was then varied by ±.20 md/Å.

[b] K(ZnN) was estimated to be 0.5 md/Å by comparing K(MN) values for $Co(NH_3)_6^{2+/3+}$. $F_{dia}(ZnCl)$ was estimated by multiplying $F_{dia}(MX)$ for trans-$[Co(NH_3)_4Cl_2]^+$ by the ratio K(ZnN)/K(MX) for trans-$[Co(NH_3)_4Cl_2]^+$, i.e., 1.41 X (.5/.91) = .7747. This was varied by ±.20 md/Å.

[c] $F_{dia}(ZnBr)$ was estimated analogous to that of $F_{dia}(ZnCl)$.

[d] Taken directly as $F_{dia}(NMN)$ for $Co(NH_3)_6^{2+}$ and varied by ±.20 md/Å.

[e] H(NZnCl) was estimated to be 0.97 md/Å (~1/2 of 0.143 md/Å for trans-$[Co(NH_3)_4Cl_2]^+$). $F_{dia}(NZnCl)$ was estimated by multiplying $F_{dia}(NMX)$ for trans-$[Co(NH_3)_4Cl_2]^+$ by the ratio H(NZnCl)/H(NMCl) for trans-$[Co(NH_3)_4Cl_2]^+$, i.e., 1.237 X (.07/143) = 0.6055. Since $F_{dia}(NMN)$ changes little from $Co(NH_3)_6^{3+}$ to $Co(NH_3)_6^{2+}$ (1.22 → 1.18), $F_{dia}(NMX)$ for trans-$[Co(NH_3)_4Cl_2]^+$ was used directly.

[f] $F_{dia}(NZnBr)$ was estimated analogous to that of $F_{dia}(NZnCl)$.

TABLE 45. RAMAN AND IR BANDS OBSERVED FOR $Zn(N_2H_4)_2X_2$ (X = Cl OR Br)[a].

X = Cl		X = Br	
Raman (cm^{-1})	IR[b] (cm^{-1})	Raman (cm^{-1})	IR[b] (cm^{-1})
3279 m	3269 s	3256	3267
3232 vs	3232 m	3213	3212
~3190 sh	3138 w	~3185	3134
~3130 sh		~3130	
1613 m	1606 s	1599	1604
1580 s	1572 s	1572	1571
1348 vw	1342 w	1342	1340
1311 w	1310 m	1309	1310
1186 m	1190 m	1190	1191
1127 w	1171 s	1130	1170
976 s	972 m	968	970
694 vw	625 m	680	619
495 vw	574 m	488	563
346 w		340	
291 w		282	
270 w		260	
151 m		139	
113 w		101?	

[a] vs = very strong, s = strong, m = medium, w = weak and vw = very weak relative intensities.

[b] This work.

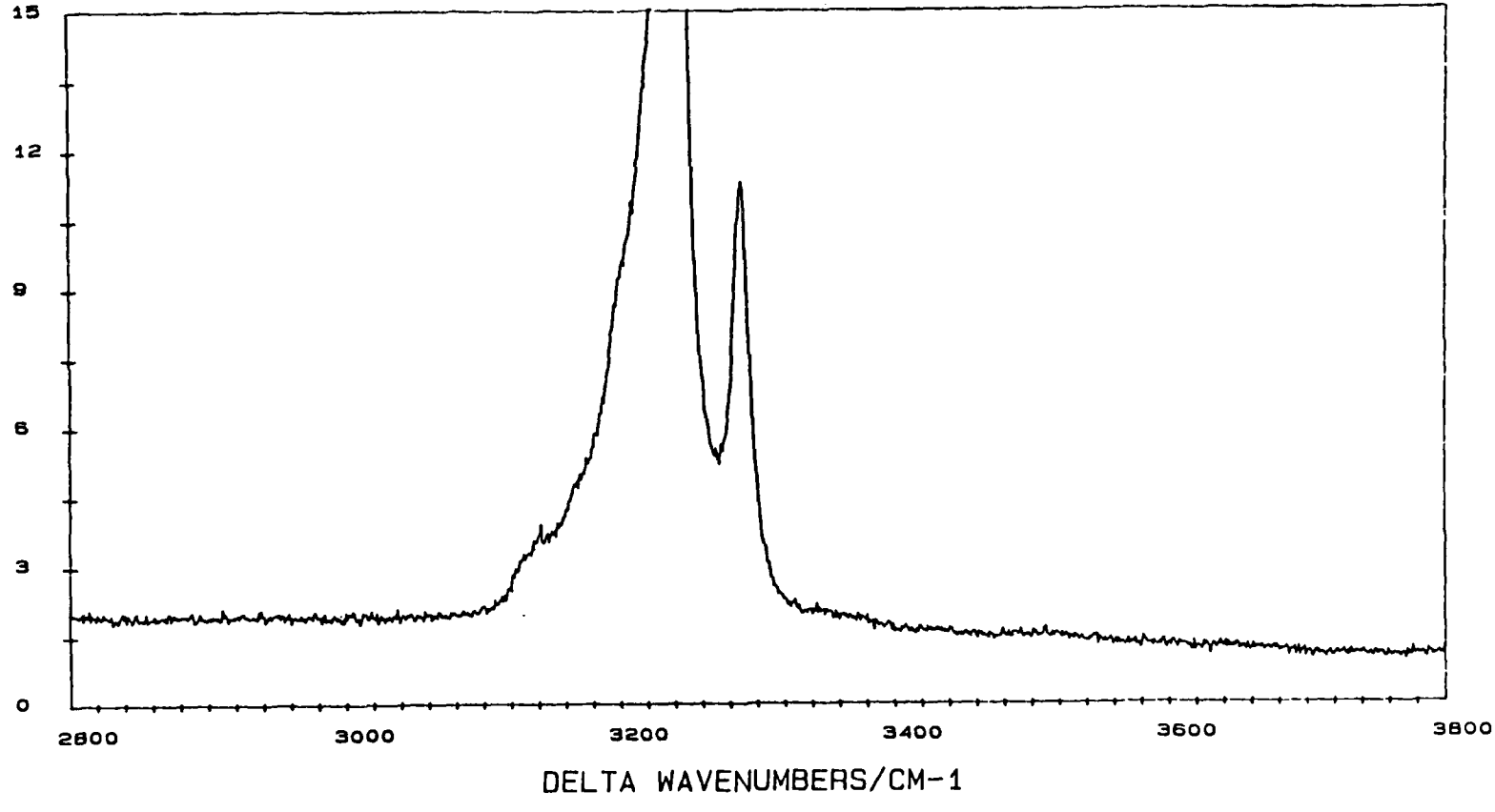

Figure 33. Raman Spectrum of Polycrystalline $Zn(N_2H_4)_2Cl_2$ in the Range 2800-3800 cm^{-1}.

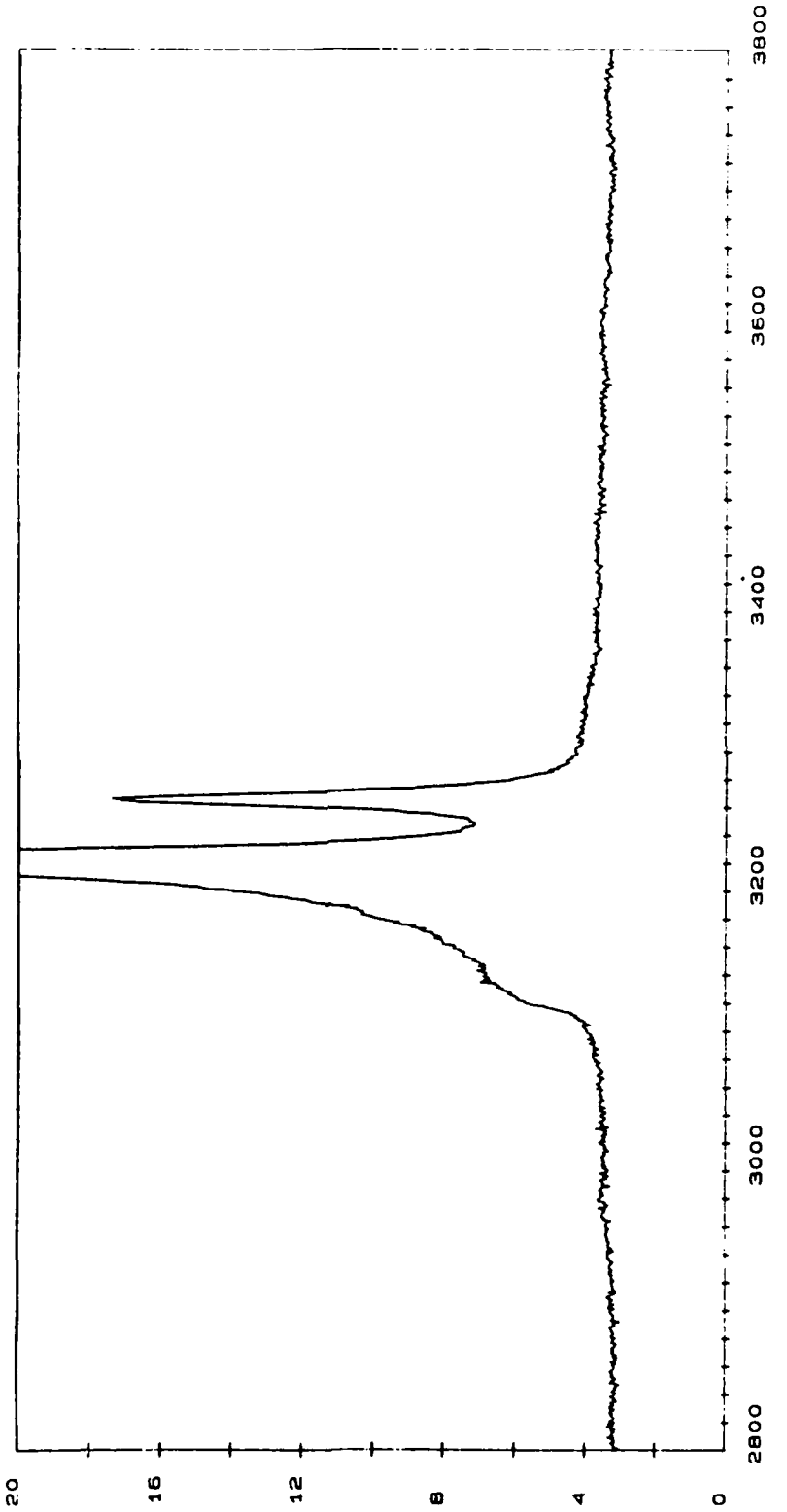

Figure 34. Raman Spectrum of Polycrystalline $Zn(N_2H_4)_2Br_2$ in the Range 2800-3800 cm^{-1}.

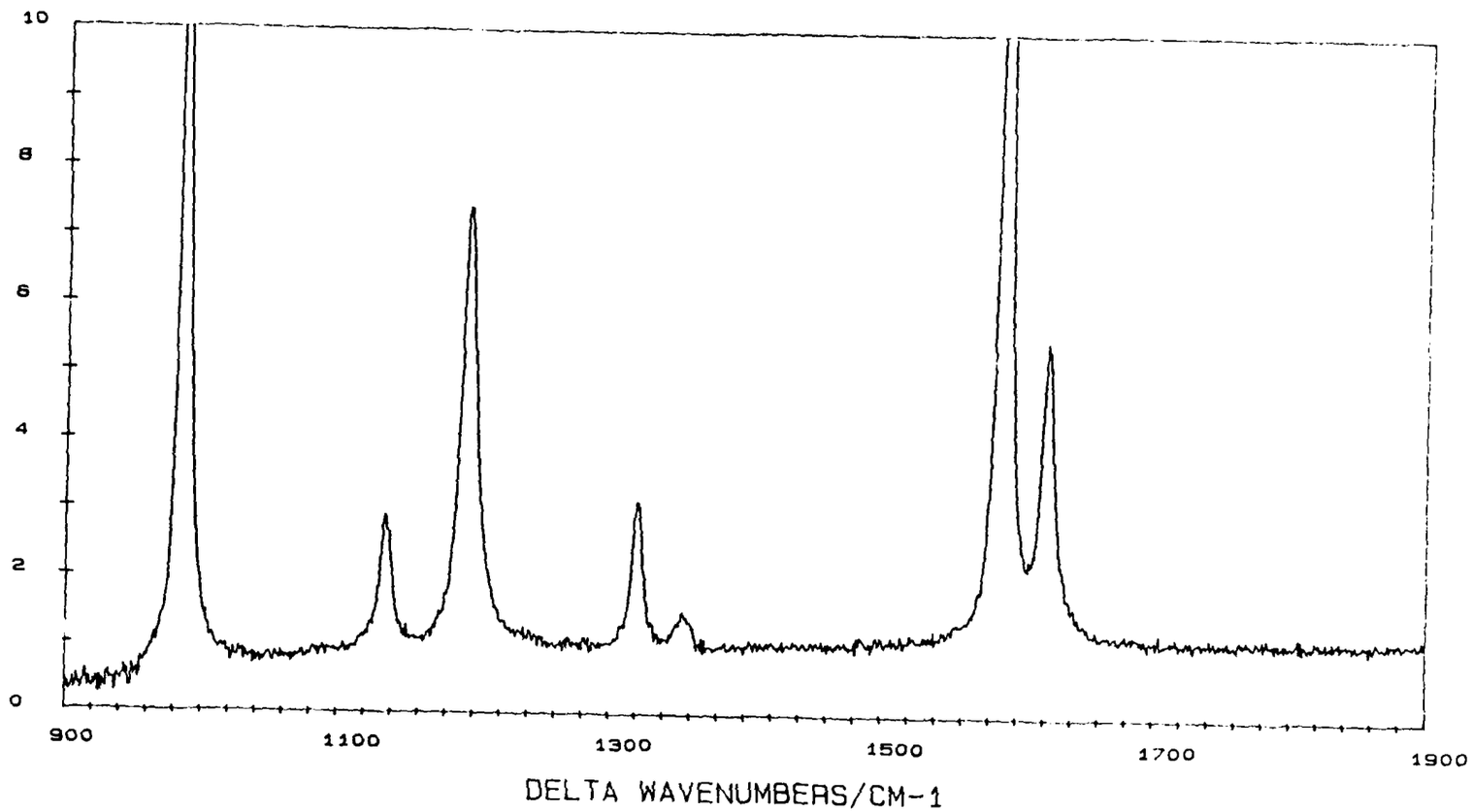

Figure 35. Raman Spectrum of Polycrystalline $Zn(N_2H_4)_2Cl_2$ in the Range 900-1900 cm^{-1}.

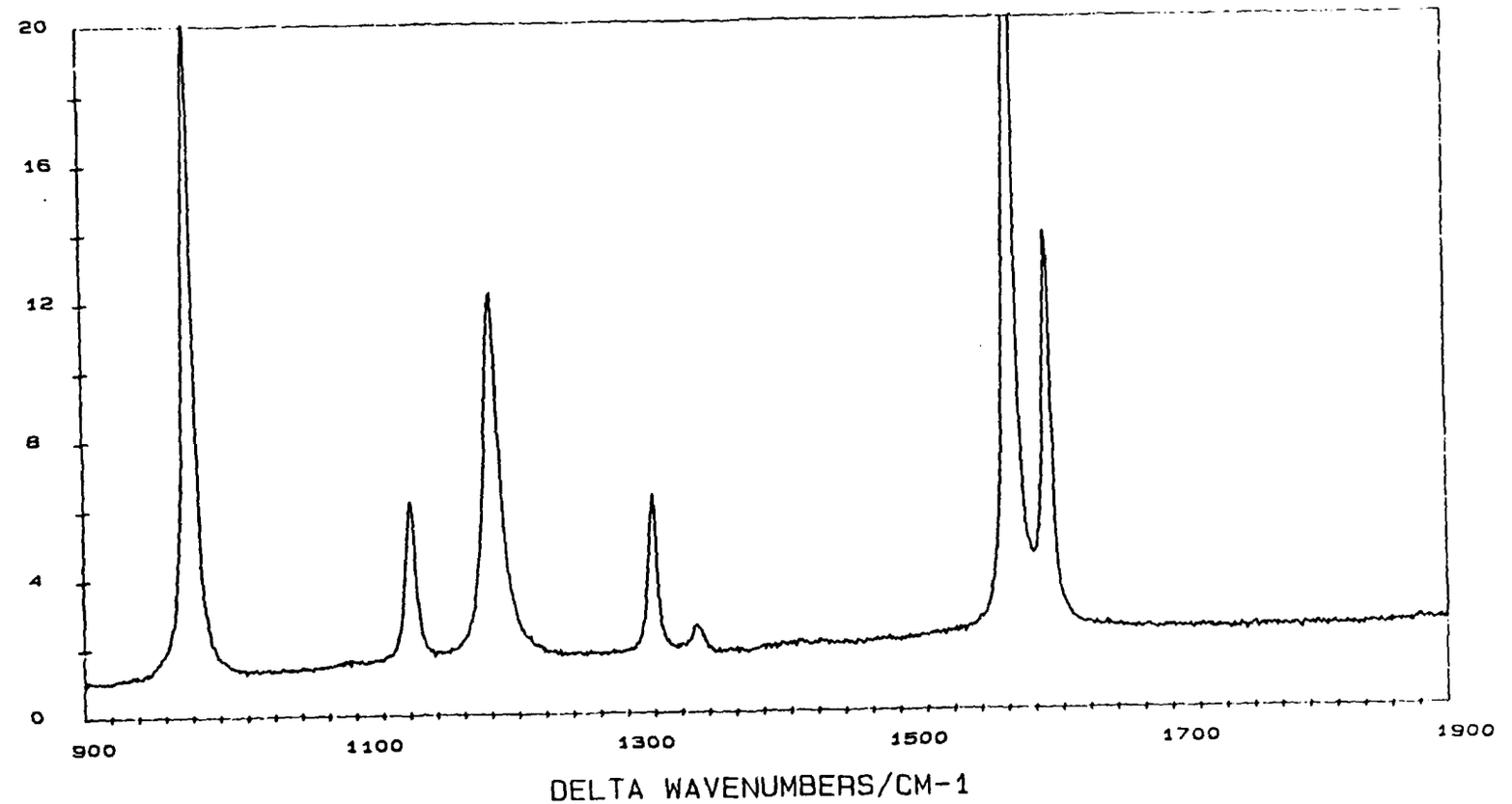

Figure 36. Raman Spectrum of Polycrystalline $Zn(N_2H_4)_2Br_2$ in the Range 900-1900 cm^{-1}.

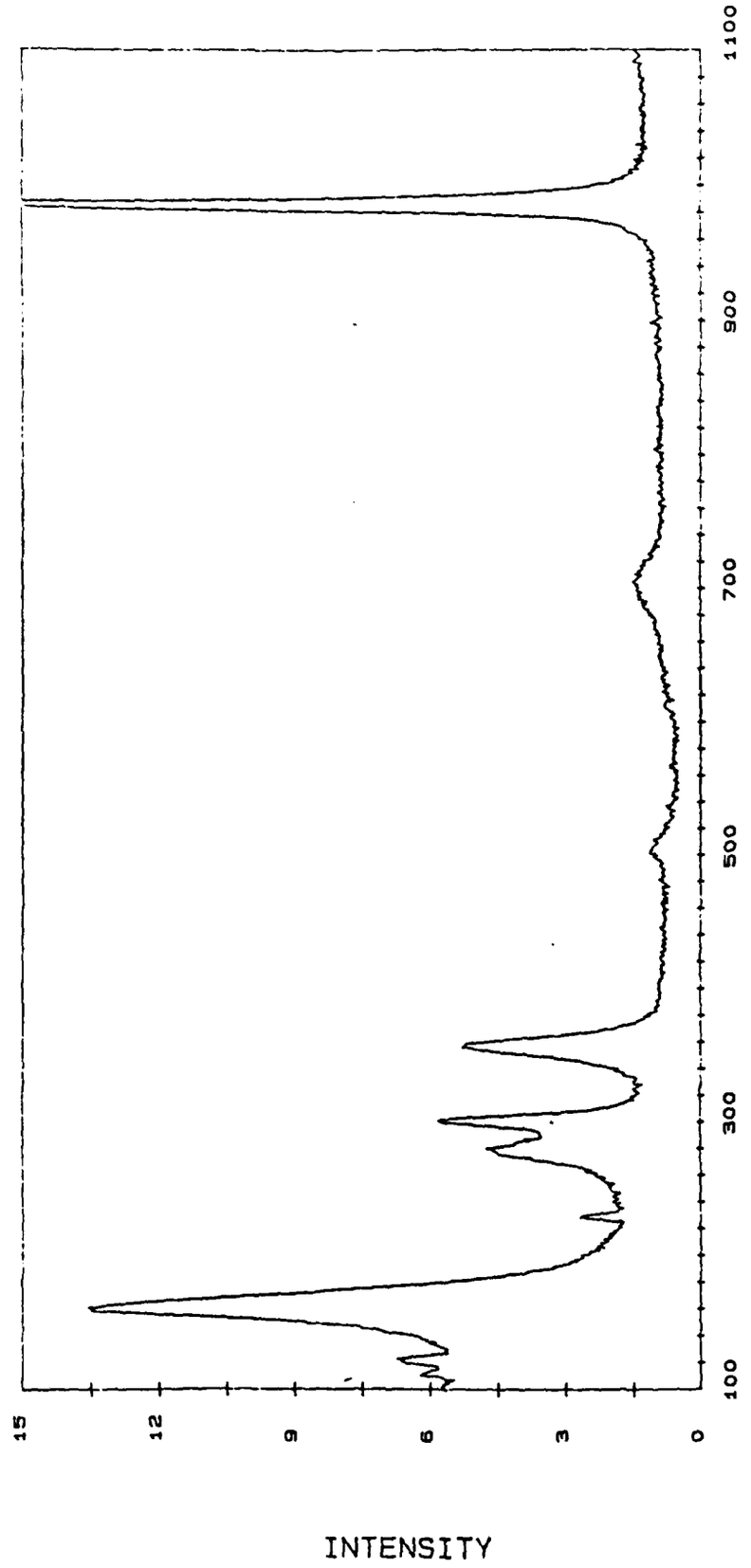

Figure 37. Raman Spectrum of Polycrystalline $Zn(N_2H_4)_2Cl_2$ in the Range 100-1100 cm^{-1}.

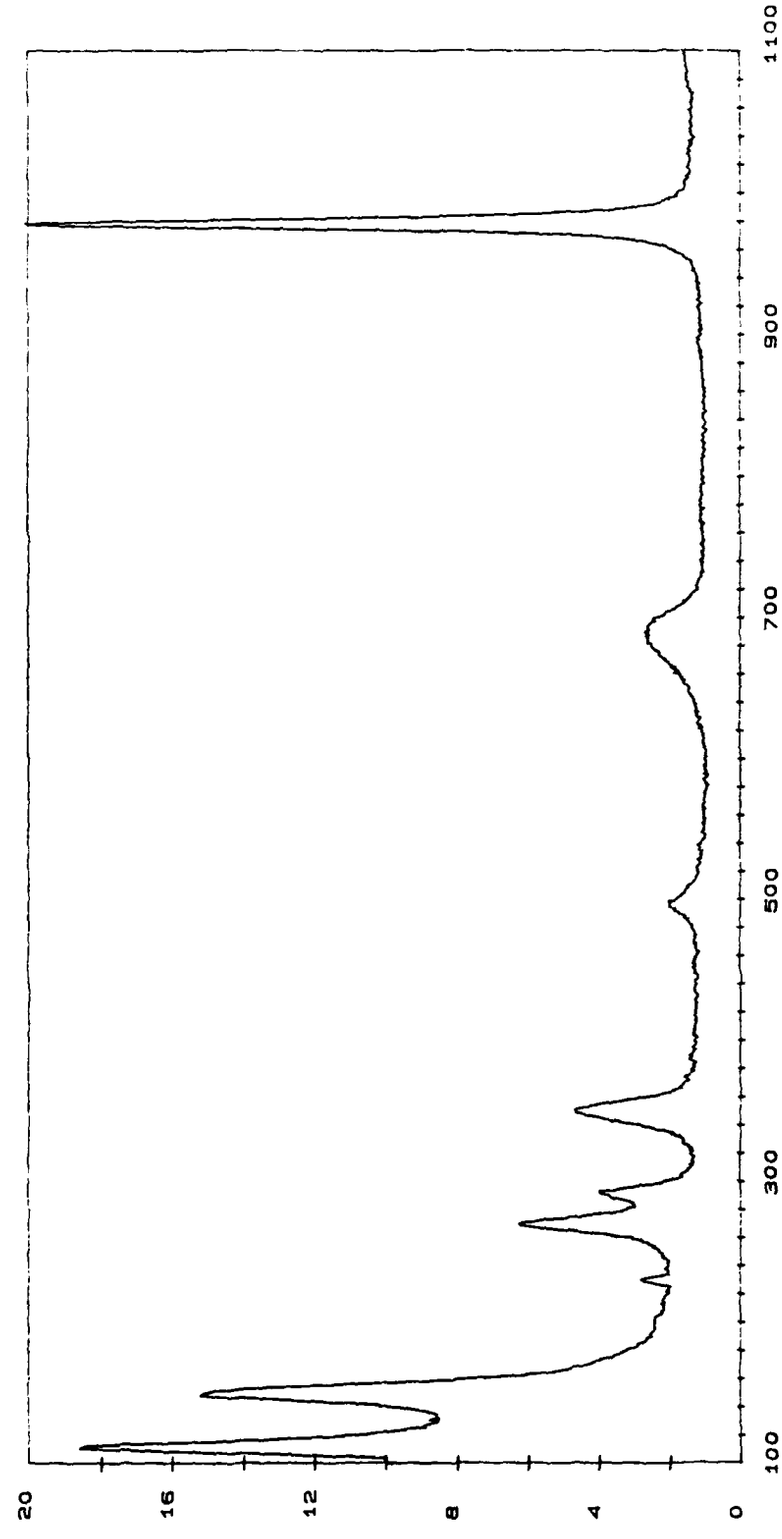

Figure 38. Raman Spectrum of Polycrystalline $Zn(N_2H_4)_2Br_2$ in the Range 100-1100 cm^{-1}.

consistent with an increase in the unit cell length along the c axis from 4.13Å to 4.18Å upon replacement of chloride with bromide (Reference V-6). Finally, if the 1186 (1190) cm^{-1} band were due to an impurity, other bands would have been expected from the impurity also. No such bands were observed; all other bands could readily be ascribed to the hydrazine-metal-halide complex.

The N-N stretching frequency has been recognized previously (Reference V-6) to be diagnostic of the type of coordination to the metal: in the range a) 931-936 cm^{-1} for unidentate complexation and (b) 948-980 cm^{-1} for bridging hydrazine. The appearance of a band at 976 (968) cm^{-1} for the present samples in both the Raman and IR is consistent with this generalization. The NN stretch is expected to exhibit a frequency close to the NH wagging vibrations. However, the polarizability change for the NN vibration is expected to be quite large, leading to a greater Raman intensity and the possibility of distinguishing it from the NH wagging modes. This is observed here: the 976 cm^{-1} band is more than 4 times as intense as the 1311 cm^{-1} band. This provides additional support that the NN band has been correctly assigned in previous IR investigations of hydrazine complexes. The fact that the NN stretch is intense in the Raman spectra of complexes could prove helpful for cases in which other vibrations partially mask its appearance, e.g. in the IR of $[Zn(N_2H_4)_{1.5}\ H_2O]SO_4$ the NN stretch appears only as a shoulder at 960 cm^{-1} and is overlapped by a band of the sulfate anion (Reference V-13). This same advantage could also be used in monitoring hydrazine in more complicated systems such as hydrazine/clay mixtures.

Two weak bands are observed at 694 (680) and 495 (488) cm^{-1} and are most probably due to the NH umbrella modes, although they are substantially displaced from the similarly-ascribed IR bands. The former band(s) could be ascribed to the first overtone of the 347 (340) cm^{-1} mode since 2 X 347 = 694 cm^{-1} and 2 X 340 = 680 cm^{-1}.

2. Metal-N and Metal-Halogen Vibrations

In the low-energy (100-400 cm^{-1}) region, five distinct bands are observed at 346(340), 291(282), 270(260), 151(139) and 113(101) cm^{-1} (cf. Fig-

ures 37, 38). In addition, incompletely eliminated plasma lines at 220 and 101 cm^{-1} have also been recorded. Since the 220 cm^{-1} plasma line is of equal intensity in both the chloride and bromide complex spectra, it is expected that other plasma lines should exhibit similar intensities in both spectra. Because of the small intensity of the plasma line at 101 cm^{-1} in the chloride complex compared to the bromide complex, we reason that the 101 cm^{-1} plasma line in the bromide complex is overlapped by a much stronger band, due to the complex.

The symmetry about the metal ion is D_{4h}:four nitrogens from different hydrazines form a square planar ligand arrangement around the Zn center with the two halides (X) lying above and below this plane on the fourfold axis (Reference V-8). Thus, all the Zn-N and Zn-X fundamental vibrations of the Zn N_4X_2 core should obey the mutual exclusivity rule governing the appearance of Raman and IR bands.

Two infrared bands have been reported (Reference V-5) in this region at 385 and 345 cm^{-1} in the chloride complex. They have been assigned to Zn-N stretching modes. This assignment is reasonable, based on the Irving-Williams order of stability of bivalent metal complexes (Reference V-14). The predicted stability order is Mn<Fe<Co<Ni<Cu>Zn>Cd. For the NH_2 twisting, symmetric and assymetric rocking, NN stretching and Metal-N stretching, the vibrational frequencies parallel the stabilities well. Reflecting their positions in this series, Co and Zn bis(hydrazine) halide complexes exhibit frequencies for these modes which are very close to each other.

The results of our normal coordinate calculations are presented in Table 46. Schematic drawings of the different modes in this range are shown in Figure 39. Table 46 shows that the band at 346 (340) cm^{-1} for the chloride (bromide) complex is assigned to the b_{2g} NZnN in-plane bending mode while the 291 (282) cm^{-1} and 270 (260) cm^{-1} modes are ascribed to the a_{1g} and b_{1g} Zn-N stretching modes. This assignment is consistent with the small shift observed when the chloride is replaced by bromide in the complex. A significantly larger shift (vide infra) is expected for the metal-halide modes.

The region below 200 cm^{-1} shows spectral bands quite different for the chloride and bromide complexes. The chloride exhibits one major band at 151 cm^{-1} (~30 cm^{-1} FWHM) and a weak band at 117 cm^{-1} while the bromide complex shows 2 major bands at 139 and 101 cm^{-1} (both ~20 cm^{-1} FWHM). The key to understanding this region is the assumption that the 151 cm^{-1} chloride band contains two bands. This assumption is supported by its broader, slightly asymmetric appearance. One component underlying the 151 cm^{-1} (Cl) band shifts upon halide replacement to 101 cm^{-1} (Br) and the other component shifts to 139 cm^{-1} (Br). The former band is assigned to a metal-halide (M-X) stretch and the latter is ascribed to a N-metal-X vibration (Table 46). Metal-bromide stretching frequencies, ν(M-Br), have been observed to parallel the metal-chloride frequencies, ν(M-Cl), usually occurring at ~0.75 ν(M-Br), although shifts in the range (0.65-0.85)·ν(M-Br) have been noted (Reference V-15). Thus, on these grounds the 151 cm^{-1} (Cl) component would be expected at ~0.75 · 151 cm^{-1} = 113 cm^{-1}, a value in reasonably good agreement with the observed band at 101 cm^{-1}. The shift of the other component from 151 cm^{-1} (Cl) to 139 cm^{-1} (Br) resembles that of the other metal-N modes, which shift ~10 cm^{-1} with a change in the halide.

TABLE 46. COMPARISON OF CALCULATED AND OBSERVED FREQUENCIES OF BIS(HYDRAZINE) ZINC CHLORO AND BROMO COMPLEXES

Observed (calculated) frequencies in cm^{-1}					
Cl		Br			Assignment
346	(328.96)	340	(328.96)	B_{2g}	NZnN in plane bond
291	(279.10)	282	(279.10)	A_{1g}, B_{1g}	Zn-N stretch
270		260			
151	(190.99)	139	(132.72)	E_g	NZnX bond
~151	(165.91)	101	(109.29)	A_{1g}	Zn-X stretch

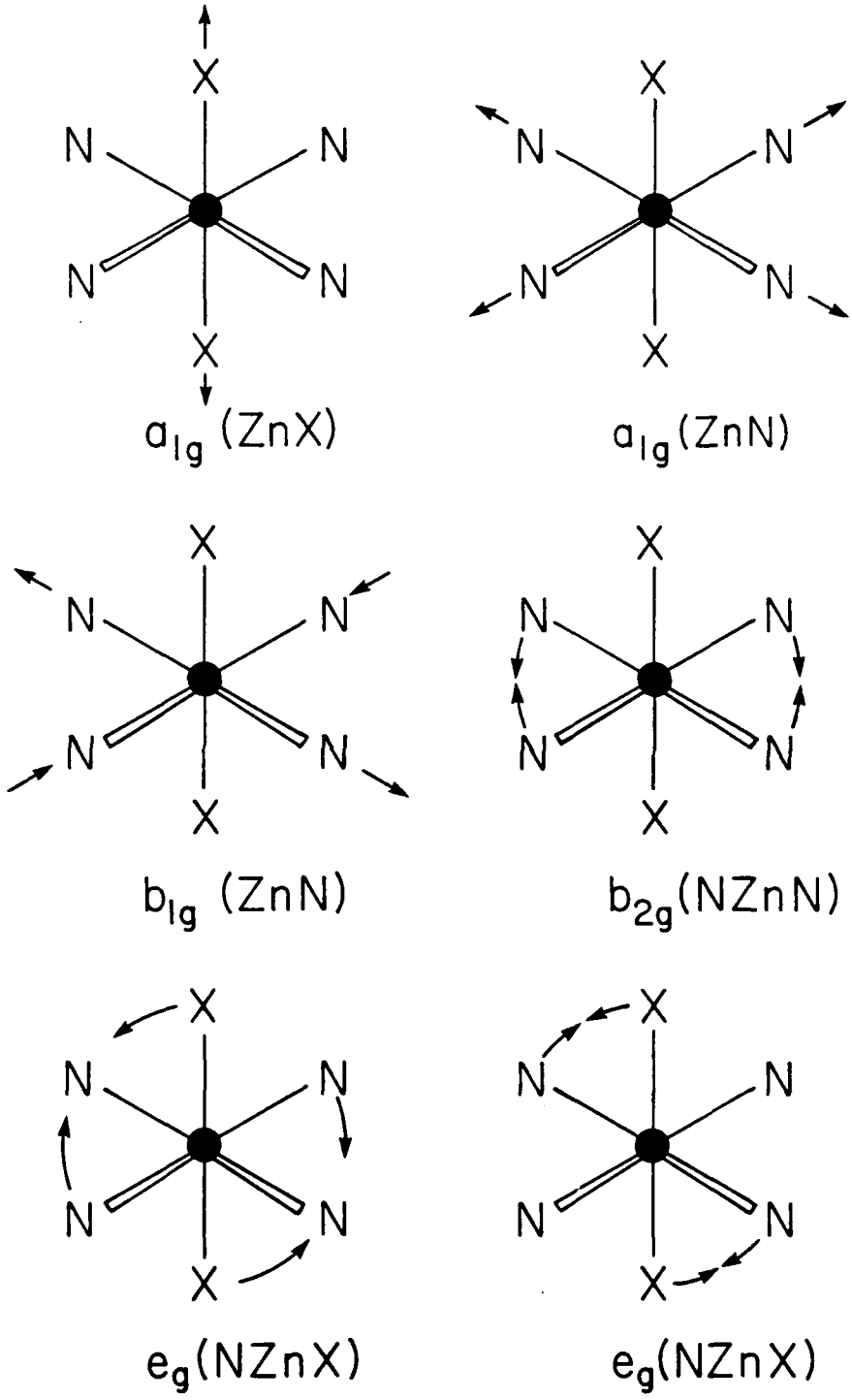

Figure 39. Schematic Diagrams of the Different ZnN_4X_2 Core Vibrational Modes.

The calculated frequencies found from the normal coordinate analysis agree with the experimental ones. A much closer fit is anticipated when the force constants are varied over a wider range. The present agreement shows that the transferability of force constants from the $CoX_2(NH_3)_4^+$ complexes is a good first approximation, as expected from the Irving-Williams stability series.

SECTION VI

VIBRATIONAL SPECTROSCOPIC STUDIES OF AROMATIC ORGANIC ADSORBATES WITH CLAY MINERALS

A. INTRODUCTION

Chemisorption and transformation of aromatic hydrocarbons have occurred on a variety of mineral surfaces. Pinnavaia and Mortland (References VI-1-2) showed that adsorbed anisole, phenol, and benzene on transition metal exchanged montmorillonites undergo single electron-transfer reactions under anydrous conditions. Under hydrated conditions, the ESR, IR, UV-vis, and resonance Raman spectra (References VI-1-5) of the aromatic organic adsorbates were minimally perturbed, in comparison to their spectra in solution. Upon dehydration, however, significant spectral changes developed. Among the most prominent were the drastic color changes of the complexes as water was removed. For example, under hydrated conditions, the Cu-exchanged montmorillonite-toluene complex (Reference VI-1) was a light pale blue color with an electronic absorption band at 27,200 cm^{-1}; upon removal of water from the clay-arene complex using P_2O_5, a bright red color developed with a red-shift (shift to lower energy) of the electronic absorption band of 5,000 to 22,200 cm^{-1}. The light blue color developed again if the clay-arene complexes were rehydrated and the dehydration process could be repeated. This reversible behavior of the complex is typical of clay-arene complexes.

Spectroscopic evidence (References VI-1-5) has shown conclusively that a single electron-transfer reaction from the organic adsorbate to the metal cation occurs; upon dehydration, the exchangeable transition-metal ions on the montmorillonite [Cu(II), Fe(III), Ru(III), and VO^{+2}] are reduced and a radical cation of the aromatic species is produced. Studies of Cu- and Fe-clay-arene complexes using electron spin resonance (ESR) spectroscopy (References VI-1-4) provided direct evidence that the interlamellar transition metal cation was reduced upon formation of the electron-transfer complexes evidenced by loss of spin intensity from the interlamellar metal cation. In addition, there was a concomitant increase in intensity of a new band in the ESR spectrum with a g-value of 2.0024. The position of the new band was near that expected for a free-spinning electron and was assigned as an organic free radical. The formation of electron-transfer complexes on both Fe(III) and

Cu(II)-exchanged montmorillonite clays indicated that the metal cation served as an oxidizing agent. Negative results were obtained for Mn(II)-, Ni(II)-, Cr(III)-, and Co(II)-exchanged montmorillonite clays which Pinnavaia et al. (Reference VI-2) attributed to unfavorable redox couples. Thus, ESR spectra of clay-arene complexes provided direct evidence that the exchangeable metal cations were reduced and that an organic free radical was produced. However, the number of organic free radical cations produced was less than 5 percent of the ESR signal loss resulting from the reduction of Cu(II) to Cu(I) or Cu metal. The chemical identities of the reaction products were shown (References VI-5, VI-6, VI-10-12) to depend strongly on the position of the substituents on the ring; if the para positions are not occupied by substituents then polymerization reactions can occur. Conversely, stable monomeric radical cations are formed on the surface of the clay if the para position is not open. In a recent study of 4-chloroanisole on Cu-montmorillonite (Reference VI-6), ESR, IR, and mass spectral analysis showed clearly that 4,4'-dimethoxybiphenyl was produced. A similar study was conducted using 4-chloroanisole in solution with CuSO4 without Cu-montmorillonite, and no 4,4'-dimethoxybiphenyl was produced. The authors concluded that the electron transfer reaction was not caused by Cu^{+2} alone, but that the negatively charged interlamellar surface of the montmorillonite clay was necessary to stabilize the radical cation intermediates.

Upon dehydration of the clay-aromatic complexes, strong perturbations were also reported in the vibrational spectra of the clay-arene complexes. IR spectra of the organic adsorbates on hydrated metal exchanged montmorillonites were not significantly perturbed in comparison to the IR spectra of the adsorbates in the liquid state (References VI-1, VI-2). Upon dehydration, however, the vibrational bands of the adsorbates were reported to shift significantly. Two of the most intense IR-active bands of substituted benzene derivatives below 2000 cm^{-1} are the out-of-plane (oop) C-H deformation band in the 700 to 850 cm^{-1} region (ν_{11} band [Reference VI-7]) and the CC stretch bands in the 1450 to 1550 cm^{-1} region (ν_{19a-b} modes [Reference VI-7]). In the case of p-xylene (Reference VI-1), as the water content decreased the ν_{11} band (C-H oop) was observed to increase from its solution value of 795 cm^{-1} to 817 cm^{-1}, a blue-shift of 22 cm^{-1}. In contrast, the ν_{19a} band was observed to decrease from its solution value of 1517 cm^{-1} to 1503 cm^{-1}, a red-shift of 14

cm^{-1}. Similar shifts in frequencies of the ν_{11} and ν_{19a} bands were observed for other substituted benzene derivatives (References VI-1-3). The C-H oop band, in particular, appeared to be a sensitive probe to changes in the local bonding environment of the organic adsorbate.

In a detailed study of the dependence of vibrational frequencies and intensities of para-substituted benzene derivatives upon the chemical nature of the substituents (Reference VI-8) , the position of the ν_{19a} band shifted significantly, depending on the electron-withdrawing character of the substituent. The greater the donor character of the substituent, the higher the observed frequency. Conversely, as the electron-withdrawing effect of the ring substituents increased (i.e., higher Hammett's sigma constant), the lower the frequency. Consequently, Varsanyi (Reference VI-7) suggested that the bond order of the C-C ring bond could be determined from the frequency of the ν_{19a} band. The opposite frequency response of the ν_{11} (C-H oop) was reported by Bellamy (Reference VI-9) who correlated the frequency of the ν_{11} band with the Hammett sigma constant for three different disubstitutions and observed that the frequency increased as the Hammett sigma value increased. Therefore, the observed red-shift of the ν_{19a} band and the concomitant blue-shift of the ν_{11} band for the p-xylene-montmorillonite are consistent with these earlier studies and indicated that the electron density of the aromatic ring decreased upon formation of the radical cation.

A decrease in the aromatic character of the organic adsorbates on the transition metal exchanged montmorillonites was expected to also influence the C-H stretching bands; however, the dispersive-IR spectra (References VI-1, VI-2) did not show any definitive perturbations in this spectral region. This was a result of the low sensitivity of dispersive-IR spectrometers and because of the high background absorption of a low-frequency electronic transition which extended into the IR region. Detailed IR spectra of p-xylene were not presented by Pinnavaia and Mortland (References VI-1, VI-2), however, they did include IR spectra of the toluene-montmorillonite complex before and after dehydration. Upon dehydration, most of the fundamental toluene bands were perturbed to some extent as discussed above. The only clear evidence of a new spectral feature induced upon drying the complex was the appearance of a band at 1300 cm^{-1} which was not observed in the hydrated spectrum and could not be

assigned to a fundamental vibration of toluene.

More recently, Soma et al. (References VI-5, VI-10-12) utilized resonance Raman spectroscopy to study clay-arene complexes. Raman spectra are resonantly enhanced when the frequency of the laser coincides with an electronic transition of the chromophore being studied. In the case of clay-arene complexes, the position of the electronic transition can vary from 400 nm to beyond 1000 nm, thus, resonantly enhanced Raman spectra can be obtained using a conventional Ar^+ or Kr^+ laser. Soma et al. (References VI-5, VI-11) obtained the Raman spectra of a Cu-benzene-montmorillonite complex and observed bands at 1600 cm^{-1} (ν_8 mode according to Wilson's numbering convention [Reference VI-13]), 1283 cm^{-1} (inter-ring stretch), 1221 cm^{-1} (CH in-plane bend) and 800 cm^{-1} (ring deformation). Upon formation of the electron transfer complex the ν_8 mode was not perturbed; the 1283 cm^{-1} mode, however, was reported to increase in frequency by 41 cm^{-1} to 1324 cm^{-1}. The 1283-1324 cm^{-1} band was tentatively assigned as an inter-ring C-C stretch based on a Raman study of the biphenyl negative ion by Takahashi et al. (Reference VI-14). However, there is some disagreement about the assignment of this band in the literature as Aleksandrov et al. (Reference VI-15) indicated that a positive shift of that magnitude (D_u = 40 cm^{-1}) of the central bond C-C central bond is not likely and that this band is extremely sensitive to the frequency of the exciting line. In the Raman spectra obtained by Soma et al. (References VI-5, VI-10-12) the hydrated complex was obtained, using the 457.5 nm line and the electron transfer complex used the 514.5 nm line. This reported sensitivity to the frequency of the exciting line may account for this discrepancy between Takahashi (Reference VI-14) and Aleksandrov (Reference VI-15). Regardless of the assignment for this particular band, Raman spectroscopy provided a useful method to observe the adsorbed species.

These initial studies of electron transfer reactions of clay-arene complexes were limited to anhydrous conditions. Rupert (Reference VI-2) extended this approach to other aromatic compounds and observed electron transfer reactions for benzene, biphenyl, naphthalene, and anthracene adsorbed on Cu-montmorillonite. In each case, electron transfer reactions were obtained under anhydrous conditions and the complexes were characterized by a loss of the Cu(II) ESR signal, formation of a new organic free radical band in

the ESR spectrum, a large red-shift in the UV-Visible spectrum which often extended into the infrared region, and by strong perturbations of the vibrational bands of the adsorbed species. In a related study, Fenn and Mortland (Reference VI-16) reported the formation of a Type II complex for anisole adsorbed on a Cu-montmorillonite clay. The general mechanism proposed to account for the formation of Type II Cu-montmorillonite-aromatic complex involved the adsorption of the aromatic species in the interlamellar region, followed by removal of water from the interlamellar transition metal (e.g., Cu[II]) cation. This step makes possible the donation of Π electrons from the aromatic adsorbate to the unfilled d orbitals of the transition metal cation which, in turn, results in the formation of a radical organic cation.

Additional Raman spectra of Type II complexes have been reported for montmorillonite clay complexed with chlorobenzene, fluorobenzene, anisole, phenol, toluene, benzonitrile, 4,4'-dimethoxybiphenyl and 4,4'-dihydroxybiphenyl (References VI-10-12). The general features of these complexes were similar to those noted above: (1) strong color change, (2) loss of metal ESR signal, (3) development of a "new" ESR band corresponding to the organic radical cation, and (4) strong perturbations observed in the vibrational spectra. In a recent ESR study of the benzene-montmorillonite system, Eastman et al. (Reference VI-4) reported that a variety of radicals are formed on the surface and that the reaction products depended on the availability of water, the identity of the metal cation, and on the reaction time.

Aromatic compounds can be chemisorbed by naturally occurring clay minerals. Early studies suggested that these reactions were restricted to anhydrous environments; however, more recent studies have indicated that they may occur in aqueous systems as well (References VI-17, VI-18). A suite of benzene substituted derivatives has been observed to chemisorb on clay surfaces and undergo chemical transformation controlled by the nature of the surface and by the type of metal cation(s) that reside on the exchange complex of the clay mineral. Preliminary attempts to remove the adsorbed species (Reference VI-19) have indicated that the chemisorbed species may be stabilized strongly by the clay surface. This fact may have important implications in the attenuation of aromatic compounds by clay mineral. The principal objective of this phase of the research was to investigate the

chemical mechanisms of interaction between aromatic organic adsorbates and naturally occurring clay minerals.

B. EXPERIMENTAL

1. CLAY MINERAL PREPARATION FOR FT-IR ANALYSIS

The clay mineral samples studied were obtained from the Source Clays Repository located at the University of Missouri and operated by the Clay Minerals Society. The kaolinite sample was the well-crystallized KGa-1 Georgia-kaolinite collected from Washington county, Georgia, and the montmorillonite sample was the SAz-1 Cheto-montmorillonite collected in Apache county, Arizona. A complete description of the physical properties of these clay samples has been given by van Olphen and Fripiat (Reference VI-20). In addition, Raman and IR spectra of the KGa-1 kaolinite clay have been reported by Johnston et. al. (References VI-21, VI-22). The colloidal behavior of 1:1 clay minerals (i.e., kaolinite and serpentine group minerals) is different from that of the 2:1 clays; therefore, separate clay mineral preparation and purification procedures were used for preparing the KGa-1 and SAz-1 clay materials.

The procedure used to prepare the SAz-1 Cheto-montmorillonite clay sample was similar to that described by Sposito et al. (Reference VI-23). Sixty grams of the crude reference clay were placed in 1-liter of distilled, de-ionized water and mixed for 2 hours with a mechanical stirrer. The fraction having an equivalent-spherical-diameter (e.s.d.) of <0.5 mm in suspension was separated by centrifugation and then flocculated by adding 800 mL of a solution containing 0.001 M HCl in 1M NaCl. Because ion-pair formation did not interfere with the FT-IR measurements, a chloride background was substituted for the perchlorate background used by Sposito et al. (Reference VI-23). The flocculated clay in the NaCl - HCl solution was centrifuged 15 minutes at 5000 revolutions per minute on a Sorvall centrifuge equipped with a Model G.S.A. head. After the clear supernatant solution was decanted carefully, the SAz-1 clay plug at the bottom of the centrifuge tube was redispersed manually into a fresh NaCl-HCl solution and the suspension was shaken on tray shaker for 20 minutes. The suspension was centrifuged again as

described above. This washing procedure was repeated about three times until the pH value of the supernatant solution dropped to 3.0. After the final NaCl-HCl wash and centrifugation, the SAz-1 clay plugs were redispersed into a 0.1 M NaCl solution and a similar washing procedure was repeated about five times using the 0.1 M NaCl solution until the pH of the supernatant solution equaled that of the 0.1 M NaCl solution (pH 5.5). After the last wash, the clay was redispersed in 0.1 M NaCl and stored in suspension prior to the spectroscopic analysis.

The clay preparation procedure used for the KGa-1 kaolinite sample was similar to that described by Johnston et al. (Reference VI-22). Two hundred grams of the the untreated KGa-1 clay were placed in 1 liter of distilled, deionized water and dispersed for size-fractionation by adjusting the pH to 9.5 by the addition of small aliquots of 0.01 M NaOH. The kaolinite suspension was size-fractionated immediately by centrifugation and the fraction have an e.s.d. of < 2.0 m was collected. The suspension then was flocculated by the addition of 1 liter of 0.001 M HCl in 1.0M NaCl. To separate the supernatant solution from the flocculated clay, the suspension was centrifuged at a relative centifugal force of 700. The supernatant solution was then decanted and its pH was measured. The kaolinite samples were redispersed manually into 1 liter of the 0.001 M HCl/1.0 M NaCl solution, and the washing procedure was repeated until the pH value of the supernatant solution equaled that of the washing solution (pH 3) this objective typically required five washed. At this point in the procedure, the clay was redispersed into 1 liter of 0.01 M NaCl, and the above procedure was repeated five more times. The treatment was adequate to raise the pH of the supernatant solution to 5.5. The final step of the procedure consisted of redispersing the clay into 0.01 M NaCl and adjusting the volume of the flocculated suspension such that a clay concentration of 20 percent (w/w) was obtained.

2. DESCRIPTION OF THE BOMEM DA3.10 FOURIER TRANSFORM SPECTROMETER

FT-IR spectra were obtained on a Bomem DA3.10 Fourier transform spectrometer. The DA3.10 spectrometer uses a Michelson interferometer with the beamsplitter positioned at a 30-degree angle to the optical axis. A Digital Equipment Corporation Vaxstation-II based data acquisition system was used to

control the DA3.10 spectrometer. A 60-degree field-of-view Infrared Associates broad-band, liquid nitrogen cooled, mercury-cadmium-telluride (MCT) detector fitted with a KRS-5 infrared window was used for these FT-IR studies. The active area of the detector element was 1.032 mm^2. The measured D* value of the detector was 3.13 x 109 $cmHz^{0.5}$ and the cutoff wavenumber was 400 cm^{-1} (25 microns). A mid infrared, water-cooled, ceramic silicon carbide source was used for the mid-IR region and a visible quartz tungsten halogen source, mounted inside the spectrometer, was used for sample alignment.

The optical resolution used in these studies ranged between 2.0 and 0.5 wavenumbers. A preliminary study showed that the spectra of kaolinite were not instrument-limited for nominal resolution values of 0.5, 1.0, 2.0 cm^{-1}. At 4.0 cm^{-1} resolution, however, the spectrum of kaolinite was instrument-limited. The FT-IR spectra of the SAz-1 Cheto-montmorillonite sample were not instrument-limited at a resolution of 2.0 cm^{-1}. A Hamming apodization function was used to weight the cosine wave interferograms. Initially, a low-resolution double-sided interferogram was collected and the phase angle deviation from zero of the interferogram was determined using the Forman method. The phase correction determined from the double-sided interferogram was stored in the HSVP and all subsequently single-sided, high resolution interferograms were corrected using these stored values. Typically, 16000 data points were collected per single sided interferogram with approximately 900 data points collected before the centerburst. Programmable low-pass and high-pass analog filters were used to optimize the signal-to-noise ratio. A low pass cut-off filter of 20 KHz, and a high-pass cut-off filter of 2 Hz (3 dB cutoff frequencies). Interferograms were collected with a moving mirror velocity of 0.5 cm/sec which corresponded to a sampling frequency of 15.8 KHz. The dynamic range of the analog-to-digital converter was 16 bits and the word length of the Vaxstation-II computer was 32 bits. One sample point was collected per laser fringe with a resolution of 16 bits per sample. Typically, 256 scans were coadded for the sample and reference files. The total measurement time for coadding 256 scans was 200 seconds for 1 cm^{-1} resolution and 600 seconds for 0.5 cm^{-1} resolution. No smoothing or interpolation algorithms were used.

The sample compartment of the Bomem DA3.10 was operated under a

reduced pressure of 0.05 torr in order to remove interferences from H_2O and CO_2 and other vapor phase constituents. The sample cover access plates were modified to accommodate two 3/8 inch MDC quick-disconnect vacuum tube feedthroughs which provided a connection through the vacuum wall of the spectrometer from the vacuum manifold to the CE-TR cell in the sample compartment.

3. DESCRIPTION OF THE VAXSTATION-II DATA ACQUISITION SYSTEM

The data acquisition system for the Bomem DA3.10 spectrometer was a Digital Equipment Corporation (DEC) Vaxstation-II computer. The Vaxstation-II computer consists of a μVAX-II cpu with a dedicated high-resolution, bit-mapped graphic display terminal. The Bomem DA3.10 spectrometer is connected directly to a dedicated high-speed vector processor (HSVP) through a 50-line parallel interface. The Vaxstation-II communicated with the HSVP through a National Instruments General Purpose Interface Bus (GPIB) Card (Model No. GPIB11V-2) which was resident on the Q-bus of the Vaxstation-II. The initial data acquisition system that was used to collect data from the Bomem was a DEC PDP 11/23 computer (which also supports the Q-bus). The use of the PDP 11/23 was limited for this application because of the 16-bit word-length and address restrictions, limited storage capability, and the extremely slow display output which resulted from the 9600 baud serial-throttle of the VT-240 terminal. The slow transmission rate to the display and the low vertical resolution (200 pixels) of the VT-240 terminal, in particular, were serious limitations of the PDP 11/23 data acquisition system. In terms of overall computational performance, the Vaxstation-II (μVax-II) system is approximately 20 times faster than the PDP 11/23. Bomem does not support their software on the Vaxstation-II, thus, the Bomem Fortran-77 and assembly-level (Macro-11) codes were modified and transferred to the Vaxstation-II. Most of the routines could be transferred directly to the Vaxstation-II with little, or no, modification; however, the HSVP routines had to be re-written altogether because of the significant differences between the VAX/VMS and RT-11 operating systems.

In addition to the HSVP routines, new codes were developed to support the VR260 graphic display terminal. The Vaxstation-II software provided two environments for the development of the graphic display codes: the VAX GKS

run-time library of graphical functions that are defined by the ANSI X3.124-1985 and ISO 7942-1985 Graphic Kernel System (GKS) standards, or the device dependent MicroVMS Workstation Graphics. The VAX GKS environment was chosen over the latter because GKS is supported on a number of different machines (e.g., DEC, IBM, HP etc.) and supports a number of different graphic output formats including the Tektronix 4010/4014, DEC VT-125, DEC Vaxstation-II VR260, LVP16, HP7470, HP7475A, LNO3, and GKS Metafile formats. The graphic display codes were developed on the Vaxstation-II operating under the VAX/VMS Version 4.5 operating system using V3.1 of the MicroVMS workstation software. The VAX GKS V2.0 run-time library of graphical functions were called from VAX Fortran-77 V4.

4. DESCRIPTION OF THE CONTROLLED-ENVIRONMENT-TRANSMISSION CELL AND MANIFOLD

The controlled-environment-transmission (CE-TR) cell was a modified 10 cm pathlength cell fitted with two Kontes Teflon® stopcocks, and two 49-mm x 3-mm ZnSe windows using Viton O-rings. The Kontes Teflon® stockcocks were modified at the glass shop to accommodate two Lab-Crest Model 571190 9-mm Solv-Seal joints. The Solv-Seal joint system incorporates a TFE seal with two viton o-rings and can be pumped down to 10^{-8} torr. Clay films were held in place in the CE-TR cell using a TFE holder which allowed the films to mounted at 90 or 60 degree angles of incidence to the modulated IR beam. The CE-TR cell was mounted on a Newport Research Corporation (NRC) Model 460XYZ-DM translation stage which was used to position the cell in the spectrometer.

The vacuum system consisted of a 195-liter/minute mechanical pump, 3 angstrom molecular sieve trap, two way valve, water-cooled Edwards Diffstak 63 oil diffusion pump (135 liter/sec), Edwards Penning & Pirani gauge head assembly, ISO63 flange to KF40 flange adapter, KF-40 isolation valve, KF16 relief valve, 1 meter KF40 stainless steel bellows, glass liquid nitrogen trap fitted with Lab-Crest Model 571190 15-mm Solv-seal joints, and a five-place Teflon®/glass Airless-ware manifold fitted with Lab-Crest Model 571190 9-mm Solv-Seal joints. Because all of the glass joints were terminated with the Lab-Crest Solv-seal joints, the vacuum manifold was highly modular. An Edwards Model 1005 controller fitted with two Pirani gauge heads and one

Penning gauge were used to monitor the pressure in the CE-TR cell and vacuum manifold in the 760 torr to 10^{-7} torr range.

5. PREPARATION OF SELF-SUPPORTING CLAY FILMS

Thin self-supporting, clay films (SSCF) of SAz-1 montmorillonite were prepared by removing the salts from the aqueous stock suspension of the SAz-1 montmorillonite by repeated washings with distilled, deionized water. After the suspension tested negative for chloride using the AgCl test, small aliquots (< 1 mL) of the dilute suspension were placed on a polystyrene surface and allowed to dry. After the clay suspension had dried the clay film deposit on the polystyrene surface was removed by running the polystyrene plastic over a knife edge.

C. RESULTS

1. COMPARISON OF PRESENTATION METHODS

A comparison of FT-IR sample presentation methods was conducted for a reference clay mineral using controlled environment transmission (CE-TR), diffuse reflectance (DR), and cylindrical internal reflectance(CIR) methods to determine the optimum presentation technique. For the purpose of this comparison, the well-crystallized KGa-1 reference kaolinite clay was chosen because its infrared and Raman spectra have been reported in the literature (References VI-20, VI-22). In addition, the cation exchange capacity, surface area, chemical composition, description of the geological deposit and location, and thermal analysis data of this clay mineral have been described by van Olphen and Fripiat (Reference VI-20).

FT-IR spectra of KGa-1 kaolinite obtained using CE-TR, DR, and CIR in the 700 to 4000 cm^{-1} region are shown in Figures 40-42. The CE-TR KGa-1 sample (Figure 40D) was prepared by deposition from a dilute KGa-1 aqueous suspension on a ZnSe window, the DR sample (Figure 40C) was a 4 percent (w/w) mixture of crude KGa-1 clay in KCl mixed together for 60 seconds in a Wig-L-Bug mixer, and the CIR sample was obtained by placing a 1 percent KGa-1 aqueous suspension directly in the CIR cell. Good agreement was obtained

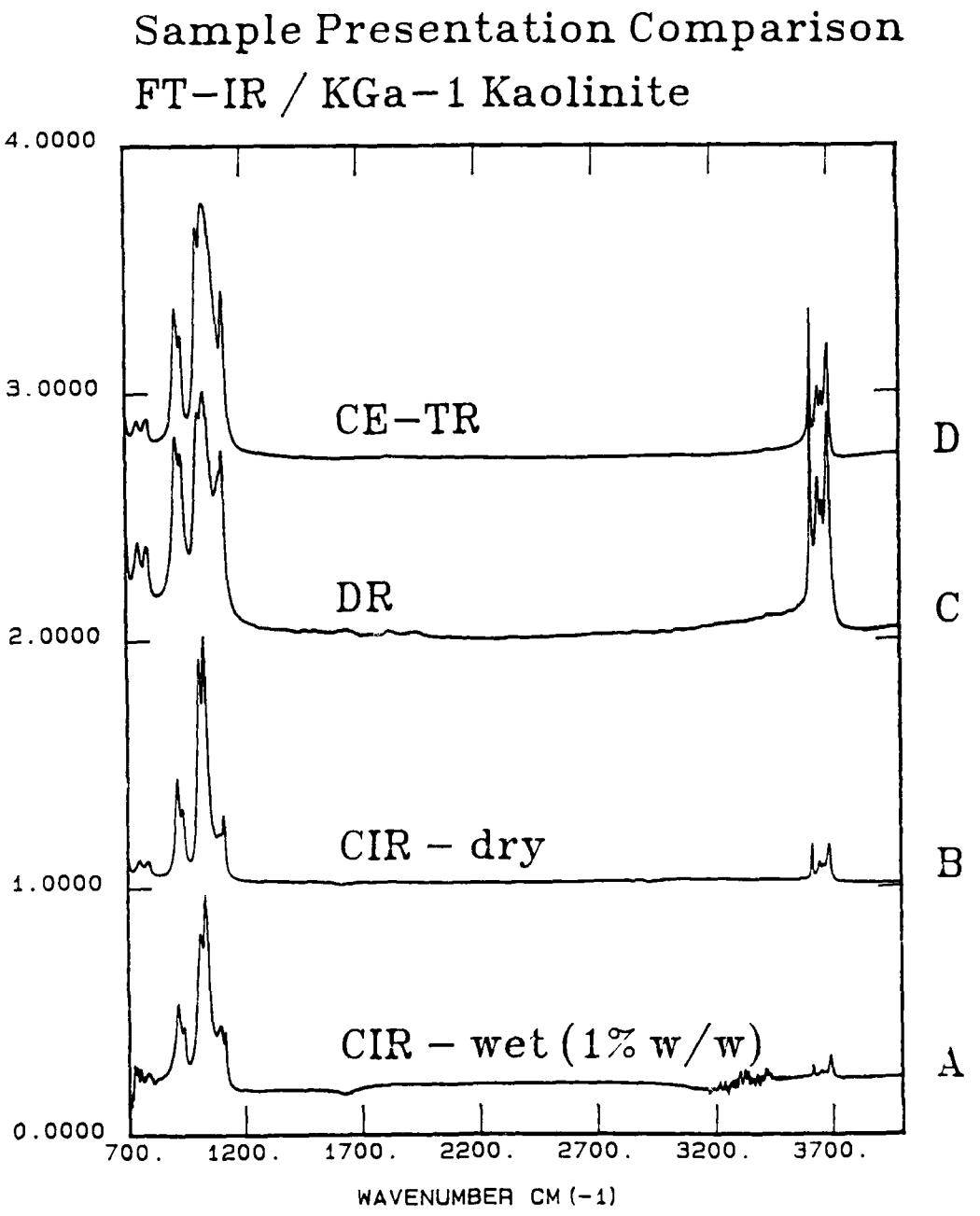

Figure 40. Comparison of FT-IR Spectra of KGa-1 Kaolinite in the 700 to 4000 cm^{-1} Region Obtained Using the Controlled Environment Transmission Cell (D), Diffuse Reflectance (C), Cylindrical Internal Reflectance Spectrum Dry (B), and the Cylindrical Internal Reflectance Spectrum Wet (A).

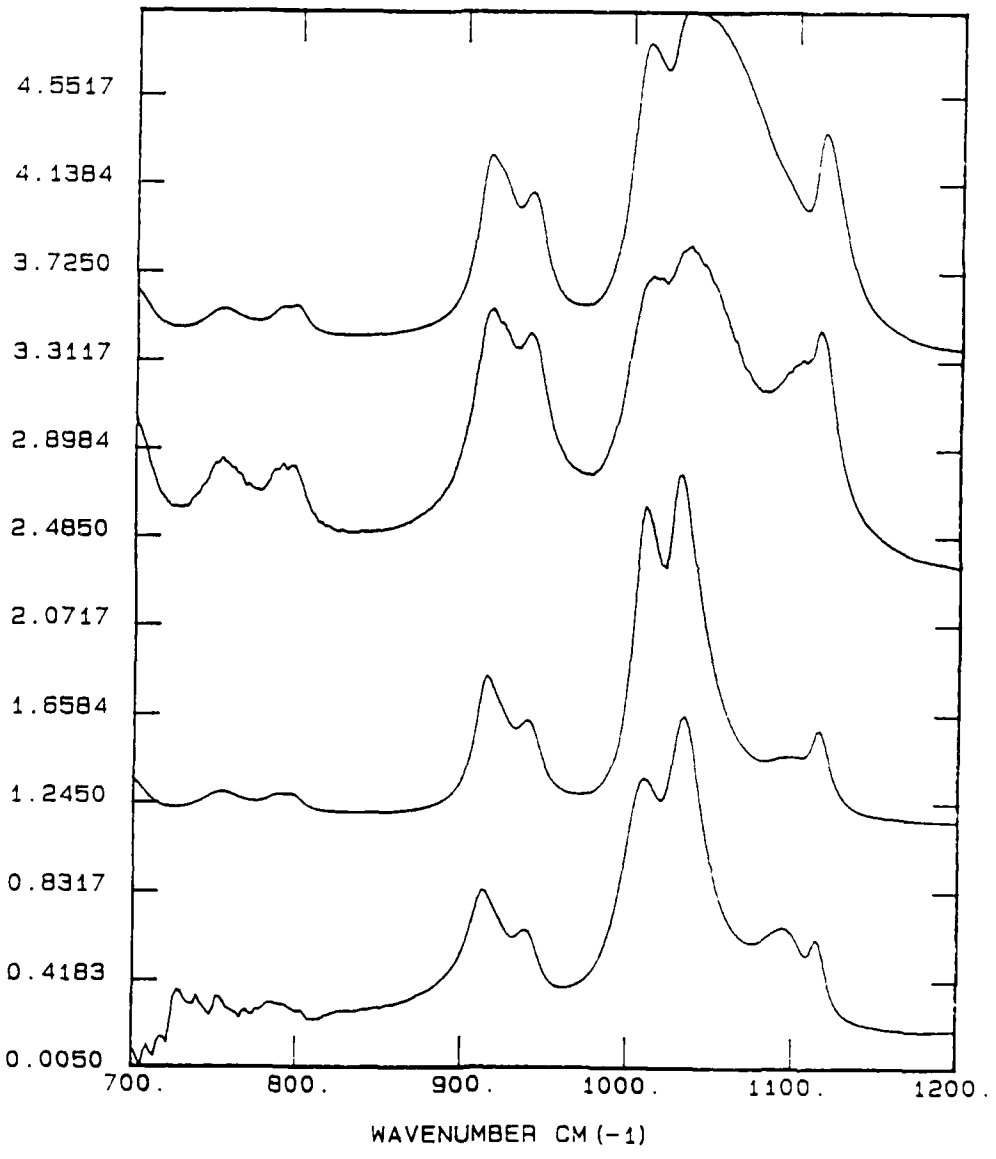

Figure 41. Comparison of FT-IR Spectra of KGa-1 Kaolinite in the 700 to 1200 cm^{-1} Region Obtained Using the Controlled Environment Transmission Cell (D), Diffuse Reflectance (C), Cylindrical Internal Reflectance Spectrum Dry (B), and the Cylindrical Internal Reflectance Spectrum Wet (A).

between the spectral band positions considering the diversity of sample presentation methods used. Insofar as these authors are aware, there have no reported FT-IR spectra of clay minerals using CIR and DR. In a spectroscopic study of structural disorder among natural kaolinite and dickite samples, Brindley et al. (Reference VI-24) showed that the spectral resolution of the 3652 and 3669 cm^{-1} bands correlated strongly with the measured XRD structural disorder of the samples (Reference VI-25). In the present study, this spectral criterion was used to evaluate the sensitivity of the three methods. As the spectra shown in Figure 42 indicated, the greatest resolution and separation of the 3652 and 3669 cm^{-1} bands were achieved using CE-TR over the DR, and CIR methods. In addition, the CE-TR spectrum had the highest signal-to-noise ratio (SNR) of the three methods. Similar results were obtained in a comparison of FT-IR spectra of the SAz-1 reference montmorillonite sample obtained using CE-TR, DR, and CIR methods (Figure 43). The SNR of the DR spectrum (Figure 43A) was much lower than that of the CE-TR, or CIR spectra. In agreement with KGa-1 sample presentation results, the CE-TR spectrum had the highest SNR of the three techniques. The low frequency optical cutoff for the CIR spectrum was 700 cm^{-1} because of the optical transmission properties of the ZnSe internal reflection element (IRE) of the CIR cell. The CETR spectrum did not have this restriction and the low frequency cutoff for the CE-TR spectra was 450 cm^{-1}. Many organic adsorbates have absorption bands in the 450 to 700 cm^{-1} region, e.g., out-of-plane C-H deformation modes of aromatic hydrocarbons; thus, CIRZnSe methods do not permit observation of these modes. Thus, in addition to the higher sensitivity of the CETR method, one additional advantage of this method over CIRZnSe is the extended frequency range. Overall, CE-TR was the most appropriate technique for noninvasive vapor-phase adsorption studies of clay minerals of the three techniques considered here.

Band positions obtained from the CE-TR spectrum (Figures 44-45) are in good agreement with the dispersive-IR and Raman literature values (References VI-26-32) for kaolinite (Table 47). For comparison, the Raman spectra of KGa-1 kaolinite in the 3600 to 3725 cm^{-1}, 100 to 1000 cm^{-1}, and 200 to 1000 cm^{-1} regions are shown in Figures 46-48. There is a strong correspondence between the Raman and IR spectra of kaolinite in the hydroxyl stretching region (Figure 46). What is not apparent from this comparison, however, were the

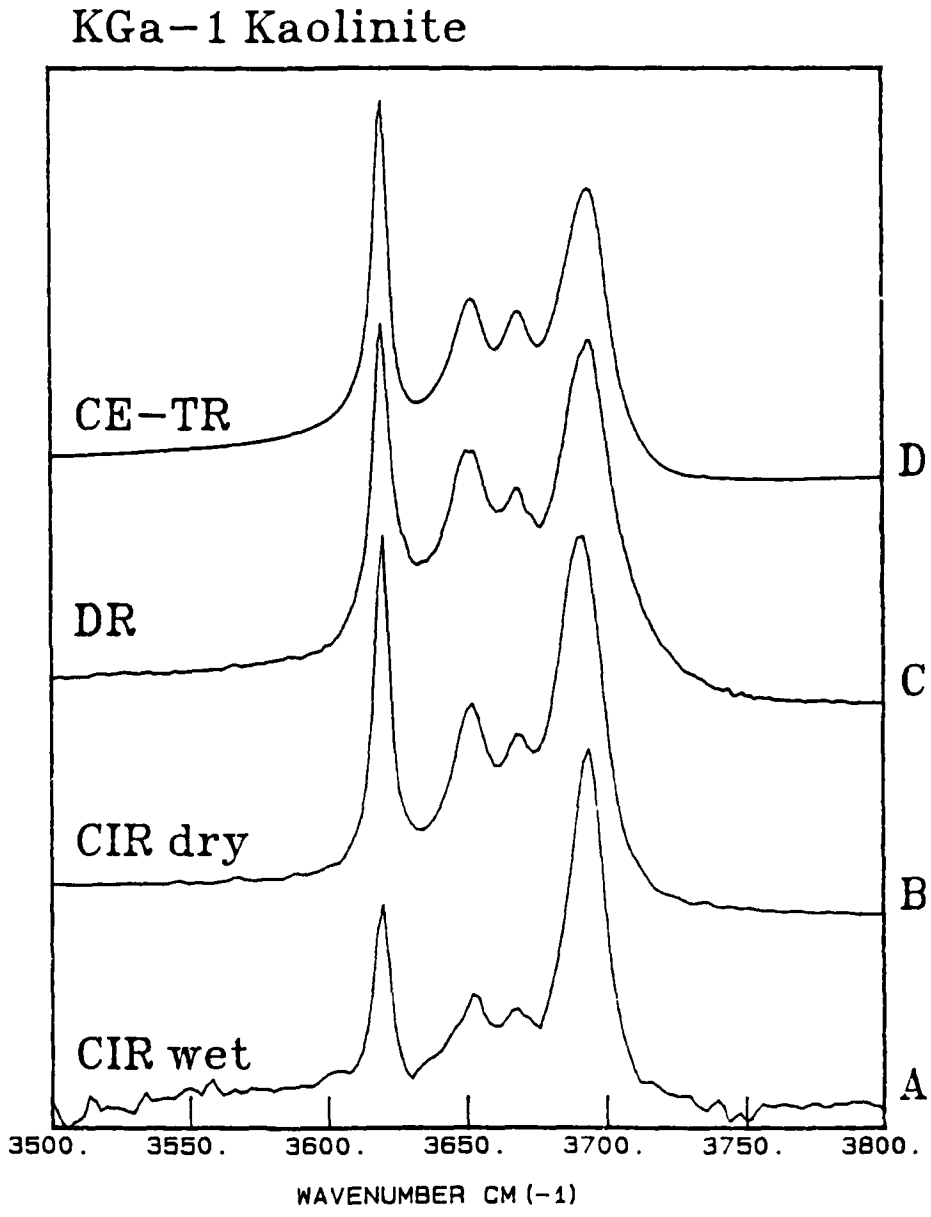

Figure 42. Comparison of FT-IR Spectra of KGa-1 Kaolinite in the 3500 to 3800 cm^{-1} Region Obtained Using the Controlled Environment Transmission Cell (D), Diffuse Reflectance (C), Cylindrical Internal Reflectance Spectrum Dry (B), and the Cylindrical Internal Reflectance Spectrum Wet (A).

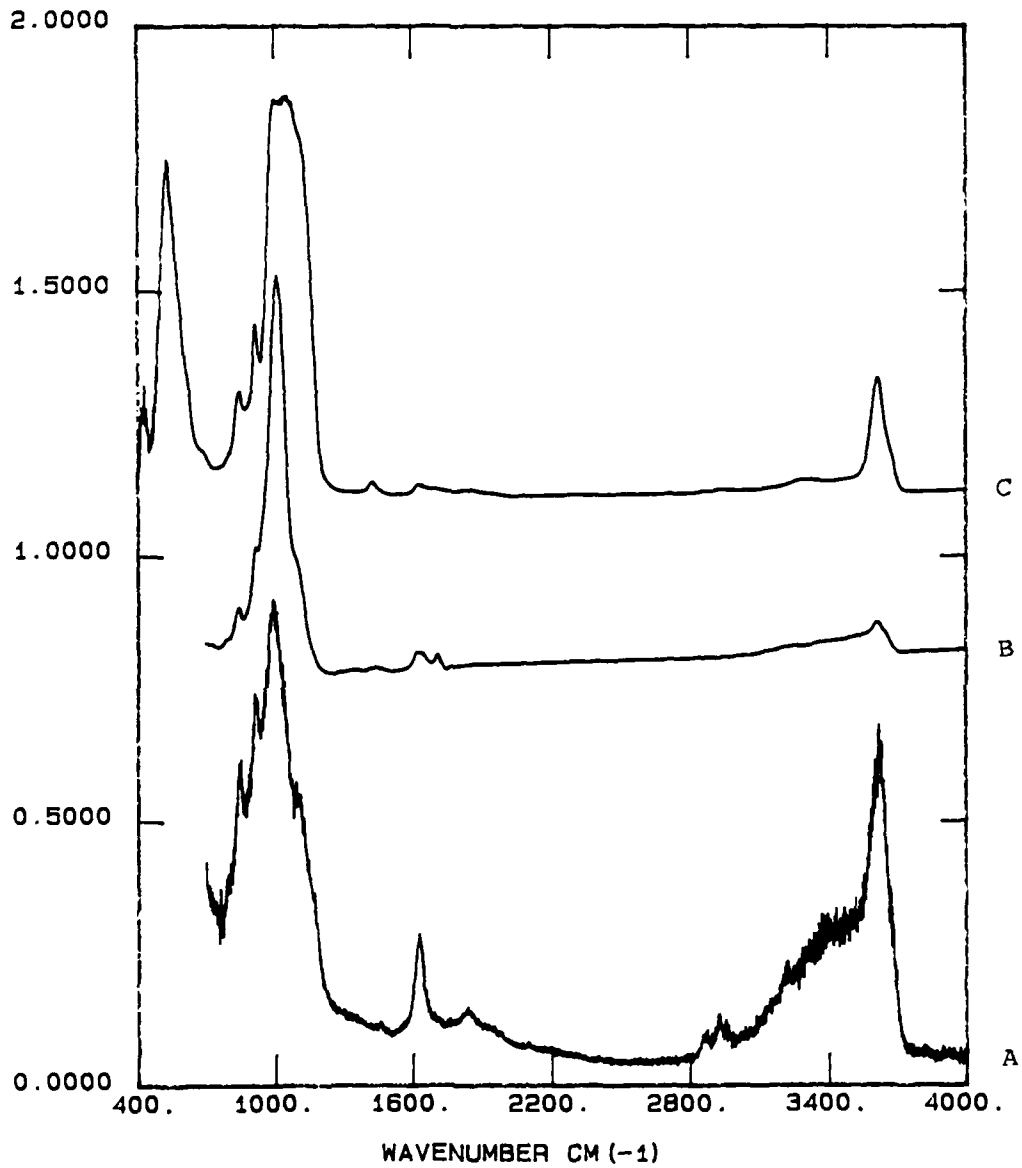

Figure 43. Comparison of FT-IR Spectra of SAz-1 Na-Montmorillonite in the 400 to 4000 cm^{-1} Region Obtained Using the Diffuse Reflectance Cell (A), Cylindrical Internal Reflectance Spectrum of Dry SAz-1 (B), and CE-TR Spectrum of a Thin Self-Supporting Clay Film of Montmorillonite in the Controlled Environment Transmission Cell (C).

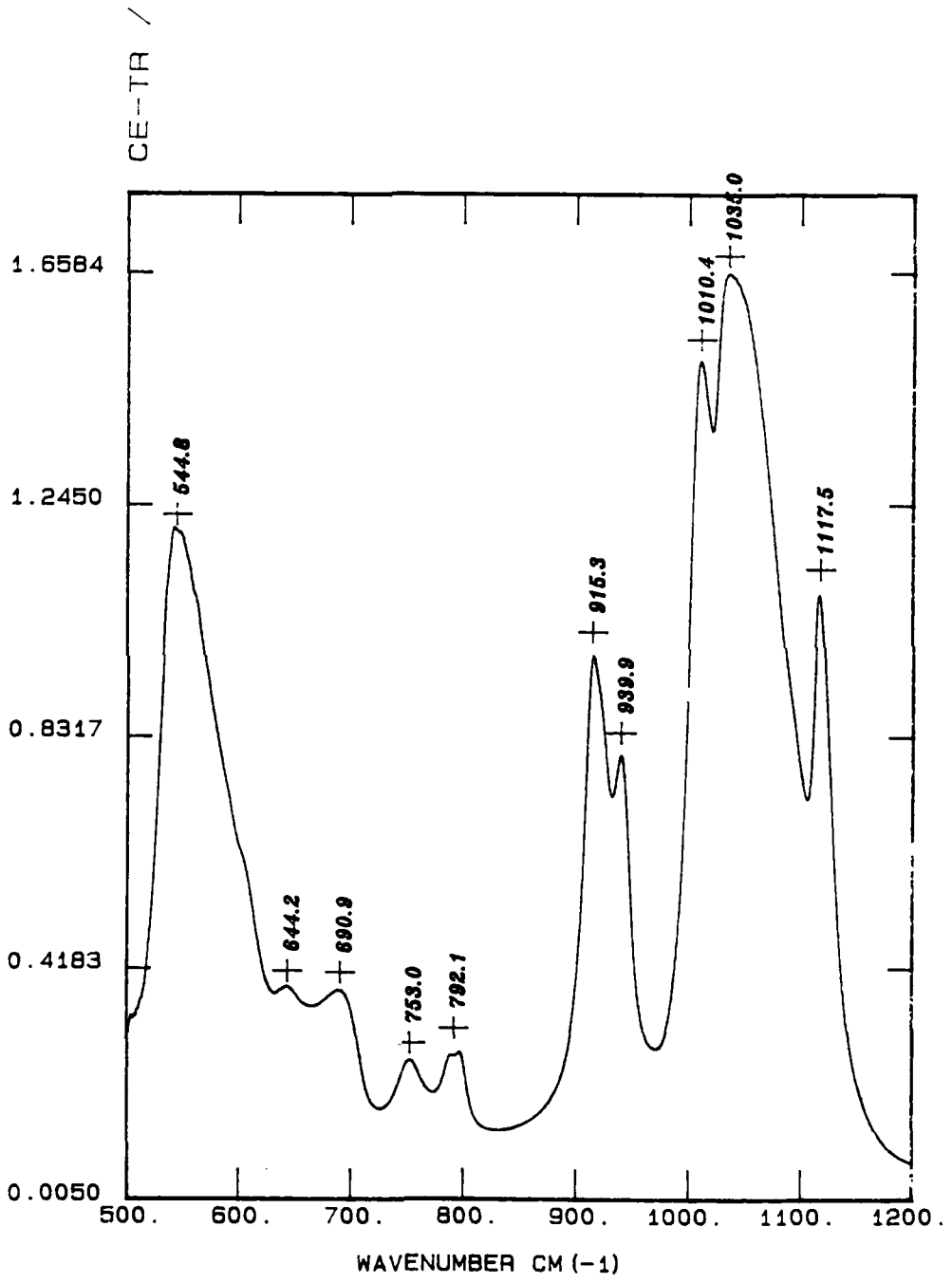

Figure 44. Absorbance FT-IR Spectrum of KGa-1 Kaolinite in the 500 - 1200 cm^{-1} Region Obtained Using the Controlled Environment Transmission Cell Under a Vacuum of 10^{-3} Torr.

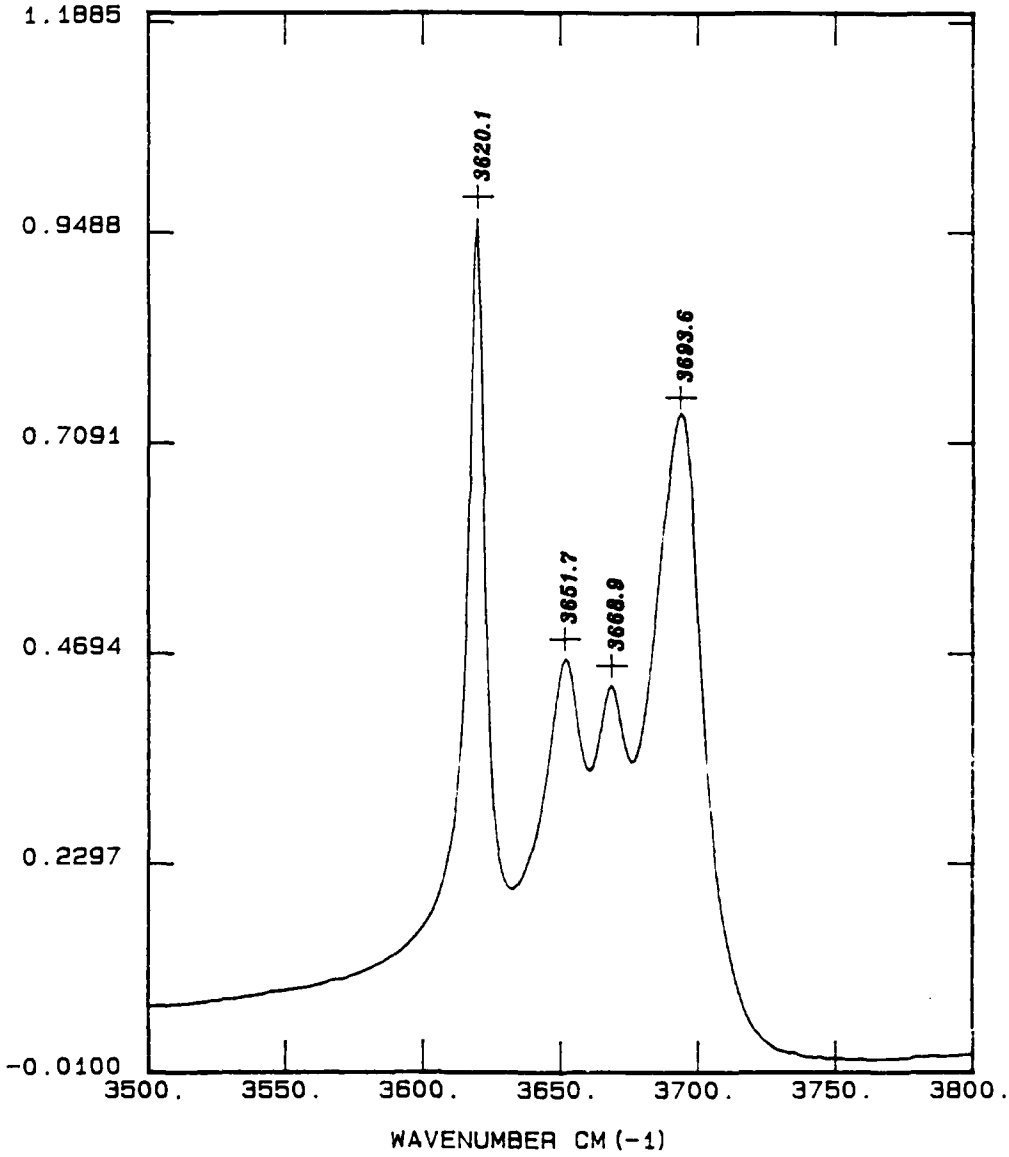

Figure 45. Absorbance FT-IR Spectrum of KGa-1 Kaolinite in the 3500 to 3800 cm^{-1} Region Obtained Using the Controlled Environment Transmission Cell Under a Vacuum of 10^{-3} Torr.

TABLE 47. COMPARISON OF OBSERVED FT-IR BANDS POSITIONS TO PUBLISHED RAMAN AND IR BAND DATA FOR KGa-1 KAOLINITE.

Observed FT-IR	Lit.[a] IR	Lit.[b] Raman	Assignment
--	130	130	
--	--	141	
--	190	201	
--	--	--	
--	--	244	
--	268	271	
--	338	335	
--	352	--	
--	366	--	
--	405	397	
--	--	--	
--	440	431	
--	--	461	
--	470	--	
--	--	512	
544	555	--	Si-O-Al Skeletal stretch
644	638	637	
691	692	700	δ(O-H) gibbsite layer
753	754	750	δ(O-H) gibbsite layer
792	792	790	
799	799	--	
915	918	915	δ(O-H) inner surface
940	941	940	δ(O-H) inner sheet (inner hyd)
1010	1018	--	ν(Si-O)
1035	1040	--	ν(Si-O)
--	1101	--	ν(Si-O)
1117	1120	--	ν(Si-O)
3620	3620	3621	ν(O-H) inner-sheet hydroxyl (inner hyd)
3652	3652	3652	ν(O-H) inner-surface hydroxyl
3669	3668	3668	ν(O-H) inner-surface hydroxyl
--	--	3688	ν(O-H) inner-surface hydroxyl
3694	3695	3696	ν(O-H) inner-surface hydroxyl

[a] Data compiled from Ledoux and White (1964), Wada (1967), Ishii et al. (1967), Estep et al. (1968), Larson et al. (1972), Farmer (1974) and Rouxhet et al. (1977).

[b] Johnston et al. (1985).

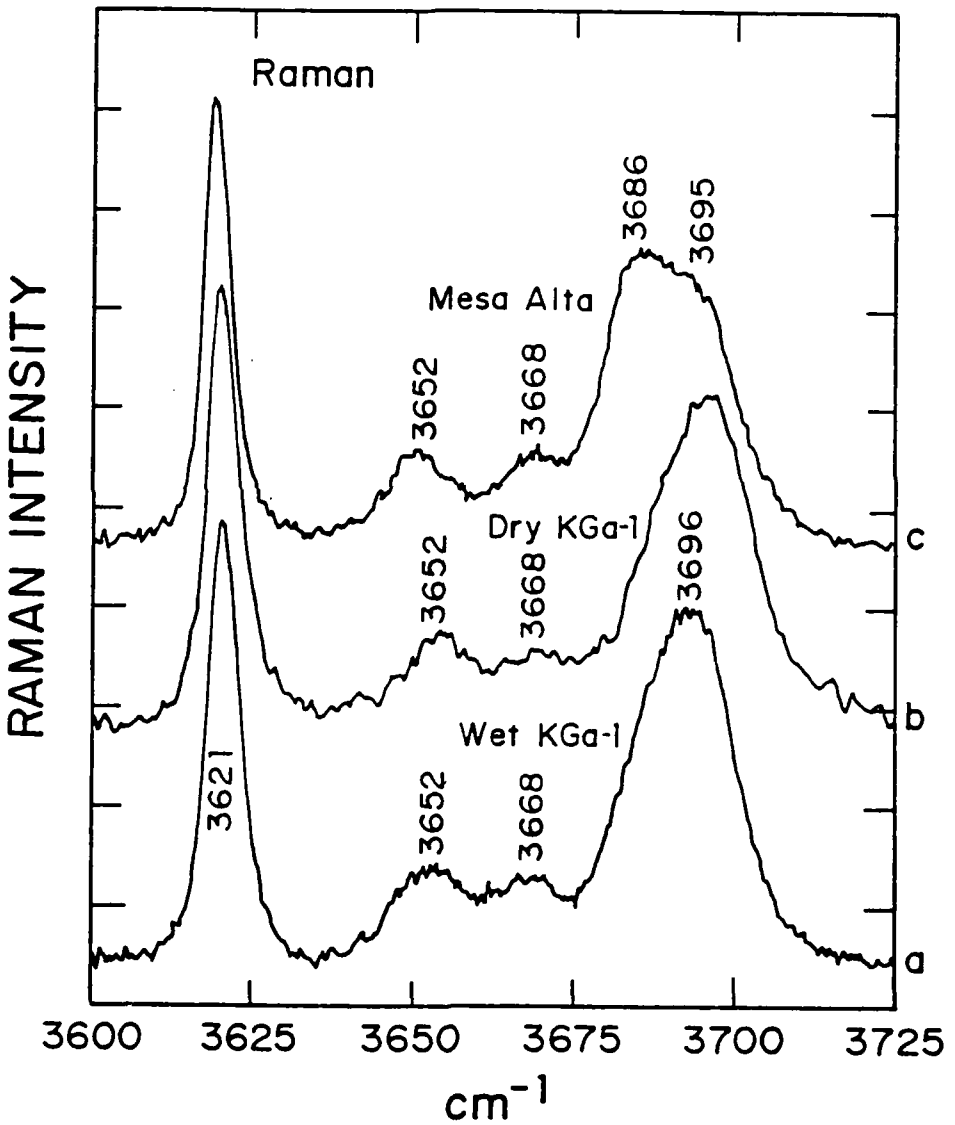

Figure 46. Raman Spectra of KGa-1 Kaolinite in Aqueous Suspension (A), Dry KGa-1 Kaolinite (B), and Dry Mesa Alta Kaolinite (C) in the 3600 to 3725 cm^{-1} Region.

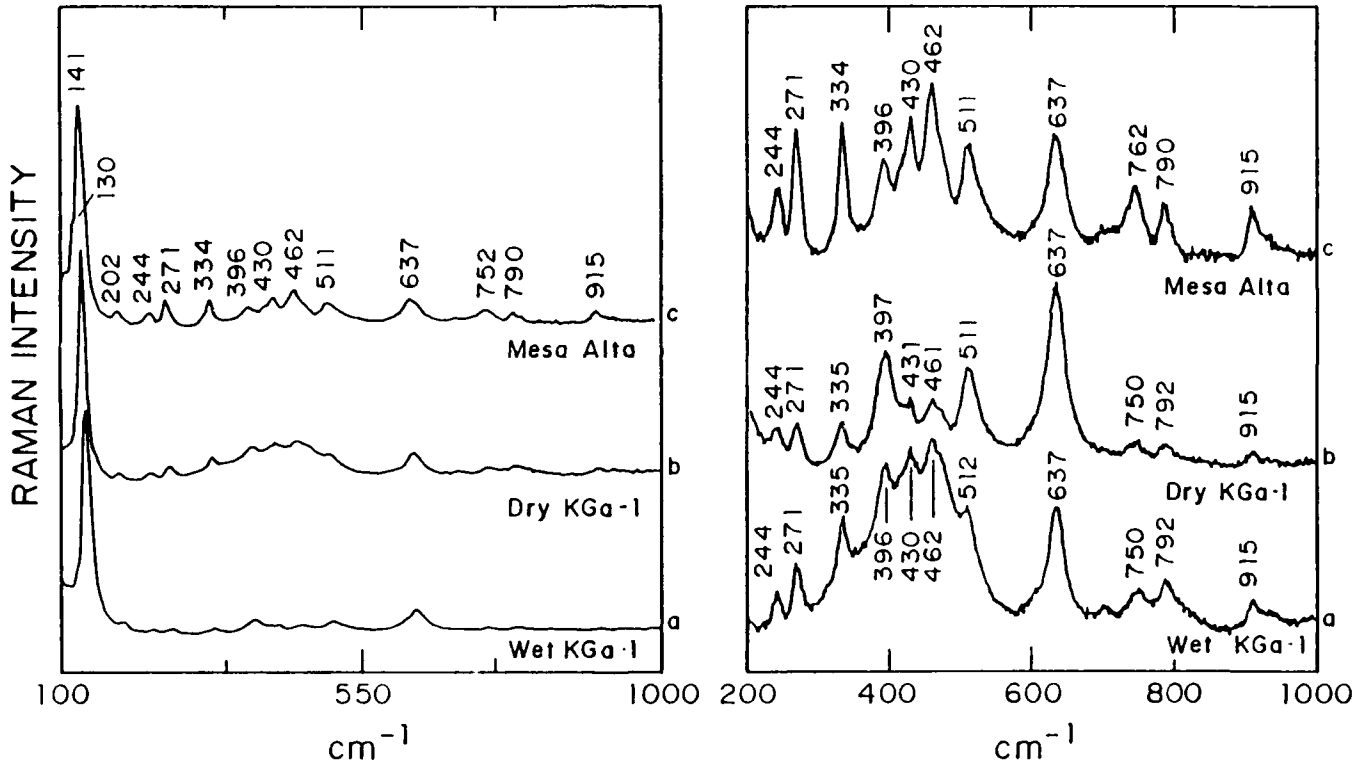

Figure 47. Raman Spectra of KGa-1 Kaolinite in Aqueous Suspension (A), Dry KGa-1 Kaolinite (B), and Dry Mesa Alta Kaolinite (C) in the 100 to 1000 cm^{-1} Region.

Figure 48. Raman Spectra of KGa-1 Kaolinite in Aqueous Suspension (A), Dry KGa-1 Kaolinite (B), and Dry Mesa Alta Kaolinite (C) in the 200 to 1000 cm^{-1} Region.

large differences in scan collections times; for a 1.0 cm^{-1} resolution Raman scan of kaolinite using a typical dwell time of 5 sec step-1 in the 100 to 4000 cm^{-1} region would require 325 minutes (5.5 hours) of sample collection time. In contrast, a comparable SNR could be obtained in approximately 1 minute using CE-TR FT-IR. Thus, CE-TR FT-IR methods are characterized by a much higher sensitivity than Raman techniques for studies of clay minerals. In the hydroxyl stretching region of kaolinite, CE-TR provides a considerable advantage over Raman methods considering the similarity of the spectra in this region and the much longer scan times required for Raman spectra. In contrast to the good overall agreement between the Raman and CE-TR spectra in the hydroxyl stretching region, there is poor correspondence between the spectral band positions and relative intensities of the Raman (Figures 47-48) and CE-TR (Figure 44) spectra in the low frequency region. Thus, a more complete characterization of the lower frequency vibrational modes of kaolinite is obtained using a combined application Raman and FT-IR methods (Reference VI-22).

2. COMPARISON OF CE-TR SPECTRA OF Na-, Ca-, AND Cu-EXCHANGED SAz-1 MONTMORILLONITE SAMPLES

Thin, self-supporting clay films (SSCF) were prepared from homoionic clay suspensions containing 0.01 M NaCl, $CaCl_2$, $CuCl_2$ salt solutions. FT-IR spectra of the Na, Ca-, and Cu-exchanged SSCFs are shown in Figures 49-51. These spectra were obtained under a roughing vacuum of 10^{-3} torr. The clay films were evacuated to minimize the interference of adsorbed water. The general features of the montmorillonite spectra were in good agreement with the published dispersive IR spectra of montmorillonite samples (Reference VI-31). The principal montmorillonite bands occur at 842, 908, 1040, and 3616 cm^{-1}, and the bands of adsorbed water occur at 1630 cm^{-1} and in the 3100 to 3500 cm^{-1} region. The montmorillonite hydroxyl deformation modes (δ(OH)) were observed at 842 and 908 cm^{-1} and have been assigned (References VI-31, VI-33) as Mg-Al-OH and Al_2OH deformation modes, respectively. The low frequency spectra of these three homoionic clay films in the 450 to 1250 cm^{-1} region were very similar (Figure 50). However, significant differences were observed in the TR FT-IR spectra in the 2600 to 3800 region (Figure 51). All of the complexes were evacuated to 10^{-3} torr, however, the Na-exchanged (Na-X) sample

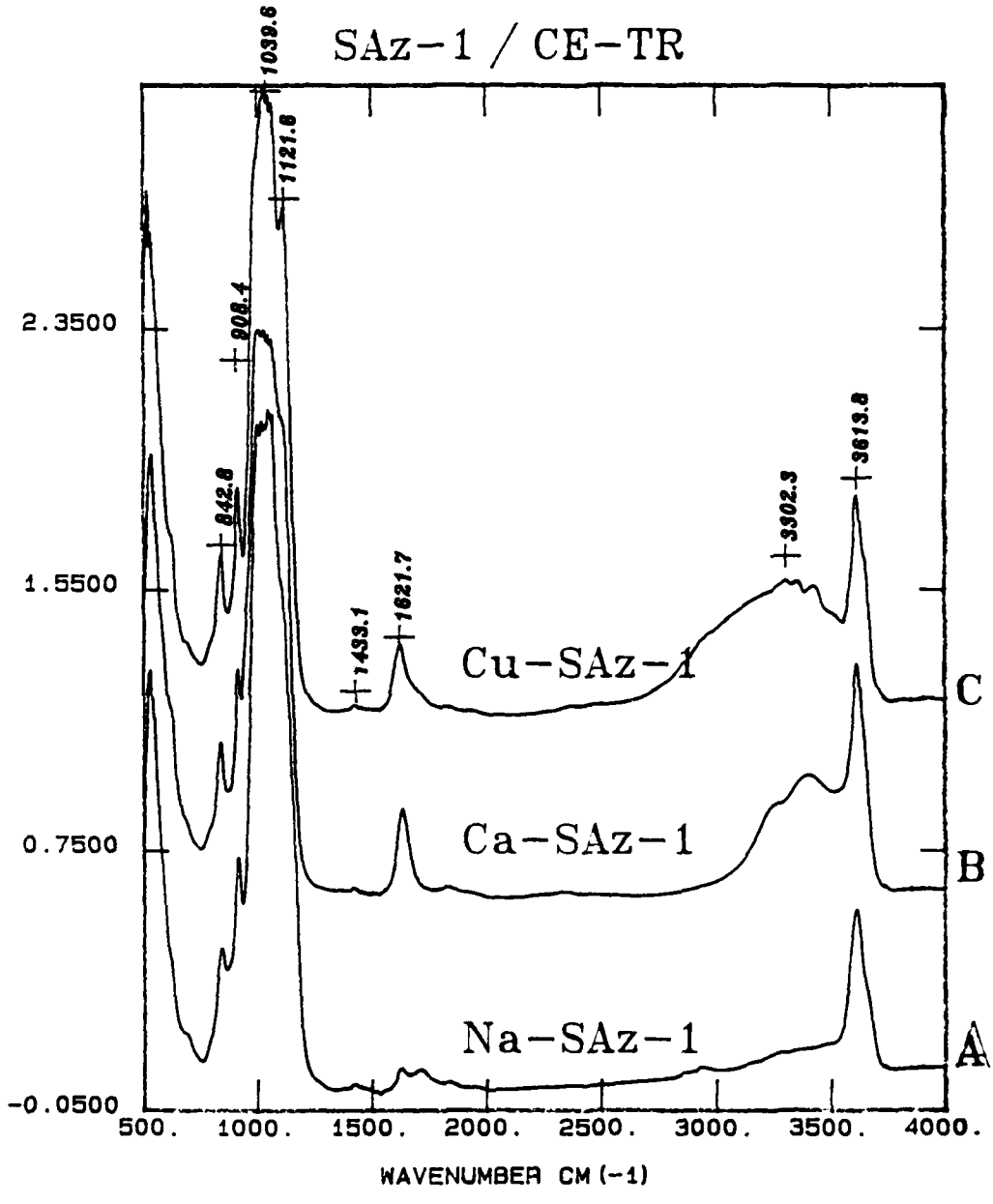

Figure 49. CE-TR FT-IR Spectra of Thin Self-Supporting Clay Films in the 500 to 4000 cm^{-1} Region of Na-SAz-1 (A), Ca-SAz-1 (B), and Cu-SAz-1 (C,top).

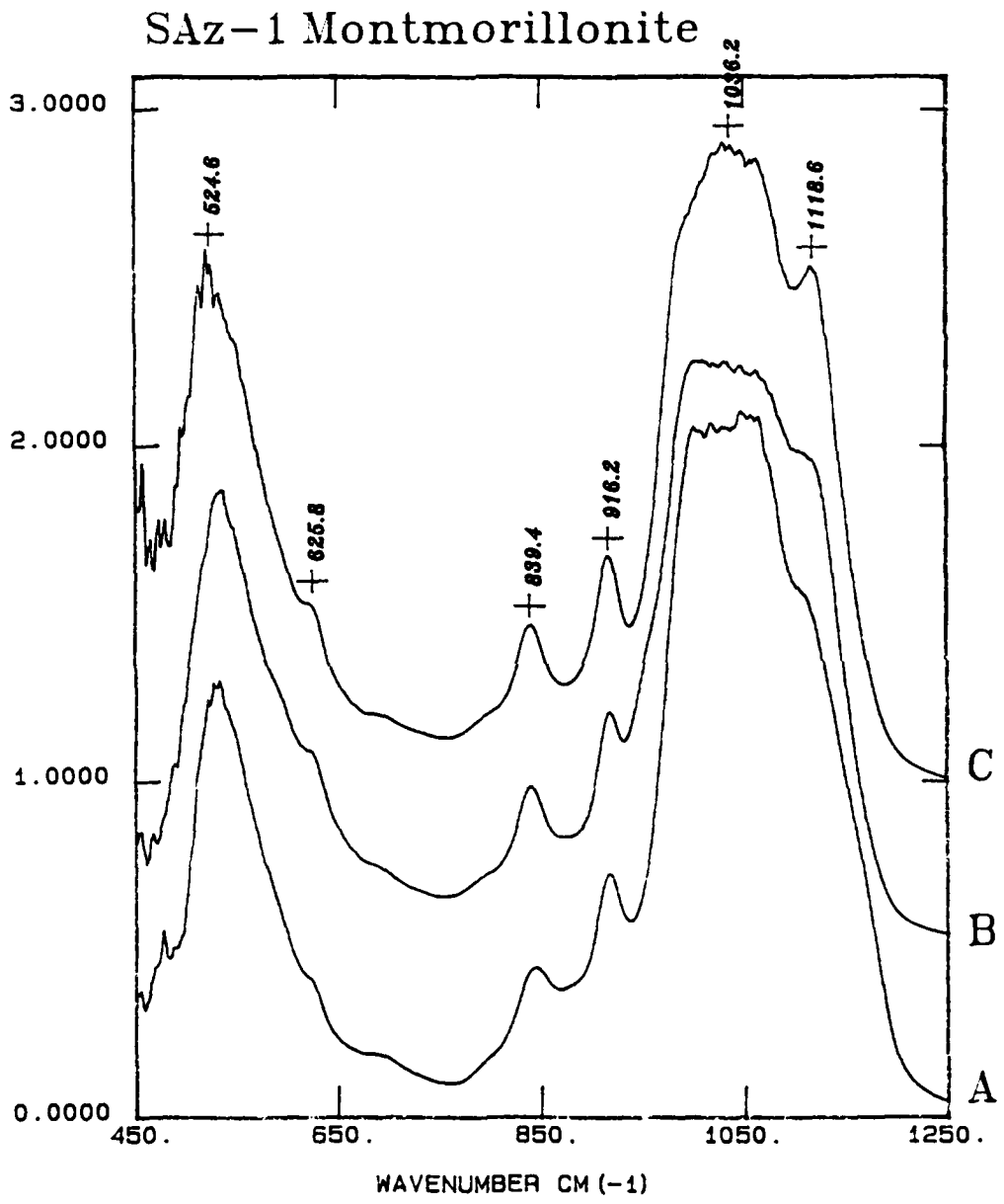

Figure 50. CE-TR FT-IR Spectra of Thin Self-Supporting Clay Films in the 450 to 1250 cm^{-1} Region of Na-SAz-1 (A), Ca-SAz-1 (B), and Cu-SAz-1 (C,top).

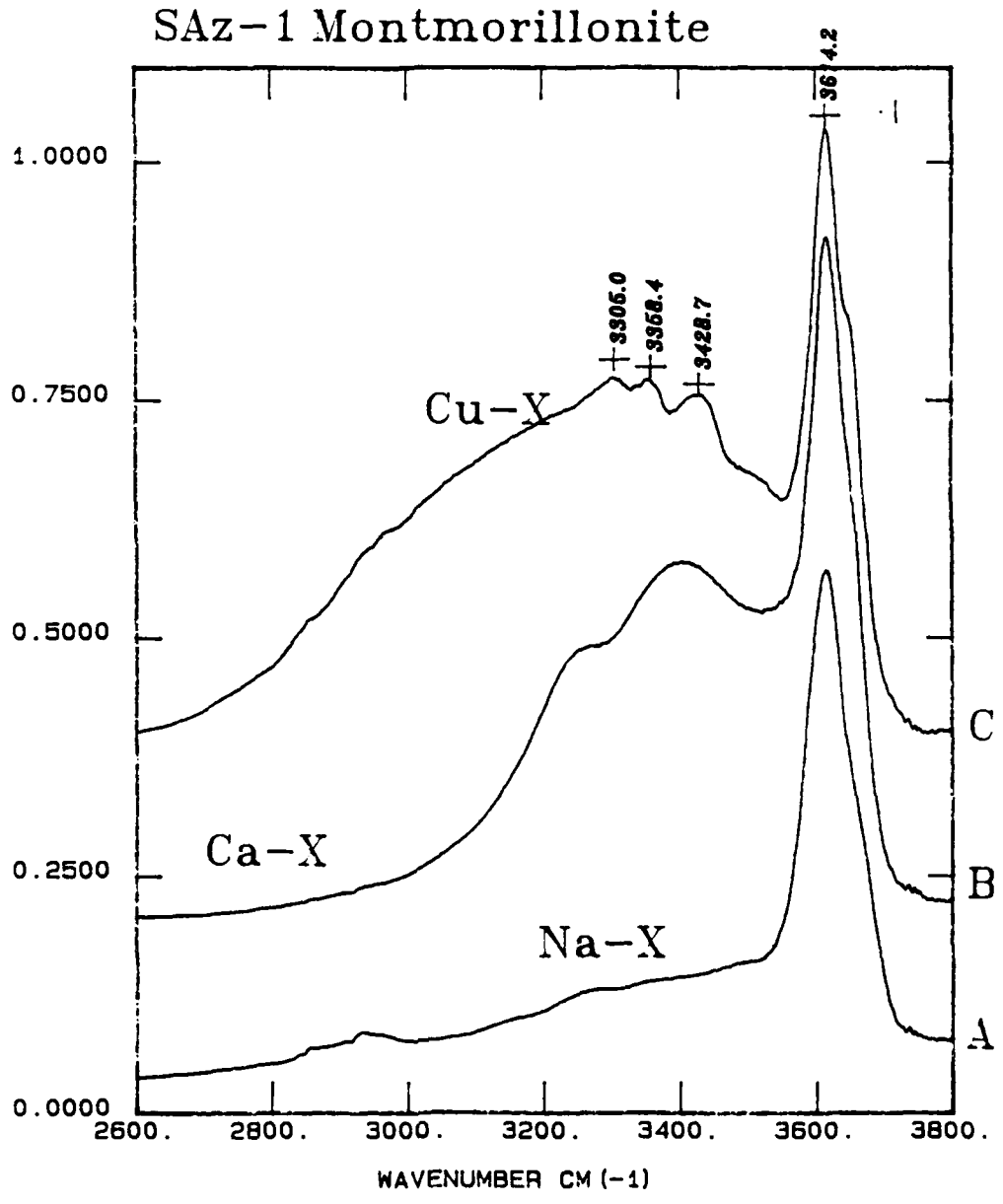

Figure 51. CE-TR FT-IR Spectra of Thin Self-Supporting Clay Films in the 2600 to 3800 cm^{-1} Region of Na-SAz-1 (A), Ca-SAz-1 (B), and Cu-SAz-1 (C,top).

contained much less adsorbed water that the Ca-X or the Cu-X clays. This is consistent with the fact that the hydration energy of Na^+ is much lower than for Ca^{+2} and Cu^{+2}. Although the integrated intensities of the of δ(O-H) band at 1622 cm^{-1} of adsorbed water on the Ca-X and Cu-X exchangers were approximately equal (Figure 49), which indicated qualitatively that the amount of water adsorbed by the two clays were similar, the vibrational structure in the ν(O-H) region of adsorbed water was considerably different (e.g., spectra shown in Figures 51B, and 51C). Similar results were obtained by Farmer et al. (Reference VI-34) who compared the IR spectra of Cu-X, Mg-X, and K-X montmorillonite samples. They proposed that the increased vibrational structure observed for Cu-X sample in comparison to K-X resulted from greater hydrogen bonding of water molecules coordinated to Cu^{+2} than for interlamellar K^+ ions. The fact that greater vibrational structure was observed for the Cu-X system in the present study indicated that the water molecules coordinated to the interlamellar Cu^{+2} ions (aquo complex) were more highly ordered around the metal cation than in the case of the Ca-X and Na-X samples. It has long been recognized that the nature of the exchange complex, i.e., what type of metal cations reside on the surface, influence strongly the behavior of water near the mineral surface. These data support this hypothesis in that the vibrational spectra of adsorbed water on the surface were shown to depend strongly on the chemical nature of the metal cation on the exchange complex.

3. ORGANIC SORPTION STUDIES

The principal objective of this phase of the investigation was to study the adsorbate-surface interactions of clay-organic complexes using CE-TR FT-IR spectroscopy. Based upon the results of the sample presentation study, the controlled-environment transmission sample presentation method was selected as the optimum technique for these vapor phase sorption experiments. Benzene and p-xylene adsorption on Cu- and Na-exchanged SAz-1 montmorillonite samples were studied in the controlled environment transmission cell. CE-TR spectra of p-xylene vapor in the Sorption/desorption CE-TR FT-IR spectra were obtained for the following systems:

Adsorbate		Metal-Clay	Technique
p-xylene	:	Na-X	Controlled Desorption
p-xylene	:	Cu-X	Controlled Desorption
p-xylene	:	Cu-X	P_2O_5
benzene	:	Cu-X	P_2O_5

4. CONTROLLED DESORPTION STUDIES

a. Na-X : p-xylene complex

Vapor phase absorbance spectra of p-xylene adsorbed on self-supporting clay films (SSCF) of Na-exchanged SAz-1 montmorillonite were obtained by placing a small aliquot (<1 mL.) of p-xylene in the CE-TR cell containing the Na-X (Na-exchanged) SAz-1 clay film. A comparison of absorbance CE-TR spectra of an evacuated (10^{-3} torr) Na-exchanged SAz-1 montmorillonite clay film before addition of the p-xylene (Figure 52A) and of the same film after a 24 hour equilibration period with 1 mL. of p-xylene (Figure 52B) indicated that p-xylene and water vapor were co-adsorbed by the clay film. Because the interlamellar siloxane surface of montmorillonite clay is hydrophyllic (Reference VI-35), more water was adsorbed by the clay film than p-xylene.

Controlled desorption spectra of the clay-organic complexes were obtained by decreasing the pressure in the CE-TR, recording the pressure value, obtaining the single beam energy spectrum, and repeating the process until a moderately high vacuum of 10^{-7} torr had been achieved for a period of at least 24 hours. A brief description of the data manipulation procedures are given below.

Definitions:

(1) $S(\bar{\nu})_i$ = Single-beam energy spectrum (SBES) of the SSCF in the CE-TR cell.

(2) $A(\bar{\nu})_j^i = \ln \dfrac{S(\bar{\nu})_j}{S(\bar{\nu})_i}$ i = sample, j = reference

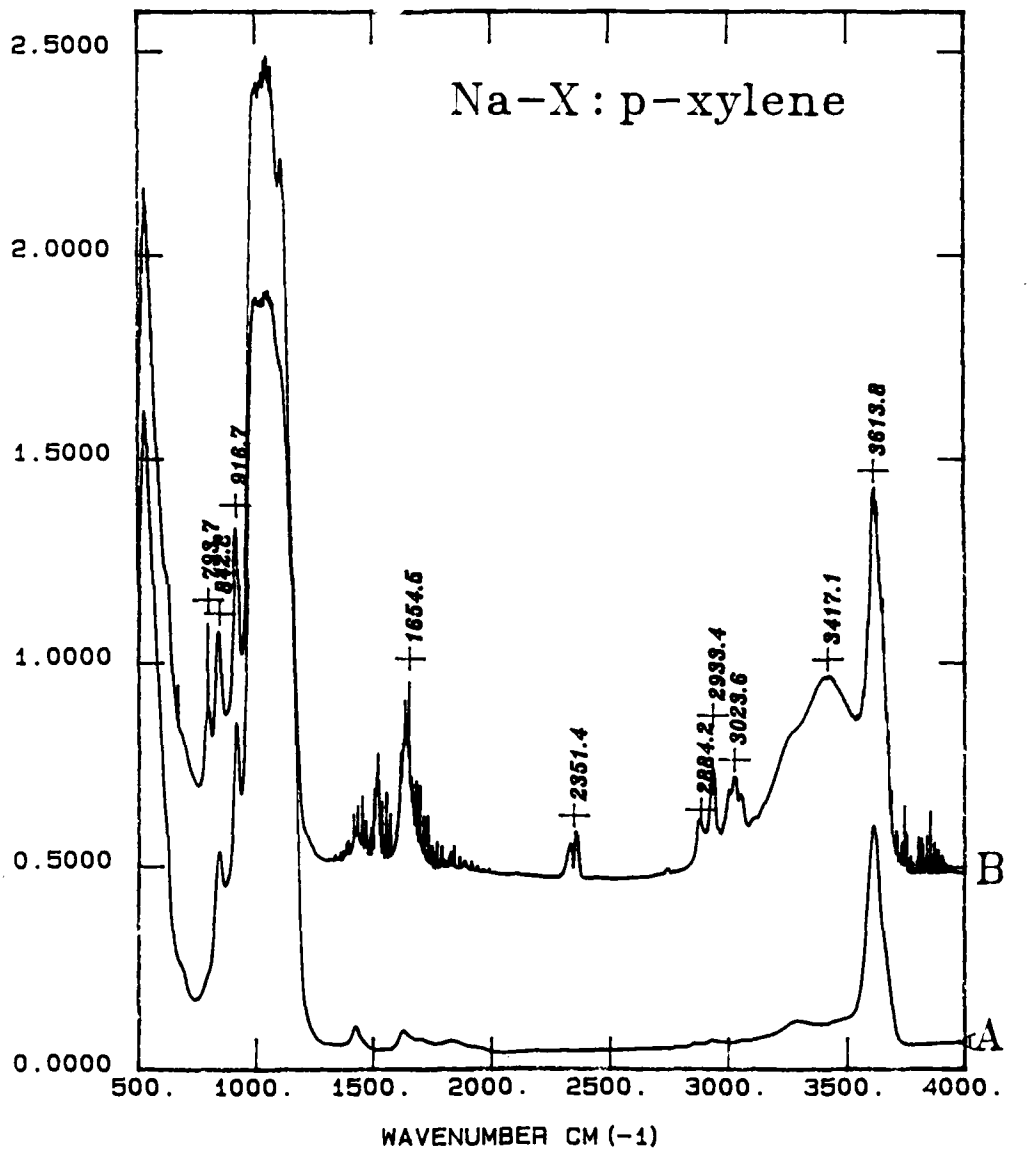

Figure 52. Absorbance CE-TR Spectra in the 500 to 4000 cm^{-1} Region of a Thin Self Supporting Clay Film of Na-SAz-1 Montmorillonite Prior to the Addition of the Organic (A), and the Same Na-SAz-1 Film Exposed to p-Xylene Vapor for 24 Hours.

$A(\bar{\nu})^{i}_{j}$ = absorbance spectrum of sample (i) ratioed against reference (j)

Controlled desorption absorbance spectra, $A(\bar{\nu})$, of the Na-exchanged (Na-X) SAz-1 : p-xylene complex are presented in Figure 53 as a function of the pressure in the CE-TR cell. These spectra were obtained by ratioing the $S(\bar{\nu})$ spectra of the clay-organic complex obtained at different pressure values against the $S(\bar{\nu})$ spectrum of the empty, evacuated CE-TR cell. The initial spectrum (Figure 53J) was characterized by vibrational bands of the SAz-1 clay at 534, 845, 912, 1040, and 3611 cm^{-1}, adsorbed p-xylene at 794,1520, 2877, 2922 and 3029 cm^{-1}, adsorbed water at 1645 and 3425 cm^{-1}, and water vapor in the CE-TE cell evidenced by the sharp bands in the 1600 to 1700 cm^{-1}, and 3500 to 3700 cm^{-1} regions.

An expanded plot of the $A(\bar{\nu})$ spectra in the 1200 to 1800 cm^{-1} region (Figure 54) indicated that p-xylene remained on the surface of the Na-SAz-1 clay film even after evacuation of the clay film to 10^{-7}torr. Although the intensity of the ν_{19} band (C-C stretch) of p-xylene was reduced by the desorption process, the band retained considerable intensity after the high vacuum treatment (Figure 54J). In addition, the position of the ν_{19} band was not observed to shift significantly from its physisorption value of 1517 cm^{-1} during the desorption process, nor were additional bands observed in this spectral region. For comparison, the spectrum of a nonreacted, evacuated Na-SAz-1 clay film is shown at the bottom of Figure 54A.

A similar result was observed in the 750 to 950 region (Figure 55); the residual intensity of the $\nu 11$ band of p-xylene at 797 cm^{-1} (out-of-plane δ(C-H) deformation) after desorption (Figure 55B) indicated that removal of p-xylene was incomplete. Two δ(O-H) deformation modes of the Na-SAz-1 montmorillonite were observed at 837 and 914 cm^{-1}. Because the vibrational modes of the SAz-1 clay were not perturbed significantly by the presence of the organic adsorbate, the data were manipulated further by choosing the $S(\bar{\nu})$ spectrum of the Na-SAz-1 clay film in the CE-TR cell as the reference spectrum. Thus, the vibrational spectrum of the SAz-1 clay was subtracted from each $A(\bar{\nu})$ spectrum of the Na-SAz : p-xylene complex. Specifically, the $S(\bar{\nu})$ spectra of the clay-organic complex were ratioed against the $S(\bar{\nu})$ spectrum of the evacuated Na-SAz-1 sample without p-xylene. These ratioed

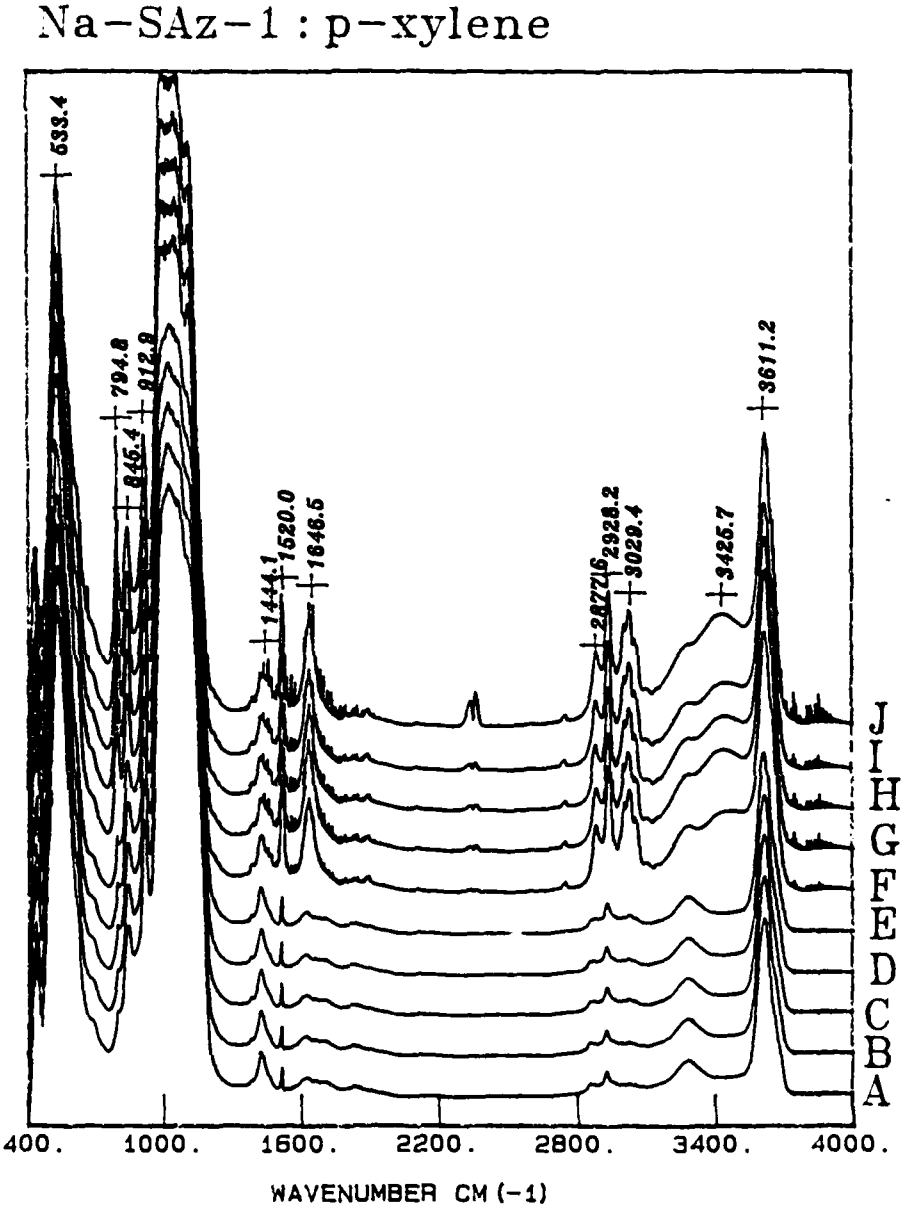

Figure 53. Controlled Desorption Spectra of the p-Xylene:Na-SAz-1 Complex in the 400 to 4000 cm^{-1} Region. Absorbance Spectra were Ratioed Against the Background Spectrum of the Empty Evacuated CE-TR cell. After an Initial 24 Hour Equilibration Period with p-Xylene at 1 atm. of Pressure (J), an Increasingly Greater Vacuum was Applied to the CE-TR Cell Until a Vacuum of 10^{-7} Torr had been Applied for 24 Hours (A).

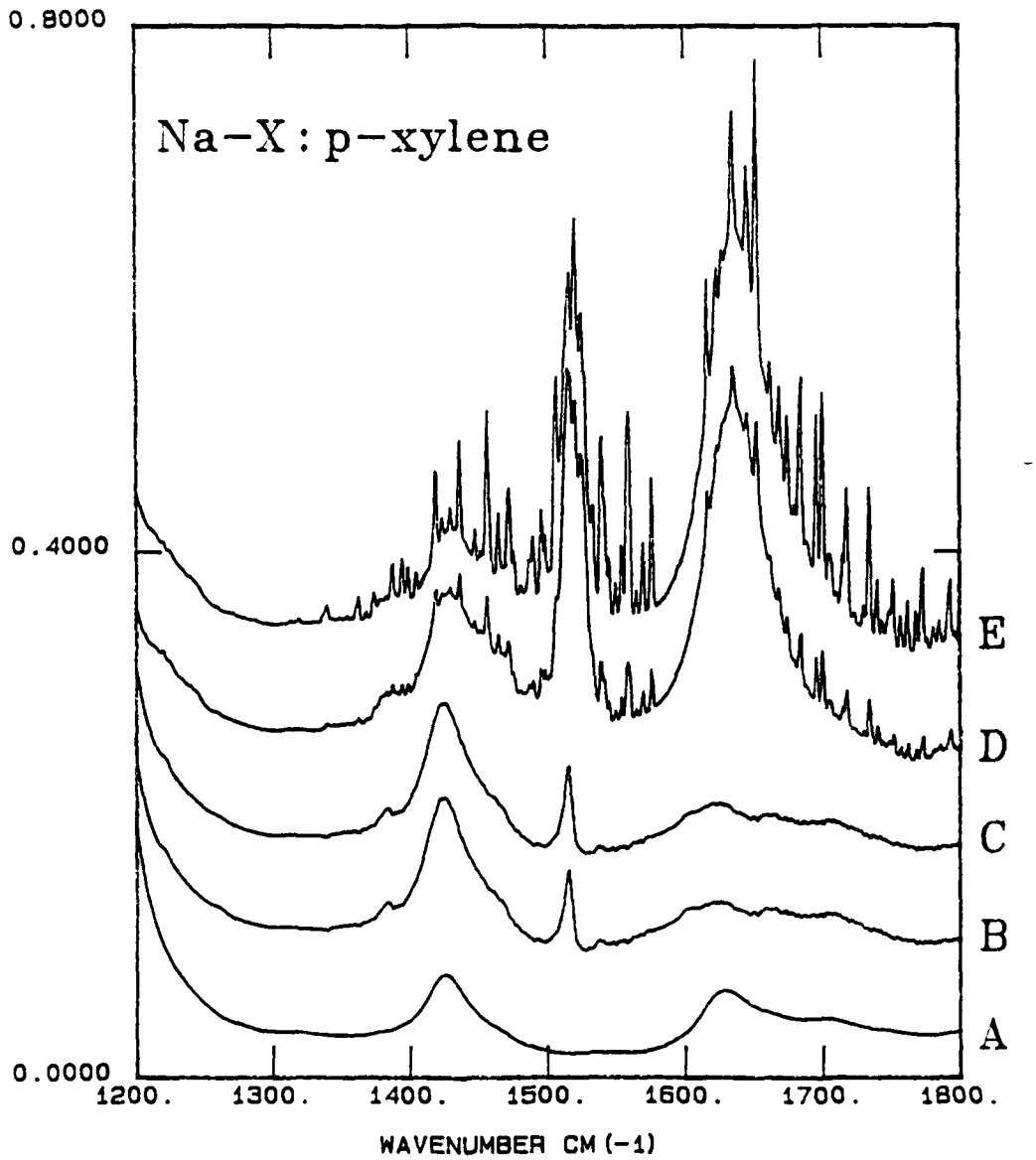

Figure 54. Controlled Desorption Spectra of the p-Xylene:Na-SAz-1 Complex in the 1200 to 1800 cm^{-1} Region. Absorbance Spectra were Ratioed Against the Background Spectrum of the Empty Evacuated CE-TR Cell. Spectra were of the p-Xylene:Na-SAz-1 Complex were Obtained at 1 atm. of Pressure (E), 10 Torr (D), 0.001 Torr (C), and 10^{-7} Torr (B). The Spectrum of an Evacuated Blank Clay Film of Na-SAz-1 Montmorillonite is Shown in A.

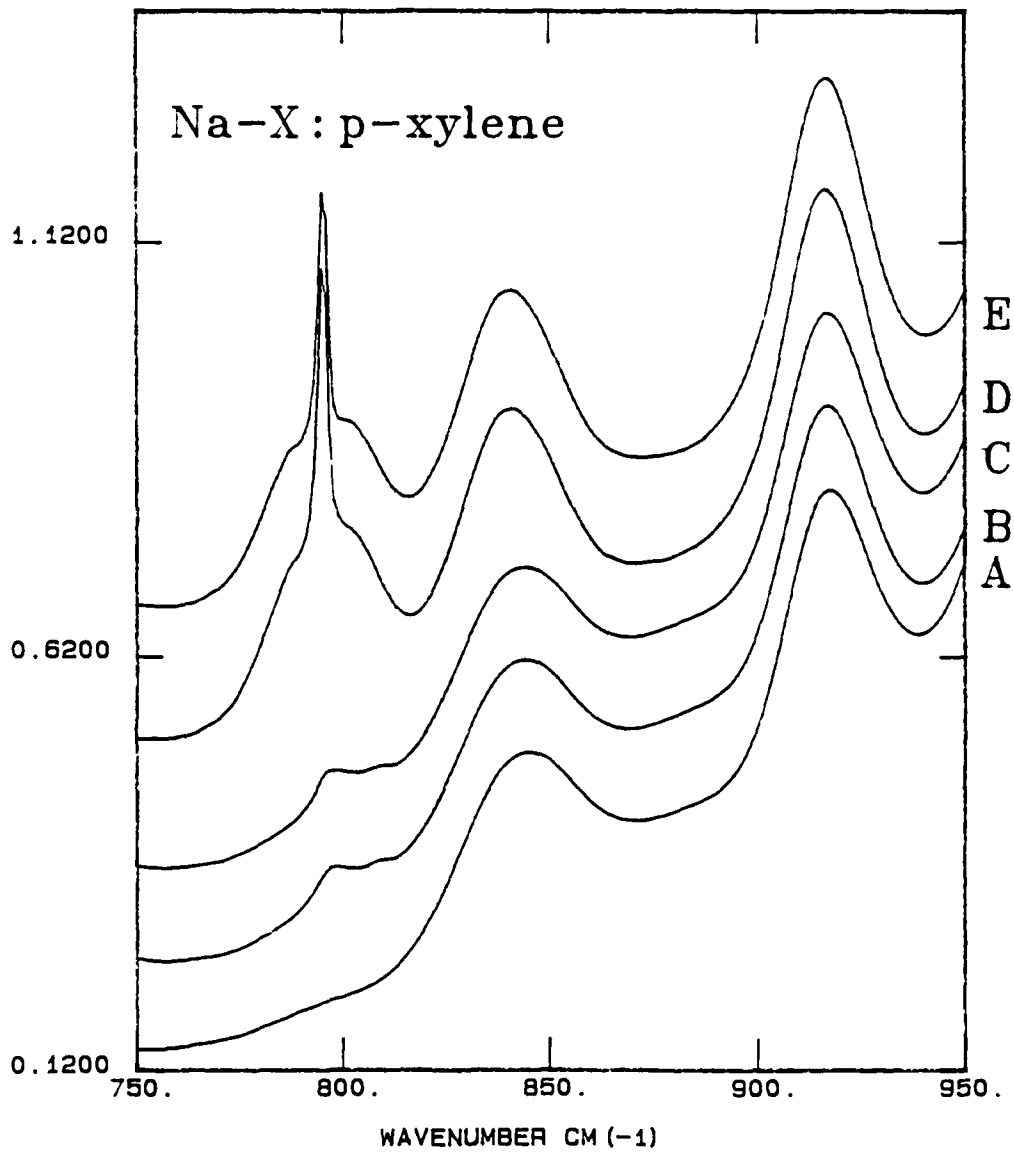

Figure 55. Controlled Desorption Spectra of the p-Xylene:Na-SAz-1 Complex in the 750 to 950 cm^{-1} Region. Absorbance Spectra were Ratioed Against the Background Spectrum of the Empty Evacuated CE-TR Cell. Spectra were of the p-Xylene:Na-SAz-1 Complex were Obtained at 1 atm. of Pressure (E), 10 Torr (D), 0.001 Torr (C), and 10^{-7} Torr (B). The Spectrum of an Evacuated Blank Clay Film of Na-SAz-1 Montmorillonite is Shown in A.

"difference" spectra show only the changes which took place between the blank clay film and the organic complex, thus, these spectra emphasize the changes in the spectra of the organic adsorbate. The resulting $A(\bar{\nu})_{diff}$ spectra in the 750 to 950 cm^{-1} region are shown in Figure 56. As the different spectra indicated (Figure 56), significant intensity was observed in the ν_{11} out-of-plane C-H deformation band even after the high vacuum desorption process. In agreement with the earlier results, the frequency of the ν_{11} was not observed to shift appreciably. However, the linewidth of the band increased relative to the physisorption spectra and a higher frequency component was observed on the shoulder of the 797 cm^{-1} band.

An expanded plot of the controlled desorption absorption spectra in the 2800 to 4000 cm^{-1} region are shown in Figure 57 for the Na-X p-xylene complex. The position and integrated intensity of the surface hydroxyl stretching mode of the SAz-1 montmorillonite at 3617 cm^{-1} was not affected significantly by the desorption of water and p-xylene. For comparison, the spectrum of an evacuated Na-X SAz-1 film without p-xylene is shown at the bottom of Figure 57A. Although the majority of the p-xylene initially adsorbed on the surface of the clay prior to the desorption procedure (top spectrum, Figure 57E) was removed by pulling a vacuum on the clay-organic complex (10^{-7} torr for 36 hours), a portion of the p-xylene remained on the surface of the clay as shown by the residual intensity of the ν(C-H) stretching modes near 2881 and 2934 cm^{-1} (Figure 57B). The significant reduction in the intensities of the p-xylene bands at 2881 cm^{-1}, 2937 cm^{-1}, and 3027 cm^{-1} bands, and of the water bands at 3268 cm^{-1} and 3412 cm^{-1} bands resulted from the removal of the adsorbates from the SAz-1 surface.

A further expansion of the aromatic and aliphatic ν(C-H) stretching region of Na-X p-xylene complex in the 2800 to 3100 cm^{-1} region is presented in Figure 58. A comparison of the initial spectrum of the Na-X : p-xylene complex prior to desorption (Figure 58C, top) to the same sample after the high vacuum step (Figure 58B) indicated that the adsorbed species had considerably less aromatic character after the desorption procedure. The significant loss in intensity of the aromatic ν(C-H) stretching bands at 3004, 3024, and 3057 cm^{-1} relative to the aliphatic ν(C-H) stretching bands at 2855 and 2925 cm^{-1} indicated a loss of aromatic character of the adsorbed p-xylene

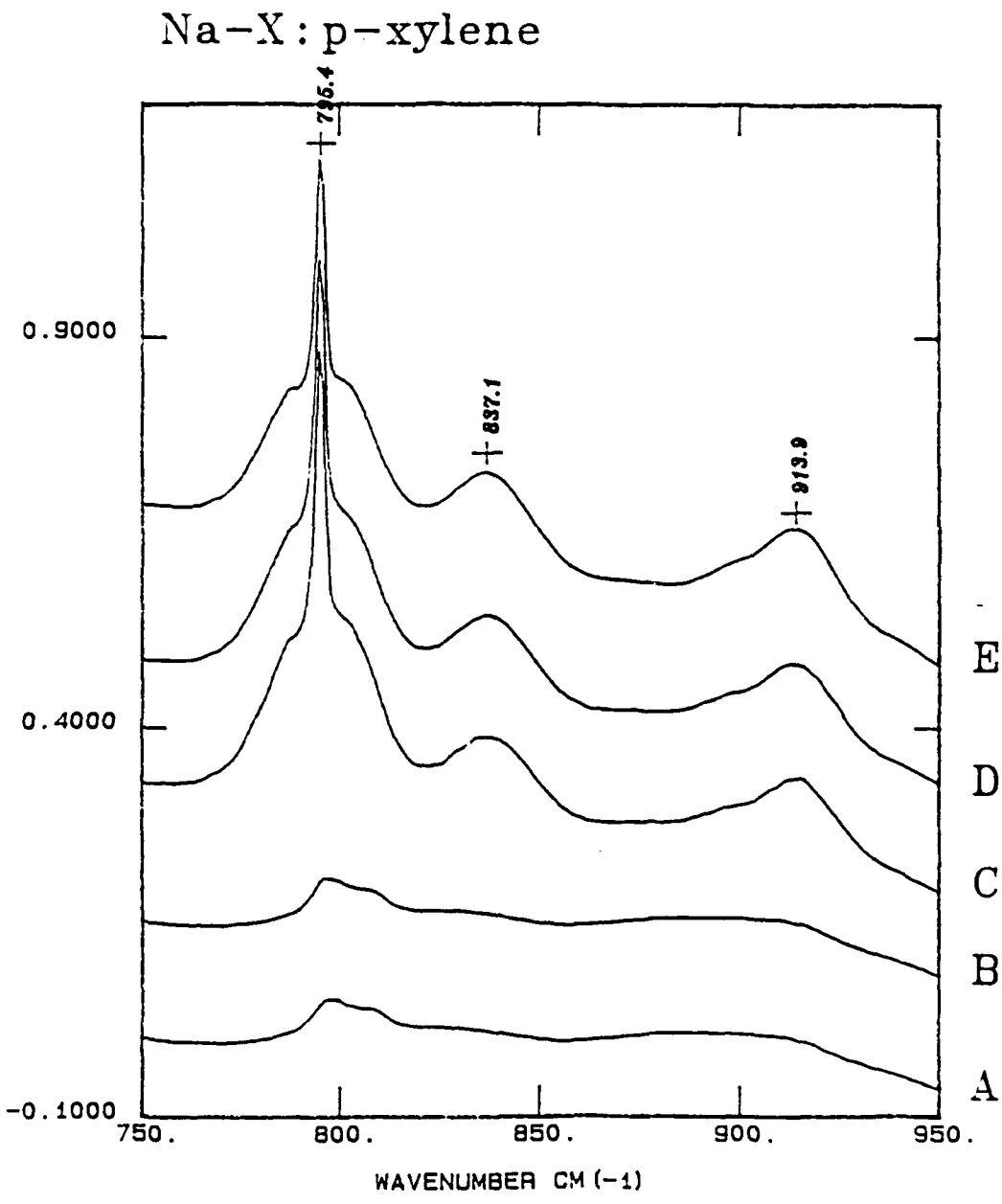

Figure 56. Controlled Desorption Difference Spectra of the p-Xylene:Na-SAz-1 Complex in the 750 to 950 cm^{-1} Region. Absorbance Spectra were Ratioed Against the Background Spectrum of an Evacuated Na-X SAz-1 Clay Film Without p-Xylene in the Empty Evacuated CE-TR Cell. Spectra were of the p-Xylene:Na-SAz-1 Complex were Obtained at 1 atm. of Pressure (E), 10 Torr (D), 1 Torr (C), 0.001 Torr (B), and 10^{-7} Torr (A). The Spectrum of an Evacuated Blank Clay Film of Na-SAz-1 Montmorillonite is Shown in A.

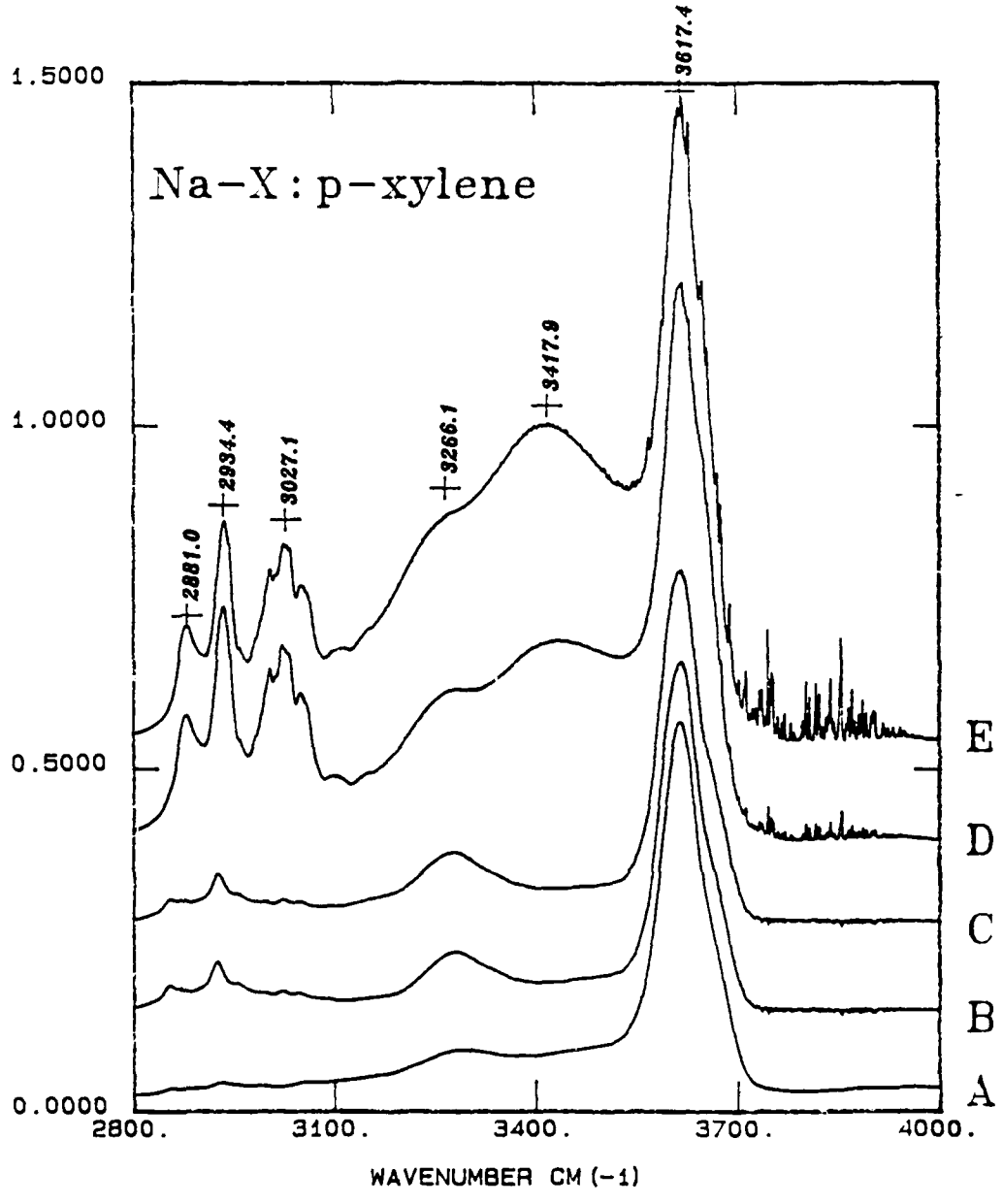

Figure 57. Controlled Desorption Spectra of the p-Xylene:Na-SAz-1 Complex in the 2800 to 4000 cm^{-1} Region. Absorbance Spectra were Ratioed Against the Background Spectrum of the Empty Evacuated CE-TR Cell. Spectra were of the p-Xylene:Na-SAz-1 Complex were Obtained at 1 atm. of Pressure (E), 10 Torr (D), 0.001 Torr (C), and 10^{-7} Torr (B). The Spectrum of an Evacuated Blank Clay Film of Na-SAz-1 Montmorillonite is Shown in A.

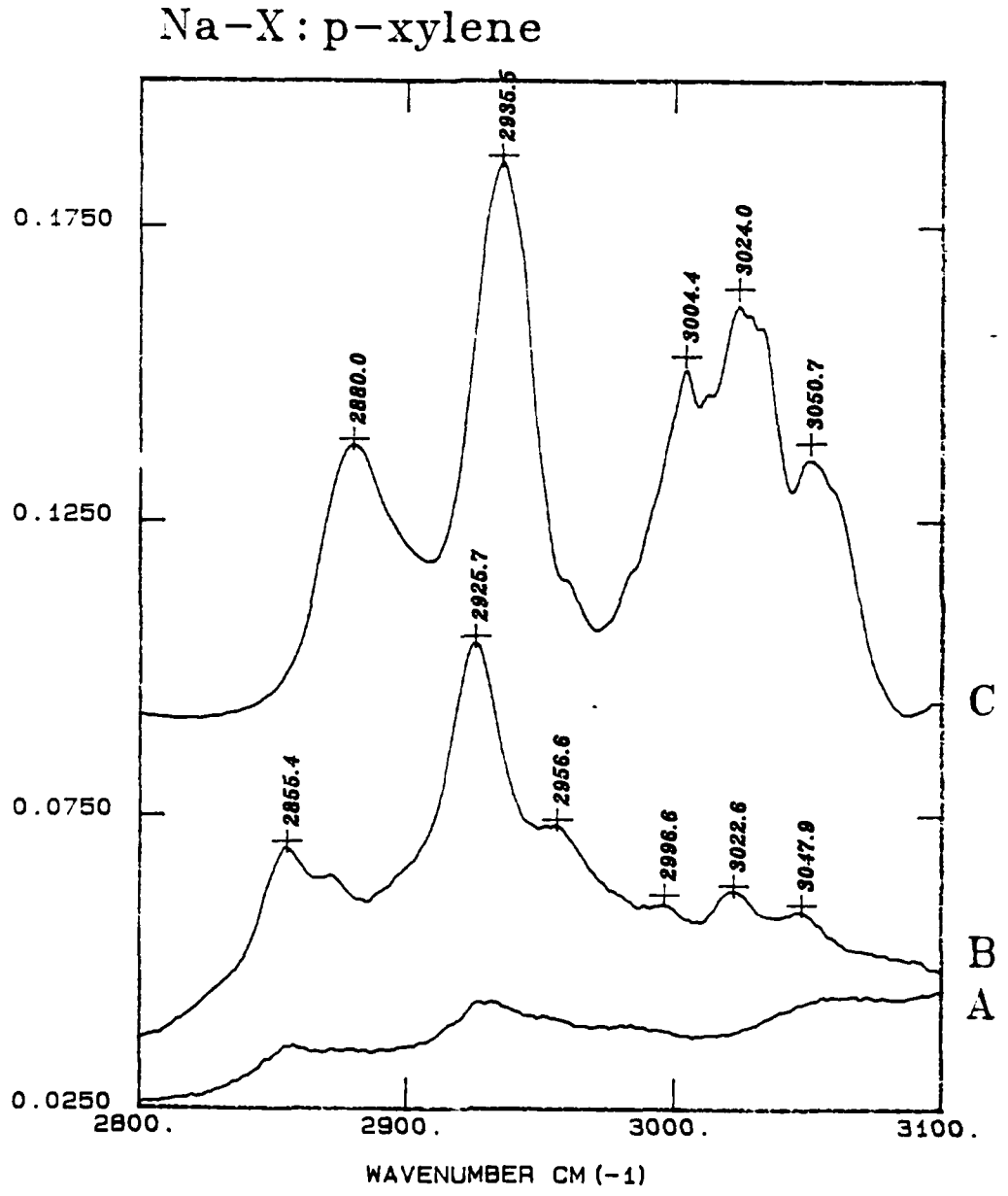

Figure 58. CE-TR Absorbance Spectra in the 2800 to 3100 cm^{-1} Region of Physisorbed p-Xylene on the Na-X SAz-1 Clay Film at 1 atm. of Pressure (C), Chemisorbed p-Xylene on the Na-X SAz-1 Clay Film at 10^{-7} Torr (B), and of the Blank Na-X SAz-1 Clay Film at 10^{-3} Torr.

species upon desorption. In addition, the position of the aliphatic ν(C-H) stretching bands at 2855 and 2925 cm^{-1} were shifted to lower frequencies in comparison to their physisorbed values of 2880 and 2936 cm^{-1}.

b. Cu-X : P-XYLENE COMPLEX

A similar experiment was conducted using a Cu-exchanged SAz-1 clay film. Similar to the results obtained for the Na-exchanged clay film, adsorbed p-xylene and water were desorbed from the surface of the SAz-1 clay as the pressure was reduced (Figure 59). Difference absorbance spectra $A(\bar{\nu})_{diff}$ of the Cu-X p-xylene were obtained by ratioing the $S(\bar{\nu})$ spectra of the Cu-X p-xylene complex against the $S(\bar{\nu})$ spectrum of an evacuated Cu-SAz-1 clay film in the CE-TR cell. $A(\bar{\nu})_{diff}$ spectra of the Cu-X p-xylene complex in the 1250 to 1750 cm^{-1} region are shown in Figure 60. The initial spectrum of the CuX p-xylene complex at 1 atm. is shown at the top of Figure 60J. The ν_{19} band of adsorbed p-xylene at 1517 cm^{-1} and the ν_2 band of adsorbed water at 1630 cm^{-1} are observed, in addition, some water vapor in the CE-TR cell was observed evidenced by the sharp vibrational bands in this spectrum. Upon reduction of the pressure in the CE-TR cell, p-xylene and water were removed from the surface of the clay as shown by the loss of intensity of the 1519 cm^{-1} and 1630 cm^{-1} bands. In contrast to the results obtained for the Na-X p-xylene clay film, a set of "new" bands were observed in this spectral region upon desorption. In addition to the ν_{19} band of p-xylene at 1522 cm^{-1}, new bands were observed at 1286, 1307, 1326, 1354, 1384, 1501, 1550, 1561, and 1596 cm^{-1}. These "new" bands were observed to increase in intensity upon desorption, despite the fact that the net surface concentration of p-xylene was reduced by the vacuum treatment. A composite plot showing the spectra of p-xylene (Figure 61D), Cu-SAz-1 : p-xylene complex before desorption (Figure 61C), Cu-SAz-1 : p-xylene after desorption (Figure 61B), and of a blank (no p-xylene) evacuated Cu-SAz-1 clay film (Figure 61A), shows clearly the presence of the new bands. A comparison of the p-xylene spectrum (Figure 61D) to that of the after-desorption Cu-X p-xylene complex (Figure 61B), indicated that these "new" bands were unique to the postdesorption Cu-X p-xylene complex, and are not absorption bands which can be attributed to fundamental vibrations of p-xylene. These results are in good agreement with the work of Pinnavaia and Mortland (References VI-1-2) wherein they reported a similar red-shift of the

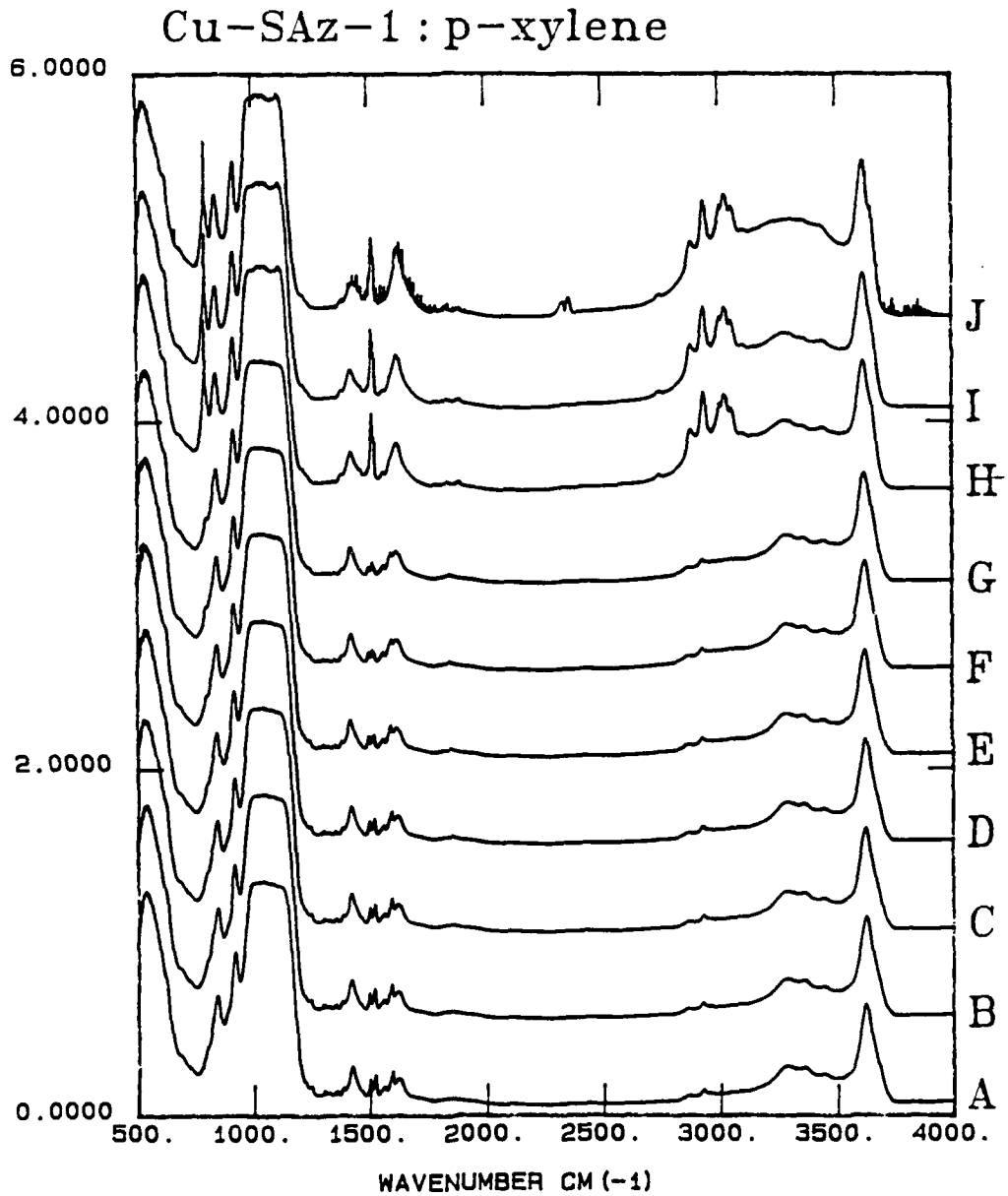

Figure 59. Controlled Desorption Spectra of the p-Xylene : Cu-SAz-1 Complex in the 500 to 4000 cm^{-1} Region. Absorbance Spectra were Ratioed Against the Background Spectrum of the Empty Evacuated CE-TR cell. After an Initial 24 hour Equilibration Period with p-Xylene at 1 atm. of Pressure (J), an Increasingly Greater Vacuum was Applied to the CE-TR cell until a Vacuum of 10^{-7} Torr had been Applied for 24 Hours (A).

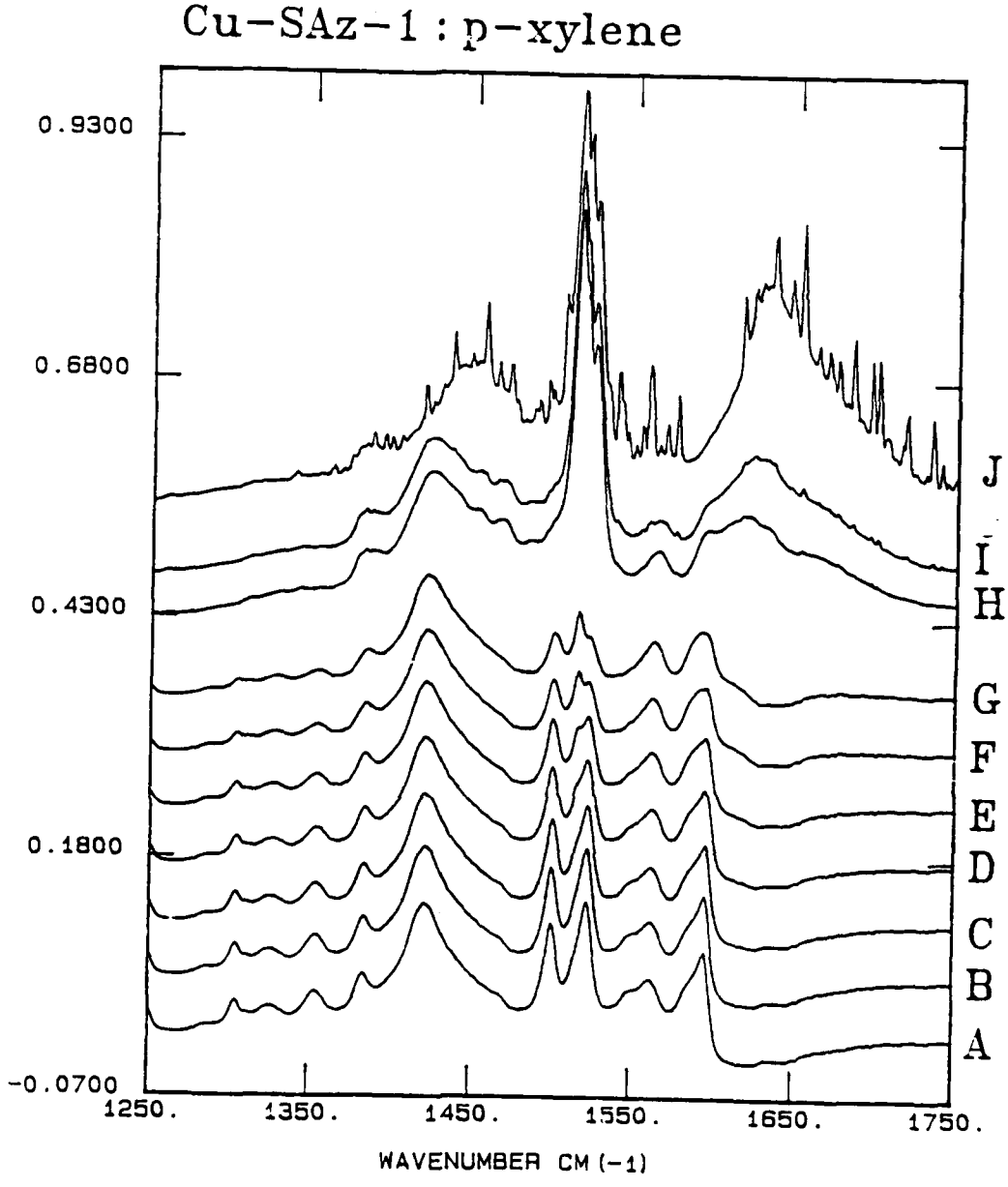

Figure 60. Controlled Desorption Difference Spectra of the p-Xylene : Cu-SAz-1 Complex in the 1250 to 1750 cm^{-1} Region. Absorbance Spectra were Ratioed Against the Background Spectrum of an Evacuated Cu-X SAz-1 Clay Film Without p-Xylene in the Empty Evacuated CE-TR Cell. Spectra were of the p-Xylene : Cu-SAz-1 Complex were Obtained at 1 atm. of Pressure (J) and Exposed to an Increasingly Greater Vacuum until a Vacuum of 10^{-7} Torr had been Applied for 24 Hours (A).

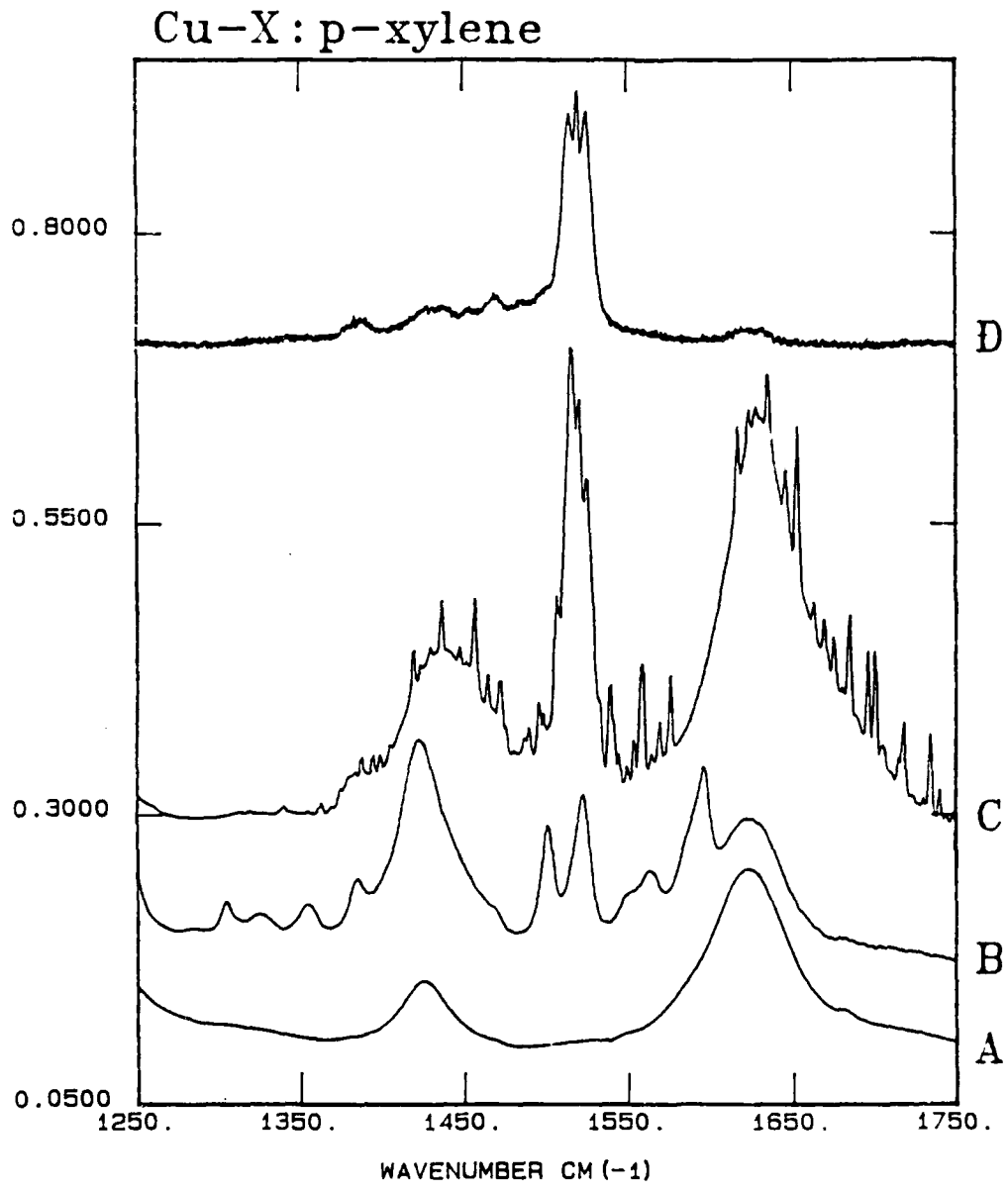

Figure 61. CE-TR Absorbance Spectra of the Cu-X p-Xylene Complex in the 1250 to 1750 cm^{-1} Region. Cu-x SAz-1 Clay Film Without p-Xylene at 10^{-3} Torr (A), Cu-X p-Xylene Complex at 10^{-7} Torr (B), Cu-X p-Xylene Complex at 1 atm. (C), and Vapor-Phase p-Xylene at 1 atm. (D).

ν_{19} band. They observed a red-shift of 14 cm^{-1} from 1521 cm^{-1} in the hydrated state to a value of 1503 cm^{-1} for the dry Cu-X p-xylene complex. In this study, we observed the ν19 fundamental at 1521 cm^{-1} and observed a decrease in frequency to 1501 cm^{-1} dehydration. However, Pinnavaia and Mortland (References VI-1-2) did not report the appearance of any "new" bands for the CuX p-xylene complex. As discussed previously, they (References VI-1-2) only presented detailed IR spectra for the Cu-X toluene complex wherein they observed the appearance of one "new" band at 1300 cm^{-1} which could not be assigned to a toluene fundamental. The appearance of the "adsorbate" bands for the Cu-X p-xylene complex here indicated clearly that the adsorbed p-xylene undergoes a chemical transformation on the surface.

Similar vibrational perturbations were observed in the out-of-plane C-H deformation region upon desorption. A comparison of the spectrum of the Cu-X p-xylene complex after desorption in the 750-850 cm^{-1} region (Figure 62B) to the spectra of p-xylene (Figure 62D) and the Cu-X p-xylene complex prior to the high vacuum treatment showed that the ν_{11} out-of-plane C-H deformation band of p-xylene was shifted to higher frequencies upon desorption. In addition, the intensity of the 795 cm^{-1} band was observed to decrease with a concomitant increase in intensity of a new band at 821 cm^{-1}. There were no IR-active bands of the Cu-SAz-1 montmorillonite sample in this region (Figure 62A) and the spectrum of p-xylene in this region is characterized by a single absorption band at 797 cm^{-1} (Figure 62D, top) agreement with the earlier study of the Cu-X p-xylene complex of Pinnavaia and Mortland (References VI-1-2). The distinct red-shift of the ν_{11} band and the concomitant blue-shift of the ν_{19} band indicated that the electron density of the p-xylene ring had decreased.

In the C-H stretch region, the data indicated that the adsorbed organic species had much less aromatic character after the desorption process similar to the results obtained in the Na-X p-xylene study. A comparison of p-xylene (Figure 63C), Cu-X p-xylene complex before desorption (Figure 63B), and of Cu-X p-xylene complex after desorption (Figure 63A) showed a large decrease in the intensity of the aromatic C-H stretching bands at 3004, 3024, and 3049 cm^{-1} relative to the aliphatic ν(C-H) bands at 2869 and 2927 cm^{-1}. The spectra of p-xylene in the vapor phase (Figure 63C) and of the CuX

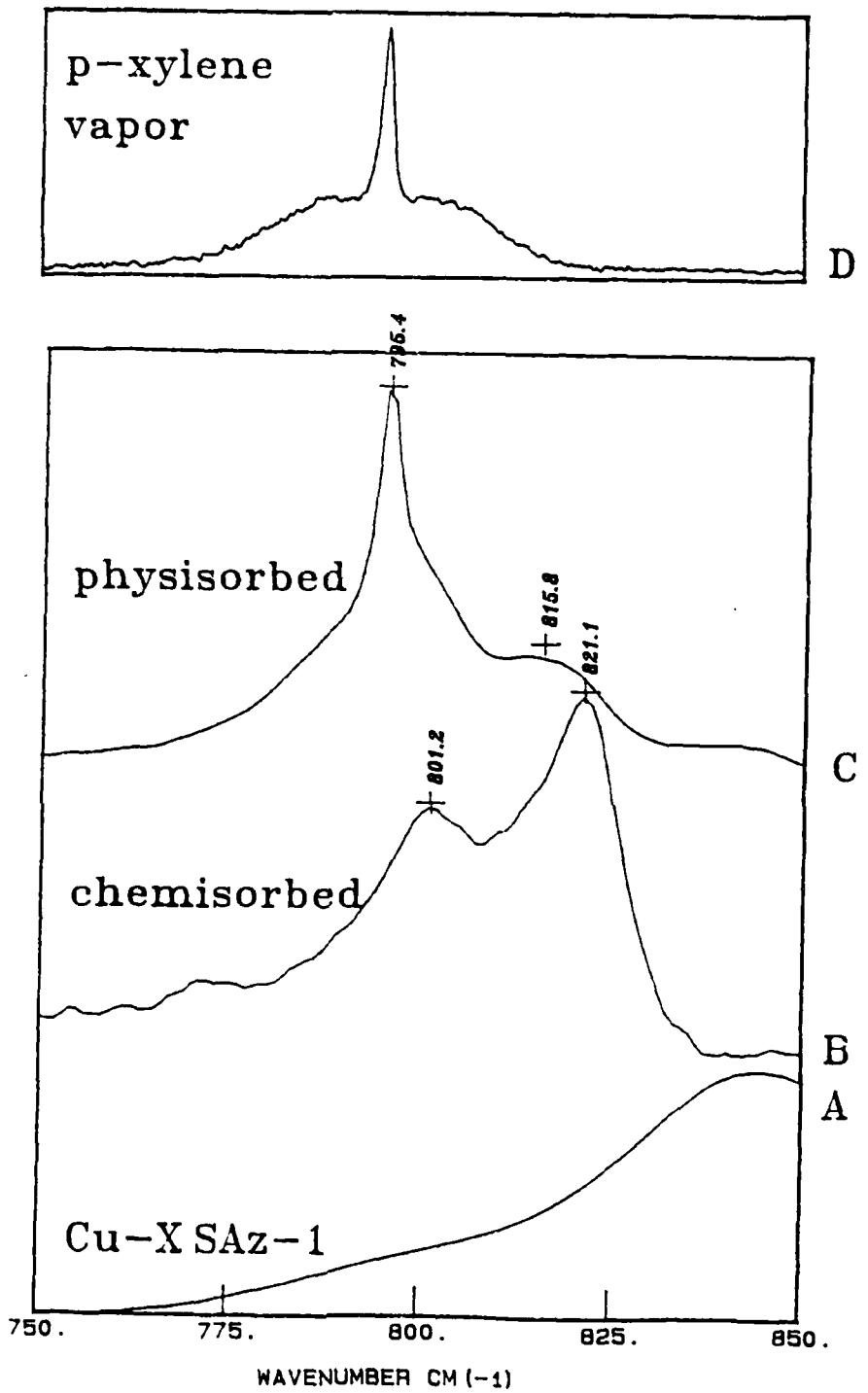

Figure 62. CE-TR Absorbance Spectra of the Cu-X p-Xylene Complex in the 750 to 950 cm^{-1} Region. Cu-X SAz-1 Clay Film Without p-Xylene at 10^{-3} Torr (A), Cu-X p-Xylene Complex at 10^{-7} Torr (B), Cu-X p-Xylene Complex at 1 atm. (C), and Vapor Phase p-Xylene at 1 atm (D).

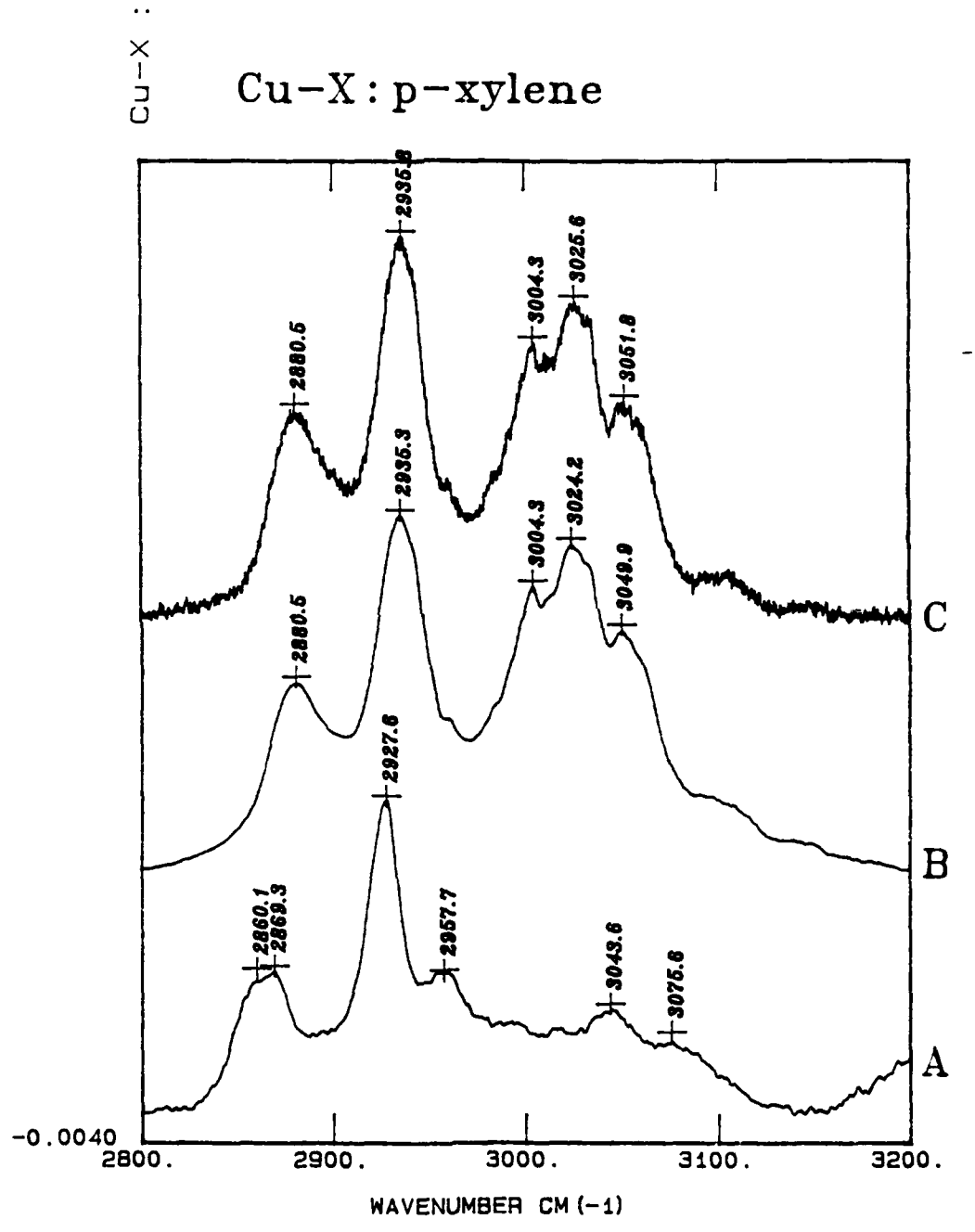

Figure 63. CE-TR Absorbance Spectra of the Cu-X p-Xylene Complex in the 2800 to 3100 cm^{-1} Region. Cu-X p-Xylene Complex at 10^{-7} Torr (A), Cu-X p-Xylene Complex at 1 atm. (B), and Vapor Phase p-Xylene at 1 atm (C).

p-xylene complex prior to desorption were very similar which suggested that the bulk of the p-xylene adsorbed at 1 atm. is not strongly bound to the surface of the clay (i.e., physisorbed). However, the significant loss in intensity of the aromatic ν(C-H) bands and the shift in frequency of the aliphatic ν(C-H) bands upon desorption indicated that a surface-induced chemical transformation of the adsorbed p-xylene had taken place. This loss in intensity of the aromatic ν(C-H) bands accompanied the appearance of the "new" bands discussed previously.

c. CLAY:ORGANIC COMPLEXES AT 1 ATM. IN THE PRESENCE OF P_2O_5

Chemical transformations of p-xylene and related arene molecules on transition metal exchanged montmorillonites are influenced largely by the presence of water. In the controlled desorption studies discussed above, water was removed from the system by pulling a vacuum on the CE-TR cell which resulted in the loss of water and p-xylene from the surface of the clay. We investigated another approach to reducing the water content of the clay-organic complexes by placing a small portion of a desiccant, P_2O_5, directly in the CE-TR cell. For these experiments, the $S(\tilde{\nu})$ spectra of the clay-organic complexes were obtained as a function of the time of exposure of the clay films to the P_2O_5 in the CE-TR cell. A vacuum was not used in these studies to remove the adsorbates. A similar result to that obtained using vacuum-desiccation was obtained; "new" bands were observed as the contact time between the Cu-X p-xylene complex increased (i.e., as more water was removed). A comparison of the results obtained using P_2O_5 and vacuum-desiccation is presented in Figure 64. Although new spectra features were observed in both spectra, there are significant differences between them. For example, relative intensity of the 1422 cm^{-1} band is much lower in the P_2O_5 spectrum, but the intensity of the 1361 cm^{-1} band is larger. The shoulder of the band at 1526 cm^{-1} in the P_2O_5 spectrum does not appear to have a counterpart in the vacuum desiccation spectrum. Conversely, the 1551 cm^{-1} band was observed only in the vacuum desiccation spectrum. These data indicate that the method of removing water from the Cu-X p-xylene complex can influence the reaction products. Qualitatively, however, a similar result was obtained; upon desiccation, a set of new spectral features was observed which indicated that the organic adsorbate had undergone a chemical transformation.

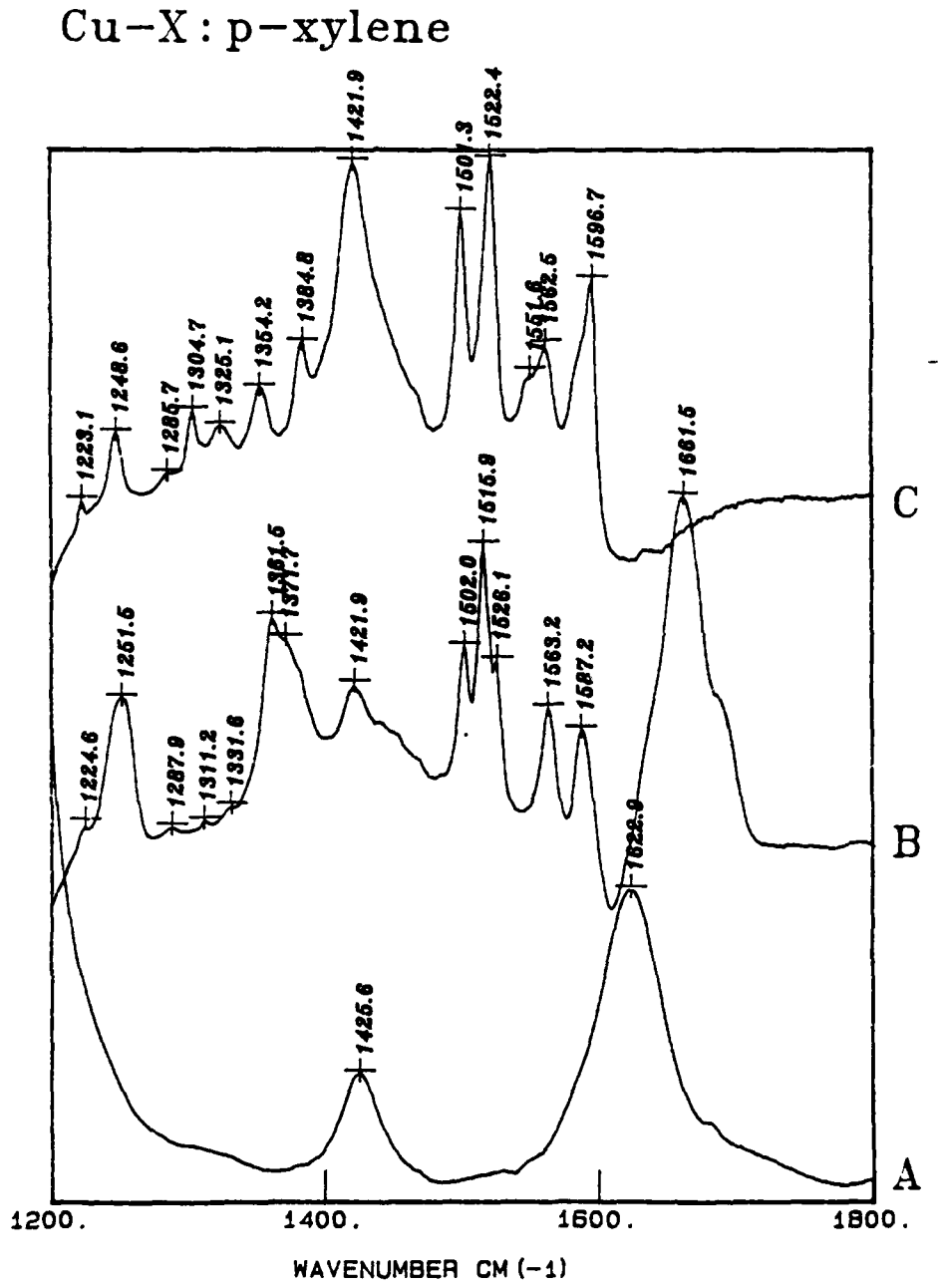

Figure 64. CE-TR Absorbance Spectra of the Cu-X p-Xylene Complex in the 1200 to 1800 cm^{-1} Region. Cu-X SAz-1 Evacuated Clay Film at 10^{-3} Torr (A), Cu-X p-Xylene Complex in the Presence of P_2O_5 (B), Cu-X p-Xylene Complex at 10^{-7} Torr (C).

d. Cu-X : BENZENE/P_2O_5

A similar result was obtained in a study of adsorbed benzene on a Cu-exchanged SAz-1 clay film in the presence of P_2O_5. As the P_2O_5 removed water vapor from the CETR cell, a new set of vibrational bands appeared which indicated that a chemical transformation of the adsorbed benzene had taken place similar to the p-xylene results. A striking color change was observed as the new bands appeared; initially, the clay-benzene complex was a light pale yellow color and upon dehydration the complex turned to a dark red color. As the water content decreased (i.e., as the dark red color developed), the intensity of the 1630 cm^{-1} band (Figure 65) decreased and a set of new bands were observed at 1294, 1303, 1321, 1357, 1421, 1470, 1498, 1522, 1549, and 1586 cm^{-1} (Figure 65). Additional evidence that a chemical transformation had taken place was observed in the CH stretching region (Figures 66-67). The initial spectrum of benzene physisorbed on the Cu-SAz-1 clay film was characterized by the aromatic C-H stretching features at 3060 cm^{-1}, and 3095 cm^{-1} (Figure 66H). However, after prolonged contact with P_2O_5, two bands at 2875, and 2932 cm^{-1} increased in intensity (Figure 66A). An expanded plot of the aliphatic CH stretching region (Figure 67) shows the growth of the new aliphatic bands upon dehydration. An expanded plot of the Cu-X benzene complex after desorption shows the large increase in relative intensity of the aliphatic ν(C-H) bands in comparison to the aromatic ν(C-H) bands (Figure 68). These bands at 2858 cm^{-1} and 2932 cm^{-1} are clearly aliphatic C-H stretching bands and provide direct evidence that the aromatic character of the adsorbate, benzene, was reduced.

A chemical transformation of the adsorbed p-xylene and benzene species takes place on the surface of transition metal exchanged montmorillonites under anhydrous conditions. Pinnavaia and Mortland (References VI-1-2) provided unambiguous ESR data 16 years ago which showed that a complete electron transfer reaction occurred between the arene and the clay surface. Although their dispersive-IR data suggested that vibrational modes of the arene were influenced by this electron transfer reaction, only two fundamental vibrational modes were affected and additional bands were not reported. This study confirms the IR results obtained by Pinnavaia and Mortland (References VI-1-2) in that similar shifts of the ν_{11} and ν_{19} bands

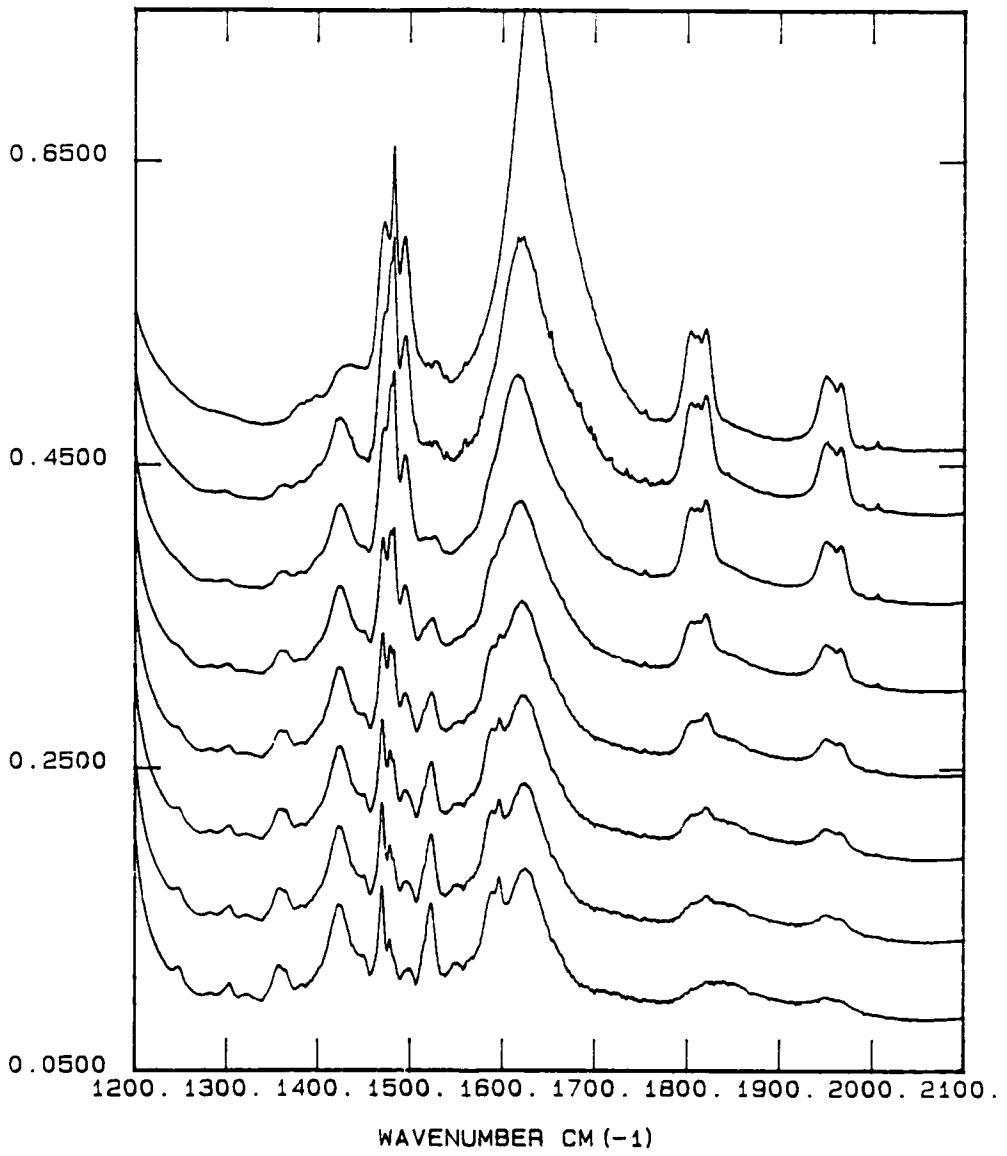

Figure 65. Controlled Desorption Spectra of the Benzene : Cu-SAz-1 Complex in the 1200 to 2100 cm^{-1} Region. Absorbance Spectra were Ratioed Against the Background Spectrum of the Empty Evacuated CE-TR cell. After an Initial 24 Hour Equilibration Period with Benzene at 1 atm. of Pressure (H), P_2O_5 was Introduced into the CE-TR Cell. The Bottom Spectrum (A) Represents the Longest Exposure Time to the P_2O_5 Desiccant (24 Hours).

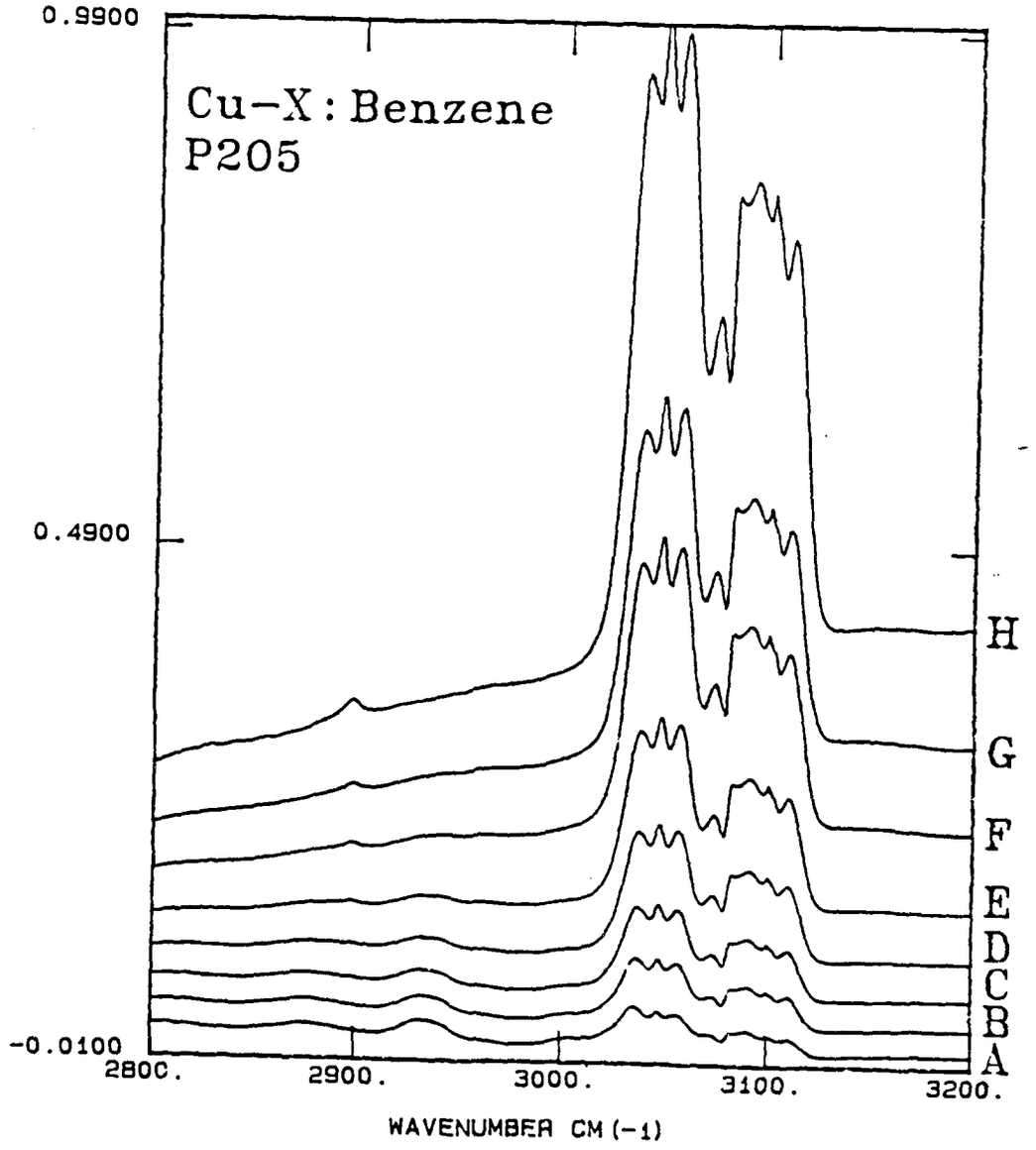

Figure 66. Controlled Desorption Spectra of the Benzene : Cu-SAz-1 Complex in the 2800 to 3200 cm^{-1} Region. Absorbance Spectra were Ratioed Against the Background Spectrum of the Empty Evacuated CE-TR Cell. After an Initial 24 Hour Equilibration Period with Benzene at 1 atm. of Pressure (H), P_2O_5 was Introduced into the CE-TR Cell. The Bottom Spectrum (A) Represents the Longest Exposure Time to the P_2O_5 Desiccant (24 Hours).

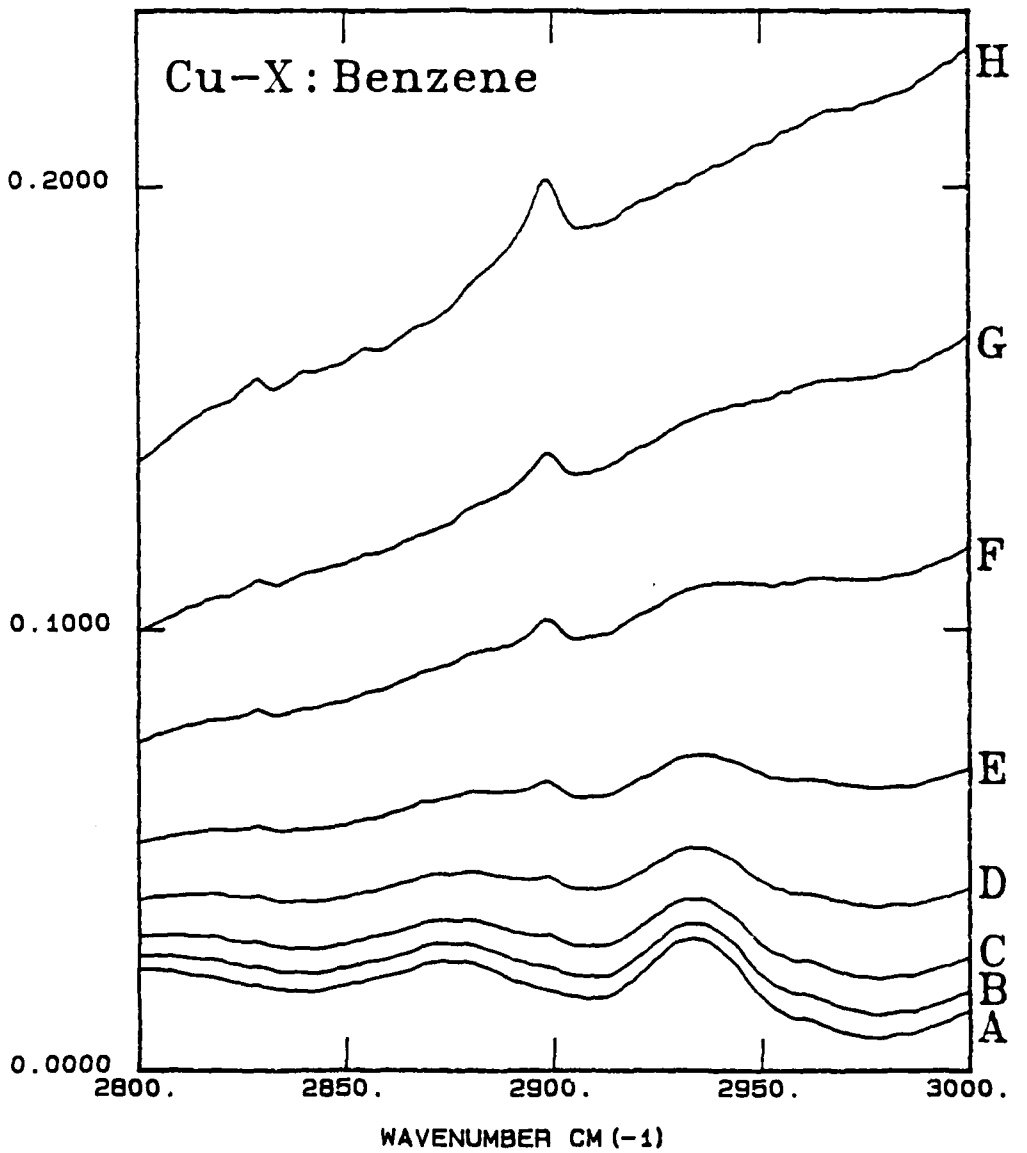

Figure 67. Controlled Desorption Spectra of the Benzene : Cu-SAz-1 Complex in the 2800 to 3000 cm^{-1} Region at 1 atm. of Pressure. Absorbance Spectra were Ratioed Against the Background Spectrum of the Empty Evacuated CE-TR Cell. After an Initial 24 Hour Equilibration Period with Benzene at 1 atm. of Pressure (H), P_2O_5 was Introduced into the CE-TR Cell. The Bottom Spectrum, (A), Represents the Longest Exposure Time to the P_2O_5 Desiccant (24 Hours).

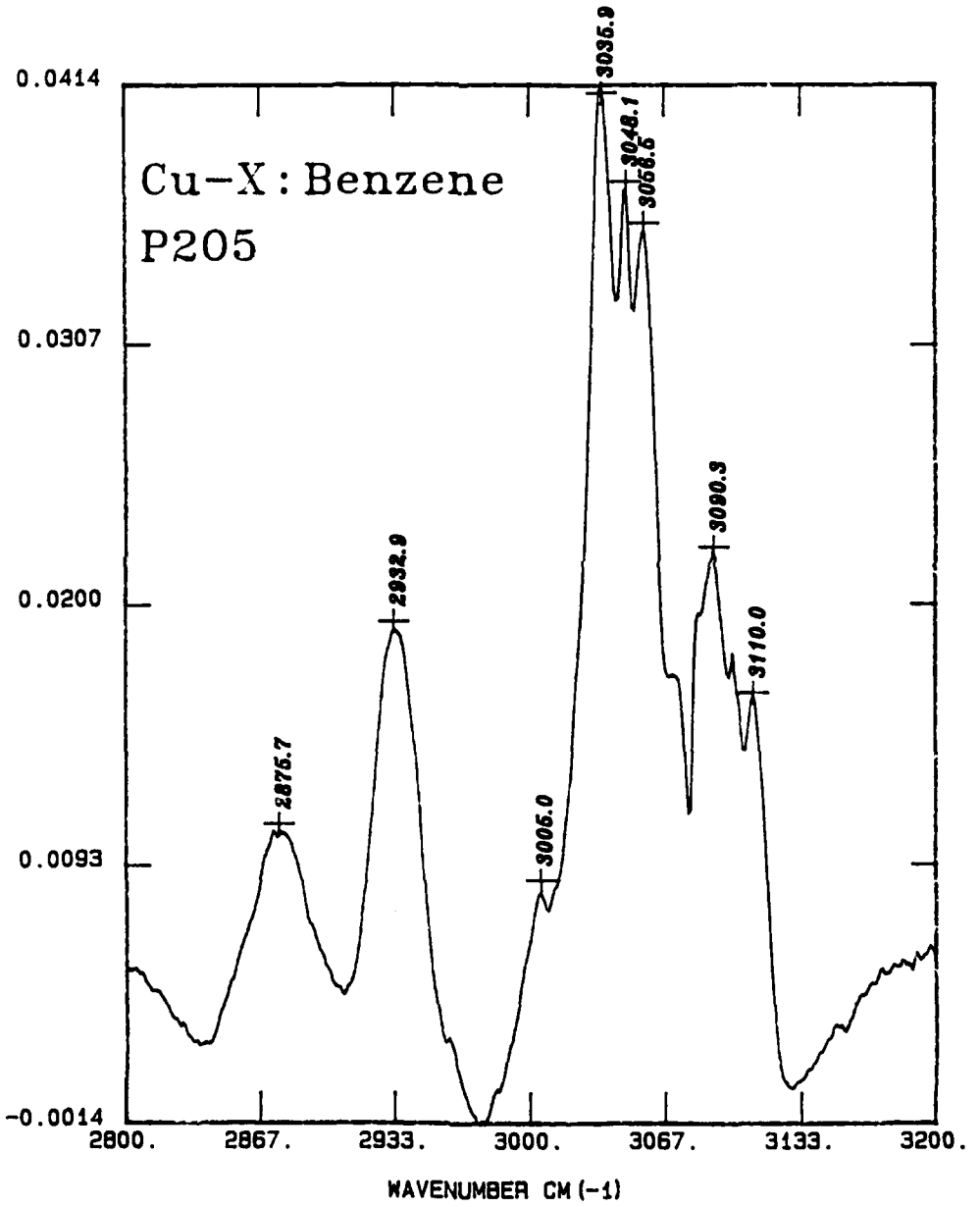

Figure 68. Expanded Plot of the CE-TR Absorbance Spectrum of the Cu-X Benzene Complex Exposed to P_2O_5 for 24 Hours in the 2800 to 3200 cm^{-1} Region at 1 atm. of Pressure.

of p-xylene were observed. The large red shift of the ν_{19} band and the concomitant blue-shift of the ν_{11} band indicated clearly that the electron density of the p-xylene ring was reduced. In addition, however, a suite of new vibrational bands observed in the present investigations has provided direct optical evidence that a chemical transformation has taken place. New vibrational features which cannot be assigned to p-xylene fundamentals have been observed and indicate that not only are p-xylene fundamentals perturbed, but that a new surface species is formed. Furthermore, the early studies on clay-arene complexes suggested that the aromatic character of the adsorbed species was reduced. This hypothesis is confirmed in the present investigation by two observations: first, the loss of aromatic character was shown clearly by the reduced intensity of the aromatic C-H stretching bands relative to the aliphatic band, and second, the combined red-shift of the ν_{19} band and the blue-shift of the ν_{11} band indicated that the electron density of the aromatic ring was reduced. A surprising result was obtained for the Na-X p-xylene system in that an electron transfer reaction was not expected because of the unfavorable redox couple of the Na-X clay. Although new bands were not observed in the lower frequency vibrational spectra upon dehydration, the significant loss in intensity of the aromatic C-H stretching bands indicated that the adsorbed species had less aromatic character. This could be a result of electron transfer reaction taking place between a structural transition metal cation (e.g., Fe[III]) in the clay lattice and the adsorbed p-xylene.

Of the three sample presentation methods evaluated, controlled-environment transmission was determined to be the optimum method for studying vapor phase adsorption of volatile organics on naturally occurring clay minerals. Diffuse reflectance (DR) and cylindrical internal reflectance (CIR) methods were shown to have a distinct set of advantages and disadvantages in comparison to the other methods. For the conditions employed in this study, however, CE-TR was shown to provide the highest sensitivity of the three techniques. The vibrational spectra of the clay minerals obtained using the three methods were in good agreement despite the diversity of the samples (i.e., aqueous suspension, powder, and thin film). In addition, good agreement of the FT-IR spectra was also obtained in comparison with Raman spectra. A distinct advantage of FT-IR spectroscopy over Raman methods was

that the data collection times for FT-IR spectra were much less than that required for Raman spectra.

Controlled-environment FT-IR spectra of p-xylene adsorption on Na- and Cu-exchanged montmorillonite were obtained. The Na-X data suggested that some of the p-xylene was irreversible adsorbed by the clay mineral. The FT-IR data in the C-H stretch region showed that the aromatic C-H stretch bands lost intensity relative to the aliphatic C-H stretch bands of p-xylene. The lower frequency FT-IR spectra suggested that, although some of the p-xylene was strongly adsorbed on the clay, there was no evidence of any new vibrational bands. These results are consistent with the expected inert behavior of Na-exchanged clays to organic catalysis.

The favorable redox properties of Cu-exchanged montmorillonite, however, can facilitate single electron transfer reactions between adsorbed aromatic compounds in the interlamellar region of the clay. Under anhydrous conditions, aromatic radical cations are produced by interactions of the π electrons of the aromatic adsorbates at vacant ligand positions of the transition metal cations (Cu[II], Fe[III], VO^{+2}). Unambiguous ESR data have shown that a complete electron transfer reaction takes place for p-xylene adsorbed on Cu-montmorillonite under dry conditions. Previous vibrational data indicated that two fundamental vibrations of p-xylene were influenced by the electron transfer reactions. The data presented in this investigation confirm this result, and, in addition, show that a suite of new bands develop under anhydrous conditions. These data provide direct vibrational spectroscopic evidence that a new surface species was produced under anhydrous conditions. Although the new vibrational features have not been assigned and the surface species has not been identified, these data suggest that this approach may provide a useful tool to characterize reaction products of organic compounds on clay mineral surfaces. These results also indicated that the aromatic character of the organic adsorbates, was reduced upon desiccation for both the Na-X and Cu-X montmorillonite clays.

SECTION VII

CONCLUSIONS AND RECOMMENDATIONS

As stated in the Introduction, the major goal of the present research program was to better understand the vibrational spectra of certain targeted metals, ligands and surfaces and the changes observed during interaction of these species. To accomplish this goal a four-pronged approach on the vibrational spectroscopy of hydrazine and its deuterated isomers, aromatic hydrocarbons, certain metals and clays was carried out. In the following paragraphs the major conclusion and suggestions for future research for each part of our four-pronged program will be presented in turn.

In the first part the vibrational spectra of hydrazine and its deuterated isomers were obtained in the vapor-phase and in frozen nitrogen and argon matrices at low temperatures (12K). This is the first exhaustive study of all nine constituent species of hydrazine and its deuterated derivatives (two of N_2H_3D, four of $N_2H_2D_2$, two of N_2HD_3 and one of N_2D_4). Temperature and concentration studies were performed to identify lines due to dimer (or higher multimer) species. With the aid of the theoretical calculations, which form the second prong of our program, the observed peaks for all isomers were identified and assigned to particular vibrational modes. The low temperature matrix-isolation method proved to be invaluable in this investigation because it invariably led to sharp, narrow vibrational peaks, which simplified spectra considerably. With this reliable data base of the vibrations of hydrazine only minimally perturbed in the noninteracting matrix, the interactions of hydrazines with environmentally significant surfaces is now possible. In addition to such studies, it would also be interesting to investigate in detail the monomethylhydrazine (MMH) and the unsymmetrical dimethylhydrazine (UDMH) derivatives. Survey spectra were recorded in this study but no detailed analysis performed.

In the second part of our program, extensive theoretical calculations of the vibrational spectra of hydrazine and all of its deuterated derivatives were carried out. Ab initio quantum mechanical calculations using the 6-31G** basis set enabled the prediction of vibrational parameters such as force constants and dipole moment derivatives which are of high enough accuracy to

give calculated vibrational frequencies and intensities which mimic experimental spectra very well. In addition potential energy distributions (PEDs) were also obtained. PEDs give the contribution of each symmetry coordinate to each one of the normal vibrational modes. All this information obtained for hydrazine and its isomers was used in the assignment of the observed bands seen in the matrix spectra. Tables of all the vibrational parameters have not been included in this report although they are extremely important if a detailed understanding of the structure and vibrations of hydrazine interacting with a complex or on a surface are to be gotten. Future research in this area would be highly interesting. Several other avenues of future research would seem profitable also. (1) Refine the force constants obtained for hydrazine by a least squares adjustment of the calculated values to the best set of experimental values obtained from hydrazine and its deuterated isomers. (2) Analyze the calculated dipole moment derivatives (Atomic Polar Tensors) to determine the extent to which they may be transferred from N_2H_4 to the methylated derivatives, MMH and UDMH. (3) Examine the calculated parameters and determine their sensitivity to intermolecular interactions such as between hydrazine and CO_2 or the metals, Cu and Fe.

In the third portion of our research, two different studies on the interaction of hydrazine with metals were performed. In the first, hydrazine was reacted with neutral Cu and Fe atoms and isolated in a solid argon matrix at 12 K and the Fourier transform infrared spectra recorded. Parallel studies on ammonia with these metals were also run. It was found that the $Cu \cdot NH_3$ and $Fe \cdot NH_3$ complexes showed large frequency shifts in the ν_2 umbrella mode region, whereas the $Cu \cdot N_2H_4$ and $Fe \cdot N_2H_4$ complexes showed much smaller shifts than the ammonia complexes. These findings were shown to be consistent with a recent theoretical study in which the bonding is ascribed to a more favorable electrostatic interaction between the NH_3 dipole moment (compared to N_2H_4) and the effective polarized metal atomic dipole moment. In the second part, complexes of hydrazine with divalent zinc ions were formed. The Raman spectra of the $Zn(N_2H_4)_2X_2$ (X = Cl, Br) complexes were measured and assigned for the first time. A normal coordinate calculation of the ZnN_4X_2 core aided in the interpretation of the low energy region (100-300 cm^{-1}). Future studies in this area which could provide further information necessary to a complete understanding of the interaction of hydrazine with environmentally important

materials include 1) FT-IR studies of hydrazine, MMH and UDMH with other metals atoms such as Ni, Mn, Co and Al, 2) Raman studies of hydrazine, MMH and UDMH complexes with other transition metal ions, Cu^{+2}, Ni^{+2}, Mn^{+2}, Co^{+2} etc. Preliminary survey spectra of the Ni^{+2} and Mn^{+2}/hydrazine complexes were measured in this research but not analyzed.

In the fourth and final part of our research program, FT-IR spectra of clay-organic complexes were measured and shown to be influenced significantly by the nature of the exchangeable metal cation. Results are presented which are consistent with a single electron transfer between the organic absorbate, p-xylene and the exchangeable metal cation, Cu^{+2}. The Cu^{+2} is reduced to Cu^{+1} or Cu metal and the aromatic is oxidized to form a radical cation. Further experimental work in this area which should be pursued would involve the FT-IR and Raman spectroscopy of hydrazine, its deuterated derivatives, plus MMH and UDMH interacting with various exchangeable metal ions on the surface of different clay materials. With the data presented in this report plus the work suggested above these results would provide much needed information on an important environmental problem.

REFERENCES

II-1. Catalano, E., R. H. Sanborn, and J. W. Frazer, "On the Infrared Spectrum of Hydrazine: Matrix-Isolation Studies of the System N_2H_4/N_2," J. Chem. Phys., vol 38, pp. 2265-2271, 1963.

II-2. Giguere, P. A., and I. D. Liu, "On the Infrared Spectrum of Hydrazine," J. Chem. Phys., vol 20, pp. 136-140, 1952.

II-3. Yamaguchi A., I. Ichishima, T. Shimanouchi, and S. Mizushima, "Torsion Band of Hydrazine," Spectrochim. Acta, vol 16, pp. 1471-1485, 1960.

II-4. Hamada Y., A. Y. Hirakawa, K. Tamagake, and M. Tsuboi, "Amino Wagging and Inversion in Hydrazines," J. Mol. Spectrosc., vol 35, pp.420-435, 1970.

II-5. Durig, J. R., S. F. Bush, and E. E. Mercer, "Vibrational Spectrum of Hydrazine-d_4 and a Raman Study of Hydrogen Bonding in Hydrazine," J. Chem. Phys., vol 44, pp. 4238-4247, 1966.

II-6. Tanaka, N., Y. Hamada, Y. Sugawara, and M. Tsuboi, "Force Field in the Hydrazine Molecule from ab Initio MO Calculation," J. Mol. Spectrosc., vol 99, pp. 245-262, 1983.

II-7. Hallam, H. E., Vibrational Spectroscopy of Trapped Species, Chap. 1, p. 6, Wiley, London, 1973.

II-8. Bentwood, R. M., A. J. Barnes, and W. J. Orville-Thomas, "Studies of Intermolecular Interactions by Matrix Isolation Vibrational Spectroscopy," J. Mol. Spectrosc., vol 84, pp. 391-404, 1980.

II-9. Ribbegard, G. "Studies of Reversible and Irreversible Temperature Effects in the Infrared Spectrum of Matrix Isolated Ammonia and Ammonia-d3," Chem. Phys., vol 8, pp. 185-191, 1975.

II-10. Pimentel, G. C., M. O. Bulanin, and M. Van Thiel, "On the Infrared Spectrum of Matrix-Isolated NH_3," J. Chem. Phys., vol 36, pp. 500-510, 1962.

II-11. Swalen J. D., and J. A. Ibers, "Inversion Barrier in NH_3," J. Chem. Phys., vol 36, pp. 1914-1920, 1962.

II-12. Barnes, A. J., and H. E. Hallam, "Infrared Cryogenic Studies," Trans. Faraday Soc., vol 66, pp. 1920-1931, 1970.

II-13. Swanson, B. I., and L. H. Jones, "Matrix-Molecule Interactions, Dynamics, and Exchange Phenomena in Low Temperature Matrices: SF_6 in Argon and Krypton," J. Chem. Phys., vol 74, pp. 3205-3215, 1981.

II-14. Tursi, A. J., and E. R. Nixon, "Matrix-Isolation Study of the Water Dimer in Solid Nitrogen," J. Chem. Phys., vol 52, pp. 1521-1528, 1970.

II-15. Ayers, G. P. and A. D. E. Pullin, "The Infrared Spectra of Matrix Isolated Water Species - I. Assignment of Bands to $(H_2O)_2$, $(D_2O)_2$ and HDO Dimer Species in Argon Matrices," Spectrochim. Acta, vol 32A, pp. 1629-1639, 1976.

II-16. Abouaf-Marguin, L., M. E. Jacox, and D. E. Milligan, "The Rotation and Inversion of Normal and Deuterated Ammonia in Inert Matrices," J. Mol. Spectrosc., vol 67, pp. 34-61, 1977.

II-17. Durig, J. R., W. C. Harris, and D. W. Wertz, "Infrared and Raman Spectra of Substituted Hydrazines: I. Methylhydrazine," J. Chem. Phys., vol 50, pp. 1449-1461, 1969.

II-18. Durig, J. R., and W. C. Harris, "Infrared and Raman Spectra of Substituted Hydrazines: II. Unsymmetrical Dimethyl Hydrazine," J. Chem. Phys., vol 51, pp. 4457-4468, 1969.

II-19. Herzberg, G., Molecular Spectra and Molecular Structure, pp. 665-666, Van Nostrand, New York, 1966.

II-20. Brown, K. G., and W. B. Person, "Infrared Spectrum of Benzene Isolated in Argon and Krypton Matrices," Spectrochim. Acta, vol 34A, pp. 117-122, 1978.

III-1. Hehre, W. J., L. Radom, Paul V. R. Schleyer and J. A. Pople, Ab Initio Molecular Orbital Theory, Wiley, New York, 1986.

III-2. Tanaka, N., Y. Hamada, Y. Sugawara, and M. Tsuboi, "Force Field in the Hydrazine Molecule from Ab Initio MO Calculation," J. Mol. Spectrosc., vol. 99, pp. 245-262, 1983.

III-3. Riggs, N. V. and L. Radom, Aust. J. Chem., 39 (1986) 1917.

III-4. Tipton, T., D. A. Stone, K. KuBulat and W. B. Person, "Experimental and Theoretical Studies of the Infrared Spectrum of Hydrazine. N_2H_4," submitted to J. Phys. Chem.

III-5. Binkley, J. S., R. A. Whiteside, K. Raghavachari, R. Seeger, D. J. DeFrees, H. B. Schlegel, S. Topiol, L. R. Kahn, M. J. Frisch, E. M. Fuder, and J. A. Pople, GAUSSIAN 82, Carnegie-Mellon University, Pittsburg, PA.

III-6. Reference III-1, p. 76.

III-7. Reference III-2, p. 82.

III-8. Kohata, K., T. Fukuyama, and K. Kuchitsu, J. Phys. Chem., 86 (1982) 602.

III-9. Califano, S. Vibrational States, Wiley, London, 1976.

III-10. Biarge, J. F., J. Herranz, and J. Morcillo, An. R. Soc. Esp. Fis. Quim. A57, 81 (1961).

III-11. Person, W. B. and J. H. Newton, J. Chem. Phys., 61 (1974) 1040.

III-12. Person, W. B. in W. B. Person and G. Zerbi, (Eds.), Vibrational Intensities in Infrared and Raman Spectroscopy, Elsevier, Amsterdam, 1982, Chaps. 4, 14.

III-13. Komornicki, A. and J. W. McIver, Jr., J. Chem. Phys., 70 (1979) 2014.

III-14. Schaad, L. J., C. S. Ewig, B. A. Hess, Jr., and D. Michalska, J. Chem. Phys., 83 (1985) 5348.

III-15. Fogarasi, G. and P. Pulay, in J. R. Durig (Ed.), Vibrational Spectra and Structure, Vol. 14, Elsevier, Amsterdam, 1985, Chap. 3.

III-16. Wiberg, K. B., V. A. Walters, K. N. Wong and S. D. Colson, J. Phys. Chem., 88 (1984) 6067.

III-17. Chin, S., I. Scott, K. Szczepaniak and W. B. Person, J. Am. Chem. Soc., 106 (1984) 3415.

III-18. Morino, Y. and K. Kuchitsu, J. Chem. Phys., 20 (1952) 1809.

III-19. Keresztury, G. and G. Jalsovszky, J. Mol. Struct., 10 (1971) 304.

IV-1. Schmidt, Eckart W., Hydrazine and Its Derivatives, p. 371 ff, Wiley-Interscience, New York, 1984.

IV-2. Bauschlicher, C. W., "Transition Metal-ligand Bonding. II," Journal of Chemical Physics, 1986, vol. 84, pp. 260-267.

IV-3. Herzberg, G., Infrared and Raman Spectra of Polyatomic Molecules, Van Nostrand Co., New York, 1945.

IV-4. Abouaf-Marguin, L., Jacox, M. E. and Milligan, D. E., "The Rotation and Inversion of Normal and Deuterated Ammonia in Inert Matrices," Journal of Molecular Spectroscopy, 1977, vol. 67, pp. 34-61 and references therein.

IV-5. Nishiya, T., Hirota, N., Shinohara, H. and Nishi, N., "Identification of Ammonia Clusters in Low Temperature Matrices Using the FTIR Short-Pulsed Matrix Isolation Technique," J. Phys. Chem. 89, 2260-2264 (1985).

IV-6. Nelander B. and Nord, L., "Complex between Water and Ammonia", Journal of Physical Chemistry, 1982, vol. 86, pp. 4375-4379.

IV-7. Süzer, S. and Andrews, L., "Infrared Spectra of Alkali Metal Atom-Ammonia Complexes," Journal of the American Chemical Society, 1987, vol. 109, pp. 300-304.

IV-8. Vala, M., Zeringue, K., Shaksemampour, J., Rivoal, J. C. and Pyzalski, Robert, "Magnetic Circular Dichroism of Matrix-isolated Atoms: Excited State Spin-orbit Coupling Constant Reduction of Copper in the Noble Gases," J. Chem. Phys., vol. 80, pp. 2401-2406, 1984, and references therein.

IV-9. Pimentel, G. C., McClellan, A. L., The Hydrogen Bond, W. H. Freeman, San Francisco, 1960.

IV-10. Tipton, T., Stone, D., Person, W. and Kubulat, K., to be published; work described elsewhere in this report.

IV-11. Johnson G. L. and Andrews, L., "Matrix Infrared Spectrum of the H_3N-HF Hydrogen-Bonded Complex", Journal of the American Chemical Society, 1982, vol. 104, pp. 3043-3047.

V-1. Bottomley, F., "The Reactions of Hydrazine with Transition-Metal Complexes" Quart. Reviews, Chemical Society 24, 617-638, 1970.

V-2. Sathyanarayana, D. N. and Nicholls, D., "Vibrational spectra of transition metal complexes of hydrazine. Normal coordinate analyses of hydrazine and hydrazine-d_4", Spectrochimica Acta, 34A, 263-267, 1978.

V-3. Franzen H. and von Meyer, O., "Über die Hydrazinate einiger Metallsalze," Z. Anorg. Allgemein. Chem. 60, 247-291 (1908).

V-4. University of Florida MicroAnalysis Service, Department of Chemistry.

V-5. Sacconi, L. and Sabatini, A., "The Infrared Spectra of Metal(II)-Hydrazine Complexes," J. Inorg. Nucl. Chem., 25, 1389-1393 (1963).

V-6. Braibanti, A., Dallavalle, F., Pellinghelli, M. A., and Leoparti, E., "The Nitrogen-Nitrogen Stretching Band in Hydrazine Derivatives and Complexes," Inorg. Chem. 7, 1430-1433 (1968).

V-7. Strommen, D. P. and Nakamoto, K., Laboratory Raman Spectroscopy, John Wiley and Sons, New York, 1984.

V-8. Ferrari, A., Braibanti, A. and Bigliardi, G., "Chains of Complexes in the Crystal Structure of Bishydrazine Zinc Chloride," Acta Cryst. 16, 498-502 (1963).

V-9. Nakagawa, I. and Shimanouchi, T., "Far infrared spectra and metal-ligand force constants of metal ammine complexes," Spectrochimica Acta. 22, 759-775, 1966.

V-10. Durig, J. R., Bush, S. F., and Mercer, E. E., "Vibrational Spectrum of Hydrazine-d_4 and a Raman Study of Hydrogen Bonding in Hydrazine," J. Chem. Phys., 44, 4238-4247 (1966).

V-11. Giguere, P. A. and Liu, I. D., "On the Infrared Spectrum of Hydrazine," J. Chem. Phys., 20, 136-140, 1952.

V-12. Szczepanski, J., Szczesniak, M., Person, W. B. and Vala, M., to be published.

V-13. Mishra, H. C., Mishra, G. and Choubey, L. N., "Some Studies on Mixed

Ligand Complexes of Co(II), Ni(II) and Zn(II) with Hydrazine and Oxalic Acid", J. Indian Chem. Soc. LX, 521-523 (1983).

V-14. Irving, H. and Williams, R. P., Nature, Lond. 162, 746 (1948); J. Chem. Soc. 3192 (1953).

V-15. Clark, R. J. H. and Williams, C. S., Inorg. Chemistry, 4, 350 (1965).

VI-1. Pinnavaia, T.J.; Mortland, M. M. (1971) Interlamellar metal complexes on layer silicates. I. Copper(II)-arene complexes on montmorillonite. J. Phys. Chem. 75, 3957.

VI-2. Pinnavaia, T.J.; Hall, P.L.; Cady, S.S.; Mortland, M.M. (1974) - Aromatic radical cation formation on the intracrystal surfaces of transition layer silicates. J. Phys. Chem. 78, 994-999.

VI-3. Rupert, J.P. (1973) Electron spin resonance spectra of interlamellar copper(II)-arene complexes on montmorillonite. J. Phys. Chem. 77, 784-790.

VI-4. Eastman, M.P.; Patterson, D.E.; Pannell, K.H. (1984) Reaction of benzene with Cu(II)- and Fe(III)-exchanged hectorites. Clays. and Clay Min. 32, 327-333.

VI-5. Soma, Y.; Soma, M.; Harada, I. (1984) The reaction of aromatic molecules in the interlayer of transition metal ion exchanged montmorillonite studied by resonance Raman spectroscopy. I. Benzene and p-phenylenes. J. Phys. Chem. 88, 3034-3038.

VI-6. Govindraj, N. Mortland, M.M.; Boyd, S.A. (1987) Single electron transfer mechanism of oxidative dechlorination of 4-chloroanisole on Copper(II)-smectite. Env. Sci. and Tech. 21, 1119- 1123.

VI-7. Varsanyi, G. (1969) "Vibrational spectroscopy of benzene derivatives," 430 p. Academic Press, New York.

VI-8. Katritzky, A.R., Simmons, P. (1958) Infrared absorption of heteroaromatic and benzenoid six membered monocyclic nuclei. Part VII para-disubstituted benzenes. J. Chem. Soc. 2051-2058.

VI-9. Bellamy, L.J. J. Chem. Soc. 2818 (1955).

VI-10. Soma, Y.; Soma, M.; Harada, I. (1983) Raman spectroscopic evidence of fomration of p-dimethoxybenzene cation on Cu- and Ru-montmorillonites. Chem. Phys. Lett. 94, 475-478.

VI-11. Soma, Y.; Soma, M.; Harada, I. (1983) Resonance raman spectra of benzene adsorbed on Cu(II) montmorillonite. Formation of poly(p-phenylene) cations in the interlayer of the clay mineral. Chem. Phys. Lett. 99, 153-156.

VI-12. Soma, Y.; Soma, M.; Harada, I. (1985) Reactions of aromatic molecules in the interlayer of transition-metal ion exchanged montmorillonite studied by resonance Raman spectroscopy. 2. Monosubstituted benzenes and 4,4'-disubstituted biphenyls. J. Phys. Chem. 89, 738-742.

VI-13. Wilson, E.B.; Decius, J.C.; Cross, P.C. (1955) Chapter 10 in "Molecular Vibrations. The theory of infrared and Raman vibrational spectra," Dover Publ., New York.

VI-14. Takahashi, C.; Maeda, S. (974) Raman spectra of biphenyl negative ion in the tetrahydrofuran solution. Chem. Phys. Lett. 24, 584-588.

VI-15. Aleksandrov, I.V.; Bobovich, Y.S.; Maslov, V.G.; Sidorov, A.N. (1975) Raman spectra of biphenyl anion radicals. Opt. Spectrosc. 38, 387-389.

VI-16. Fenn, D.B.; Mortland, M.M.; Pinnavaia, T.J. (1973) The chemisorption of anisole on Cu(II) Hectorite. Clays and Clay Min. 21, 315-322.

VI-17. Cloos, P.; Moreale, A.; Broers, C.; Badot, C. (1979) Adsorption and

oxidation of aniline and p-chloroaniline by montmorillonite. Clay Minerals 14, 307-321.

VI-18. Moreale, A.; Cloos, P., Badot, C. (1985) Differential behavior of Fe(III)- and Cu(II) montmorillonite with aniline: I. suspensions with constant solid:liquid ratio. Clay Minerals 20, 29-37.

VI-19. Mortland, M.M.; Halloran, L.J. (1976) Polymerization of aromatic molecules on smectite. Soil Sci. Soc. of Amer. J. 40, 367-370.

VI-20. van Olphen, H.; Fripiat, J.J. (1979) Data handbook for clay materials and other non-metallic minerals. Pergamon Press, Oxford, 346 pp.

VI-21. Johnston, C.T.; Sposito, G.; Bocian, D.F.; Birge, R.R. (1984) Vibrational spectroscopic study of the kaolinite-dimethylsulfoxide complex. J. Phys. Chem. 88, 5959-5964.

VI-22. Johnston, C.T.; Sposito, G.; Birge, R.R. (1985) Raman spectroscopic study of kaolinite in aqueous suspension. Clays and Clay Min. 33, 483-489.

VI-23. Sposito, G., Holtzclaw, K.H., Johnston, C.T., and LeVesque-Madore, C.S. (1981) Thermodynamics of Sodium-Copper Exchange on Wyoming Bentonite at 298 K. Soil Sci. Soc. Am. J. 45 1079-1084.

VI-24. Brindley, G.W.; Kao, C.C.; Harrison, J.L.; Lipsicas, M.; Rayathatha, R. (1986) Relation between structural disorder and other characteristics of kaolinites and dickites. Clays and Clay Min. 34, 239-249.

VI-25. Plancon, A.; Tchoubar, C. (1977) Determination of structural defects in phyllosilicates by X-ray powder diffraction. I. Principle of calculations of the diffraction phenomenon. Clays and Clay Min. 25, 430-435.

VI-26. Ledoux, R.L.; White, J.L. (1964) Infrared study of selective

deuteration of kaolinite and halloysite at room temperature. Science 145, 47-49.

VI-27. Wada, K. (1967) A study of hydroxyl groups in kaolin minerals utilizing selective deuteration and infrared spectroscopy. Clay Minerals 7, 51.

VI-28. Rouxhet, P.G.; Samudacheata, N.; Jacobs, H.; Anton, O. (1977) Attribution of the OH strecthing bands of kaolinite. Clay Minerals 12, 171-178.

VI-29. Ishii, M.; Shimanouchi, T.; Nakahira, M. (1967) Far infra-red absorption spectra of layer silicates. Inorg. Chim. Acta, 1. 387-392.

VI-30. Larson, S.J.; Pardoe, G.W.F.; Gebbie, H.A.; Larson, E.E. (1972) The use of far infrared interferometric spectroscopy for mineral identification. Amer. Minera. 57, 998-1002.

VI-31. Farmer, V.C. (1974) Chapeter 15 in "The infrared spectra of minerals," Ed. Farmer, V.C. Publ. by the Mineral Society of London.

VI-32. Estep, P.A.; Kouach, J.J.; Karr, C. (1968) Quantitative infrared multicomponent determinations of minerals in coal. Anal. Chem. 40, 358-363.

VI-33. Sposito, G.; Prost, R.; Gaultier, J.P. (1983) Infrared spectroscopic study of adsorbed water on reduced charge Na/Li montmorillonites. Clays and Clay Min. 31, 9-16.

VI-34. Farmer, V.C.; Russell, J.D. (1971) Interlayer complexes in layer silicates. The structure of water in lamellar ionic solutions. Trans. Farad. Soc. 67, 2737-2749.

VI-35. McBride, M.B.; Pinnavaia, T.J.; Mortland, M.M. (1977) Adsorption of aromatic molecules by clays in aqueous suspension. Adv. environ. Sci. Technol. 8, 145-154.

APPENDIX A

FORTRAN PROGRAM FOR BASELINE AND VAPOR CORRECTIONS OF FT-IR MATRIX-ISOLATION SPECTRA

APPENDIX A

FORTRAN PROGRAM FOR BASELINE AND VAPOR CORRECTIONS OF FT-IR MATRIX-ISOLATION SPECTRA

Matrix-isolation spectra usually exhibit broad interference fringes. To make these spectra more suitable for plotting, an automated baseline-correction program was written. This program divides the single-beam sample spectrum into blocks, and locates the frequency of maximum detector intensity for each quarter of the block. Whichever of these four maxima is in a region where the integrated absolute second derivatives is smallest is assigned as the baseline point for the block. This procedure tends to prevent saddle points from being chosen as baseline points. All baseline points between the reference baseline points are generated by cubic spline interpolation. A transmittance can, thereby, be obtained for every data point in the single-beam spectrum. The background spectrum is handled in the same manner using the same baseline frequencies that were obtained from the sample spectrum. When the resulting single-beam spectra are ratioed, the transmittance is exactly 100 percent at the reference frequencies previously determined from the sample spectrum. Broad spectral features are thereby removed while narrow ones are unaffected. The size of the data blocks can be enlarged if the solute molecules in the matrix have unusually broad asorptions.

An optional part of the computer program can be used to reduce the intensities of unwanted CO_2 and H_2O vapor absorptions. The frequencies of these absorptions are often affected by a matrix-induced calibration error of the FT-IR spectrometer. The frequency shifts are approximately a constant multiple of the original frequencies, and are on the order of 0.01 cm^{-1} at 2000 cm^{-1}. Although such shifts are of no concern for matrix absorptions, they have a very noticeable effect on vapor subtractions. The computer program corrects these shifts by computing several sets of S/B (S = sample, B = background) peak-height ratios for several selected H_2O absorptions using stepwise-adjusted calibration factors. The true calibration factor is assumed to be the one that gives the most consistent set of peak intensity ratios. The consistency is determined by counting the number of peaks that are within a specified deviation from the median peak-height ratio (averaged ratios are not desirable one or more of the H_2O vapor reference frequencies may be overlapped with matrix absorptions).

After the frequency calibration has been determined, the H_2O vapor absorptions of the background spectrum are multiplied by whatever constant factor yields the best intensity matchup between the sample and background vapor peaks. The H_2O vapor peaks will then be eliminated in the S/B ratioing process if these peaks are not totally absorbing.

The CO_2 vapor absorptions can be processed in the same manner as for H_2O, but the outcome is less satisfactory because of strong intensities and overlappings of the component rovibrational bands.

Areas of the sample spectrum that have large vapor absorptions but virtually no matrix absorptions can be further corrected by simply blanking them.

```
C SBBLN.FOR
      INTEGER BRDATA(512),SRDATA(512),IDATA(512),ODATA(512),
     1        SWDATA(512),BWDATA(512),ILIM(8)    ,BLKSKP(2) ,
     2        IC(2,2)     ,ICSEC(2,2) ,NVP(4)    ,NR(4,2)   ,
     3        BLKCNT,BLKREL,BASCNT,BGBLSZ,BSLINE,BLKSIZ,BLKOPT,
     4        Q23CO2,PR2CO2,OBFSEC,OSFSEC,OXFSEC,RESUME,WRDLOW,
     5        ENDATA,VAPSEC,VAPOPT,OLDSEC,OZFSEC,BSFIND,BSCORR,
     6        WRDHI ,SFSEC ,BFSEC ,WATOPT,CO2OPT,OZFN  ,OXFN  ,
     7        ASFN  ,ABFN  ,ADFN  ,OSFN  ,OBFN  ,ODFN
      DIMENSION FSKIP(2,2),VRANGE(8) ,VRAT(4,2) ,VPWVN(4,10),
     1          XINTRP(10),BVPK(30)  ,SVPK(30)  ,RVPK(30)  ,
     2          BBAS(16)  ,SBAS(10)  ,RBAS(10)  ,BFRQ(10)  ,
     3          CB(10,3)  ,CS(10,3)  ,CSC(10,3) ,CCB(3)    ,
     4          CCS(3)    ,DEL(3)    ,Y(10)     ,WSHIFT(4,2),
     5          YB(10)    ,YS(10)
      CHARACTER VAPNAM(4)*10
      COMMON /IO/    IVFSEC,OBFSEC,OSFSEC,OXFSEC,IWRSEC,INODE,
     1               IWR,LSEC,BGBLSZ,PPWVN,BRDATA,SRDATA,IDATA
      COMMON /VAPRAT/ PCTOL
      COMMON /VAPSHF/ XINTRP,Y,CB,CS
C
      DATA VAPNAM/'H2O V2','H2O V3','CO2 V2','CO2 V3'/
      DATA VRANGE/1360.,2070.,3400.,4000.,625.,715.,2230.,2400/
C
      DATA VAPCUT/97.0/, SIGMIN/99.0/
C
      DATA NBLANK/0/, LASTPT/0/,
     1     WATOPT/2/, ICUBIC/0/, CO2OPT/2/,
     2     Q23CO2/1/, ISHIFT/1/, PR2CO2/1/, MXBLNK/2/,
     3     BASCNT/0/, ISTART/1/, IQUIT /0/, ENDATA/512/
C
      DATA ISFN/2/ ,IBFN/3/ ,ODFN/44/,OSFN/42/,OBFN/43/,IVFN/0/,
     1     ASFN/52/,ABFN/53/,ADFN/54/,OXFN/41/,OZFN/40/
C
C ***************************************************************
C REFERENCE VAPOR PEAKS:
C
      NVP(1)   =10
      VPWVN(1,1) =1419.5
      VPWVN(1,2) =1436.8
      VPWVN(1,3) =1496.4
      VPWVN(1,4) =1539.0
      VPWVN(1,5) =1554.5
      VPWVN(1,6) =1616.9
      VPWVN(1,7) =1675.2
      VPWVN(1,8) =1717.4
      VPWVN(1,9) =1734.5
      VPWVN(1,10)=1844.2
      NVP(2)   =6
      VPWVN(2,1) =3649.2
      VPWVN(2,2) =3744.7
      VPWVN(2,3) =3816.0
      VPWVN(2,4) =3854.1
```

```
      VPWVN(2,5) =3885.7
      VPWVN(2,6) =3917.3
      NVP(3)   =6
      VPWVN(3,1) =647.4
      VPWVN(3,2) =651.9
      VPWVN(3,3) =659.6
      VPWVN(3,4) =676.0
      VPWVN(3,5) =685.6
      VPWVN(3,6) =695.3
      NVP(4)   =6
      VPWVN(4,1) =2307.0
      VPWVN(4,2) =2323.1
      VPWVN(4,3) =2347.5
      VPWVN(4,4) =2364.1
      VPWVN(4,5) =2372.6
      VPWVN(4,6) =2378.8
C
      FSKIP(1,1)=666.5
      FSKIP(1,2)=670.0
      FSKIP(2,1)=2280.0
      FSKIP(2,2)=2400.0
C
C ***************************************************************
C ************** ENTER INPUT DATA ***************************
C
      PRINT *,'BASLIN.DAT: 0=EXISTS, 1=CREATE, -1=NOT 0 OR 1:  '
      READ *,BSFIND
      PRINT *,'BASELINE-CORRECTION?            (0=NO, 1=YES):  '
      READ *,BSCORR
          IF (BSFIND.NE.-1) OPEN(11,FILE='BASLIN.DAT',
     1                      FORM='FORMATTED',STATUS='UNKNOWN')
      PRINT *,'VAPOR CORRECTION? 0=NO,1=YS,2=YS/DEFAULT PARAMS:'
      READ *,VAPOPT
      IVPOPT=(1+VAPOPT)/2
C
         IF (VAPOPT.NE.0.AND.BSCORR.EQ.0.AND.BSFIND.EQ.0) THEN
               IBFN=OBFN
               ISFN=OSFN
               OBFN=ABFN
               OSFN=ASFN
               ODFN=ADFN
               ENDIF
      WRITE(2,2100) IBFN,ISFN,OBFN,OSFN,ODFN
2100  FORMAT('0','THE DEFAULT FILES ARE: IBFN=',I2,'  ISFN=',I2,
     1       '  OBFN=',I2,'  OSFN=',I2,'  ODFN=',I2)
      WRITE(2,2200)
2200  FORMAT('0','USE THESE DEFAULT DATA FILES? 0=NO, 1=YES:')
      READ *,ISCRAT
           IF (ISCRAT.EQ.1)                              GO TO 31
      PRINT *,'BACKGROUND FILE # FOR INPUT DATA:                '
      READ *,IBFN
      PRINT *,'    SAMPLE  "   "  "    "    "  :               '
      READ *,ISFN
```

```
      PRINT *,'BACKGROUND  "   "  "  OUTPUT "  :                '
      READ *,OBFN
      PRINT *,'    SAMPLE  "   "  "    "    "  :                '
      READ *,OSFN
      PRINT *,'ABSORBANCE  "   "  "    "    "  :                '
      READ *,ODFN
          IF (BSFIND.EQ.0)                                GO TO 31
      PRINT *,'BASELINE    "   "  "    "    "  :                '
      READ *,OZFN
C
C THE FOLLOWING STATEMENT GUARDS AGAINST TRYING TO READ FROM A
C NONEXISTANT BASELINE FILE.
C
31        IF (BSFIND.EQ.0) THEN
               READ(11,8300) BLKSIZ
               READ(11,8500) FRQMIN,RFXF,RLXF
             ELSE
      PRINT *,' 1ST FREQ OF CORRECTION RANGE:                   '
      READ *,RFXF
      PRINT *,'LAST FREQ OF CORRECTION RANGE:                   '
      READ *,RLXF
      PRINT *,'WORDS PER BASELINE BLOCK (USE - SIGN IF 6000C): '
      READ *,BLKSIZ
      BLKSIZ=16*(BLKSIZ/16)
             ENDIF
C
61                          NICMOD=6000
          IF (BLKSIZ.GT.0)  NICMOD=740
          IF (BLKSIZ.LT.0)  BLKSIZ=-BLKSIZ
          IF (BLKSIZ.LT.16) BLKSIZ=16
          IF (VAPOPT.NE.1)                                GO TO 91
      PRINT *,'FILE # FOR INPUT VAPOR REF SPECTRUM (0=NONE)   :'
      READ *,IVFN
      PRINT *,'CO2 CORRECTIONS: 0=NONE, 1=V3(PQR)&V2(Q), 2=ALL:'
      READ *,CO2OPT
      PRINT *,'H2O VAPOR CORRECTIONS: 0=NONE, 1=V2 ONLY, 2=ALL:'
      READ *,WATOPT
      PRINT *,'VAPOR BLANKING? 0=NO,1=YES,2=YS/DEFAULT PARAMS: '
      READ *,BLKOPT
      IBLOPT=(1+BLKOPT)/2
           IF (BLKOPT.NE.1)                               GO TO 81
           IF (CO2OPT.EQ.0)                               GO TO 71
      PRINT *,'BLANK V3(PQR) & V2(Q) OF CO2? (0=NO,1=YES):     '
      READ *,Q23CO2
           IF (Q23CO2.EQ.1) THEN
      PRINT *,'CO2-V2: LOW CM-1 KILL LIMIT (-/DEFAULT; 0=NONE):'
      READ *,B
      IF (B.GT.-0.001) FSKIP(1,1)=B
      PRINT *,'CO2-V2: HIGH  "   "     "         "        "   :'
      READ *,B
      IF (B.GT.-0.001) FSKIP(1,2)=B
      PRINT *,'CO2-V3: LOW   "   "     "         "        "   :'
      READ *,B
```

```
      IF (B.GT.-0.001) FSKIP(2,1)=B
      PRINT *,'CO2-V3: HIGH  "   "     "         "        "   :'
      READ *,B
      IF (B.GT.-0.001) FSKIP(2,2)=B
           ENDIF
      PRINT *,'INTERPOLATE V2(PR) OF CO2? (0=NO,1=YES)        :'
      READ *,PR2CO2
71    PRINT *,'%T CUTOFF FOR 1-BEAM VAPOR PKS (- FOR DEFAULT): '
      READ *,VC
      IF (VC.GT.0.0) VAPCUT=VC
      PRINT *,'%T CUTOFF FOR IGNORING SAMPLE  (- FOR DEFAULT): '
      READ *,SG0
      IF (SG0.GT.0.0) SIGMIN=SG0
      PRINT *,'MAX CONSEC BLANK PTS WHEN SIG>MIN (-/DEFAULT):  '
      READ *,MXB
      IF (MXB.GT.-1) MXBLNK=2*(MXB/2)
C
C     "OXFN"  IS THE # OF THE OUTPUT FILE WHICH INDICATES WHAT
C PARTS OF THE SPECTRUM HAVE BEEN BLANKED TO REMOVE VAPOR LINES.
C
      PRINT *,'FILE # FOR OUTPUT BLANKING-INDICATION SPECTRUM: '
      READ *,OXFN
81    PRINT *,'TRY TO CORRECT VAPOR FREQ CALIBR? (0=NO,1=YES): '
      READ *,ISHIFT
C
C ****************************************************************
C ****************** FTIR PARAMETERS *************************
C
91       IXSP=RFXF+.001
         IXEP=RLXF+.99
         CALL IRPUT(14025,0,IXSP)
         CALL IRPUT(14026,0,IXEP)
         CALL IRPUT(14036,0,OBFN)
         CALL IRPUT(14015,0,OSFN)
         CALL IRPUT(14022,0,ODFN)
C
C ****************************************************************
C ************** PRINT INPUT DATA ****************************
C
      PR2CO2=PR2CO2*(CO2OPT/2)
      Q23CO2=Q23CO2*((CO2OPT+1)/2)*IBLOPT
      WRITE(2,7100) IXSP,IXEP
7100  FORMAT('0','CORRECTION RANGE:  ',I5,'  TO  ',I5,' CM-1')
      WRITE(2,7200) IVPOPT
7200  FORMAT('0',' ENABLE VAPOR CORRECTIONS?:              ',I1)
      WRITE(2,7300) WATOPT*IVPOPT
7300  FORMAT(' ',' H2O CORRECTIONS?: 0=NONE, 1=V2, 2=ALL   ',I1)
      WRITE(2,6800) CO2OPT*IVPOPT
6800  FORMAT(' ',' CO2 CORRECTIONS?: 0=NONE,1=V3&V2Q,2=ALL ',I1)
      WRITE(2,7400) IBLOPT*IVPOPT
7400  FORMAT(' ',' ENABLE VAPOR BLANKING?:                 ',I1)
      WRITE(2,7500) Q23CO2*IVPOPT*IBLOPT
7500  FORMAT(' ',' ENABLE CO2(V3-PQR,V2-Q) BLANKING?:      ',I1)
```

```
      WRITE(2,7600) PR2CO2*IVPOPT*IBLOPT
7600  FORMAT(' ','ENABLE CO2(V2-PR) BLANKING?:            ',I1)
      WRITE(2,7700) ISHIFT*IVPOPT
7700  FORMAT(' ','ENABLE SPECTRUM SHIFTING?:              ',I1)
      WRITE(2,7900) VAPCUT
      VAPCUT=0.01*VAPCUT
7900  FORMAT(' ','BLANKING THRESHOLD (% TRANSMITTANCE): ',F5.1)
      WRITE(2,8100) SIGMIN
      SIGMIN=0.01*SIGMIN
8100  FORMAT(' ','SAMPLE      "       "       "       : ',F5.1)
      WRITE(2,8200) MXBLNK
8200  FORMAT(' ','MAX # CONSEC BLANKED PTS (SIG > MIN):  ',I2)
      WRITE(2,9000) BLKSIZ
9000  FORMAT('0','THE BASELINE CORRECTION INTERVAL IS',I4,
     1' WORDS')
      WRITE(2,5000) ISFN,IBFN
      WRITE(2,6000) OSFN,OBFN,ODFN
      WRITE(2,4000) OXFN,OZFN
5000  FORMAT('0','INPUT FILES:   1-BEAM SAMPLE =',I3,4X,
     1'BACKGROUND =',I3)
6000  FORMAT('0','OUTPUT FILES:  1-BEAM SAMPLE =',I3,4X,
     1'BACKGROUND =',I3,3X,'ABSORBANCE =',I3)
4000  FORMAT(' ',10X,'BLANKING-INDICATOR =',I3,6X,'BASELINE =',
     1I3)
C
C ****************************************************************
C OBTAIN ADDITIONAL SPECTRAL PARAMETERS:
C
      CALL FTPARM(NICMOD,RFXF,RLXF,FRQMIN,FRQMAX,IISEC,IFSEC,
     1            INDXSP,INDXEP,INODE,NSECS,PPWVN)
C
C COMPUTE SECTOR INDICES FOR USE IN IRTISK AND IWTISK ROUTINES:
C
      IBFSEC=IBFN*NSECS+88-1
      ISFSEC=ISFN*NSECS+88-1
      IVFSEC=IVFN*NSECS+88-1
      OSFSEC=OSFN*NSECS+88-1
      OBFSEC=OBFN*NSECS+88-1
      OXFSEC=OXFN*NSECS+88-1
      OZFSEC=OZFN*NSECS+88-1
      IF (IVFN.EQ.0) IVFSEC=OBFSEC
C
C****************************************************************
C READ FILE STATUS BLOCKS TO GET EXPONENTS AND NUMBERS OF SCANS:
C
      CALL IRTISK(BRDATA,512,IBFSEC+NSECS,INODE)
      IBEXP=BRDATA(6)
      NSB=BRDATA(3)
      CALL IRTISK(SRDATA,512,ISFSEC+NSECS,INODE)
      ISEXP=SRDATA(6)
      NSS=SRDATA(3)
      WRITE(2,2000) NSS,NSB,IBEXP,ISEXP
2000  FORMAT('0','NSS= ',I4,4X,'NSB= ',I4,4X,'IBEXP='
```

```
     1,I2,4X,'ISEXP=',I2)
C
C ***************************************************************
C COPY FILE STATUS BLOCK OF ISFN INTO OSFN; AND IBFN INTO OBFN:
C
      CALL IWTISK(SRDATA,512,OSFSEC+NSECS,INODE)
      CALL IWTISK(BRDATA,512,OBFSEC+NSECS,INODE)
C ***************************************************************
C
C ******************* INITIALIZE VARIABLES ********************
C
      IF(IBEXP.GT.ISEXP) SCALE=(1.0*NSS)/NSB*2**(IBEXP-ISEXP)
      IF(IBEXP.LT.ISEXP) SCALE=(1.0*NSS)/(NSB*2**(ISEXP-IBEXP))
      IF(IBEXP.EQ.ISEXP) SCALE=(1.0*NSS)/NSB
      SSCALE=1.0E5
      BSCALE=SSCALE/SCALE
      NBLKS=512/BLKSIZ
      BLKREL=(IISEC-1)*NBLKS
C
C COMPUTE ARRAY INDICES CORRESPONDING TO THE CM-1 LIMITS OF
C V2-Q (I=1) AND V3-PQR (I=2) OF CO2.
C
      DO 101 I=1,2
      DO 101 J=1,2
      IX=PPWVN*FSKIP(I,J)
      IC(I,J)=1+IX-(IX/512)*512
      BLKSKP(J)=IX/BLKSIZ+1-BLKREL
101   ICSEC(I,J)=IX/512+1
C
      PCTOL0=1.0
      PCTOL =PCTOL0
      BGBLSZ=32
      SWRSEC=OSFSEC+IISEC
      BWRSEC=OBFSEC+IISEC
      NX=-524288
      IF (BSFIND.EQ.0)                                    GO TO 261
      WRITE (2,8000)
8000  FORMAT('0','BEGIN BASELINE-LOCATOR ALGORITHM')
C***************************************************************
C
C ***************** LOCATE BASELINE POINTS *******************
C
      DO 251 M=IISEC,IFSEC
      DO 131 I=1,512
131           BWDATA(I)=NX
              IH=4
      DO 141 I=1,IH
              K=IH+1-I
141           IF (IBSWRD.GE.513-I)
     1           BWDATA(K)=BSCALE*(1+.1*(512+K-IBSWRD))
              IIBLK=1
              WRDDIF=512*(M-1)-1
              CALL IRTISK(BRDATA,512,IBFSEC+M,INODE)
```

```
            CALL IRTISK(SRDATA,512,ISFSEC+M,INODE)
            IF (M.NE.IISEC)                                  GO TO 161
C
C ***************************************************************
C
C FIRST SECTOR ONLY:
C DETERMINE THE INDEX OF THE 1ST WORD OF THE SPECTRUM (INDXSP):
C
      DO 151 I=1,512
151         IF (SRDATA(I).EQ.NX.AND.BRDATA(I).EQ.NX) NBLANK=I
            IF (INDXSP.LT.NBLANK+1) INDXSP=NBLANK+1
            IIBLK=INDXSP/BLKSIZ+1
            BLKCNT=IIBLK-1
            FRQMIN= (WRDDIF+INDXSP)/PPWVN
            WRITE(11,8300) BLKSIZ
            WRITE(11,8500) FRQMIN,RFXF,RLXF
C ***************************************************************
C
C LAST SECTOR ONLY:
C DETERMINE THE INDEX OF THE LAST WORD OF THE SPECTRUM (INDXEP)
C
161         IF (M.NE.IFSEC)                                  GO TO 191
      DO 171 I=1,512
            IF(SRDATA(I).GT.NX.AND.BRDATA(I).GT.NX)  GO TO 171
            ENDATA=I-1
                                                             GO TO 181
171         CONTINUE
181         IF (ENDATA.LT.INDXEP) INDXEP=ENDATA
C ***************************************************************
C
191   DO 241  LOCBLK=IIBLK,NBLKS
            BLKCNT=BLKCNT+1
C ***************************************************************
C
C IF THE CURRENT BLOCK IS WITHIN THE V3 BAND OF CO2, READ THE
C NEXT DATA BLOCK WITHOUT SEARCHING FOR A BASELINE PT.
C
      IF (BLKCNT.GT.BLKSKP(1).AND.BLKCNT.LT.BLKSKP(2)) GO TO 241
C
C ***************************************************************
C
C THE CURRENT SAMPLE DATA BLOCK IS DIVIDED INTO QUARTERS, AND
C THE MAXIMUM DETECTOR INTENSITY IS FOUND FOR EACH QUARTER.
C THE BEST BASELINE PT FOR THE BLOCK IS CHOSEN FROM THESE 4
C MAXIMA BY COMPARING SUMS OF THE ABSOLUTE VALUES OF SEVERAL
C 2ND DERIVATIVES OBTAINED FROM THE NEIGHBORHOOD OF EACH OF THE
C 4 MAXIMA.  THE MAXIMUM HAVING THE SMALLEST SUCH SUM IS CHOSEN
C AS THE BASELINE PT BECAUSE IT IS THE ONE THAT IS LEAST LIKELY
C TO BE A SADDLE PT.
C
            JMIN=1
            IF (BASCNT.EQ.0) JMIN=4
            IF (M.EQ.IFSEC.AND.LOCBLK*BLKSIZ.GE.INDXEP) THEN
```

```
                JMIN=4
               - LASTPT=INDXEP
                ENDIF
            SUMMIN=1.0E10
      DO 231 J=JMIN,4
            ILAST=LOCBLK*BLKSIZ-(4-J)*BLKSIZ/4
            IFIRST=ILAST-JMIN*BLKSIZ/4+1
            IF (BASCNT.EQ.0) IFIRST=INDXSP
            IF (LASTPT.NE.0) ILAST =INDXEP
            IBQ=IFIRST
      DO 201 I=IFIRST,ILAST
201         IF (SRDATA(I).GT.SRDATA(IBQ)) IBQ=I
            SUM=0.0
            IF (LASTPT.NE.0.OR.BASCNT.EQ.0)          GO TO 221
            IMIN=IBQ-2
            IF (IMIN.LT.1) IMIN=1
            IF (IMIN+4.GT.512) IMIN=512-4
      DO 211 I=IMIN,IMIN+4
211         SUM=SUM+ABS(1.*SRDATA(I+2)-2.*SRDATA(I+1)+
     1                  1.*SRDATA(I))
221         IF (SUM.LT.SUMMIN.AND.(J.NE.1.OR.JOLD.NE.4)) THEN
               SUMMIN=SUM
               IBSWRD=IBQ
               JOLD=J
               ENDIF
231         CONTINUE
            BWDATA(IBSWRD)=BSCALE
      DO 235 I=1,IH
            IF (IBSWRD.GT.I)    BWDATA(IBSWRD-I)=BSCALE*(1+.1*I)
235         IF(IBSWRD+I.LE.512)BWDATA(IBSWRD+I)=BSCALE*(1+.1*I)
C
C ***************************************************************
C     THE CM-1 OF EACH BASELINE PT IS SENT TO FILE "BASLIN.DAT"
C ALONG WITH THE BG & SAMPLE INTENSITIES AT THIS CM-1.
C
            BFRQ(1)=(IBSWRD+WRDDIF)/PPWVN
            BASCNT=BASCNT+1
                YB(1)=BRDATA(IBSWRD)
                YS(1)=SRDATA(IBSWRD)
               WRITE(11,8400) BFRQ(1),YB(1),YS(1)
            IF (LASTPT.EQ.0)                         GO TO 241
            FRQMAX=-(WRDDIF+INDXEP)/PPWVN
            WRITE(11,8400) FRQMAX
                                                     GO TO 251
241         CONTINUE
251         CALL IWTISK(BWDATA,512,OZFSEC+M,INODE)
            CLOSE(11)
C
C ***************************************************************
C    THE SET OF BASELINE FREQUENCIES AND INTENSITIES PREVIOUSLY
C SENT TO FILE "BASLIN.DAT" ARE READ FROM THIS FILE, AND
C CUBIC SPLINE FITS ARE DONE ON SETS OF 4 CONSECUTIVE BASELINE
C PTS.  THE COEFFICIENTS DESCRIBING THE RANGE FROM PTS 2 TO 3
```

```
C ARE USED FOR BASELINE INTERPOLATION.  THEN, ARRAY INDICES 2-4
C ARE REINDEXED AS 1-3, A SEARCH IS MADE FOR THE NEXT BASELINE
C PT #4, AND ANOTHER CUBIC FIT IS PERFORMED, ETC.  FOR THE
C INITIAL AND FINAL SETS OF PTS, ADDITIONAL INTERPOLATIONS ARE
C DONE OUTSIDE OF THE USUAL 2-3 RANGE.
C    THE SAMPLE AND BACKGROUND SPECTRA ARE ADJUSTED SO THAT
C THEIR BASELINE PTS ARE EQUAL TO SSCALE AND BSCALE.  ALL OTHER
C PTS ARE ADJUSTED SO THAT (BASELINE-SIGNAL)/BASELINE REMAINS
C UNCHANGED FROM THE ORIGINAL SPECTRUM.
C
261           IF (BSCORR.EQ.0)                          GO TO 391
              WRITE(2,6700)
6700   FORMAT('0','BEGIN BASELINE CORRECTIONS')
              M=IISEC
              BASCNT=2
              CALL IRTISK(BRDATA,512,IBFSEC+IISEC,INODE)
              CALL IRTISK(SRDATA,512,ISFSEC+IISEC,INODE)
              IF (BSFIND.NE.0) READ(11,8300) BLKSIZ
              IF (BSFIND.NE.0) READ(11,8500) FRQMIN
              INDXSP=NINT(FRQMIN*PPWVN+1-(IISEC-1)*512)
              IMIN=INDXSP
      DO 271 I=1,4
271           READ(11,8400) BFRQ(I),YB(I),YS(I)
              WRDHI=NINT(BFRQ(1)*PPWVN+1-(IISEC-1)*512)
              WRDLOW=WRDHI
281           IMAX=512
              IF (IMAX.GT.WRDHI) IMAX=WRDHI
      DO 291 I=IMIN,IMAX
              BRDATA(I)=BSCALE*BRDATA(I)/YB(1)
291           SRDATA(I)=SSCALE*SRDATA(I)/YS(1)
              IF (IMAX.EQ.512)                          GO TO 381
301           IMIN=IMAX+1
311           IF (IQUIT-1)                          321,315,381
C
C CHANGE THE REF PT OF THE FINAL CUBIC EQN FROM PT 3 TO PT 4 FOR
C EXTRAPOLATION OF THE CUBIC FIT BEYOND THE FINAL BASELINE PT.
C
315           D=BFRQ(4)-BFRQ(3)
              CB(3,1)=3*CB(3,3)*D*D+2*CB(3,2)*D+CB(3,1)
              CS(3,1)=3*CS(3,3)*D*D+2*CS(3,2)*D+CS(3,1)
              CB(3,2)=0.0
              CS(3,2)=0.0
              IQUIT=IQUIT+1
C
321           BASCNT=BASCNT+1
              IF (BASCNT.EQ.4.OR.IQUIT.NE.0)            GO TO 351
              IF (BASCNT.EQ.3)                          GO TO 341
C
C THE (I+1)TH BASELINE INDEX FOR THE OLD BASELINE ARRAYS
C BECOMES THE ITH BASELINE INDEX FOR THE NEW ARRAYS.
C
      DO 331 I=1,3
              BFRQ(I)=BFRQ(I+1)
```

```
                YB(I)=  YB(I+1)
331             YS(I)=  YS(I+1)
              READ(11,8400) BFRQ(4),YB(4),YS(4)
              IF (BFRQ(4).LT.0.0) THEN
                  IQUIT=1
                  BFRQ(4)=-BFRQ(4)
                  ENDIF
341           IF (IQUIT.EQ.0) THEN
                 CALL SPLINE(1,4,BFRQ,YB,0.0,0.0,CB)
                 CALL SPLINE(1,4,BFRQ,YS,0.0,0.0,CS)
                 ENDIF
351           J=2+(IQUIT/2)-ISTART
              K=2+(IQUIT+1)/2-ISTART
              ISTART=0
              WRDLOW=WRDHI
              WRDHI=NINT(BFRQ(J+1)*PPWVN+1-(M-1)*512)
361           IMAX=512
              IF (IMAX.GT.WRDHI) IMAX=WRDHI
      DO 371 I=IMIN,IMAX
              XD=(I-WRDLOW)/PPWVN
              BGBASE=YB(J)+CB(K,1)*XD+CB(K,2)*XD*XD+CB(K,3)*XD**3
              SMBASE=YS(J)+CS(K,1)*XD+CS(K,2)*XD*XD+CS(K,3)*XD**3
              BRDATA(I)=BSCALE*BRDATA(I)/BGBASE
371           SRDATA(I)=SSCALE*SRDATA(I)/SMBASE
              IF (IMAX.NE.512)                              GO TO 301
381           CALL IWTISK(BRDATA,512,OBFSEC+M,INODE)
              CALL IWTISK(SRDATA,512,OSFSEC+M,INODE)
              M=M+1
              IF (M.GT.IFSEC)                               GO TO 391
              CALL IRTISK(BRDATA,512,IBFSEC+M,INODE)
              CALL IRTISK(SRDATA,512,ISFSEC+M,INODE)
              IMIN=1
              WRDLOW=WRDLOW-512
              WRDHI=WRDHI-512
              IF (WRDHI.EQ.0)                                GO TO 311
              IF (ISTART)                                  1999,361,281
C
C LEAVE PROGRAM IF NO VAPOR CORRECTIONS ARE TO BE MADE:
391           IF (VAPOPT.EQ.0)                               GO TO 1999
C
C*****************************************************************
C*************   BEGIN VAPOR CORRECTIONS     ********************
C
C THICK MATRIX DEPOSITS CAN CAUSE THE SAMPLE SPECTRUM TO SHIFT
C RELATIVE TO THE BACKGROUND SPECTRUM.  THIS SHIFT IS
C PROPORTIONAL TO FREQUENCY AND CAN BE DETERMINED BY EXAMINING
C WATER VAPOR PEAKS.
C
              WRITE(2,9100)
9100  FORMAT('0','BEGIN VAPOR CORRECTIONS')
C
C IF THE INPUT AND OUTPUT FILES FOR VAPOR CORRECTIONS ARE NOT
C THE SAME (I.E. IF BASELINE CORRECTIONS WERE SKIPPED), COPY
```

```
C THE UNCORRECTED INPUT DATA INTO THE OUTPUT FILES:
C
            IF (BSCORR.EQ.0) THEN
      DO 395        M=IISEC,IFSEC
                    CALL IRTISK(BRDATA,512,IBFSEC+M,INODE)
                    CALL IRTISK(SRDATA,512,ISFSEC+M,INODE)
                    CALL IWTISK(BRDATA,512,OBFSEC+M,INODE)
395                 CALL IWTISK(SRDATA,512,OSFSEC+M,INODE)
                    ENDIF
C
      DO 489 IVAP=1,4
            IF (ISHIFT.EQ.0) F=0.0
C
C      FOR EACH VAPOR REFERENCE PEAK CM-1 (VPWVN), PUT THE PEAK
C POINT AND THE TWO POINTS ON EITHER SIDE OF THE PEAK INTO THE
C SVPK, BVPK, AND RVPK ARRAYS.  ALSO, PUT THE LOCAL BASELINES
C INTO THE SBAS, BBAS, AND RBAS ARRAYS.  REPEAT THE CALCULATION
C FOR EACH VAPOR BAND (IVAP=1 IS H2O-V2, IVAP=2 IS H2O-V3,
C IVAP=3 IS CO2-V2, AND IVAP=4 IS CO2-V3).
C
            CALL VAPREF(IVAP,NVP,VPWVN,BVPK,SVPK,RVPK,BBAS,
     1                  SBAS,RBAS)
      DO 485 J=1,2
            IF (IVAP.GT.2.AND.J.EQ.2)               GO TO 485
      DO 481 I=1,2
            PCTOL=I*PCTOL
C
C   DETERMINE THE VAPOR CM-1 CALIBRATION ERROR (BG-SM) FOR EACH
C VAPOR BAND.  IF A REFERENCE PURE VAPOR SPECTRUM IS AVAILABLE
C (J=2), CALCULATE THE RF-BG CALIBRATION ERROR ALSO:
C
            IF (ISHIFT.NE.0.AND.J.EQ.1)
     1          CALL VAPSHF(IVAP,NVP,BVPK,SVPK,F,N)
            IF (ISHIFT.NE.0.AND.J.EQ.2)
     1          CALL VAPSHF(IVAP,NVP,RVPK,BVPK,F,N)
            WSHIFT(IVAP,J)=F
C
C      CALCULATE THE (SAMPLE ABSORBANCE / BG ABSORBANCE) RATIO
C FOR THE GIVEN BAND.  IF A REFERENCE PURE VAPOR SPECTRUM IS
C AVAILABLE, COMPUTE ABSORBANCE(REF)/ABSORBANCE(BG) ALSO.
C
            IF (J.EQ.1) CALL VAPRAT(IVAP,J,NVP,SVPK,BVPK,SBAS,
     1                              BBAS,F,VRAT,NR)
            IF (J.EQ.2) CALL VAPRAT(IVAP,J,NVP,BVPK,RVPK,BBAS,
     1                              RBAS,F,VRAT,NR)
            IF (NR(IVAP,J).GT.0.OR.ISHIFT.EQ.0)     GO TO 483
481         CONTINUE
483       WRITE(2,9200) NR(IVAP,J),NVP(IVAP),VAPNAM(IVAP),PCTOL
485         CONTINUE
            IF (IVAP.EQ.1.OR.IVAP.EQ.3)             GO TO 489
C
C   IF THE VAPOR-RATIO DETERMINATION FAILS FOR 1 OF 2 BANDS OF 1
C MOLECULE, SET BOTH RATIOS EQUAL TO THAT OF THE 1 GOOD BAND.
```

```
C IN THE EVENT OF TOTAL FAILURE, SET BOTH RATIOS TO UNITY.
C
      DO 487 J=1,2
             IF (IVAP.NE.2.AND.J.EQ.2)                GO TO 487
             IF (NR(IVAP,J).EQ.0.AND.NR(IVAP-1,J).EQ.0) THEN
                VRAT(IVAP,J)   =1.0
                VRAT(IVAP-1,J) =1.0
               ELSEIF (NR(IVAP,J).EQ.0) THEN
                VRAT(IVAP,J)   =VRAT(IVAP-1,J)
               ELSEIF (NR(IVAP-1,J).EQ.0) THEN
                VRAT(IVAP-1,J) =VRAT(IVAP,J)
                ENDIF
487          CONTINUE
489          CONTINUE
      DO 491 I=1,4
491          BFRQ(I)=-WSHIFT(I,1)/PPWVN
             WRITE(2,9600) BFRQ(1),BFRQ(2),BFRQ(3),BFRQ(4)
            WRITE(2,9700)VRAT(1,1),VRAT(2,1),VRAT(3,1),VRAT(4,1)
C
C IDENTIFY THE FIRST AND LAST SECTORS FOR EACH VAPOR BAND:
C
       DO 511 I=1,8
511           ILIM(I)=PPWVN*VRANGE(I)/512+1
C
C ***************************************************************
C ***************************************************************
C      USE THE PREVIOUSLY CALCULATED VAPOR ABSORBANCE RATIOS
C & VAPOR CALIBRATION ERRORS TO CORRECT THE BG & SAMPLE SPECTRA.
C
      DO 799 IVAP=1,4
             IF (IVAP.EQ.1.AND.WATOPT.EQ.0)           GO TO 799
             IF (IVAP.EQ.2.AND.WATOPT.NE.2)           GO TO 799
             IF (IVAP.GE.3.AND.CO2OPT.EQ.0)           GO TO 799
             IF (IVAP.EQ.3.AND.CO2OPT.EQ.1.AND.
     1           ICSEC(1,1).LT.IISEC)                 GO TO 799
                                        IRFSEC=OBFSEC
             IF (IVAP.LT.3.AND.IVFN.GT.0) IRFSEC=IVFSEC
             IF (IVAP.GE.3) VRAT(IVAP,2)=1.
             EXP=VRAT(IVAP,2)*(VRAT(IVAP,1)-1)
             ISP=1
             IF (WSHIFT(IVAP,1)*WSHIFT(IVAP,2).LT.0) ISP=2
             IF (WSHIFT(IVAP,1).LT.0) IDIR=-1
             IF (WSHIFT(IVAP,1).GE.0) IDIR=1
             MI=ILIM(2*IVAP-(IDIR+1)/2)
             MF=ILIM(2*IVAP+(IDIR-1)/2)
      DO 791 M=MI,MF,IDIR
             CALL IRTISK(BRDATA,512,OBFSEC+M,INODE)
             CALL IRTISK( IDATA,512,IRFSEC+M,INODE)
          IF(ISHIFT.EQ.1.)CALL IRTISK(SRDATA,512,OSFSEC+M,INODE)
C
             IF (M.EQ.IISEC.AND.INDXSP.GT.1) THEN
      DO 705         I=1,INDXSP-1
705                  SWDATA(I)=NX
```

```
                ELSEIF (M.EQ.IFSEC.AND.INDXEP.LT.512) THEN
      DO 711    -     I=INDXEP+1,512
711                   SWDATA(I)=NX
                      ENDIF
C
            IF (ISHIFT.EQ.0)                                  GO TO 739
C  ***********************************************************
C
C    SHIFT THE SAMPLE SPECTRUM TO COMPENSATE FOR THE CALIBRATION
C ERROR DETERMINED EARLIER.  THE SIGN OF THE SAMPLE INTENSITY
C CORRECTION IS ALWAYS:
C
C  -(SIGN OF THE SLOPE OF FREQ VS INTENSITY)*(SIGN OF BFRQ-SFRQ)
C
C WHEN THE SHIFT IS +, THE I AND I-1 POINTS ARE USED TO COMPUTE
C THE SLOPE.  OTHERWISE, THE I AND I+1 POINTS ARE USED.
C
            IF (WSHIFT(IVAP,1).LT.0) THEN
                  IL=1
                  IU=511
                  K=512
               ELSE
                  IL=2
                  IU=512
                  K=1
                  ENDIF
            IF (M.EQ.IISEC) IL=IL+INDXSP-1
            IF (M.EQ.IFSEC) IU=INDXEP
            IF (M.EQ.MI)                                      GO TO 715
C
C SHIFT THE PT ADJACENT TO THE SECTOR BOUNDARY:
C
                           SWDATA(K)= SRDATA(K)+
     1                        IDIR*WSHIFT(IVAP,1)*(S-SRDATA(K))
            IF (ISP.EQ.2) ODATA(K)=  IDATA(K)+
     1                        IDIR*WSHIFT(IVAP,2)*(BR-IDATA(K))
            IF (ISP.EQ.1) ODATA(K)=  BRDATA(K)+
     1                        IDIR*WSHIFT(IVAP,2)*(BR-BRDATA(K))
C
C SHIFT THE REST OF THE DATA:
C
715   DO 721 I=IL,IU
721         SWDATA(I)=SRDATA(I)+IDIR*(SRDATA(I-IDIR)-SRDATA(I))
     1                                          *WSHIFT(IVAP,1)
C
C SHIFT THE BG OR THE REF DATA, DEPENDING ON WHICH SHIFT HAS
C THE SAME SIGN AS THE SHIFT OF BG VS SAMPLE.
C
            IF (ISP.EQ.2) THEN
      DO 725        I=IL,IU
725                 ODATA(I)=IDATA(I)+IDIR*(IDATA(I-IDIR)-
     1                      IDATA(I))*WSHIFT(IVAP,2)
               ELSE
```

```
      DO 731       I=IL,IU
731               ODATA(I)=BRDATA(I)+IDIR*(BRDATA(I-IDIR)-
     1                         BRDATA(I))*WSHIFT(IVAP,2)
                ENDIF
C
C SAVE THE PT NEXT TO THE SECTOR BOUNDARY FOR LATER USE:
C
                            S=  SRDATA(513-K)
              IF (ISP.EQ.2) BR= IDATA (513-K)
              IF (ISP.EQ.1) BR= BRDATA(513-K)
C
C THE FOLLOWING STEPS MATCH THE BG VAPOR PEAK ABSORBANCES TO THE
C SAMPLE ABSORBANCES.  THIS MATCHING IS DONE WITH RESPECT TO A
C SECONDARY BASELINE WHICH HAS A HIGHER DENSITY OF BASELINE PTS
C THAN THE PRIMARY BASELINE.
C "BSLINE" AND "IDATA(I)" APPLY TO EITHER THE VAPOR REFERENCE
C SPECTRUM OR THE BACKGROUND SPECTRUM DEPENDING ON WHETHER A
C REFERENCE SPECTRUM HAS BEEN SPECIFIED.
C
739                  IL=1
                     IU=512
              IF (IVAP.EQ.3.AND.CO2OPT.EQ.1) THEN
                     IL=IC(1,1)
                     IU=IC(1,2)
                ELSEIF (M.EQ.IISEC) THEN
                     IL=INDXSP
                ELSEIF (M.EQ.IFSEC) THEN
                     IU=INDXEP
                     ENDIF
C
              IF (IL.LT.1.OR.IL.GT.512)                GO TO 761
              IZ=BGBLSZ*((IL-1)/BGBLSZ)
      DO 755 J=1+(IL-1)/BGBLSZ, 1+(IU-1)/BGBLSZ
              ILOW =IZ+BGBLSZ*(J-1)+1
              IHIGH=IZ+BGBLSZ*J
              IF (IL.GT.ILOW)  ILOW =IL
              IF (IU.LT.IHIGH) IHIGH=IU
              BSLINE=0
      DO 741  I=ILOW,IHIGH
              IF (IDATA(I).LE.0)                       GO TO 755
741           IF (IDATA(I).GT.BSLINE) BSLINE=IDATA(I)
C
              IF (ISP.EQ.1) THEN
      DO 751     I=ILOW,IHIGH
751               BRDATA(I)=ODATA(I)*(1.*IDATA(I)/BSLINE)**EXP
                ELSE
      DO 753     I=ILOW,IHIGH
753               BRDATA(I)=BRDATA(I)*(1.*ODATA(I)/BSLINE)**EXP
                  ENDIF
755           CONTINUE
C
761         IF(ISHIFT.NE.0)CALL IWTISK(SWDATA,512,OSFSEC+M,INODE)
785           CALL IWTISK(BRDATA,512,OBFSEC+M,INODE)
```

```
791          CONTINUE
799          CONTINUE
             IF (IBLOPT.EQ.0)                              GO TO 1999
C ************************************************************
C
C    POINTS IN THE SINGLE-BEAM SPECTRA WHERE THE VAPOR IS
C STRONGEST ARE REPLACED VIA INTERPOLATION.  THIS METHOD IS
C APPLIED TO THE WATER BANDS AND THE V3(PR) BAND OF CO2:
C
C INITIALIZE THE BLANKING-INDICATOR FILE IF BLANKING OPTION =YES
C
      DO 801 J=1,512
801          BRDATA(J)=NX
      DO 805 M=IISEC,IFSEC
805          CALL IWTISK(BRDATA,512,0XFSEC+M,INODE)
             IF (CO2OPT.EQ.0.OR.Q23CO2.EQ.0)          GO TO 823
C
823   DO 999 IVAP=1,3
             IF (IVAP.EQ.1.AND.WATOPT.EQ.0)           GO TO 999
             IF (IVAP.EQ.2.AND.WATOPT.NE.2)           GO TO 999
             IF (IVAP.EQ.3.AND.PR2CO2.EQ.0)           GO TO 999
             ISEC=ILIM(2*IVAP-1)
             LSEC=ILIM(2*IVAP)
             IWR=0
             RESUME=0
             ISAMP=0
             LSTVAP=NX
             IVAP0=0
             IWRSEC=ISEC
             ISTART=3
C
C    'XINTRP' IS AN ARRAY OF 4 INDICES WHICH IS USED FOR EITHER
C LINEAR OR CUBIC SPLINE INTERPOLATION.  INTERPOLATIONS ARE
C ALWAYS DONE BETWEEN POINTS 2 AND 3.  THE OTHER 2 POINTS ARE
C NEEDED FOR CUBIC INTERPOLATION ONLY.  THE SECOND DERIVATIVES
C AT PTS 1 AND 4 ARE FIXED AT 0 FOR THE CUBIC INTERPOLATIONS.
C    'ISTART' IS THE INITIAL DATA ARRAY INDEX USED IN SEARCHING
C FOR THE 3RD INTERPOLATION PT.  IT IS SUPERCEDED FOR THE
C INITIAL SECTOR IF THIS SECTOR CONTAINS BLANKED PTS, AND FOR
C THE V2 BAND OF CO2 WHEN THE BLANKING OPTION IS CHOSEN FOR THE
C Q BRANCH BUT NOT THE P AND R BRANCHES.
C
             IF (ISEC.NE.IISEC) THEN
                   XINTRP(1)=1.0
                   XINTRP(2)=2.0
                ELSE
                   XINTRP(1)=INDXSP
                   XINTRP(2)=INDXSP+1.0
                   ENDIF
C
825   DO 991 M=ISEC,LSEC
             LL=1
             LU=512
```

```
            IF (M.EQ.IISEC) LL=INDXSP
            IF (M.EQ.IFSEC) LU=INDXEP
            I=ISTART
            IF (M.EQ.IISEC.AND.LL.GT.ISTART) I=LL
            CALL IRTISK(BRDATA,512,OBFSEC+M,INODE)
            CALL IRTISK(SRDATA,512,OSFSEC+M,INODE)
      DO 827 J=1,512
827         IDATA(J)=NX
C
C LOCATE ALL BACKGROUND BASELINE PTS IN THE CURRENT SECTOR:
C
      DO 831 J=1,512/BGBLSZ
            ILOW =BGBLSZ*(J-1)+1
            IHIGH=BGBLSZ*J
            BBAS(J)=0
      DO 829 K=ILOW,IHIGH
829         IF(BRDATA(K).GT.BBAS(J)) BBAS(J)=BRDATA(K)
831         CONTINUE
C
C     A NONZERO 'RESUME' INDICATES WHERE THE SEARCH FOR
C INTERPOLATION PTS WAS HALTED DUE TO AN END-OF-SECTOR FLAG.
C
            IF(RESUME.EQ.3)                          GO TO 885
            IF(RESUME.EQ.4)                          GO TO 901
            IF(ISTART.EQ.1)                          GO TO 841
            ISTART=1
C
C INITIALIZE THE OUTPUT ARRAYS:
C
       DO 835 J=1,512
            ODATA(J)=IDATA(J)
            BWDATA(J)=BRDATA(J)
835         SWDATA(J)=SRDATA(J)
C
C ***************************************************************
C
C        USING THE LOCAL BASELINE ARRAY "BBAS", COMPUTE THE
C "1-BEAM TRANSMITTANCE" (BGTRAN) OF THE BACKGROUND VAPOR PT,
C AND COMPARE IT TO THE ARBITRARY MINIMUM BLANKING TRANSMITTANCE
C (VAPCUT).  IF VAPOR SIGNAL IS FOUND, GO TO LINE 861 AND
C INCREASE EITHER THE PURE VAPOR COUNTER (IVAP0) OR THE
C CONSECUTIVE SAMPLE+VAPOR COUNTER (ISAMP).  IF NOT, EITHER
C RESET THE INTERPOLATION INDICES OR SEARCH FOR THE 4TH
C INTERPOLATION PT DEPENDING ON WHETHER BOTH VAPOR COUNTERS ARE
C ZERO OR ONE IS NONZERO, RESPECTIVELY.
C
841         BGTRAN=1.*BRDATA(I)/BBAS(1+(I-1)/BGBLSZ)
            IF(BGTRAN.LT.VAPCUT)                     GO TO 861
            IF (ISAMP.NE.0.OR.IVAP0.NE.0)            GO TO 891
            XINTRP(1)=XINTRP(2)
            XINTRP(2)=XINTRP(2)+1.0
845         IF (NINT(XINTRP(1)).GE.1.AND.IWR.EQ.1)
     1          CALL SBBOUT(BWDATA,SWDATA,ODATA)
```

```
                I=I+1
                IF (I.LE.LU)                                    GO TO 841
                                                                GO TO 981
C ***************************************************************
C
C LINE LABEL 861 IS EXECUTED ONLY AFTER A VAPOR PEAK HAS BEEN
C FOUND.  LINES 861 TO 891 ARE USED TO DETERMINE XINTRP(3).
C
C CHECK WHETHER THE POINT WHICH HAS BEEN MARKED FOR POSSIBLE
C BLANKING HAS A SIGNIFICANT (> SIGMIN) SAMPLE SIGNAL COMPONENT.
C IF SO, COUNT THE NUMBER OF CONSECUTIVE POINTS (ISAMP) WHICH
C HAVE BOTH SIGNAL AND VAPOR.  AS SOON AS A SPECIFIED COUNTING
C LIMIT (MXBLNK) IS REACHED, PICK OUT THE POINT IN THE SET
C WHICH HAS THE LEAST VAPOR SIGNAL, AND RETAIN IT AS
C INTERPOLATION POINT #3.
C      FOR PTS WHICH HAVE BOTH SIGNAL AND VAPOR, USE 'ILSTVP'
C AND 'LSTVAP' TO KEEP TRACK OF WHICH POINT IN A GIVEN SET HAS
C THE LEAST VAPOR SIGNAL.
C     IF SAMPLE+VAPOR IS ENCOUNTERED AFTER 2 OR MORE PURE VAPOR
C POINTS HAVE BEEN COUNTED (IVAP0), USE THE LAST PURE VAPOR
C POINT FOR INTERPOLATION.
C
861     IF (SRDATA(I)/(SCALE*BRDATA(I)).GT.SIGMIN)      GO TO 875
             ISAMP=ISAMP+1
             IF(BRDATA(I).GE.LSTVAP) THEN
                ILSTVP=I
                LSTVAP=BRDATA(I)
                ENDIF
             IF (ISAMP.LT.MXBLNK)                       GO TO 881
             IF (NINT(XINTRP(2))+1.EQ.ILSTVP)           GO TO 871
C
             IF (IVAP0.GE.2) THEN
                   I=I-MXBLNK
                   XINTRP(3)=I*1.0
                ELSE
                   ICUBIC=1
                   XINTRP(3)=ILSTVP*1.0
                ENDIF
                                                        GO TO 891
C
C IF POINTS 2 AND 3 OF THE XINTRP ARRAY ARE ONLY 1 UNIT APART,
C RESET INTERPOLATION INDICES AND LOOK FOR ANOTHER XINTRP(3)
C VALUE.
C
871          XINTRP(1)=XINTRP(2)
             XINTRP(2)=ILSTVP*1.0
             I=I+1
             LSTVAP=NX
             ISAMP=0
             IF (NINT(XINTRP(1)).GE.1.AND.IWR.EQ.1)
     1           CALL SBBOUT(BWDATA,SWDATA,ODATA)
                                                        GO TO 861
C
```

```
C RESET COUNTERS TO INDICATE A PURE VAPOR PT HAS BEEN FOUND
C
875           ISAMP=0
              LSTVAP=NX
              IVAP0=IVAP0+1
C
C INCREMENT THE DATA ARRAY INDEX AND CONTINUE THE SEARCH FOR
C INTERPOLATION PT 3 AT LINE 841.
C
881           I=I+1
              IF (I.GT.LU) RESUME=3
              IF (I.GT.LU)                                    GO TO 981
885           XINTRP(3)=I*1.0
              RESUME=0
                                                              GO TO 841
C ***************************************************************
C
C LOCATE XINTRP(4) IF CUBIC INTERPOLATION IS TO BE APPLIED.
C THIS CASE OCCURS WHENEVER THE INTERPOLATION COVERS A RANGE
C THAT HAS NO CONSECUTIVE PURE VAPOR PTS.  XINTRP(4) IS THE 1ST
C PT ENCOUNTERED THAT IS EITHER VAPOR-FREE OR HAS SAMPLE SIGNAL.
C
891           ISAMP=0
              IVAP0=0
              LSTVAP=NX
              IF (ICUBIC.EQ.0)                                GO TO 915
              RESUME=4
895           I=I+1
              IF (I.GT.LU)                                    GO TO 981
901           XINTRP(4)=I*1.0
        IF (SRDATA(I)/(SCALE*BRDATA(I)).LE.SIGMIN)            GO TO 909
C
              BGTRAN=1.*BRDATA(I)/BBAS(1+(I-1)/BGBLSZ)
              IF (BGTRAN.LT.VAPCUT)                           GO TO 895
C
C ***************************************************************
909           NXTCUB=1
911           ISAMP=0
              LSTVAP=NX
C
C USE INTERPOLATION ON BOTH THE SAMPLE (ISPEC=1) AND
C BACKGROUND (ISPEC=2) FILES FOR THE CURRENT XINTRP ARRAY:
C
915           RESUME=0
      DO 961 ISPEC=1,2
              ICASE=0
      DO 921 J=1,3
921           IF(NINT(XINTRP(J)).LT.1) ICASE=ICASE+1
              IF(ICASE.EQ.0)                                  GO TO 931
      DO 925 J=1,ICASE
              Y(J)=SWDATA(NINT(XINTRP(J))+512)
925           IF(ISPEC.EQ.2) Y(J)=BWDATA(NINT(XINTRP(J))+512)
931   DO 935 J=ICASE+1,3+ICUBIC
```

```
            Y(J)=SRDATA(NINT(XINTRP(J)))
935         IF(ISPEC.EQ.2) Y(J)=BRDATA(NINT(XINTRP(J)))
      DO 941 J=1,3
941         DEL(J)=XINTRP(J+1)-XINTRP(J)
C
C ***************************************************************
C USE LINEAR INTERPOLATION IN MOST CASES:
C
            IF (INT(DEL(2)).GT.5.OR.ICUBIC.NE.1) THEN
                CSC(2,1)=(Y(3)-Y(2))/DEL(2)
                CSC(2,2)=0.0
                CSC(2,3)=0.0
                ENDIF
C
C USE CUBIC SPLINE INTERPOLATION WHERE VAPOR PEAKS COINCIDE
C WITH SAMPLE PEAKS AND THE INTERPOLATION RANGE IS SHORT:
C
            IF (INT(DEL(2)).LE.5.AND.ICUBIC.EQ.1)                    -
     1          CALL SPLINE(1,4,XINTRP,Y,0.0,0.0,CSC)
C
C ***************************************************************
            II=XINTRP(2)+1.0
            IL=XINTRP(3)-1.0
            XI=0.0
C
      DO 955 J=II,IL
            XI=XI+1.0
          YY=CSC(2,3)*XI*XI*XI+CSC(2,2)*XI*XI+CSC(2,1)*XI+Y(2)
            JI=J+512*IWR
            K=NINT(XINTRP(1))
C
C SAMPLE CORRECTIONS ARE SENT TO SWDATA UNLESS A FULL SET OF
C PREVIOUS CORRECTIONS HAVE BEEN MADE ON SWDATA AND HAVE NOT
C YET BEEN SENT TO DISK. IN THE LATTER CASE, THE CORRECTIONS
C ARE SENT TO THE INPUT ARRAY SRDATA.  THE BLANKING-INDICATOR
C ARRAYS, IDATA AND ODATA, ARE HANDLED ANALAGOUSLY.
C
            IF (ISPEC.EQ.1.AND.J.GT.0.AND.K.LT.1) THEN
                SRDATA(J)=YY
                IDATA(J)=BSCALE
              ELSEIF (ISPEC.EQ.1.AND.(J.LE.0.OR.K.GE.1)) THEN
                SWDATA(JI)=YY
                ODATA(JI)=BSCALE
              ELSEIF (ISPEC.EQ.2.AND.J.GT.0.AND.K.LT.1) THEN
                BRDATA(J)=YY
              ELSE
                BWDATA(JI)=YY
              ENDIF
955         CONTINUE
961         CONTINUE
C
            IF (ICUBIC.NE.0)                          GO TO 965
            XINTRP(1)=XINTRP(2)
```

```
            XINTRP(2)=XINTRP(3)
                                                        GO TO 845
965         ICUBIC=NXTCUB
            NXTCUB=0
C ***************************************************************
C
C   IF THE LAST 2 INTERPOLATION INDICES ARE 1 UNIT APART, RESET
C THE 1ST 2 INTERPOLATION INDICES AT THESE LAST 2 POINTS AND
C RESTART THE SEARCH FOR INTERPOLATION POINT 3.
C      OTHERWISE, SHIFT INDICES AT LINE LABEL 940 AND, AFTER
C POSSIBLE DISK WRITING, START LOOKING FOR XINTRP(4).
C
            IF (INT(DEL(3)).EQ.1)                       GO TO 975
      DO 971 J=1,3
971         XINTRP(J)=XINTRP(J+1)
            IF (NINT(XINTRP(1)).GE.1.AND.IWR.EQ.1)
     1          CALL SBBOUT(BWDATA,SWDATA,ODATA)
                                                        GO TO 891
975         XINTRP(1)=XINTRP(3)
            XINTRP(2)=XINTRP(4)
                                                        GO TO 845
C
C ***************************************************************
C LINE LABEL 981 IS EXECUTED ONLY AFTER THE END OF A SECTOR HAS
C BEEN REACHED:
C
981    DO 985 J=1,3
985         XINTRP(J)=XINTRP(J)-512.0
            IWR=1
991         CONTINUE
C
C ***************************************************************
C SEND THE LAST SECTOR OF THE CURRENT VAPOR REGION TO DISK:
C
995         CALL SBBOUT(BWDATA,SWDATA,ODATA)
999         CONTINUE
C
C BLANK THE V2(Q) AND V3(PQR) BANDS OF CO2 BY SETTING SETTING
C ALL SAMPLE WORDS EQUAL TO -524288:
C
            IF (Q23CO2.EQ.0)                        GO TO 1999
      DO 1031 I=1,2
            IF (ICSEC(I,1).LT.IISEC)                GO TO 1031
            IMIN=IC(I,1)
            IMAX=512
      DO 1021 M=ICSEC(I,1),ICSEC(I,2)
            IZ=IMIN+512*(ICSEC(I,1)-M)
            CALL IRTISK(SRDATA,512,OSFSEC+M,INODE)
            IF (M.EQ.ICSEC(I,2)) IMAX=IC(I,2)
      DO 1011 J=IMIN,IMAX
1011        SRDATA(J)=NX
            IMIN=1
1021        CALL IWTISK(SRDATA,512,OSFSEC+M,INODE)
```

```
1031          CONTINUE
C
C ***************************************************************
8300          FORMAT(I10)
8400          FORMAT(F10.3,2F10.0)
8500          FORMAT(3F10.3)
9200  FORMAT('0',I2,' OF ',I2,1X,A6,' PKS PASSED TOLERANCE
     1 SPECIFICATION OF',F4.1,' PERCENT')
9300  FORMAT('0',I2,' OF ',I2,' H20(V3) PKS PASSED TOLERANCE
     1 SPECIFICATION OF',F4.1,' PERCENT')
9600  FORMAT(' ','SAMPLE VS BG CM-1 FOR H2O(V2,V3) & CO2(V2,V3)
     1: ',4F6.3)
9700  FORMAT(' ','FINAL S/B VAPOR RATIOS FOR H2O(V2,V3) & CO2
     1(V2,V3): ',4F7.3)
9800  FORMAT('0',I2,' OF ',I2,' CO2(V2) PKS PASSED TOLERANCE
     1 SPECIFICATION OF',F4.1,' PERCENT')
9900  FORMAT('0',I2,' OF ',I2,' CO2(V3) PKS PASSED TOLERANCE
     1 SPECIFICATION OF',F4.1,' PERCENT')
1999          CALL EXIT
              END
```

```
      SUBROUTINE VAPRAT(IVAP,IR,NVP,IN,ID,BN,BD,FRACPT,VRAT,NR)
      REAL IN(30),ID(30),BN(10),BD(10)
      DIMENSION RAT(30),NVP(4),VRAT(4,2),NR(4,2)
      COMMON /VAPRAT/ PCTOL
C
C THIS SUBROUTINE DETERMINES AN AVERAGE ABSORBANCE RATIO (VRAT)
C BETWEEN CORRESPONDING VAPOR PEAKS IN TWO 1-BEAM SPECTRA. IT
C IS CALLED BY 'SBBLN.FOR'.
C
C INPUT:
C
C   IVAP   = BAND ID #.
C   IR     = RATIO TYPE (1= S/B, 2= B/R)
C   NVP    = # OF INPUT REFERENCE PEAKS FOR THE VAPOR BAND.
C   IN(I)  = INTENSITIES OF PEAKS IN THE NUMERATOR  SPECTRUM.
C   ID(I)  =     "       "   "     "  " DENOMINATOR   "    .
C   BN(I)  = BASELINE INTENSITY AT PEAK I FOR THE IN(I) DATA.
C   BD(I)  =    "          "     "   "   "  "   "  ID(I)   " .
C   FRACPT= CALIBRATION ERROR (DENOMINATOR WORD MINUS NUMERATOR
C           WORD); I.E. IF THE DENOMINATOR SPECTRUM IS SHIFTED
C           IN THE - CM-1 DIRECTION WITH RESPECT TO THE
C           NUMERATOR SPECTRUM, FRACPT WILL BE NEGATIVE.
C
C OUTPUT:
C
C   VRAT   = ABSORBANCE RATIO.
C   NR     = # OF PEAKS WHICH SATISFIED THE ABSORBANCE RATIO
C            TOLERANCE "PCTOL" AND WERE USED TO DERIVE "VRAT".
C ***************************************************************
C
C   EACH OF THE ARRAYS (IN,ID,BN,BD) IS COMPRISED OF 3-WORD
C SUBSETS.  THE SUBSETS CONTAIN THE INTENSITY AT THE REF CM-1
C AND THE INTENSITIES OF THE NEAREST PRECEDING & FOLLOWING PTS.
C
            NPTS=3*NVP(IVAP)
      DO 101 K=1,NPTS
            IP=0
            IF (3*((K+1)/3).EQ.K+1.AND.FRACPT.GT.0) IP=1
            JM=(K+2)/3
            J=K/3+JM*2+IP
            TD=(ID(K)+(ID(J)-ID(J-1))*FRACPT)/BD(JM)
            TN=IN(K)/(BN(JM)*1.0)
101         RAT(K)=LOG(TN)/LOG(TD)
            N=0
            SUM=0.0
      DO 201 J=1,NVP(IVAP)
            I1=3*(J-1)+1
            I2=I1+1
            I3=I2+1
            AV=(RAT(I1)+RAT(I3))/2
            DEV=ABS(RAT(I1)-AV)+ABS(RAT(I3)-AV)
            AVGDEV=DEV/2
            TOL=0.01*AV*PCTOL
```

```
            IF (RAT(I3).GT.RAT(I2).AND.RAT(I1).GT.RAT(I2))
     1        TOL=0.02*AV*PCTOL
            IF (RAT(I3).LT.RAT(I2).AND.RAT(I1).LT.RAT(I2))
     1        TOL=0.02*AV*PCTOL
            IF (AVGDEV.GE.TOL)                          GO TO 201
            SUM=SUM+AV
            N=N+1
201         CONTINUE
            IF (N.NE.0) VRAT(IVAP,IR)=SUM/N
            IF (N.EQ.0) VRAT(IVAP,IR)=1.
            NR(IVAP,IR)=N
            RETURN
            END
```

```
      SUBROUTINE SBBOUT(BWDATA,SWDATA,ODATA)
      INTEGER BWDATA(512),SWDATA(512),SRDATA(512),BRDATA(512),
     1        IDATA(512),ODATA(512),OBFSEC,OSFSEC,OXFSEC,BGBLSZ
      COMMON /IO/   IVFSEC,OBFSEC,OSFSEC,OXFSEC,IWRSEC,INODE,
     1              IWR,LSEC,BGBLSZ,PPWVN,BRDATA,SRDATA,IDATA
C
            CALL IWTISK(BWDATA,512,OBFSEC+IWRSEC,INODE)
            CALL IWTISK(SWDATA,512,OSFSEC+IWRSEC,INODE)
            CALL IWTISK(SRDATA,512,OXFSEC+IWRSEC,INODE)
            IF (IWRSEC.EQ.LSEC)                         GO TO 999
      DO 101 J=1,512
            ODATA(J)=IDATA(J)
            BWDATA(J)=BRDATA(J)
101         SWDATA(J)=SRDATA(J)
            IWRSEC=IWRSEC+1
999         IWR=0
            RETURN
            END
```

```
      SUBROUTINE VAPREF(IVAP,NVP,VPWVN,BVPK,SVPK,RVPK,BBASE,
     1                  SBASE,RBASE)
      COMMON /IO/    IVFSEC,OBFSEC,OSFSEC,OXFSEC,IWRSEC,INODE,
     1               IWR,LSEC,BGBLSZ,PPWVN,BRDATA,SRDATA,IDATA
      INTEGER BRDATA(512),SRDATA(512),IDATA(512),NVP(4),OLDSEC,
     1        OBFSEC,OSFSEC,BGBLSZ,OXFSEC
      DIMENSION VPWVN(4,10),BVPK(30),SVPK(30),RVPK(30),BBASE(10)
     1          ,SBASE(10),RBASE(10)
C
C THIS SUBROUTINE GENERATES INTENSITY ARRAYS FROM INPUT WAVE-
C NUMBERS OF VAPOR REFERENCE PEAKS.  IT IS CALLED BY "SBBLN.FOR"
C
C ************************  INPUT  ******************************
C   IVAP     = BAND ID #
C   NVP(IVAP)= # OF INPUT REFERENCE PEAKS FOR THE VAPOR BAND.
C   VPWVN    = WAVENUMBERS OF THE INPUT VAPOR PEAKS.
C
C ************************  OUTPUT  *****************************
C   BVPK  : INTENSITY ARRAYS (BG, SAMPLE, AND REFERENCE,
C   SVPK  : RESPECTIVELY) COMPRISED OF 3-WORD SUBSETS. THE
C   RVPK  : SUBSETS CONTAIN THE INTENSITY AT THE REF CM-1 & THE
C           INTENSITIES OF THE NEAREST PRECEDING & FOLLOWING PTS
C   BBASE:  BASELINE INTENSITIES (BG, SAMPLE, AND REFERENCE)
C   SBASE   AT THE REFERENCE WAVENUMBERS.
C   RBASE
C ***********************************************************
      DO 301 I=1,NVP(IVAP)
             IWORD=1+PPWVN*VPWVN(IVAP,I)
             IVPSEC=IWORD/512+1
             IPK=IWORD+(1-IVPSEC)*512
             IF(IVPSEC.NE.OLDSEC) THEN
                OLDSEC=IVPSEC
                CALL IRTISK(BRDATA,512,OBFSEC+IVPSEC,INODE)
                CALL IRTISK(SRDATA,512,OSFSEC+IVPSEC,INODE)
                CALL IRTISK( IDATA,512,IVFSEC+IVPSEC,INODE)
                ENDIF
      DO 101 J=1,3
             JI=3*(I-1)+J
             JR=IPK-2+J
             RVPK(JI)= IDATA(JR)
             BVPK(JI)=BRDATA(JR)
101          SVPK(JI)=SRDATA(JR)
             ILOW= BGBLSZ*((IPK-1)/BGBLSZ)+1
             IHIGH=ILOW+BGBLSZ-1
             IBASE=ILOW
      DO 201 J=ILOW,IHIGH
201          IF (SRDATA(J).GT.SRDATA(IBASE)) IBASE=J
             BBASE(I)=BRDATA(IBASE)
             SBASE(I)=SRDATA(IBASE)
301          RBASE(I)= IDATA(IBASE)
             RETURN
             END
```

```
      SUBROUTINE VAPSHF(IVAP,NVP,BVPK,SVPK,FRACPT,NSH)
      DIMENSION XINTRP(10),Y(10),BVPK(30),SVPK(30),CB(10,3),
     1          CS(10,3),WRDSHF(10),NVP(4)
      COMMON /VAPSHF/ XINTRP,Y,CB,CS
C
C ****************************************************************
C THIS SUBROUTINE DETERMINES THE AVERAGE CALIBRATION ERROR
C (BG - SAMPLE) OF A SET OF VAPOR PEAKS.  IT IS CALLED BY
C "SBBLN.FOR".
C
C INPUT:
C
C IVAP       = BAND ID #.
C NVP(IVAP)  = # OF INPUT REFERENCE PEAKS FOR THE VAPOR BAND.
C BVPK,SVPK  = INTENSITY ARRAYS COMPRISED OF 3-WORD SUBSETS. THE
C              SUBSETS CONTAIN THE INTENSITY AT THE REF CM-1 AND
C              THE INTENSITIES OF THE NEAREST-NEIGHBOR PTS.
C
C OUTPUT:     FRACPT = AVERAGE CALIBRATION ERROR.
C             NSH    = # OF REF PTS USED TO CALCULATE 'FRACPT'.
C ****************************************************************
C
              IS=0
              XINTRP(1)=0
              XINTRP(2)=1
              XINTRP(3)=2
      DO 101 J=1,NVP(IVAP)
              J3=3*(J-1)
      DO  11 I=1,3
11            Y(I)=BVPK(J3+I)
              CALL SPLINE(1,3,XINTRP,Y,0.0,0.0,CB)
      DO  21 I=1,3
21            Y(I)=SVPK(J3+I)
              CALL SPLINE(1,3,XINTRP,Y,0.0,0.0,CS)
C
              KB=2
              IF (BVPK(J3+1).LT.BVPK(J3+3)) KB=1
              ARG=4*CB(KB,2)*CB(KB,2)-12*CB(KB,3)*CB(KB,1)
              IF (ARG.LT.0)                                  GO TO 101
              XB=(-2*CB(KB,2)+SQRT(ARG))/(6*CB(KB,3))
              IF (XB.LT.0.OR.XB.GT.1)
     1             XB=(-2*CB(2,2)-SQRT(ARG))/(6*CB(2,3))
              IF (XB.LT.0.OR.XB.GT.1)                        GO TO 101
C
              KS=2
              IF (SVPK(J3+1).LT.SVPK(J3+3)) KS=1
              ARG=4*CS(KS,2)*CS(KS,2)-12*CS(KS,3)*CS(KS,1)
              IF (ARG.LT.0)                                  GO TO 101
              XS=(-2*CS(KS,2)+SQRT(ARG))/(6*CS(KS,3))
              IF (XS.LT.0.OR.XS.GT.1)
     1             XS=(-2*CS(2,2)-SQRT(ARG))/(6*CS(2,3))
              IF (XS.LT.0.OR.XS.GT.1)                        GO TO 101
              IS=IS+1
```

```
            WRDSHF(IS)=XB-XS+KB-KS
101         CONTINUE
C
C ***************************************************************
C SORT THE INDIVIDUAL CALIBRATION ERRORS:
C
      DO 131 I=1,IS-1
      DO 131 K=I+1,IS
            IF (WRDSHF(K).LT.WRDSHF(I))                GO TO 131
               TEMP      = WRDSHF(I)
               WRDSHF(I)= WRDSHF(K)
               WRDSHF(K)= TEMP
131         CONTINUE
C
C ***************************************************************
C DISCARD INDIVIDUAL CALIBRATION ERRORS THAT DIFFER FROM THE
C AVERAGE VALUE BY MORE THAN THE TOLERANCE LIMIT.
C
      PRINT *,'IS,WRDSHF(1,IS)',IS,WRDSHF(1),WRDSHF(IS)
            IL=1
            IU=IS
            NDUMP=0
201         SUM=0.0
      DO 221 I=IL,IU
221         SUM=SUM+WRDSHF(I)
            FRACPT=SUM/(1+IU-IL)
            NPTS=1+IU-IL
            PRINT *,'FRACPT,NPTS',FRACPT,NPTS
            ABSL=ABS(WRDSHF(IL)-FRACPT)
            ABSU=ABS(WRDSHF(IU)-FRACPT)
            IF (ABSU.LT.0.02.AND.ABSL.LT.0.02)         GO TO 299
            IF (ABSU.GT.ABSL) IU=IU-1
            IF (ABSU.LE.ABSL) IL=IL+1
            NDUMP=NDUMP+1
            IF (NDUMP.LT.NVP(IVAP)/2)                  GO TO 201
            FRACPT=0.0
299         PRINT *,'FRACPT',FRACPT
            NSH=IS-NDUMP
            RETURN
            END
```

```
      SUBROUTINE FTPARM(NICMOD,RFXF,RLXF,FRQMIN,FRQMAX,IISEC,
     1          -        IFSEC,INDXSP,INDXEP,INODE,NSECS,PPWVN)
C ***************************************************************
C
C PURPOSE OF SUBROUTINE:
C      OBTAIN SELECTED FTIR PARAMETERS FROM COMPUTER MEMORY.
C
C INPUT:
C
C NICMOD       : SPECTROMETER MODEL CODE (740 OR 6000).  EACH
C                HAS A SLIGHTLY DIFFERENT PPWVN VALUE.
C RFXF,RLXF    : INITIAL AND FINAL WAVENUMBERS OF THE SPECTRAL
C                REGION UNDER CONSIDERATION.
C
C OUTPUT:
C
C FRQMIN,FRQMAX: RFXF AND RLXF ARRANGED IN ASCENDING ORDER.
C IISEC,IFSEC  : RELATIVE INITIAL & FINAL SECTORS CORRESPONDING
C                TO FRQMIN & FRQMAX (WITH SECTOR 1 DEFINED AS
C                BEGINNING AT 0 CM-1 OF THE CURRENT SPECTRUM).
C INDXSP,INDXEP: RELATIVE INITIAL AND FINAL WORDS CORRESPONDING
C                TO FRQMIN AND FRQMAX (EACH REFERENCED TO THE
C                START OF THE SECTOR IN WHICH IT IS LOCATED).
C INODE        : DISK LOCATION OF FTIR SCRATCH FILES.
C NSECS        : # OF SECTORS PER FTIR SCRATCH FILE.
C PPWVN        : RATIO OF WORD RANGE TO WAVENUMBER RANGE.
C ***************************************************************C
C
      NSECS=IRVAL(14001,0)
      INODE=IRVAL(13004,0)
      NDPW =IRVAL(14000,0)
      IF (NICMOD.EQ.6000) R=0.032408016
      IF (NICMOD.EQ. 740) R=0.032409085
      PPWVN=R*NDPW
      FRQMIN=RFXF
      FRQMAX=RLXF
      IF (RLXF.LT.RFXF) FRQMIN=RLXF
      IF (RLXF.LT.RFXF) FRQMAX=RFXF
C
C IIWORD IS OBTAINED BY TRUNCATION.  IFWORD IS OBTAINED BY
C TRUNCATION FOLLOWED BY ADDING AN EXTRA 1.
C
      IIWORD=1+INT(PPWVN*FRQMIN)
      IISEC =(IIWORD-1)/512+1
      INDXSP=IIWORD+(1-IISEC)*512
      IFWORD=2+INT(PPWVN*FRQMAX)
      IFSEC =(IFWORD-1)/512+1
      INDXEP=IFWORD+(1-IFSEC)*512
      RETURN
      END
```

```
C SPLINE.FOR
C
C THIS SUBROUTINE COMPUTES COEFFICIENTS FOR CUBIC INTERPOLATION
C FORMULAS.
C ***************************************************************
C
C  INPUT:
C        SPLOPT:  + VALUE: CUBIC INTERPOLATION.
C                 0      : SET ALL COEFFICIENTS TO 0.
C                 - VALUE: LINEAR INTERPOLATION.
C        NPTS = # OF DATA POINTS
C        XDATA(I),YDATA(I) = DATA ARRAYS
C        Y2DI,Y2DF = ESTIMATES OF THE 2ND DERIVATIVES AT THE
C                    INITIAL AND FINAL INTERPOLATION POINTS,
C                    RESPECTIVELY.
C
C  OUTPUT:
C        C(I,J) = ARRAY OF COEFFICIENTS (J = 1,2,3)
C
C ***************************************************************
C   THE COEFFICIENTS FOR THE ITH CUBIC EQN (COVERING RANGE I TO
C I+1) ARE GIVEN BY:
C
C   Y = C(I,3)*X**3 + C(I,2)*X**2 + C(I,1)*X + YDATA(I)
C
C    THE COEFFICIENTS ARE DEFINED SO THAT XDATA(I) CORRESPONDS
C TO X=0.
C ***************************************************************
C
      SUBROUTINE SPLINE(SPLOPT,NPTS,XDATA,YDATA,Y2DI,Y2DF,C)
      DIMENSION XDATA(10),YDATA(10),C(10,3),XUPDIF(2),YUPDIF(2),
     1          DIFRAT(2),R(10),CY2D(10,10),Y2D(10)
      INTEGER SPLOPT
C
            NDIM=NPTS-2
C
C      COMPUTE 2ND DERIVATIVES FROM AN ITERATIVE FORMULA
C DERIVED FROM BOUNDARY MATCHING CONDITIONS FOR 2ND DERIVATIVES.
C
            Y2D(1)=Y2DI
            Y2D(NPTS)=Y2DF
            MAXDIM=10
      DO 11 I=1,MAXDIM
            R(I)=0.0
      DO 11 J=1,3
11          C(I,J)=0.0
            IF (SPLOPT) 15,999,19
15    DO 17 I=1,MAXDIM
            DENOM=XDATA(I+1)-XDATA(I)
            IF (ABS(DENOM).LT.1.0E-6) GO TO 999
17          C(I,1)=(YDATA(I+1)-YDATA(I))/DENOM
            GO TO 999
19    DO 21 I=1,2
```

```
            XUPDIF(I)=XDATA(I+1)-XDATA(I)
            YUPDIF(I)=YDATA(I+1)-YDATA(I)
21          DIFRAT(I)=YUPDIF(I)/XUPDIF(I)
            R(1)=-XUPDIF(1)*Y2D(1)
      DO 51 I=1,NDIM
            IF (I.EQ.1) GO TO 31
            CY2D(I,I-1)=XUPDIF(1)
31          CY2D(I,I)=2*(XUPDIF(1)+XUPDIF(2))
            IF (I.EQ.NDIM) GO TO 41
            CY2D(I,I+1)=XUPDIF(2)
41          R(I)=6*(DIFRAT(2)-DIFRAT(1))+R(I)
            IF (I.EQ.NDIM) GO TO 51
            XUPDIF(1)=XUPDIF(2)
            XUPDIF(2)=XDATA(I+3)-XDATA(I+2)
            YUPDIF(2)=YDATA(I+3)-YDATA(I+2)
            DIFRAT(1)=DIFRAT(2)
51          DIFRAT(2)=YUPDIF(2)/XUPDIF(2)
            R(NDIM)=R(NDIM)-XUPDIF(2)*Y2D(NPTS)
C
C INVERT THE MATRIX OF 2ND-DERIVATIVE COEFFICIENTS:
C
            CALL MATINV(NDIM,CY2D)
C
C ***************************************************************
C COMPUTE 2ND DERIVATIVES FOR POINTS 2,3,...NPTS-1.
C
      DO 131 I=2,NPTS-1
            Y2D(I)=0.0
      DO 131 J=1,NDIM
131         Y2D(I)=Y2D(I)+CY2D(I-1,J)*R(J,1)
C
C ***************************************************************
C
C THE FOLLOWING EXPRESSIONS FOR THE CUBIC COEFFICIENTS ARE TRUE
C IN GENERAL BUT THE 2ND DERIVATIVES THAT APPEAR IN THESE
C EXPRESSIONS ARE DEPENDENT ON INPUT BOUNDARY CONDITIONS.
C
      DO 301 I=1,NPTS-1
      Q=      XDATA(I+1)-XDATA(I)
      C(I,3)= (Y2D(I+1)-Y2D(I))/(6*Q)
      C(I,2)= Y2D(I)/2
      C(I,1)= (YDATA(I+1)-YDATA(I)-Q*Q*(Y2D(I)/3+Y2D(I+1)/6))/Q
301   CONTINUE
999   RETURN
      END
```

```
      SUBROUTINE MATINV(N,A)
      DIMENSION A(10,10),IP(10,3)
      D=1.0
      DO 51 J=1,N
51          IP(J,3)=0
      DO 901 I=1,N
            AM=0.0
      DO 201 J=1,N
            IF (IP(J,3).EQ.1) GO TO 201
      DO 101 K=1,N
            IF (IP(K,3).EQ.1) GO TO 101
            IF (AM.GE.ABS(A(J,K))) GO TO 101
            IR=J
            IC=K
            AM=ABS(A(J,K))
101         CONTINUE
201         CONTINUE
            IF (AM.LE.1.0E-30) GO TO 1201
            IP(IC,3)=1
            IP(I,1)=IR
            IP(I,2)=IC
            IF (IR.EQ.IC) GO TO 351
      DO 301 L=1,N
            SW=A(IR,L)
            A(IR,L)=A(IC,L)
301         A(IC,L)=SW
351         PV=A(IC,IC)
            D=D*PV
            A(IC,IC)=1.0
      DO 401 L=1,N
401         A(IC,L)=A(IC,L)/PV
      DO 601 L1=1,N
            IF (L1.EQ.IC) GO TO 601
            T=A(L1,IC)
            A(L1,IC)=0.0
      DO 501 L=1,N
501         A(L1,L)=A(L1,L)-A(IC,L)*T
601         CONTINUE
901         CONTINUE
            NS=0
      DO 1101 I=1,N
            L=N-I+1
            IF (IP(L,1).EQ.IP(L,2)) GO TO 1101
            JR=IP(L,1)
            JC=IP(L,2)
            NS=NS+1
      DO 1001 K=1,N
             SW=A(K,JR)
             A(K,JR)=A(K,JC)
1001         A(K,JC)=SW
1101         CONTINUE
1201         RETURN
             END
```


(The reverse of this page is blank.)